Yang-Baxter Integrable Dimers and Fused Restricted-Solid-On-Solid Lattice Models

Alessandra Vittorini Orgeas

Submitted in total fulfilment of the requirements of the degree of

Doctor of Philosophy

School of Mathematics and Statistics
THE UNIVERSITY OF MELBOURNE

April 2019

Abstract

The main objects of investigation in this thesis are two Yang-Baxter integrable lattice models of statistical mechanics in two dimensions: nonunitary RSOS models and dimers. At criticality they admit continuum descriptions with nonunitary conformal field theories (CFTs) in (1+1) dimensions. CFTs are quantum field theory invariant under conformal transformations. They play a major role in the theory of phase transition and critical phenomena. In quantum field theory unitarity is the requirement that the probability is conserved, hence realistic physical problems are associated with unitary quantum field theories. Nevertheless, in statistical mechanics this property loses a physical meaning and statistical systems like polymers and percolations, which model physical problems with long-range interactions, in the continuum scaling limit give rise to nonunitary conformal field theories.

Both the nonunitary RSOS models and dimers are defined on a two-dimensional square lattice. Restricted solid-on-solid (RSOS) models are so called because their degrees of freedom are in the form of a finite (therefore restricted) set of heights which live on the sites of the lattice and their interactions take place between the four sites around each face of the lattice (solid-on-solid). Each allowed configuration of heights maps to a specific Boltzmann weight. RSOS are integrable in the sense that their Boltzmann weights and transfer matrices satisfy the Yang-Baxter equation. The CFTs associated to critical RSOS models are minimal models, the simplest family of rational conformal field theories. The process of fusion on elementary RSOS models has a different outcome on the CFT side depending on both the level of fusion and the value of their crossing parameter λ. Precisely, in the interval $0 \leq \lambda \leq \pi/2$, the 2×2 fused RSOS models correspond to higher-level conformal cosets with integer level of fusion equal to two. Instead in the complementary interval

$\pi/n \leq \lambda \leq \pi$ the 2×2 fused RSOS models are related to minimal models with integer level of fusion equal to one. To prove this conjecture one-dimensional sums, deriving from the well-known Yang-Baxter corner transfer matrix method, have been calculated, extended in the continuum limit and ultimately compared to the conformal characters of the related minimal models.

The dimer model has been for a long time object of various scientific studies, firstly as simple prototype of diatomic molecules and then as equivalent formulation to the well-known domino tilings problem of statistical mechanics. However, only more recently it has attracted attention as conformal field theory thanks to its relation with another famous integrable lattice model, the six-vertex model. What is particularly interesting of dimers is the property of being a free-fermion model and at the same time showing non-local properties due to the long-range steric effects propagating from the boundaries. This non-locality translates then in the dependance of their bulk free energy on the boundary conditions. We formulate the dimer model as a Yang-Baxter integrable free-fermion six-vertex model. This model is integrable in different geometries (cylinder, torus and strip) and with a variety of different integrable boundary conditions. The exact solution for the partition function arises from the complete spectra of eigenvalues of the transfer matrix. This is obtained by solving some functional equations, in the form of inversion identities, usually associated to the transfer matrix of the free-fermion six-vertex model, and using the physical combinatorics of the pattern of zeros of the transfer matrix eigenvalues to classify the eigenvalues according to their degeneracies. In the case of the cylinder and torus, the transfer matrix can be diagonalized, while, in the other cases, we observe that in a certain representation the double row transfer matrix exhibits non trivial Jordan-cells. Remarkably, the spectrum of eigenvalues of dimers and critical dense polymers agree sectors by sectors. The similarity with critical dense polymers, which is a logarithmic field theory, raises the question whether also the free-fermion dimer model manifests a logarithmic behaviour in the continuum scaling limit. The debate is still open. However, in our papers we provide a final answer and argue that the type of conformal field theory which best describe dimers is a logarithmic field theory, as it results by looking at the numerically estimate of the finite size corrections to the critical free energy of the free-fermion six-vertex-equivalent dimer

model.

The thesis is organized as follows. The first chapter is an introduction which has the purpose to inform the reader about the basics of statistical mechanics, from one side, and CFTs, on the other side, with a specific focus on the two lattice models that have been studied (nonunitary RSOS and dimers) and the theories associated to the their continuum description at criticality (minimal models and logarithmic CFTs). The second chapter considers the family of non-unitary RSOS models with $\pi/n \leq \lambda \leq \pi$ and brings forward the discussion around the one-dimensional sums of the elementary and fused models, and the associated conformal characters in the continuum scaling limit. The third and fourth chapters are dedicated to dimers, starting with periodic conditions on a cylinder and torus, and then more general integrable boundary conditions on a strip. In each case, a combinatorial analysis of the pattern of zeros of the transfer matrix eigenvalues is presented and extensively treated. It follows then the analysis of the finite-size corrections to the critical free energy. Finally, the central charges and minimal conformal dimensions of critical dimers are discussed in depth with concluding remarks about the logarithmic hypothesis. Next, there is a conclusion where the main results of these studies are summarized and put into perspective with possible future research goals.

Declaration

This is to certify that

1. the thesis comprises only my original work towards the PhD except where indicated in the Preface,
2. due acknowledgement has been made in the text to all other material used,
3. the thesis is less than 100,000 words in length, exclusive of tables, maps, bibliographies and appendices.

Alessandra Vittorini Orgeas, April 2019

Acknowledgements

My first mention goes to my supervisor. I would like to thank him for giving me this incredible opportunity of starting a new PhD in Mathematics at the University of Melbourne. Then, I would like to thank Jan de Gier and Peter Forrester who formed my supervisor committee and have been a valuable guide through the course of these three years of PhD. Many other people in our school also have been extraordinary supportive and helpful, David Ridout, Thomas Quella, Omar Foda, Kirsten Hoak, Susan Wei. A special thank you goes to Elena Tartaglia who kindly assisted me in many different ways, not just answering my maths questions, bust also cheering my afternoon at the university with tea breaks and chats, and also providing me some technical support to settle in this new city. Another special thank you goes to Alexander Garbali and Gyorgy Feher for their thoughtful advices and their guidance in solving interesting maths problems. Thank you to Lachlan McIntosh, Tianshu Liu, Charl Ras, Luna Liu for sharing ideas, problems, solutions and experiences as well as lots of laughs and great companionship. All of this could have never been started without the support and encouragement of my whole family overseas. To all of them I dedicate this thesis.

Preface

Each chapter refers to a publication or preprint in this precise order

- Chapter 2 is based on G. Z. Fehér, P. A. Pearce, A. Vittorini-Orgeas, "One-Dimensional Sums and Finitized Characters of 2×2 Fused RSOS Models," J. Stat. Mech. 073104, 2018.
- Chapter 3 is based on P. A. Pearce, A. Vittorini-Orgeas, "Yang-Baxter Solution of Dimers as a Free-Fermion Six-Vertex Model," *Journal of Physics A: Mathematical and Theoretical*, vol. 50, no. 434001, p. 1-28, 2017.
- Chapter 4 is based on P. A. Pearce, J. Rasmussen, A. Vittorini-Orgeas, "Yang-Baxter Integrable Dimers on a strip," unpublished.

To my family.

Contents

List of Figures

Chapter 1
Introduction

1.1 Statistical Mechanics

Statistical mechanics is the theory which defines and justifies the connection between the microscopic description provided by classical mechanics and the macroscopic description of theories such as thermodynamics and fluid dynamics [1–3].

A classical physical system, such as a gas, can be defined in first approximation as a collection of N point-like particles, or molecules, subject to the laws of classical mechanics. Its time evolution is then determined by the Hamiltonian equations of motion and is described by a set of canonical coordinates $(\boldsymbol{q},\boldsymbol{p})$ where each component q_i and p_i refers to coordinates and momenta of the ith particle of this system in a $6N$-dimensional phase space. This method offers a solution which is in principle exact and complete, in the sense that it is not approximated, and contains all the possible information relative to the system under study. However, it does not work efficiently when the number of particles becomes extremely large. This is often the case in real life since physical systems typically contain a number of particles as large as Avagadro's number, 6.02×10^{23}.

Theormodynamics and fluid dynamics look at the problem from a different perspective. In fact they base their description on macroscopic quantities such as density, pressure, temperature etc. If the state variables (usually temperature, pressure, volume and number of particles) don't change in time, a physical system is said to be in thermodynamic equilibrium with its surroundings and a thermodynamic approach is used in this case. If, instead, there are some macroscopic movements involved in it (such as flux of material, heat transfer, propagation of sounds waves etc.) a fluid dynamic description is required.

Statistical mechanics is able to connect the macroscopic and microscopic formulations by using a probabilistic approach. Within this approach, the macroscopic variables are computed as expectation values of certain functions of the microscopic states (microstates) of the system with respect to a probability density function in a suitable statistical ensembles. The determination of this density function and the associated partition function constitute an important aspect of the theory of statistical mechanics.

The fundamental statistical ensembles are: microcanonical, canonical and grand canonical. Each of them depends on a few observable parameters which are in statistical equilibrium. The canonical ensemble applies when the mechanical system is in thermal equilibrium with the external environment at fixed temperature T. In this case, the probability that a microstate s with energy $E(s)$ occurs is

$$P(s) = \frac{1}{Z} \exp^{-\frac{E(s)}{k_B T}} \tag{1.1.1}$$

where k_B denotes the Boltzmann's constant and the exponential term $\exp^{-\frac{E(s)}{k_B T}}$ is known as the Boltzmann factor. The canonical partition function is then defined as the normalization factor of this probability distribution and in a discrete setting is given by

$$Z = \sum_{\{s\}} \exp^{-\frac{E(s)}{k_B T}} \tag{1.1.2}$$

If $\mathcal{O}$ is a generic observable of this system, with values $\mathcal{O}(s)$ on each microstate s, then we calculate its expectation value as follows

$$\langle \mathcal{O} \rangle = \frac{1}{Z} \sum_{\{s\}} \mathcal{O}(s) \exp^{-\frac{E(s)}{k_B T}} \tag{1.1.3}$$

The importance of the partition function goes beyond the normalization of the probability distribution. In fact, the expectation values of many physical properties of interest (such as total energy, entropy, pressure) can be expressed in terms of the partition function or its derivatives. For example, the internal energy U in the canonical ensemble is defined as

$$\langle U \rangle = \frac{1}{Z} \sum_{\{s\}} E(s) \exp^{-\frac{E(s)}{k_B T}} = k_B T^2 \frac{\partial}{\partial T} \log Z \tag{1.1.4}$$

In this manner, we see the importance of the partition function Z as a thermodynamic potential from which a set of thermodynamic quantities defining a statistical model in thermodynamic equilibrium can be obtained by differentiation.

1.1.1 Phase transition

The theory of statistical mechanics is often used in the context of phase transitions [4,5].

A phase transition describes the situation where a particular state of matter changes to a different one in response to a variation of external conditions such as temperature, pressure, chemical potential, magnetic or electric field and others. The fundamental (classical) states of matter are four: solid, liquid, gas and plasma. Yet, a comprehensive list of states of matter is very long. It includes forms of matter which show hybrid properties compared to the classical phases, and also others which only exist under extreme conditions. Typical examples of the former case are glass, liquid crystal and magnetically ordered materials, and of the latter case Bose-Einstein condensates and neutron-degenerate matter which are, respectively, low temperature and high density states of matter. Finally, in this list there are some non-classical states of matter, such as fermionic condensate or quark-gluon plasma, which are not even composed by molecules.

A phase transition usually manifests itself with a sudden appearance of order in an otherwise disordered system. As examples, it could be a liquid (disordered phase) which freezes into a solid (ordered phase), or a material characterized by permanent magnetisation (ferromagnetic or ordered phase) which loses its magnetic property above a critical temperature, the so called Curie temperature, to enter into a paramagnetic phase (disordered phase) where magnetization can only be induced by an external magnetic field.

Two different types of phase transitions are distinguished: *first order* (discontinuous) and *second order* (continuous). This classification relies on the concept of *correlation length* (ξ), the characteristic distance over which the system's microscopic properties are correlated. ξ is an intrinsic length scale of a physical system, and it depends on thermodynamic variables, such as temperature, pressure, external magnetic field and others, therefore it can be experimentally measured. It behaves differently in the two types of phase transition. Since first order phase transitions are characterized by phase coexistence, ξ, which is

of the order of the size of the correlated clusters, remains finite while the transition is taking place. Differently, in second order phase transitions, correlations among microscopic variables extend to the whole system and in proximity of the transition ξ becomes infinite. This exceptional behaviour, with the loss of a natural length scale, accounts for an important symmetry of continuous phase transitions, known as *scale invariance*: the physics of the system remains invariant under any change of length scale.

Second order phase transitions are typically defined in one specific point (*critical point*) of the so called phase diagram, the graph which displays the thermodynamic conditions under which different phases occur and coexist in equilibrium. In the proximity of the critical point, ξ, as well as other thermodynamic quantities, exhibit a power law behaviour. Remarkably, it is observed that the critical exponents characterizing these power law behaviours depend not on the microscopic details of the model under study but only on its fundamental symmetries. This interesting phenomenon is called *universality*, and it finds a formal theoretical explanation in the *renormalization group theory* [6–16].

1.1.2 Critical phenomena

Various classes of critical phenomena [4,5,15–18] are characterized by divergence of some physical quantities of interest as the system approaches the critical point. This behaviour is mathematically expressed with power law functions of the form $|t|^{-r}$, where t is the reduced temperature, $(T - T_c)/T_c$, measuring the departure from criticality and r is the *critical exponent* [11,12,19]. A set of critical exponents $\{\alpha, \beta, \gamma, ...\}$ rigorously describes the singular behaviour in the vicinity of a continuous phase transition. A simple example is the ferromagnetic transition of the two-dimensional Ising model.

The Ising ferromagnet model

In the classical description of the two-dimensional Ising model [20], elementary spin variables $\sigma_i = \pm 1$ are located at each node (site) i of a two-dimensional square lattice, as shown in figure 1.1. Each spin interacts with the four closest neighbours and, in principle, also with an external magnetic field. The contribution of each single vertex to the total energy

of the system is given by a Hamiltonian function of this type

$$H = -J \sum_{<i,j>} \sigma_i \sigma_j - h \sum_j \sigma_j \tag{1.1.5}$$

where $< i, j >$ indicates that the sum is over every nearest neighbour pair of nodes and h is the strength of the magnetic field. The first term in this sum is the interaction between neighbouring spins, while the second term measures the interaction between each individual spin and the external field. In the ferromagnetic model the exchange energy parameter J is positive, so the configuration with parallel alignment of adjacent spins lowers the energy which means that is energetically favoured (1.1.5). This is the case that we are interested to discuss. On the other hand, when J is negative, the anti-alignment of spins is favoured. The system then is classified as anti-ferromagnetic.

The Ising ferromagnet model describes a simple magnet in two dimensions. For an infinitely large system with no external magnetic field ($h = 0$) it exhibits a continuous phase transition at the Curie temperature T_c. More precisely, the net magnetic moment, either induced or spontaneous, is

$$m = \langle \sum_j \sigma_j \rangle \tag{1.1.6}$$

and the transition is between a paramagnetic phase with $m = 0$ and a ferromagnetic phase where the alignment of spins results in $m > 0$. For $T < T_c$, instead, there is a first order phase transition characterized by the coexistence of paramagnetic and ferromagnetic phases. In addition to the magnetization (or net magnetic moment), the susceptibility and heat capacity are two other observables of interest in this case. The critical exponents [15] of these physical quantities in the Ising ferromagnet model are listed in Table 1.1 (here the critical exponent β differs from the factor $\beta = 1/(k_B T)$ which appears in the definition of the partition function).

Physical quantity	**Exponent**	**Relationship**
Specific heat	α	$C_0 \sim \lvert t\rvert^{-\alpha},\ t \to 0,\ h = 0$
Spontaneous magnetisation	β	$m_0 \sim \lvert t\rvert^{\beta},\ t \to 0-,\ h = 0$
Zero field susceptibility	γ	$\chi_0 \sim \lvert t\rvert^{-\gamma},\ t \to 0,\ h = 0$
Magnetisation	δ	$m \sim h^{1/\delta},\ t = 0,\ h \to 0$

Table 1.1: Critical exponents for the Ising ferromagnet model.

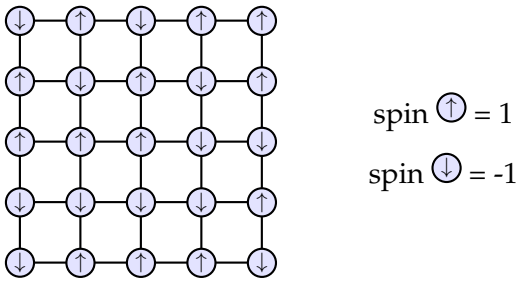

Figure 1.1: Ising ferromagnet on the square lattice

Since these physical quantities are connected through various thermodynamic relations, the critical exponents are not completely independent of each other. In fact, the scaling relations [14]

$$\begin{aligned} \alpha + 2\beta + \gamma &= 2 \\ \gamma &= \beta(\delta - 1) \end{aligned} \tag{1.1.7}$$

show that only two of the exponents listed in Table 1.1 are independent.

1.1.3 Renormalization group theory

The renormalization group (RG) theory offers a suitable mathematical framework to explain critical exponents and universality classes of systems showing a second order phase transition [7–10, 15, 16]. The first crucial assumptions of this theory is that ξ is the most important length scale of a critical system. The second assumption is that ξ is solely responsible for the singular contributions to thermodynamic quantities around the critical

point. These assumptions are grounded on the fundamental principle of scaling invariance, which states that the properties of a critical system don't change under different length scales provided that ξ diverges in the proximity of a critical point. As the temperature approaches the critical temperature T_c, the rate of divergence of ξ is controlled by the critical exponent ν

$$\xi \sim |t|^{-\nu}, \qquad t \to 0 \qquad h = 0 \tag{1.1.8}$$

In the example of the Ising ferromagnet, ξ is the characteristic distance over which two spins at different locations are statistically correlated. More explicitly, away from criticality, the two-spin correlation function G is asymptotically given by

$$G(\boldsymbol{r_1} - \boldsymbol{r_2}) \sim |\boldsymbol{r_1} - \boldsymbol{r_2}|^{2-d-\eta} \exp\Big(-\frac{|\boldsymbol{r_1} - \boldsymbol{r_2}|}{\xi}\Big), \quad |\boldsymbol{r_1} - \boldsymbol{r_2}| \gg 1, \quad 2 - d - \eta < 0 \tag{1.1.9}$$

here d is the dimension of the system. At criticality, the critical exponent η describes the power law decay of G

$$G(\boldsymbol{r_1} - \boldsymbol{r_2}) \sim |\boldsymbol{r_1} - \boldsymbol{r_2}|^{2-d-\eta}, \quad t = 0, \quad \xi \to \infty, \quad |\boldsymbol{r_1} - \boldsymbol{r_2}| \gg 1, \quad 2 - d - \eta < 0 \tag{1.1.10}$$

We can generalise the result above (1.1.10) to a generic physical observable ϕ, whose leading singularities near a critical point are described by a set of *relevant scaling variables* u_i [14], so that

$$\langle \phi_i(\boldsymbol{r_1}) \phi_i(\boldsymbol{r_2}) \rangle \sim |\boldsymbol{r_1} - \boldsymbol{r_2}|^{-2x_i}, \quad \xi \to \infty, \quad |\boldsymbol{r_1} - \boldsymbol{r_2}| \gg 1 \tag{1.1.11}$$

The quantity x_i is the *scaling dimension* of the physical observable ϕ_i associated to u_i. For the Ising ferromagnet and other examples of interest, the relevant scaling variables are t and h.

The RG theory introduces further relations among the critical exponents. Indeed, the critical exponents are related to the renormalisation group eigenvalues y_i associated with

the scaling variables u_i. These relations read as follows

$$2-\alpha = d/y_t, \quad \beta = (d-y_h)/y_t, \quad \gamma = (2y_h - d)/y_t, \quad \delta = y_h/(d-y_h) \tag{1.1.12}$$

$$\nu = 1/y_t, \qquad \eta = d + 2 - 2y_h$$

After the due substitutions, the scaling relations (1.1.10) become

$$\begin{aligned} \alpha &= 2 - d\nu \\ \gamma &= \nu(2-\eta) \end{aligned} \tag{1.1.13}$$

The critical exponents of the two dimensional Ising's ferromagnet model have been exactly calculated by Onsager and others [4, 18, 21–24]

$$\alpha = 0 \text{ (log divergence)}, \quad \beta = 1/8, \quad \gamma = 7/4, \quad \delta = 15, \quad \eta = 1/4, \quad \nu = 1 \tag{1.1.14}$$

and this result agree with the predictions [7, 9, 13] of the RG theory: $y_t = 1$, $y_h = 15/8$.

It is a fundamental result of statistical mechanics that critical theories of two-dimensional lattice models in the continuum scaling limit are equivalent to conformally invariant quantum field theories. In this correspondence, scaling dimensions are precisely linked to conformal dimensions. This point will be addressed in subsection 1.2 with the help of a well-studied, illustrative example. Here, we simply anticipate a result [14], without the details of its derivations, that will be used later

$$x_i = d - y_i \tag{1.1.15}$$

This equation, which relates renormalisation group eigenvalues to scaling dimensions, is one of the most fundamental and general results of the RG theory.

The corresponding values for the two-dimensional Ising's ferromagnet model are $x_t = 1$ and $x_h = 1/8$.

1.1.4 Integrable systems

Classical theory

The foundations of classical integrability have been established mainly through the pioneering works of Kawalewskaya, Fuchs, Painlevé, Liuoville more than a century ago, and some other contempories [25]. There are many definitions of integrability but this topic goes far beyond the purpose of this thesis. Among these definitions the most referred to, in the classical theory of Hamiltonian systems, is the Liouville one where integrability is strictly tied to the existence of *action-angle variables*.

To explain this concept we introduce a Hamiltonian system on a $2n$-dimensional phase space Ω with total energy $H(q(x,t), p(x,t))$. Its time evolution in terms of the canonical coordinates $(q,\ p)$ is described by a set of nonlinear equations, the Hamilton's equations, which read as follows

$$\dot{p} = -\frac{\partial H}{\partial q}, \qquad \dot{q} = \frac{\partial H}{\partial p} \qquad (q,p) \in \mathbb{R}^{2n} \tag{1.1.16}$$

Using the Poisson brackets, $\{A(q,p), B(q,p)\} = \frac{\partial A}{\partial q}\frac{\partial B}{\partial p} - \frac{\partial A}{\partial p}\frac{\partial B}{\partial q}$ for functions A and B on phase space Ω, we call I a conserved quantity of this system (or else first integral) if $\{I, H\} = 0$. Such a system is said to be integrable if there exist additional functions $H_1(q,p), \ldots, H_n(q,p)$ (referred to as Hamiltonians) such that they are independent and all Poisson brackets $\{H_j, H_k\}$ vanish. The Hamiltonian formalism is invariant under canonical transformations, $(q,p) \to (q',p')$, $\Omega \to \Omega'$, which preserve Hamilton's equations. The Liouville-Arnold theorem ensures that in integrable systems it is possible to find a canonical transformation that leads from the old set of coordinates to a system of action-angle variables, $(a(\lambda), b(\lambda,t))$, and it is such that the new Hamiltonian becomes dependent only on the action coordinates, explicitly $H = H(a)$. In this case the dynamical equations

$$\dot{a} = -\frac{\partial H}{\partial b} = 0, \qquad \dot{b} = \frac{\partial H}{\partial a} = \omega \tag{1.1.17}$$

can be trivially solved and, moreover, we get $a(\lambda)$ as the generator of the conserved quantities (one of these conserved quantities is the total energy). The number of such indepen-

dent conserved quantities in integrable systems coincides with the number of degrees of freedom of the system and in interacting quantum models it becomes infinite.

The notion of action-angle variables originates from the theory of the inverse scattering method (ISM) [26, 27]. This method is used in non-linear partial differential equations and it works by solving an equivalent linear scattering problem where the scattering matrix data are action-angle variables and the scattering potential is the inverse action-angle map. The exact solution to the original nonlinear problem is then obtained by finding the canonical mapping from the action-angle variables to the original coordinate fields. This is an *inverse method* for the reason that it retrieves the scattering potential from the scattering matrix as opposed to the usual problem of recovering some scattering data from a given potential.

Quantum theory

The scattering description generalises also to the quantum case [28] and the well-known *Algebraic Bethe-Ansatz* (ABA) construction [29] (details will be given in the next section) provides an effective way to solve for the spectrum of eigenvalues and eigenvectors of the Hamiltonian matrix and the conserved quantities. Hence, infinite quantum systems which exhibit a scattering behaviour can be solved and they are said to be integrable systems. A finite-dimensional integrable system with Poisson commuting Hamiltonians admits a quantization such that the quantum Hamiltonians commute and the resulting quantum system is also integrable. However, the general notion of integrability is quite broad and it usually depends on the model on hand. Also, it must be noted that often the term *exactly solved* or *soluble* are used interchangeably with the term *integrable*.

1.1.5 Lattice models

Two-dimensional lattice models constitute an important category of discrete models in statistical mechanics, which attract interest not only for their versatility in describing physical problems of various types (spin chains, phase transitions, polymers and percolation, just to name few) but also because they have the potential to offer exact solutions to non trivial

problems. In regards to critical behaviour, the current state of knowledge provides powerful insight into the relation between two-dimensional critical lattice models and established quantum field theory in (1+1) dimensions.

Two-dimensional lattice models are defined on a finite two-dimensional lattice graph and the lattice space is organized through the repetition of a fundamental unit (less frequently there are more than one) with regular geometric shape, the most common of which are square, triangular and rhomboid. The degrees of freedom are discrete or continuous variables, assigned to regular positions in the lattice which usually are lattice sites (in *face type* models) or bonds between those sites (in *vertex type* models). These variables are often interpreted either as particles or spins, borrowing the terminology from physics, even though the underlying physical context is not always evident. The discrete setting allows many simplifications in the study of a real physical problem and then the connection with the continuum description is established once the so called *continuum scaling* limit is performed. This limit corresponds to extending the lattice size to infinity, $N \to \infty$, while reducing the lattice spacing to zero, $a \to 0$, in such a way that the continuum space is restored provided that $Na \to x$. In some contexts it is also used the so called *thermodynamic limit*, which simply implies that the system size is increased to infinity to match the situation of real physical systems with a large number of particles.

The square lattice: face and vertex type models.

We will present here a general overview of face and vertex type models defined on the square lattice since these are the main focus of this thesis.

These two types of lattice models are illustrated in figure 1.2. For face type models each unit square, or face of the lattice, is surrounded by a configuration of four heights. Face models are also referred to as *interaction-round-a-face* (IRF) models, since the interactions involve the four sites sharing a common face. For vertex type models, each vertex, formed by the four edges incident on a given site, is associated to a configuration of four arrow (or particle occupation) states. Each allowed configuration of heights/arrow states is assigned to a Boltzmann weight function, which depends not only on the height/arrow state variables but also on an extra parameter, u, called the *spectral parameter*. Formally, we use the

following notation to indicate the Boltzmann weight of face and vertex models

$$W\left(\begin{matrix} b_1 & b_2 \\ a_1 & a_2 \end{matrix}\middle| u\right) \qquad W\left(\sigma_1 \begin{matrix} \gamma_1' \\ \gamma_1 \end{matrix} \sigma_2 \middle| u\right) \tag{1.1.18}$$

face type vertex type

The local configurations $\{a_1, a_2, b_2, b_1\}$ and $\{\sigma_1, \gamma_1, \sigma_2, \gamma_1'\}$ are ordered, by convention, using the marked corner which is shown in figure 1.2 with a red arc. The first entries in these configurations are, for the face type model, the height state of the marked corner and, for vertex models, the arrow state to the left of the marked corner. The next entries are then listed in a counterclockwise order.

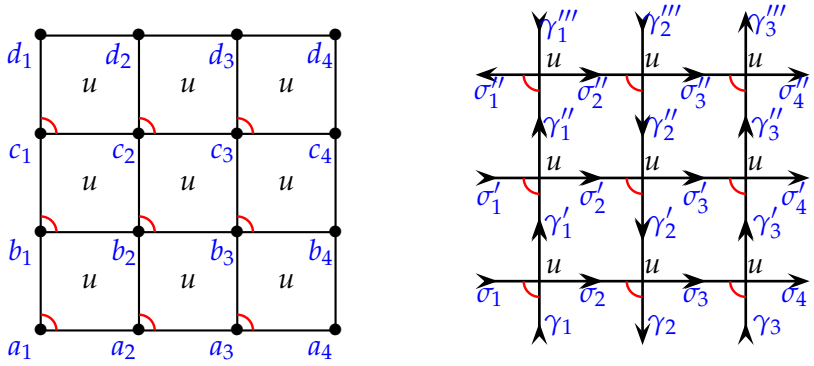

(a) Face type (b) Vertex type

Figure 1.2: Two dimensional square lattice models: face and vertex type.

The real spectral parameter u controls the spatial anisotropy of the Boltzmann weights through the *anisotropy angle* (ϑ) which is defined as

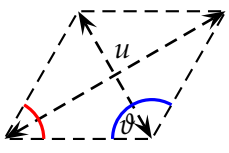

$$\vartheta = \frac{\pi u}{\lambda} \tag{1.1.19}$$

Here λ is the *crossing parameter*, a model-dependent parameter that we will introduce later. The spectral parameter plays a fundamental role in the integrability of lattice models and is often treated as a complex variable.

Integrability and Bethe ansatz

To explain integrability in the context of two-dimensional lattice models, we introduce the *single row transfer matrix*.

Let's consider a face model on a $M \times N$ square lattice with periodic boundary configurations on the vertical edges. The entries of the single row transfer matrix are

$$\boldsymbol{T}(u)_{\boldsymbol{a},\boldsymbol{b}} =$$

$$=$$

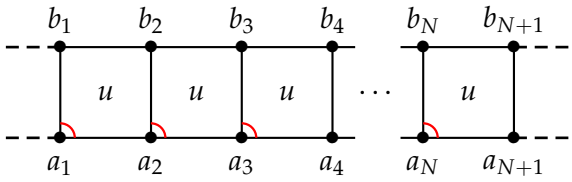

$$= \quad W\left(\begin{matrix} b_1 & b_2 \\ a_1 & a_2 \end{matrix}\middle| u\right) W\left(\begin{matrix} b_2 & b_3 \\ a_2 & a_3 \end{matrix}\middle| u\right) \ldots W\left(\begin{matrix} b_N & b_1 \\ a_N & a_1 \end{matrix}\middle| u\right) \tag{1.1.20}$$

here the periodic boundaries ($a_{N+1} = a_1, b_{N+1} = b_1$) are indicated by dashed lines. Let's consider now a vertex model on a $M \times N$ square lattice and periodic boundary conditions on the horizontal rows. The entries of the single row transfer matrix are

$$\boldsymbol{T}(u)_{\boldsymbol{\gamma},\boldsymbol{\gamma}'} =$$

$$=$$

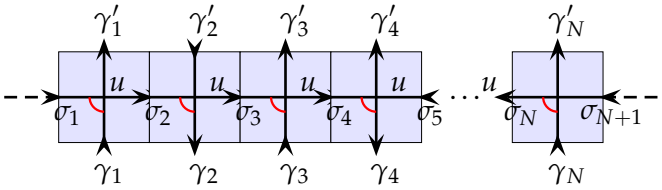

$$= \quad \sum_{\sigma_1}\sum_{\sigma_2}\cdots\sum_{\sigma_N} W\left(\sigma_1 \begin{matrix} \gamma'_1 \\ \gamma_1 \end{matrix} \sigma_2\middle| u\right) W\left(\sigma_2 \begin{matrix} \gamma'_2 \\ \gamma_2 \end{matrix} \sigma_3\middle| u\right) \ldots W\left(\sigma_N \begin{matrix} \gamma_{N'} \\ \gamma_N \end{matrix} \sigma_1\middle| u\right) \tag{1.1.21}$$

here the periodic boundaries ($\sigma_{N+1} = \sigma_1$) are indicated by dashed lines and in (1.1.21) the sum runs over all arrow states (occupation numbers). If the local vertex is not allowed, the Boltzmann weight is zero. Thus, the single row transfer matrix encodes the probability of transition from a particular height/arrow state configuration along a horizontal line of the lattice to the height/arrow state configuration of the next line.

M single rows are necessary to build the whole square lattice and the probability of occurrence of any allowed configurations is obtained by multiplying M single rows transfer matrices. Tracing out this product yields the *partition function* on a torus as

$$Z_{MN} = \mathrm{Tr}\, \boldsymbol{T}^M = \sum_{i=1}^{N} \Lambda_i^M \tag{1.1.22}$$

where the trace glues together the top and bottom edges of the cylinder in the shape of a torus. In the presence of non-periodic boundary conditions it is more useful to act with a double row transfer matrix which propagates across two single rows of the lattice.

For both periodic and non-periodic boundary conditions, the partition function is given by the sum of the eigenvalues of the transfer matrix, Λ_i, raised to the power of M. If Λ_1 is the largest eigenvalue of the transfer matrix, by the Perron-Frobenius theorem, it is a positive real number such that

$$\Lambda_1 > |\Lambda_2| \geq |\Lambda_3| \geq \ldots |\Lambda_N| \tag{1.1.23}$$

It is also the leading term in the continuum scaling limit

$$Z_{MN} = \sum_{i=1}^{N} \Lambda_i^M = \Lambda_1^M (1 + \Big(\frac{\Lambda_2}{\Lambda_1}\Big)^M + \ldots) \sim \Lambda_1^M, \quad M, N \to \infty \tag{1.1.24}$$

Integrable systems are associated with an infinite family of mutually commuting transfer matrices which can then be simultaneously diagonalized

$$[\boldsymbol{T}(u), \boldsymbol{T}(v)] = 0 \tag{1.1.25}$$

Members of this family are identified by their value of the spectral parameter and they share the same set of eigenvectors which, consequently, do not depend on the spectral parameter.

The task of diagonalising the transfer matrix and finding the eigenvalues and eigenvectors can be addressed using the *Bethe ansatz approach*. This is an important method in quantum integrability, originally proposed by Hans Bethe [30] to solve the XXX spin chain

problem (1.1.27) and nowadays applied to many different integrable systems [28, 29]. The key point of this method is that it solves the problem by regarding it as a two-body scattering process with conserved particles and momenta (even if they can be redistributed among particles). It is indeed the quantum equivalent of the inverse scattering method in classical theory, with the difference that the interaction is between virtual particles which belong to an unphysical space, called auxiliary space. The transfer matrix corresponds then to the product of those scattering matrices, which act on both the physical and unphysical spaces, summing over the degrees of freedom in the auxiliary space so that only the physical variables enter into its definition. In this setting the eigenvectors are constructed as elementary excitation of a pseudo-vacuum. The consistency conditions for the existence of such a solution for the eigenstates is precisely expressed by the *Yang-Baxter equation*, which will be the topic of section 1.1.6.

Examples of two-dimensional lattice models

The first formulation of a two-dimensional lattice model is the Ising model [20, 31]. This model represents the physics of elementary spins (up or down) located at the sites of a square lattice with only nearest-neighbour interaction in an external magnetic field. It is also the simplest example of a two dimensional lattice model whose partition function can be calculated and solved explicitly on the square lattice [21]. The Ising model can be further generalized in the Q-state Potts model [32] where the lattice sites are occupied by scalar spins which can assume one of the Q values and the nearest-neighbour interaction is given by a Kronecker delta. Another Ising-type model is the n-vector model, introduced by Stanley in 1968 [33] also known as the O(n) model since the spins have the symmetry of the orthogonal group. In this model, each spin is a unit vector with n components.

Similarly to the Ising model, the six-vertex models have been known for a long time. It was first introduced by Linus Pauling [34] in the 1935 to describe the two-dimensional structure of water ice. In fact, in this model an edge between two vertices of the square lattice corresponds to an oxygen-hydrogen bond and is visualized on the lattice by an arrow associated with a double-valued degree of freedom (spin $+$ or $-$). Its name accounts for the number of allowed configurations of vertices. Thirty years later, the six-vertex model

was reformulated and solved by Lieb [35–38] and then Sutherland [39] in presence of an external electric field, both using a transfer matrix approach. Interestingly, the six-vertex and Ising models can be considered as special cases of a more general model, the zero-field eight-vertex model [40, 41]. From a purely physical point of view, the eight-vertex model describes a ferroelectric material in absence of external electrical field whose polarization, corresponding to the average over the microscopic electric dipoles, represented in the lattice in the form of arrows.

An important feature of the eight-vertex model is that, in the continuum scaling limit, it exactly reproduces the one-dimensional XYZ spin chain quantum integrable system [31, 42]. The XYZ spin chain model is the quantum mechanical model of ferromagnetism and it is represented by the following Hamiltonian

$$H = -\frac{1}{2}\sum_{j=1}^{N}(J_x\sigma_j^x\sigma_{j+1}^x + J_y\sigma_j^y\sigma_{j+1}^y + J_z\sigma_j^z\sigma_{j+1}^z) \tag{1.1.26}$$

Here J_x, J_y, J_z are constants associated with the interactions between nearest neighbouring spins along, respectively, the x, y, z directions. $\sigma_x, \sigma_y, \sigma_z$ are Pauli matrices. The partition function of this model is

$$Z = \mathrm{Tr}\exp(-H/k_BT) \tag{1.1.27}$$

If $J_x = J_y = J_z$, this is the well-known Heisenberg or XXX model [43–45]. Considering more specific cases, $J_x = J_y = 0$ reproduces the nearest-neighbour one-dimensional Ising model where spins are aligned in the z direction, $J_z = 0$ is known as the XY model (it is related to the Ising ferromagnet model), $J_x = J_y$ is the XXZ model. It can be proven that the Hamiltonian in (1.1.26) corresponds to the logarithmic derivative of the eight-vertex transfer matrix [46, 47]. This result is valid for any values of J_x, J_y, J_z. In a similar way the XY spin chain is related to the Ising model and the XXZ spin chain to the six-vertex model. These facts highlight, indeed, a well-proven correspondence between the transfer matrix of 2-dimensional vertex models and the Hamiltonian of 1-dimensional spin chains of quantum mechanics [28, 31] .

Regarding face type models, the hard hexagon problem (the triangular lattice gas with

nearest-neighbour exclusion) was the first to be exactly solved [48,49]. However, few year later it was pointed out that it belongs to a larger class of models, the so called restricted Solid-on-Solid models discovered by Andrews, Baxter and Forrester [50] (detailes will be given in section 1.1.8) which in turn is related to the eight-vertex model.

From these considerations it appears clear that there must exist a remarkable equivalence between the two-dimensional lattice models mentioned so far. Technically, this equivalence relies on the fact that certain elementary matrices, whose product makes up the transfer matrices and so indirectly are related to the partition function, lie in the same algebra, known as the *Temperley-Lieb algebra*, for each model (details about this algebra in section 1.1.7).

1.1.6 Yang-Baxter integrability

The Yang-Baxter equation is the cornerstone of classical and quantum integrability in two dimensions [29,31]. In particular, it provides the consistency condition for the integrability of two-dimensional lattice models on a torus. The validity of this equation ensures that there exist an infinite family of commuting transfer matrices which can be simultaneously diagonalized. Then, if the spectrum of eigenvalues is known, the model under study is *solved* because we can calculate the partition function and derive from it other thermodynamic variables of interest. It is not always obvious that the spectrum of eigenvalues is analytically soluble. However, since ultimately we are interested in the thermodynamic limit, the solution for the partition function reduces to the problem of finding its dominant term for $N >> 1$ where N is the size of the finite system.

In the following we elucidate the meaning and fundamental implications of the Yang-Baxter equation. For clarity we decide to use the symbolic language of face models as we have introduced in the previous section. We formulate the Yang-Baxter equation in the planar algebra notation [51] as

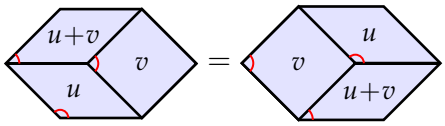

(1.1.28)

where each plaquette corresponds to a Boltzmann face weight and it's implied that all external degrees of freedom are fixed while the internal degrees of freedom are summed over. When the limiting value $u = 0$ is reached, the Boltzmann weights are subject to this condition

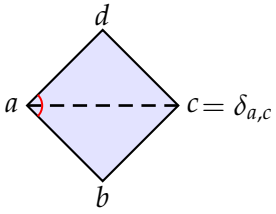

(1.1.29)

This is also known as *initial condition*. The plaquette on the left side of (1.1.29) is a collapsed face where the nodes linked by the dashed line are identified, and it represents a Kronecker delta function so, in the operator language, is an identity. The Boltzmann face weights of the lattice models studied in this thesis satisfy also another important local equation, the so called *inversion relation* [52]

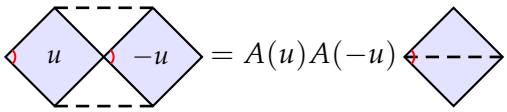

(1.1.30)

where $A(u)$ is a function which depends on the type of model under study.

The Yang-Baxter equation and inversion relation have also an interpretation in the operator formalism, where the elementary face operator, $\mathbb{X}_j(u)$, reproduces the action of adding a single face to the lattice in the position indexed by j

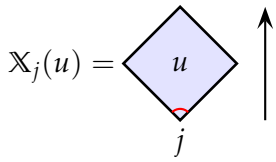

(1.1.31)

More appropriately, we shall refer to (1.1.31) as *face transfer operator* [31, 53]. The direction of action is fixed, by convention, along the diagonal that connects the site with the marked

corner to the one opposite to it. In the operator form, (1.1.28) and (1.1.30) then become

$$\mathbb{X}_j(u)\mathbb{X}_{j+1}(u+v)\mathbb{X}_j(v) = \mathbb{X}_{j+1}(v)\mathbb{X}_j(u+v)\mathbb{X}_{j+1}(u) \tag{1.1.32}$$

$$\mathbb{X}_j(u)\mathbb{X}_j(-u) = A(u)A(-u)I \tag{1.1.33}$$

where I is the identity operator. Often these equations are expressed in the diagrammatic form

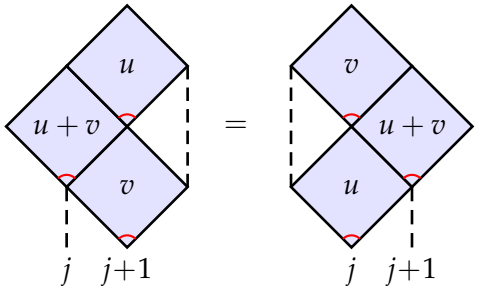

(1.1.34)

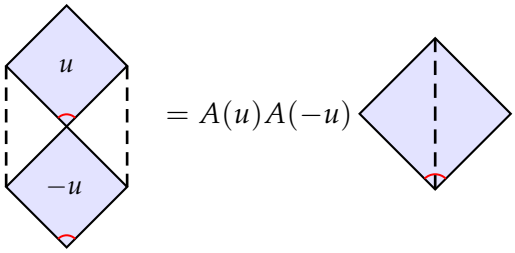

(1.1.35)

In this notation the plaquettes represent the Boltzmann face operators and the collapsed face on the right-hand side of the inversion relation is the identity operator.

Using the local face operators we can construct the periodic single row transfer matrix of size N

$$\boldsymbol{T}(u) = \tag{1.1.36}$$

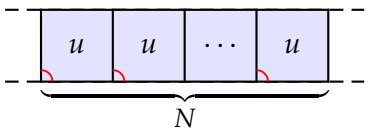

The symbolic representation is identical to the one introduced before (1.1.20). The periodic boundary conditions, indicated by dashed lines, make the right and left edges of the single row identical. The importance of the Yang-Baxter equation and inversion relation resides

in the fact that they imply the commutativity of single row transfer matrices for generic values of the spectral parameter which means

$$[\boldsymbol{T}(u), \boldsymbol{T}(v)] = 0 \tag{1.1.37}$$

In the following we illustrate the proof of this fact

$$\boldsymbol{T}(u)\boldsymbol{T}(v) = \tag{1.1.38}$$

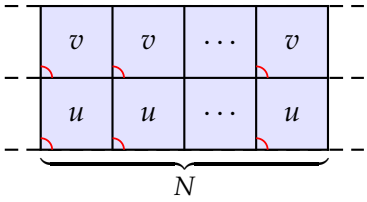

$$= A(v-u)^{-1}A(u-v)^{-1} \tag{1.1.39}$$

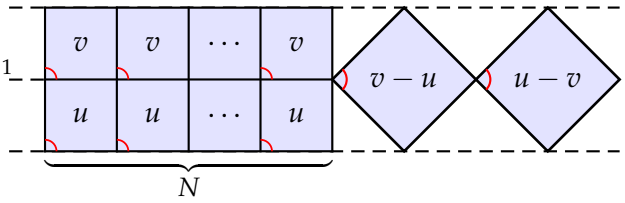

$$= A(v-u)^{-1}A(u-v)^{-1} \tag{1.1.40}$$

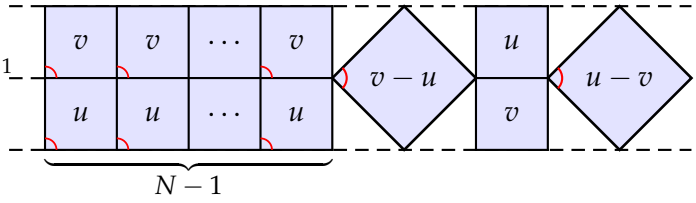

$$= A(v-u)^{-1}A(u-v)^{-1} \tag{1.1.41}$$

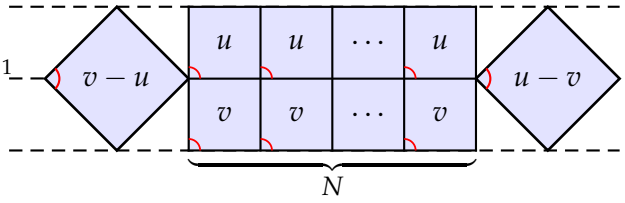

$$= A(u-v)^{-1}A(v-u)^{-1} \tag{1.1.42}$$

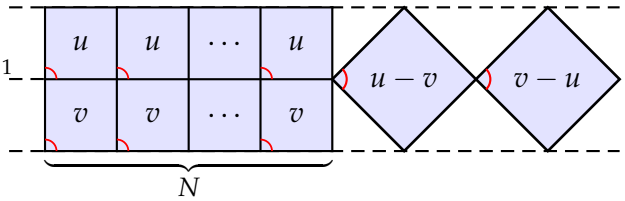

$$= \quad = \boldsymbol{T}(v)\boldsymbol{T}(u) \tag{1.1.43}$$

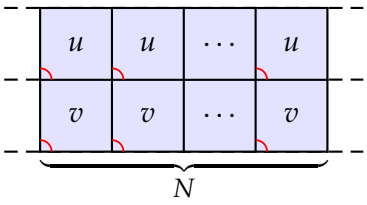

In (1.1.39) the identity operator is inserted at the right side of the double row and is then replaced by the inversion relation. Thanks to the Yang-Baxter equation the face operator immediately attached to the right end of the double row can be pushed backwards (1.1.40),

till it reaches the left end (1.1.41) where it connects to the face operator at the right end by virtue of the periodicity (1.1.42). Finally, we recognise that, by following these steps, we have reconstructed the inversion relation again, so at the end we are left with the product of the two initial transfer matrices (1.1.38) but reversed (1.1.43).

Typically the spectral parameter is a continuous variable, so it means that there exists an infinite family of transfer matrices which commute and, provided that they are diagonalizable, the transfer matrices in this family can be simultaneously diagonalized. In the simplest case the transfer matrix is a normal matrix and hence diagonalizable by standard techniques. Other times, the transfer matrix satisfy additional functional equations and because the eigenvalues (but not the eigenvectors) are function of the spectral parameter, we can write down similar equations for the eigenvalues. The spectrum of eigenvalues can then be found by solving these functional equations. The ultimate problem concerning integrable models, is thus related to the solution of the spectrum of eigenvalues of their transfer matrix. From its solution the partition function can be calculated and the model in question is technically considered *exactly solved*.

The lattice models that will be considered in this thesis belong to two different classes of Yang-Baxter integrable models: the Restricted Solid-on-Solid models and dimers (free-fermion model). They will be reviewed carefully in two separate sections of this introduction.

1.1.7 Temperley-Lieb algebra

Solutions to the Yang-Baxter equation can be constructed through representations of the Temperley-Lieb (TL) algebra. TL_N is an associative algebra generated by the unimodular complex number $q \in \mathbb{C}$ and operators I and e_j $(j = 1, 2, \ldots, N)$ which satisfy the following

relations

$$Ig = gI = g \tag{1.1.44}$$

$$e_j^2 = (q + q^{-1})e_j \tag{1.1.45}$$

$$e_j e_{j\pm1} e_j = e_j \tag{1.1.46}$$

$$e_i e_j = e_j e_i, \qquad |i - j| \geq 2 \tag{1.1.47}$$

where g can be any element of the TL_N algebra and $\beta = (q + q^{-1})$ is often referred to as *loop fugacity* and is a real number. In the case of the models considered in this thesis, we choose $q = e^{i\lambda}$ (λ is the crossing parameter and will be introduced later) and, hence, $\beta = 2\cos(\lambda)$. In the diagrammatic language, TL_N algebra is represented by monoids e_j acting on N strings

$I =$

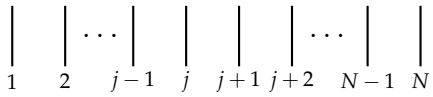

(1.1.48)

$e_j =$

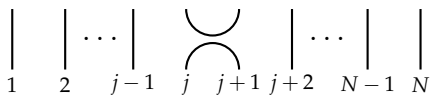

(1.1.49)

Thus, the defining relations of TL algebra (1.1.45) - (1.1.47) translate in the following diagrammatic relations

$$Ie_j = \quad = \quad = e_j \tag{1.1.50}$$

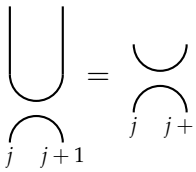

$$e_j^2 = \quad = (q+q^{-1}) \quad = (q+q^{-1})e_j \tag{1.1.51}$$

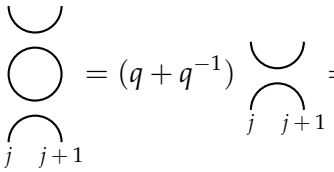

$$e_j e_{j+1} e_j = \quad = \quad = e_j \tag{1.1.52}$$

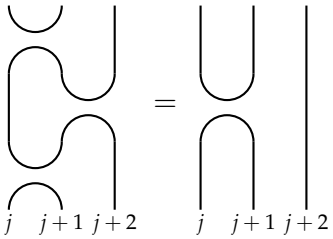

$$e_i e_j = \cdots \quad = \quad \cdots = e_j e_i, \quad j-i \geq 2 \tag{1.1.53}$$

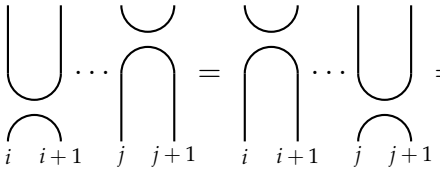

From (1.1.51) it is made clear that β is associated with the weight of the loop. In the planar algebra, the monoids I and e_j become

$$I = \quad e_j = \tag{1.1.54}$$

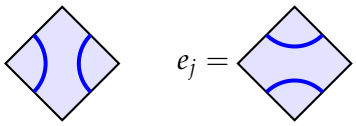

and hence the diagrammatic relations (1.1.50)-(1.1.53) take this form

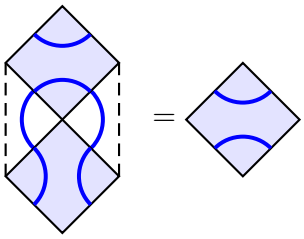

(1.1.55)

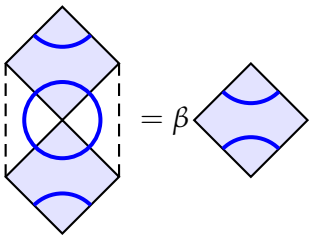

(1.1.56)

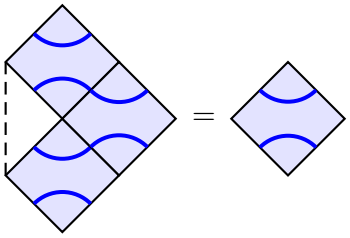

(1.1.57)

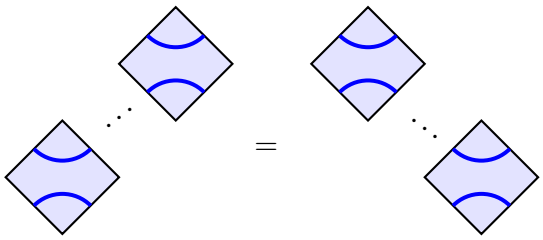

(1.1.58)

where the dashed lines indicate that the corners and internal edges are identified.

1.1.8 Restricted solid-on-solid model

Critical models

The restricted solid-on-solid (RSOS) models form a class of two-dimensional exactly solvable models defined on a square lattice. They were introduced by Andrews, Baxter and Forrester in 1984 and are described in these two seminal papers [50, 54]. They belong to face type models, the dynamic variables are therefore called heights and are assigned to

each lattice face with the requirement that adjacent heights must differ by ± 1.

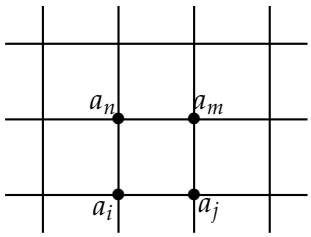

$$|a_i - a_j| = |a_j - a_m| = |a_m - a_n| = |a_n - a_i| = 1$$

Figure 1.3: RSOS model: heights arrangements round a face of a square lattice.

Any arrangement of four heights around the corners of the square face, compatible with these restrictions, corresponds to a specific Boltzmann weight (1.1.18). Two coprime integers m, m' with $2 \leq m < m'$ completely identify any RSOS model. In fact, they specify the crossing parameter $\lambda = (m' - m)\pi/m'$ and also impose a restriction on heights which are integer numbers in the range $a = 1, 2, \ldots, m' - 1$. Exactly six types of of face configurations respect the height restrictions described above, and their Boltzmann weights in the critical regime read

$$W\left(\begin{matrix} a \pm 1 & a \\ a & a \mp 1 \end{matrix}\middle| u\right) = \begin{array}{ccc} & {\scriptstyle a\pm 1} & \\ {\scriptstyle a} & u & {\scriptstyle a} \\ & {\scriptstyle a\mp 1} & \end{array} = s(\lambda - u) \tag{1.1.59}$$

$$W\left(\begin{matrix} a & a \pm 1 \\ a \mp 1 & a \end{matrix}\middle| u\right) = \begin{array}{ccc} & {\scriptstyle a} & \\ {\scriptstyle a} & u & {\scriptstyle a\pm 1} \\ & {\scriptstyle a\mp 1} & \end{array} = \frac{g_{a\mp 1}}{g_{a\pm 1}} \frac{s((a \pm 1)\lambda)}{s(a\lambda)} s(u) \tag{1.1.60}$$

$$W\left(\begin{matrix} a & a \pm 1 \\ a \pm 1 & a \end{matrix}\middle| u\right) = \begin{array}{ccc} & {\scriptstyle a} & \\ {\scriptstyle a} & u & {\scriptstyle a\pm 1} \\ & {\scriptstyle a\pm 1} & \end{array} = \frac{s(a\lambda \pm u)}{s(a\lambda)} \tag{1.1.61}$$

Here $s(u) = \sin u / \sin \lambda$, u is the spectral parameter ($0 < u < \lambda$) and g_a are arbitrary gauge factors. The initial condition applies

$$W\left(\begin{matrix} d & c \\ a & b \end{matrix}\middle| 0\right) = \delta(a, c), \tag{1.1.62}$$

These Boltzmann weights satisfy two important local relations, the Yang-Baxter equation

(1.1.28)

$$\sum_g W\left(\begin{matrix} f & g \\ a & b \end{matrix}\middle| u\right) W\left(\begin{matrix} e & d \\ f & g \end{matrix}\middle| u+v\right) W\left(\begin{matrix} d & c \\ g & b \end{matrix}\middle| v\right) = \sum_g W\left(\begin{matrix} e & g \\ f & a \end{matrix}\middle| v\right) W\left(\begin{matrix} g & c \\ a & b \end{matrix}\middle| u+v\right) W\left(\begin{matrix} e & d \\ g & c \end{matrix}\middle| u\right) \tag{1.1.63}$$

and the inversion relation (1.1.30)

$$\sum_g W\left(\begin{matrix} d & g \\ a & b \end{matrix}\middle| u\right) W\left(\begin{matrix} d & c \\ g & b \end{matrix}\middle| -u\right) = s(\lambda-u)s(\lambda+u)\,\delta_{a,c} \tag{1.1.64}$$

The Boltzmann weights of the RSOS models also show some interesting symmetries. The first is the invariance under height reflection about the leading diagonal, the second is the invariance under height reversal

$$W\left(\begin{matrix} d & c \\ a & b \end{matrix}\middle| u\right) = W\left(\begin{matrix} b & c \\ a & d \end{matrix}\middle| u\right), \quad W\left(\begin{matrix} d & c \\ a & b \end{matrix}\middle| u\right) = W\left(\begin{matrix} m'-d & m'-c \\ m'-a & m'-b \end{matrix}\middle| u\right) \tag{1.1.65}$$

In the principal series (m=$m'-1$) of RSOS models, also known as *unitary* models, where all weights are positive, the gauge for the transfer matrices is commonly chosen to be $g_k = \sqrt{s(k\lambda)}$ ($k = a, b, c, d$) (*symmetric gauge*). The Boltzmann weights in this gauge can be rewritten as

$$W\left(\begin{matrix} d & c \\ a & b \end{matrix}\middle| u\right) = s(\lambda-u)\delta_{a,c}A_{a,b}A_{a,d} + \sqrt{\frac{s(a\lambda)s(c\lambda)}{s(b\lambda)s(d\lambda)}}s(u)\delta_{b,d}A_{a,b}A_{b,c} \tag{1.1.66}$$

where $A_{i,j}$ are entries of the $(m'-1)\times(m'-1)$ adjacency matrix. In the non-principal series models ($m < m'-1$), so called *non-unitary* models, some weights are not positive, therefore a *non-symmetric* gauge must be chosen in order to avoid square roots of negative numbers. A convenient choice of the gauge is $g_k = 1$ if $k = b, d$ (heights along the principal diagonal), and $g_k = \epsilon_k = (-1)^{\left\lfloor \frac{k-1}{2} \right\rfloor}$, if $k = a, c$ (heights along the non-principal diagonal). The last factor is either positive or negative according to

$$\begin{cases} \epsilon_i\epsilon_j = +1, & |i-j| = 1 \\ \epsilon_i\epsilon_j = -1, & |i-j| = 2 \end{cases} \tag{1.1.67}$$

In this gauge, the Boltzmann weights become

$$W\left(\begin{matrix} d & c \\ a & b \end{matrix}\middle| u\right) = s(\lambda - u)\delta_{a,c}A_{a,b}A_{a,d} + \frac{\epsilon_a}{\epsilon_c}\frac{s(c\lambda)}{s(d\lambda)}s(u)\delta_{b,d}A_{a,b}A_{b,c} \tag{1.1.68}$$

Let's consider a square lattice wound around a cylinder. Then the boundary conditions are periodic because the last column is glued to the first one. Given a $M \times N$ lattice under these conditions, we define the single row transfer matrix $\boldsymbol{T}$ with the lower and upper row height sequences given respectively by $\boldsymbol{a} = \{a_1, \ldots, a_N\}$ and $\boldsymbol{a}' = \{a'_1, \ldots, a'_N\}$ as

$$\boldsymbol{T}(u)_{\boldsymbol{a},\boldsymbol{a}'} = \prod_{j=1}^{N} W\left(\begin{matrix} a'_j & a'_{j+1} \\ a_j & a_{j+1} \end{matrix}\middle| u\right), \qquad a_{j+N} = a_j, \;\; a'_{j+N} = a'_j \tag{1.1.69}$$

In conclusion, the RSOS models are Yang-Baxter integrable models, which means that their transfer matrices with different spectral parameters commute and if they are also diagonalizable they share a common set of u-independent eigenvectors and the whole family of commuting matrices can be simultaneously diagonalized.

Off-critical RSOS models

Off-criticality, the sine functions in (1.1.59), (1.1.60) and (1.1.61) are replaced by elliptic theta functions $\vartheta_1(u,t)$ depending on u and an extra variable $t = e^{-\epsilon}$, the elliptic nome, which measures the perturbation from criticality

$$\vartheta_1(u,t) = 2t^{1/4}\sin u \prod_{n=1}^{\infty}(1 - 2t^{2n}\cos 2u + t^{4n})(1 - t^{2n}) \tag{1.1.70}$$

It is easily shown that, when $t = 0$, quotients of theta functions simplify to quotients of trigonometric functions and the theory becomes critical. For the purpose of this thesis, we are concerned with RSOS models in the so called regime III: $0 < u < \lambda$ and $0 < t < 1$. The initial condition and the local relations (Yang-Baxter equation and inversion relation) still hold.

An important quantity associated with off-critical RSOS models is the *one-dimensional configurational sum*. It derives from the corner transfer matrix formalism introduced by Baxter [55,56] and enables the calculation of local one-point functions (fundamental objects

in theoretical physics). Let $\sigma = \{\sigma_1, ..., \sigma_N\}$ and $\sigma' = \{\sigma'_1, ..., \sigma'_N\}$ denote the heights at the edges of the region in figure 1.1.71 with boundaries $(\sigma_N, \sigma_{N+1}) = (b, c)$.

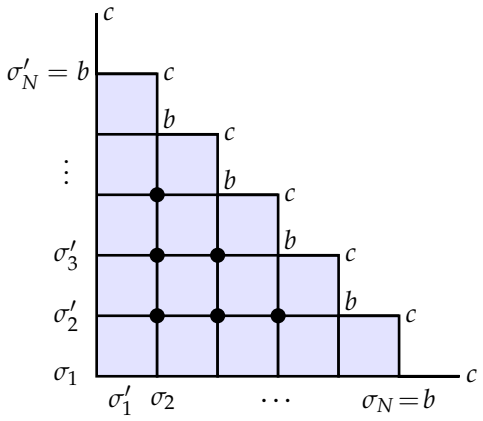

(1.1.71)

The corner transfer matrix $A(u)$ is defined as

$$A(u)_{\sigma,\sigma'} = \sum\prod W\left(\begin{matrix}\sigma_n & \sigma_m \\ \sigma_i & \sigma_j\end{matrix}\middle| u\right) \qquad \text{if } \sigma_1 = \sigma'_1 \tag{1.1.72}$$

$$= 0 \qquad \text{if } \sigma_1 \neq \sigma'_1 \tag{1.1.73}$$

where the product is over the $\frac{1}{2}N(N+1)$ faces in (1.1.71) and the sum is over all spins on sites denoted by solid circles. The concept of one-dimensional sums relates to the local height probability $P_{a'}$ [50] which is defined as the probability to find a center site with height a' in the square lattice divided into 4 quadrants as shown in figure 1.4. Formally this probability reads as follow

$$P_{a'} = Z^{-1} \sum \delta(\sigma_1, a') \prod W\left(\begin{matrix}\sigma_n & \sigma_m \\ \sigma_i & \sigma_j\end{matrix}\middle| u\right) \tag{1.1.74}$$

$$= \frac{\mathrm{Tr}(\delta(\sigma_1,a')\boldsymbol{A}(u)\boldsymbol{B}(u)\boldsymbol{C}(u)\boldsymbol{D}(u))}{\mathrm{Tr}(\boldsymbol{A}(u)\boldsymbol{B}(u)\boldsymbol{C}(u)\boldsymbol{D}(u))} \tag{1.1.75}$$

where Z is the partition function and the sum is over all heights $1 \leq \sigma_i \leq m' - 1$ and the product over all faces of the square lattice having a' as height of the center site σ_1.

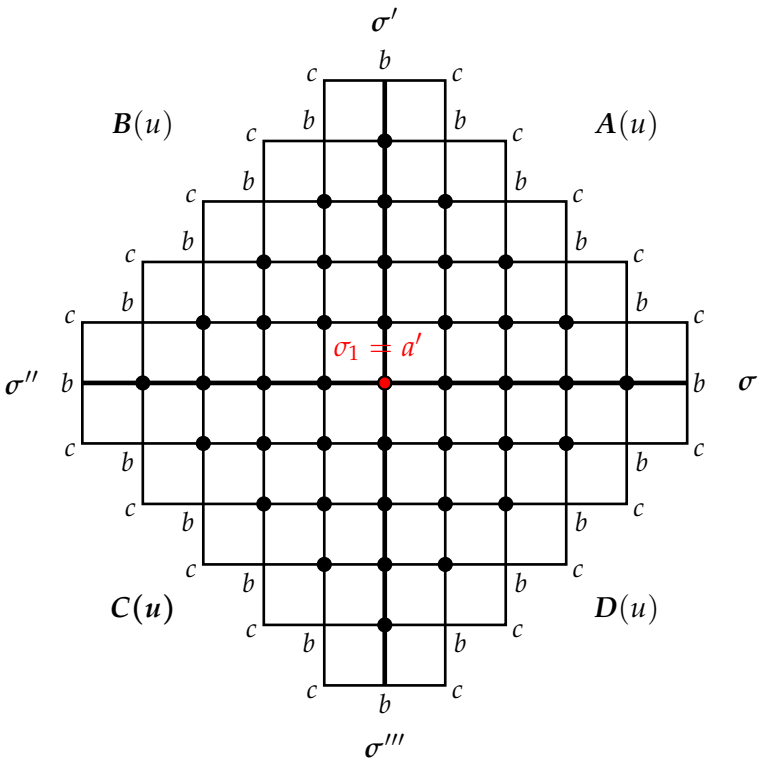

Figure 1.4: Corner transfer matrices $\boldsymbol{A}(u)$, $\boldsymbol{B}(u)$, $\boldsymbol{C}(u)$, $\boldsymbol{D}(u)$ build up each quadrant of the square lattice.

One finds that the local height probability in regime III can be rewritten as

$$P_{a'} = \frac{E(x^{a'}, x^{m'}) X_N(a', b, c; q)}{\sum_{1 \le a \le m'-1} E(x^a, x^{m'}) X_N(a, b, c; q)}, \qquad x = e^{-4\pi^2/(m'\epsilon)} \tag{1.1.76}$$

$$X_N(a', b, c; q) = q^{-E_0} \sum_{\sigma_2, \sigma_3 \ldots \sigma_{N-1}} q^{\sum_{j=1}^{N} jH(\sigma_{j-1}, \sigma_j, \sigma_{j+1})} = \sum_{\sigma} q^{E(\sigma) - E_0} \tag{1.1.77}$$

where $E(w, p)$ is related to the elliptic theta function as defined in appendix A.1. The new function X_N is the one-dimensional configurational sum. The sum is over the sequence of heights $\sigma = (\sigma_1, \sigma_2, \ldots, \sigma_N, \sigma_{N+1})$ of length N subject to the restriction that $|\sigma_j - \sigma_{j+1}| = 1$ with boundaries $\sigma_1 = a'$, $\sigma_N = b$ and $\sigma_{N+1} = c$.

We can interpret the one-dimensional sum as weighted sum of the energies $E(\sigma)$ associated to *the lattice path* σ which starts off at height a' and terminates at height c following height b as shown in figure 1.5. The energy $E_0 = \min_{\sigma} E(\sigma)$ is the energy of the groundstate path.

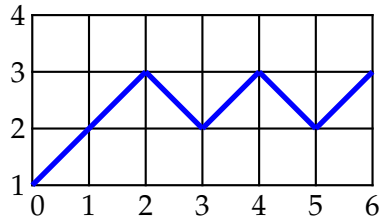

Figure 1.5: An example of lattice path $\sigma = \{1, 2, 3, 2, 3, 2, 3\}$ in model $(m, m') = (2, 5)$ with boundary conditions $(a, b, c) = (1, 2, 3)$ and $N = 5$ steps from $a = 1$ to $c = 3$.

The importance of the one-dimensional sum goes beyond its statistical interpretation as generating function for the lattice path configurations. In fact, it is well known that it generates the conformal characters of the associated CFT in the thermodynamic limit [57–60]. The one-dimensional sums have proven very helpful for studying characters in CFT, not only because they represent a finitized version of their conformal counterparts but also because the recurrence relations between one-dimensional sums are easier to handle mathematically than the equations of the conformal algebra.

1.1.9 Six-vertex model

The six-vertex model is an important lattice model of statistical mechanics in two dimensions. It is a vertex type model defined on a square lattice and the spin variables take the form of arrows placed on the bonds connecting neighbouring lattice points. The spins configurations are in agreement with the ice-rule [34], so at each lattice point (vertex) there are exactly two ingoing and two outgoing spins regardless of the order in which they are sorted. Only six types of vertices satisfy this condition as shown in the figure below

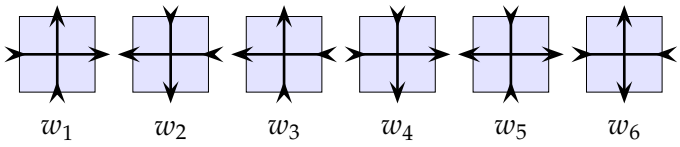

Figure 1.6: Allowed arrow configurations in the six-vertex model.

Each vertex is assigned a Boltzamnn weight w_i. In the symmetric case, these weights are invariant under simultaneous reversal of all arrows, that means $w_1 = w_2 = a$, $w_3 = w_4 = b$, $w_5 = w_6 = c$. We are interested, however, in a different case where the last two configurations in figure 1.6 cannot be identified under arrow reversal and therefore they are mapped to different weights, $w_5 = c_1$ and $w_6 = c_2$. The most general parametrization of the Boltzmann weights of the integrable six-vertex model is

$$a(u) = \rho \frac{\sin(\lambda - u)}{\sin \lambda}, \quad b(u) = \rho \frac{\sin u}{\sin \lambda}, \quad c_1(u) = \rho g, \quad c_2(u) = \frac{\rho}{g} \tag{1.1.78}$$

$$\Delta = (a^2 + b^2 - c_1 c_2)/(2ab) \tag{1.1.79}$$

where $\lambda \in (0, \pi)$ is the *crossing parameter*, g a gauge factor and $\rho \in \mathbb{R}$ a normalization constant. Under different choices of λ, g and ρ, the six-vertex model exhibits different behaviours, according to the value of the parameter Δ. In particular, when $\lambda = \frac{\pi}{2}$, which implies $\Delta = 0$, this is the *free-fermion* model and it is well known its relation to dimers and domino tilings [41, 61].

1.1.10 Dimers

The term "dimer" refers to a specific arrangement of units (often referred to as tiles) on a regular lattice whose peculiarity is that they can be decomposed into two elementary subunits. The classical example is on a square lattice where horizontal and vertical dimers are viewed as dominos (see figure 1.8). Originally the model was formulated to address a simple enumeration problem, the problem of counting the number of ways the sites of a finite regular lattice can be covered by tiles (dimers) such that two adjacent sites are covered by exactly one tile and no single site is left uncovered [62], as shown in figure 1.8. This is the also known as the close-packed limit and, if not otherwise stated, it is implicitly assumed to hold when we talk about dimers. There are also variations to this problem in which additional vacancies are taken into account [63–68] but it won't be covered in this thesis. As mentioned in section 1.1.9, dimers can be considered as a special case of the six-vertex model at the free fermion point. The mapping between vertex and dimer configurations is well known [61,69] and it is shown in Figure 1.7. It is clear that this mapping is not bijective since the vertex w_5 relates to two possible dimer arrangements. Moreover, dimers exhibit a 45° orientation, differently from the classical model where they can only have horizontal and vertical orientation.

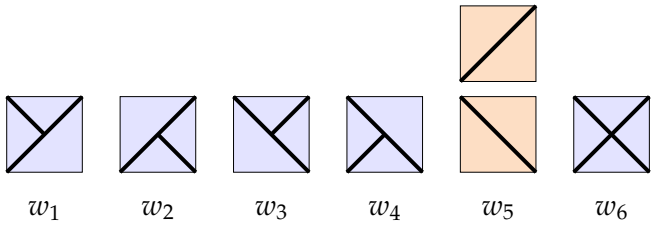

Figure 1.7: Mapping between vertex and dimer configurations

The problem of counting dimer configurations is equivalent to calculating the partition function of the free-fermion six-vertex model with the proper choice of Boltzmann weights (1.1.78). Indeed, thanks to a freedom of gauge, it is always possible to find the special gauge transformation that, given a suitable choice of the normalization constant and spectral parameter, sets the weights to one and two (only for the doubly degenerated configuration). Under these conditions, the partition function, which sums the Boltzmann

weights over all possible dimer configurations compatible with the boundary conditions, exactly counts the number of dimer tilings on a square lattice.

In the thermodynamic limit the dimer model exhibits interesting properties from the point of view of its critical behaviour. The relation between dimers and its conformal field theory limit will be discussed in section 1.2.4.

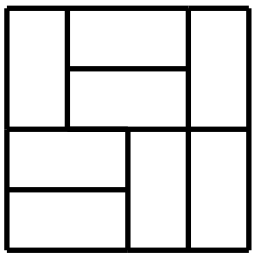

Figure 1.8: Domino tiling of a square lattice.

In tracing back the history of the dimer model, we find out that it was first introduced in the 1937 by Fowler and Rushbrook [70] as model for the adsorption of diatomic molecules on a two-dimensional substrate. Yet quickly it became a general problem studied in various scientific communities. The first important results regarding the statistical properties of dimers were obtained in the sixties. It was initially exactly solved in one dimension [71,72], then in two dimensions the solution on the square lattice with free boundary conditions was independently calculated by Kasteleyn 1961 [73] and Temperley and Fisher 1961 [74] using a combinatorial method involving Pfaffians. Kasteleyn also studied dimers with toroidal boundary conditions. Later in the sixties Lieb [75] reformulated and calculated the partition function of the dimer model using a particular transfer matrix method which doesn't involve Yang-Baxter integrability. Lieb's approach is based on a map from dimer configurations to spin configurations and thus sets the ground for a more recent application of this method linked to a particular spin chain representation of the Temperley-Lieb algebra [76]. Afterwards, almost no significant progress has been made to further explore the statistical properties of dimers, until the late 80's when the discover of high temperature superconductors promoted new interest in this topic. In fact, the new superconductive materials were described as a quantum hard-core dimer gas on a two-dimensional square lattice [77]. In the 1996 a paper by Cohn et al. [78] on the domino tilings of an Aztec

diamond raised a crucial issue about dimers: small changes in the boundary conditions can have a dramatic effect on the bulk free energy as it is evident from the behaviour of domino tilings of a typical planar region under such conditions. Since then, there have been great efforts to gain a better understanding of the finite-size effects of the boundary conditions under the influence of infinitely repulsive hard-core local interactions. Finally, in the last two decades the interest in the dimer model has moved towards its properties as critical system and the connection with conformal field theories in the continuum scaling limit [69,79–90].

1.2 Conformal Field Theories

Conformal field theories (CFTs) [91,92] are quantum field theories invariant under conformal transformations, i.e. coordinates transformations which preserve angles between vectors. Let's consider a generic manifold endowed with a flat metric $g_{\mu\nu}$, then, by definition, the coordinates transformation $x \to x'$ is conformal if it leaves the metric invariant up to a change of scale

$$g_{\mu\nu}(x) \to g'_{\mu\nu}(x') = \Omega(x) g_{\mu\nu}(x), \qquad \Omega(x) = |\partial x'/\partial x|^2 \tag{1.2.1}$$

CFTs play a major role in classical and quantum statistical mechanics since they are able to effectively describe second order phase transitions of critical phenomena. As we already mentioned in (1.1.3), critical lattice models in the continuum scaling limit show scale invariance. In fact, near the critical point the correlation length diverges, consequently correlations of all sizes are equally important and this also means that any change of scale doesn't affect the physics of the model. While in dimensions greater or equal to three conformal invariance is simply equivalent to ordinary scale invariance, two dimensions is a rather special case because there is an infinite family of analytic transformations which are conformal (they constitute the conformal algebra in two dimensions) but they only apply locally so they are not always globally defined. These transformations may look complicated in first instance and yet understanding their nature is crucial because sometimes it leads to the exact solution and ultimately a classification of possible two-dimensional crit-

ical phenomena. A subset of these local transformations are conformal analytic functions which are invertible and globally well defined in two dimensions. They form a group known as the *global conformal group* represented by

Poincaré group $\Omega(x) = 1$

dilatations $\Omega(x) = \lambda^{-2}$

special conformal transformations $\Omega(x) = (1 + 2b_\mu x^\mu + b^2 x^2)^2$

The next sections are devoted to a deeper analysis of two-dimensional CFTs and, in particular, the minimal and logarithmic theories will be studied in more details given their relevance to the topic of this thesis.

1.2.1 Two-dimensional CFTs

At the classical level, a field theory has conformal symmetry if its action is invariant under conformal transformations. Without entering in details of the quantization process, we start with the flat Euclidean time and space coordinates (x^1, x^2), then we construct a set of complex coordinates composed of the holomorphic $\zeta = x^1 + ix^2$ and anti-holomorphic $\bar{\zeta} = x^1 - ix^2$ part, where the spatial component is compactified on a cylinder, so $x^1 = x^1 + 2\pi$. These are the Euclidean analogs of the standard light-cone coordinates $x^1 \pm ix^2$ in the Minkowski space and describe the geometry of an infinite cylinder. Through the conformal map $f(\zeta) = exp(\zeta) = z^1 \pm z^2$ we finally study the theory on the complex z-plane. This procedure is particularly advantageous because it allows the use of well-known methods of complex analysis to compute conserved charges, operator expansions and other characteristic quantities of a quantum conformal field theory in the Euclidean regime.

Concerning local conformal transformations we are interested to define the algebra of their generators. We look for infinitesimal transformations which act on the coordinate components as $x^\nu \to x'^\nu = x^\nu + \varepsilon^\nu(x)$ and satisfy the conformal constraint in two dimensions

$$\bar{\partial}\varepsilon = \partial\bar{\varepsilon} = 0 \tag{1.2.2}$$

Here, ∂ and $\bar{\partial}$ denote partial derivatives with respect to z and $\bar{z}$ respectively. Consequentially, any holomorphic infinitesimal transformation in two dimensions may be expressed as

$$z' = z + \varepsilon(z), \qquad \varepsilon(z) = \sum_{n=-\infty}^{\infty} c_n z^{n+1} \tag{1.2.3}$$

where, by hypothesis, the infinitesimal mapping admits a Laurent expansion around $z = 0$. Similar expressions apply to the anti-holomorphic component.

A spinless dimensionless field $\phi(z, \bar{z})$ under such a transformation changes in the following way

$$\phi'(z', \bar{z}') = \phi(z, \bar{z}) = \phi(z', \bar{z}') - \varepsilon(z')\partial'\phi(z', \bar{z}') - \bar{\varepsilon}(\bar{z}')\bar{\partial}'\phi(z', \bar{z}') \tag{1.2.4}$$

where the first equality expresses the invariance of ϕ at any point under change of the coordinate system. Therefore, the infinitesimal change in the field is

$$\delta\phi = -\varepsilon(z')\partial'\phi(z', \bar{z}') - \bar{\varepsilon}(\bar{z}')\bar{\partial}'\phi(z', \bar{z}') = \sum_n [c_n \ell_n \phi(z, \bar{z}) + \bar{c}_n \bar{\ell}_n \phi(z, \bar{z})] \tag{1.2.5}$$

where the differential operators $\ell_n = -z^{n+1}\partial$, $\bar{\ell}_n = -\bar{z}^{n+1}\bar{\partial}$ generate a Lie algebra called the *conformal algebra*, defined by these commutation relations

$$\begin{aligned} [\ell_n, \ell_m] &= (n-m)\ell_{n+m} \\ [\bar{\ell}_n, \bar{\ell}_m] &= (n-m)\bar{\ell}_{n+m} \\ [\ell_n, \bar{\ell}_n] &= 0 \end{aligned} \tag{1.2.6}$$

with $n, m \in \mathbb{Z}$. This algebra is two commuting copies of the *Witt algebra*. Its generators are ℓ_{-1}, ℓ_0 and ℓ_1 (and their antiholomorphic counterparts). They correspond to translations (l_{-1} and $\bar{l}_{-1}$), dilatations ($l_0 + \bar{l}_0$), rotations (i($l_0 - \bar{l}_0$)) and special conformal transformations (l_1 and $\bar{l}_{-1}$).

The Witt algebra contains a subalgebra associated with the global conformal group, the group of transformations which are invertible and well defined everywhere on the

Riemann sphere (i.e., the complex plane plus the point at infinity). The conformal transformations in this group are mappings of this kind:

$$f(z) = \frac{az+b}{cz+d} \qquad \text{with } ad - cd = 1 \tag{1.2.7}$$

where a, b, c, and d are complex numbers. These are projective transformations and to each of them we can associate the matrix

$$A = \begin{pmatrix} a & b \\ c & d \end{pmatrix} \tag{1.2.8}$$

It is easily verified that the composition of two maps $f_1 \circ f_2$ corresponds to the matrix multiplication $A_2 A_1$. Therefore, the global conformal group in two dimensions is isomorphic to the group of complex invertible 2×2 matrices with unit determinant, $SL(2, \mathbb{C})$, which in turn is isomorphic to the Lorentz group in four dimensions $SO(3,1)$.

Quantum generators obey an algebra similar to the Witt algebra (1.2.6) defined just above, but differ from it by the presence of the central extension c

$$\begin{aligned} [L_n, L_m] &= (n-m)L_{n+m} + \frac{c}{12} n(n^2-1)\delta_{n+m,0} \\ [\bar{L}_n, \bar{L}_m] &= (n-m)\bar{L}_{n+m} + \frac{c}{12} n(n^2-1)\delta_{n+m,0} \\ [L_n, \bar{L}_n] &= [L_n, c] = [\bar{L}_n, c] = 0 \end{aligned} \tag{1.2.9}$$

with $n, m \in \mathbb{Z}$. These relations define the so called *Virasoro algebra*. The quantum operators $L_n, \bar{L}_n$ are the generators of the local conformal transformations on the Hilbert space, in the same way $\ell_n, \bar{\ell}_n$ are the generators of conformal mappings on the space of functions. The operator c commutes with all other Virasoro generators and hence it can be thought of as a constant known as the *central charge*. From the point of view of physics, the central charge turns out to be proportional to the Casimir energy, the change in the vacuum energy density that arises from the periodic boundary conditions on the cylinder. For example, $c = 1$ corresponds to the case of the free boson, $c = 1/2$ to the free fermion.

Because the holomorphic and anti-holomorphic part of this algebra are independent

and they satisfy the same relations, for simplicity of exposition, we will continue the discussion considering only the holomorphic sector, keeping in mind that same considerations apply to the anti-holomorphic counterpart.

In the quantization process dilations $(z, \bar{z}) \to \lambda(z, \bar{z})$ become time translations. Thus, the generator of these transformations, L_0, is proportional to the Hamiltonian of the system and the basis of eigenstates of this operator can be chosen as basis of states of the Hilbert space of the theory. An important remark here is that in the Hilbert space of conformal field theories the vacuum state $|0\rangle$ must be invariant under global conformal transformations. Hence, if the ground state energy is set to zero, $|0\rangle$ must be annihilated by L_{-1}, L_0 and L_1 and their anti-holomorphic counterparts.

$$L_n|0\rangle = 0, \qquad n > -1 \qquad \langle 0|L_n = 0, \qquad n < -1 \tag{1.2.10}$$

We are interested to construct an irreducible finite-dimensional representation of the Virasoro algebra. This task is addressed by first finding a universal representation with a given highest-weight and then quotient from it to obtain a representation with the desired properties. In the highest-weight representation of the Virasoro algebra, otherwise known as the *Verma module*, the dilatation operator L_0 is chosen to be diagonal. Also, an inner product is assumed to exist on the representation space such that $L_n^\dagger = L_{-n}$ and this condition implies that the dilatation operator is Hermitian with a real spectrum of eigenvalues. The highest-weight state $|\Delta\rangle$ is an eigenstate of L_0 with eigenvalue Δ

$$L_0|\Delta\rangle = \Delta|\Delta\rangle \tag{1.2.11}$$

From the commutation relation (1.2.9) it follows that

$$[L_0, L_n] = -nL_n, \qquad L_0(L_n|\Delta\rangle) = L_n(L_0|\Delta\rangle) - nL_n|\Delta\rangle = (\Delta - n)L_n|\Delta\rangle \tag{1.2.12}$$

This suggests that $L_{n>0}$ and $L_{n<0}$ can be viewed as lowering and raising operators respectively and, thanks to this fact, excited states are obtained by successive applications of the

last operators

$$|\Delta'\rangle = L_{-k_1} L_{-k_2} \dots L_{-k_n} |\Delta\rangle, \qquad 1 \leq k_1 \leq \dots \leq k_n \tag{1.2.13}$$

The resulting state, called descendant, is an eigenstate of the L_0 operator with eigenvalue

$$\Delta' = \Delta + k_1 + k_2 + \dots k_n = \Delta + N \tag{1.2.14}$$

By convention, the sequence of operators L_k appears with an increasing order of the k_j and a different ordering can always be converted into a linear combination of the well ordered states by applying the commutation rules. Through all possible combinations of raising operators applied to the highest weight state, we obtain a basis of states in this representation and the integer N is called the level of the descendant. The number of distinct, linearly independent states at level N is simply the number $\mathrm{p}(N)$ of partitions of the integer N. By Taylor expanding, it is easy to prove that the generating function of the partition numbers is

$$\sum_{n=0}^{\infty} p(n) q^n = \frac{1}{(q)_\infty}, \qquad (q)_\infty = \prod_{k=1}^{\infty} (1 - q^k) \tag{1.2.15}$$

Let $V_{c,\Delta}$ and $\overline{V}_{c,\bar{\Delta}}$ denote the Verma modules generated respectively by the holomorphic and anti-holomorphic Virasoro generators $\{L_n\}$ and $\{\bar{L}_n\}$ with central charge c and highest weights Δ and $\bar{\Delta}$. The full Hilbert space is a direct sum over all values of the highest weights of the tensor product of the holomorphic and anti-holomorphic Verma modules

$$\sum_{\Delta,\bar{\Delta}} V_{c,\Delta} \otimes V_{c,\bar{\Delta}} \tag{1.2.16}$$

The *character* $\chi_{c,\Delta}(q)$ of a Verma module $V_{c,\Delta}$ is the generating function for the number of linearly independent states at each level N, denoted by $\dim V_{c,\Delta}^{(N)}$, and is defined as follows

$$\chi_{c,\Delta}(q) = \mathrm{Tr}\, q^{L_0 - c/24} = \sum_{N=0}^{\infty} \dim V_{c,\Delta}^{(\Delta+N)}\, q^{\Delta+N-c/24} \tag{1.2.17}$$

This formula can be easily explained. Since the trace term $\mathrm{Tr}\, q^{L_0}$ corresponds to the sum of the eigenvalues of L_0 and the multiplicity of each eigenvalue is equal to the dimension of its corresponding eigenspace $V_{c,\Delta}^{(\lambda)}$, it follows that

$$\mathrm{Tr}\, q^{L_0} = \sum_{\lambda} \dim V_{c,\Delta}^{(\lambda)}\, q^{\lambda} \tag{1.2.18}$$

After making the substitution $\lambda = \Delta + N$ and multiplying by the constant factor $q^{-c/24}$ in (1.2.18), we retrieve the expression above (1.2.17) for the character of a generic Verma module $V_{c,\Delta}$. Noticing that the dimension of $V_{c,\Delta}^{(\lambda)}$ is precisely the partition number $p(N)$, we use the definition given in (1.2.15) and finally write the expression of a Virasoro character for a generic Verma module as

$$\chi_{c,\Delta}(q) = q^{-c/24+\Delta}\, \frac{1}{(q)_\infty} \tag{1.2.19}$$

1.2.2 Minimal models

The simplest CFTs are *rational* CFTs which admit a finite number of irreducible representations of the Virasoro Algebra which close under fusion. From the reducible Verma module it is possible to construct a rational CFT with irreducible representations whose spectrum consists of a finite number of conformal dimensions. These representations form the building blocks of the so called *minimal models* [93, 94]. A pair of coprime integers m, m', satisfying $2 \leq m < m'$, uniquely identifies each minimal model $\mathcal{M}(m, m')$ with central charge given by

$$c = c^{m,m'} = 1 - \frac{6(m-m')^2}{mm'}, \qquad 2 \leq m < m', \qquad \gcd(m, m') = 1 \tag{1.2.20}$$

All admissible conformal weights of the primary fields are derived from the Kac 's determinant formula [95]

$$\Delta_{r,s}^{m,m'} = \frac{(rm'-sm)^2 - (m-m')^2}{4mm'}, \quad 1 \leq r \leq m-1,\ 1 \leq s \leq m'-1 \tag{1.2.21}$$

and given this symmetry $\Delta^{m,m'}_{m-r,m'-s} = \Delta^{m,m'}_{r,s}$ there are $(m-1)(m'-1)/2$ distinct primary fields in the model. The corresponding Virasoro characters [96] are

$$\mathrm{ch}^{m,m'}_{r,s}(q) = \frac{q^{-c/24+\Delta^{m,m'}_{r,s}}}{(q)_\infty} \sum_{k=-\infty}^{\infty} \left[q^{k(kmm'+rm'-sm)} - q^{(km+r)(km'+s)}\right] \tag{1.2.22}$$

In this formula q is the modular nome and the above series is uniformly convergent since $|q| < 1$. Because we are working on the infinite plane the holomorphic and anti-holomorphic sectors can be treated independently. For clarity of exposition we decide to use only the holomorphic coordinates, q, knowing that same equations also apply identically to the anti-holomorphic counterpart, $\bar{q}$. The set of all possible conformal dimensions for each pair of quantum numbers (r,s), as it appears in (1.2.21), are systematically arranged in a two-dimensional table, called *Kac table*.

A representation of the Virasoro Algebra is called unitary if every non-zero vector has a positive norm. When $m = m' - 1$ in (1.2.20) and (1.2.21), we obtain the sequence of unitary highest weight representations of the Virasoro algebra with $0 < c < 1$. These models are of particular interest because they provide a complete set of possible two-dimensional critical behaviours which find realization in well-known models of statistical mechanics [92, 97]. The unitary condition in field theories is the statement that the probability is conserved and hence it can describe a quantum mechanical system. However, in statistical mechanics it shouldn't be interpreted as a physical condition. In fact, many examples of physical systems, such as the so called hard objects (i.e. bulky objects that cannot overlap and are subject to simple enough interactions) or polymers in two dimensions, have phases described by non-unitary minimal models. In the non-unitary representation, some negative conformal dimensions appear but the spectrum of eigenvalues is still real. The central charges and conformal dimensions of a non-unitary CFT are given by the previous formula (1.2.20) and (1.2.21) for $m' \neq m+1$, where, differently from the unitary case, negative values are also allowed.

Historical background

check it out The discovery of rational CFTs and their identification with known statis-

tical models mark an important breakthrough in understanding the principle of conformal invariance and its application to physics . In 1984 Belavin-Polyakov-Zamolodchikov (BPZ) [93] formulated the theory of minimal models, and at the same time Andrews-Forrester-Baxter (ABF) [50] introduced exactly solvable RSOS models on the square lattice that exhibit generic $\mathbb{Z}_2$ multicriticality. Remarkably, by analyzing the multicritical exponents, Huse [98] observed that in the continuum scaling limit, the critical RSOS models, in regime III and IV (respectively low-temperature and high-temperature regions), are precisely realized by the minimal models of BPZ, which are unitary theories. Nonunitary RSOS lattice models, although they lack of a clear probabilistic interpretation, are nevertheless associated with well-defined minimal models in the continuum scaling limit in the same regimes III and IV [99–101]. The consequences of conformal invariance of lattice models in unitary and non-unitary theories were studied in depth by Cardy [97, 102]. Itzykson, Saleur and Zuber [103] discussed the general application of conformal invariance to nonunitary two-dimensional models, and in particular they analyzed the case of the Lee-Yang edge singularity. It is essentially a non-unitary critical point and is associated with the critical behaviour of an Ising-type model, a ferromagnet in a purely imaginary non-zero magnetic field, above the critical temperature.

Riggs [104] pointed out that the finitized conformal characters of the nonunitary minimal models can be interpreted in terms of the *one-dimensional configurational sums* of the nonunitary RSOS models. Next, Foda and Welsh [105] explored this relation more in detail and provided a useful combinatorial interpretation of the fermionic expressions of these finitized characters. Interestingly, this interpretation can also be applied to describe patterns of zeros of the eigenvalues of the transfer matrix of the associated RSOS lattice models [106].

Through lattice fusion is it possible to construct a hierarchy of solid-on-solid lattice models [107, 108], in a similar way as higher spins representations can be generated in vertex lattice models [109]. When fusion is implemented on elementary RSOS models, it results in new Yang-Baxter integrable RSOS lattice models [110–112]. It was shown that fused RSOS models in the unitary case are identified in the thermodynamic limit with higher fusion level minimal models [112–117]. Tartaglia and Pearce [118] worked further

on the CFT classification of fused RSOS models in the non-unitary case and particularly they found an exact correspondence between models whose crossing parameter ranges in the interval $0 \geq \lambda \geq \pi/n$ (n level of fusion) and higher-level cosets theories of CFT. Recently, in a joint publication, Fehér et al. argue that in the complementary interval of the crossing parameter, for $n = 2$, the fused RSOS models converge to the elementary minimal models in the thermodynamic limit.

The Ising CFT

To complete the discussion around minimal theories we use an example, the simplest unitary minimal model, $\mathcal{M}(3,4)$, which describes the critical behaviour of the two-dimensional Ising ferromagnet model of statistical mechanics (1.1.2). Central charge and conformal dimensions are respectively

$$c = \frac{1}{2}, \qquad \Delta^{3,4}_{r,s} = \frac{(4r-3s)^2-1}{48}, \quad r = 1,2, \;\; s = 1,2,3 \tag{1.2.23}$$

As consequence of the Kac table symmetry $\Delta^{3,4}_{3-r,4-s} = \Delta^{3,4}_{r,s}$, the conformal dimensions can be collected in pairs

$$\Delta^{3,4}_{2,3} = \Delta^{3,4}_{1,1} = 0, \qquad \Delta^{3,4}_{2,2} = \Delta^{3,4}_{1,2} = \tfrac{1}{16}, \qquad \Delta^{3,4}_{2,1} = \Delta^{3,4}_{1,3} = \tfrac{1}{2} \tag{1.2.24}$$

The Kac table of $\mathcal{M}(3,4)$ is explicitly shown in table (1.2).

s		
3	$\frac{1}{2}$	0
2	$\frac{1}{16}$	$\frac{1}{16}$
1	0	$\frac{1}{2}$
	1	2 r

Table 1.2: Kac table for the Ising model $\mathcal{M}(3,4)$.

The critical behaviour of two-dimensional statistical models is defined in terms of a set

of critical exponents as explained in (1.1.3). In the case of the Ising model, this set includes the critical exponents η and ν which are associated, respectively, to the spatial correlation of spins, G, and the temperature dependence of the correlation length ξ

$$G(i-j) \sim |i-j|^{-\eta}, \qquad \xi \sim |T-T_c|^{-\nu}, \qquad t \to 0, \qquad |\boldsymbol{i}-\boldsymbol{j}| \gg 1 \tag{1.2.25}$$

The critical exponents of two-dimensional critical systems are related to the spectrum of their associated conformal field theory. Precisely, scaling dimensions are related to conformal dimensions through this relation

$$x = \Delta + \bar{\Delta} \tag{1.2.26}$$

where $\Delta = \bar{\Delta}$ for spinless operators. For the Ising model this becomes

$$x_t = \Delta_t + \bar{\Delta}_t = 1, \qquad x_h = \Delta_h + \bar{\Delta}_h = \tfrac{1}{8} \tag{1.2.27}$$

which agrees with the prediction of the RG theory (1.1.15). Here the conformal dimensions have been labelled in terms of temperature t and applied magnetic field h (as usual in the statistical mechanics description) and in the CFT operator formalism they correspond to the energy density ε and magnetisation σ respectively. In a complete CFT description, there is also a third operator, the identity I, which is always dimensionless. So, the set of conformal dimensions for the critical Ising model are explicitly

$$\Delta_I = 0, \qquad \Delta_\sigma = \tfrac{1}{16}, \qquad \Delta_\varepsilon = \tfrac{1}{2} \tag{1.2.28}$$

Operators, corresponding to the scaling fields, are realized in a boundary setting by applying the appropriate conjugate boundary conditions for the associated critical lattice model. In this particular example, the possible boundary configurations are all spins up (identity), all spins down (energy density), fixed spins or free boundary (magnetisation).

$$\Delta_I \leftrightarrow +, \qquad \Delta_\sigma \leftrightarrow \text{ free }, \qquad \Delta_\varepsilon \leftrightarrow - \tag{1.2.29}$$

1.2.3 Logarithmic minimal models

Minimal models describe the critical behaviour of lattice models with local degrees of freedom, such as the Ising, 3-state Potts and ABF RSOS models, whose Boltzmann weights are locally defined and are not subject to global constraints. In contrast, there are models of statistical mechanics with non-local degrees of freedom. This is the case of polymers (dense or dilute) which are made of connected subunits and percolation with the formation of long-range connectivities. In the continuum scaling limit at criticality they are associated with logarithmic CFTs (LCFTs).

The Virasoro minimal models described in the previous section (1.2.2) are rational CFTs meaning that they admit a finite number of irreducible representations. An irreducible representation cannot be the direct sum of any two non-zero subrepresentations. Any irreducible representation is also indecomposable.

Logarithmic theories form another class of CFTs characterized by some reducible yet indecomposable representations. The distinction between rational and logarithmic CFTs is made clear by looking at certain matrix representations of the dilatation Virasoro generator L_0. If the matrix can be diagonalized, the representation is the direct sum of irreducible subrepresentations. If not, it has reducible but indecomposable subrepresentations. This latter one entails the appearance of non trivial Jordan cells.

A rational CFT [93] is fully characterised by its *conformal data* which means conformal dimensions, scaling dimensions, central charge and operator product expansion coefficients (three-point correlators) of the primary operators. The same does not apply to the LCFT. In fact, it can be the case that two distinct LCFTs share the same conformal data but they exhibit different Jordan cell structure.

The simplest and most studied LCFTs are the logarithmic minimal models [119–125] $\mathcal{LM}(p, p')$, also known as *logarithmic minimal CFTs*. The first few members of the principal series $\mathcal{LM}(p, p+1)$ are critical dense polymers (p=1), critical percolation (p=2), Logarithmic Ising model (p=3). The conformal data of the logarithmic minimal CFTs is related to the one of rational minimal models. The relationship between them can be understood in

terms of the *logarithmic limit* [122] which is symbolically expressed by

$$\lim_{m,m'\to\infty,\ \frac{m'}{m}\to\frac{p'}{p}+} \mathcal{M}(m,m') = \mathcal{LM}(p,p'), \qquad 1 \leq p < p', \quad gcd(p,p') = 1 \tag{1.2.30}$$

where the one-sided limit is taken through coprime pairs (m, m') with $2 \leq m < m'$ and $\frac{m'}{m} > \frac{p'}{p}$ to ensure the correct limiting ground states. The equality indicates that taking the limit of the conformal data for the rational minimal models $\mathcal{M}(m, m')$ yields the conformal data of the logarithmic minimal models $\mathcal{LM}(p, p')$. The logarithmic limit is taken in the continuum scaling limit, after the thermodynamic limit 1.1.5. The resulting CFT is not rational nor unitary and the conformal data are explicitly given by

$$c^{p,p'} = 1 - \frac{6(p'-p)^2}{pp'}, \qquad 1 \leq p < p', \quad gcd(p,p') = 1 \tag{1.2.31}$$

$$\Delta^{p,p'}_{r,s} = \frac{(rp'-sp)^2-(p'-p)^2}{4pp'}, \qquad r,s = 1,2,\ldots \tag{1.2.32}$$

For each value of the central charge, the set of conformal dimensions of logarithmic minimal models yields an infinitely extended Kac table. Similarly, the logarithmic limit for the conformal characters yields

$$\chi^{p,p'}_{r,s}(q) = q^{-\frac{c}{24}+\Delta^{p,p'}_{r,s}} \frac{(1-q^{rs})}{(q)_\infty} \tag{1.2.33}$$

Through the continuum scaling limit of well-defined integrable lattice models, the so called *logarithmic lattice minimal models* [123], we can study the properties of logarithmic minimal CFTs.

Hamiltonian limit

In the context of lattice models, the transfer matrix commute with the integrals of motions of the theory and particularly with the Hamiltonian. In fact, the Hamiltonian ($\mathcal{H}$), which is proportional to the Virasoro operator L_0, is the first order term in the Taylor expansion of the single row transfer matrix about the spectral parameter. The Hamiltonian limit is

defined, up to a factor $\alpha > 0$, as

$$\boldsymbol{T}(u) = \boldsymbol{I} - \alpha u \mathcal{H} + \mathcal{O}(u^2) \tag{1.2.34}$$

where $T(u)$ is the normalized single row transfer matrix. If we choose the eigenstates of L_0 as basis of the Hilbert space of states of a LCFT, from (1.2.34) it is clear that the Jordan block structure of L_0 is then reflected into the transfer matrix.

1.2.4 The dimer CFT

It is widely accepted that the close-packed dimer model on the square lattice is conformally invariant [65, 81–83, 126]. From the point of view of statistical mechanics, dimers are classically studied in the framework of free fermion models. However, differently from the statistics of free fermions, the lattice structure and boundary conditions strongly influences the dimers free energy, and not only the geometry, also the parity of the dimensions of the lattice grid has non negligible effect. This fact has been known for a long time [127]. In the last two decades, universality, scaling, finite-size corrections to the free energy of critical systems have been dominating the research area of integrable lattice models. In this context, the interest for the dimer model has shifted towards a major question: the central charge of dimers as conformal field theory. This question has opened a crucial debate that nowdays is still on. Briefly, the discussion moves around two alternatives, $c = -2$, logarithmic CFT, and $c = 1$, Gaussian free field theory. Arguments based on the equivalence with spanning trees (rectangular geometry or cylinder) support the $c = -2$ theory [83, 88, 128]. On the other side, the ones that uses the height function to define dimers configurations claim the consistency of the the $c = 1$ description [80, 89, 129]. Due to the appearance of the Temperly-Lieb algebra with zero loop fugacity in the formulation of the transfer matrix of dimers on the square lattice [76], it has been observed a connection with critical dense polymers, which is a logarithmic field theory [130], and this reinforces the logarithmic interpretation. The strong argument in favour of the second alternative is the proof that the fluctuations of the height functions are precisely described in the scaling limit by a massless free scalar field which is consistent with $c = 1$. Studies about the correlation functions in

the dimer model support the dual interpretation [131]. Using the Lieb's transfer matrix approach, Morin-Duchesne and others [87], present further evidence in favour of the $c = -2$ description of the close-packed planar dimer model. Their conclusion is not definitive yet, since it doesn't exclude that a transfer matrix built upon different degrees of freedom may bring to a conformal description consistent with $c = 1$. More recently, Izmailian [90] published a work where finite-size corrections to the critical free energy and boundary effects have been analyzed for the dimer model on a square lattice under free, periodical, toroidal, Möbius and Klein bottle boundary conditions. In this paper they compute the exact asymptotic expansion of the free energy and they found that there is a dependance on the type of boundaries as well as the parity of the number of lattice sites along the lattice axes: such peculiar behaviour can be fully understood in the framework of the $c = -2$ universality class. In our paper about dimers with periodic boundary conditions [132], we provide further proof that dimers can be classified unambiguously as a logarithmic CFT with central charge $c = -2$.

Chapter 2

One-Dimensional Sums and Finitized Characters of 2×2 Fused RSOS Models

The nonunitary $n \times n$ fused Forrester-Baxter RSOS(m, m') models are described, in the continuum scaling limit, by the minimal models $\mathcal{M}(M, M', n)$ constructed as the higher-level conformal cosets $(A_1^{(1)})_k \otimes (A_1^{(1)})_n / (A_1^{(1)})_{k+n}$ at integer fusion level $n \geq 1$ and fractional level $k = nM/(M'-M) - 2$ with $(M, M') = \big(nm - (n-1)m', m'\big)$. These results rely on Yang-Baxter integrability and are valid in Regime III for models determined by the crossing parameter $\lambda = (m'-m)\pi/m'$ in the interval $0 < \lambda < \pi/n$. Combinatorially, Baxter's one-dimensional sums generate the finitized branching functions as weighted walks on the $A_{m'-1}$ Dynkin diagram. The ground state walks terminate within shaded n-bands, consisting of n contiguous shaded 1-bands. The shaded 1-bands occur between heights $(\rho, \rho+1)$ where $\rho = \rho(r) = \left\lfloor \frac{rm'}{m} \right\rfloor$, $r = 1, 2, \ldots, m-1$. These results do not extend to the interval $\pi/n < \lambda < \pi$ since, for these models, there are no shaded n bands to support the ground states. Here we consider the 2×2 RSOS(m, m') models in the interval $\frac{\pi}{2} < \lambda < \pi$ and investigate the associated one-dimensional sums. In this interval, we verify that the one-dimensional sums produce new finitized Virasoro characters $\mathrm{ch}_{r,s}^{(N)}(q)$ of the minimal models $\mathcal{M}(m, m', 1)$ with $m' > 2m$. We further conjecture finitized bosonic forms and check that these agree with the ground state one-dimensional sums out to system sizes $N = 12$. The 2×2 RSOS(m, m') models thus realize new Yang-Baxter integrable models in the universality classes of the minimal models $\mathcal{M}(m, m', 1)$. For the series $\mathcal{M}(m, 2m+1, 1)$ with $m \geq 2$, the spin-1 one-dimensional sums were previously analysed by Jacob and Mathieu without the underlying Yang-Baxter structure. Finitized Kac characters $\chi_{r,s}^{m,m';(N)}(q)$ for the logarithmic minimal models $\mathcal{LM}(p, p', 1)$ are also obtained for $p' \geq 2p$ by taking the logarithmic limit *$m, m' \to \infty$ with $m'/m \to p'/p+$.*

2.1 Introduction

The RSOS(m,m') lattice models [50, 54] are Yang-Baxter integrable [31] both at criticality and off-criticality. In the continuum scaling limit, the off-critical RSOS(m,m') lattice models realize the integrable $\varphi_{1,3}$ thermally perturbed minimal models of Zamolodchikov [133–135]. Further Yang-Baxter integrable models, denoted by RSOS$(m,m')_{n\times n}$, are constructed by using fusion [109] to build face weights from $n \times n$ blocks of elementary face weights of the RSOS(m,m') lattice models. On the CFT side, the related minimal models $\mathcal{M}(M,M',n)$ are constructed [136] as the higher-level Goddard-Kent-Olive (GKO) cosets

$$\text{COSET}(k,n): \quad \frac{(A_1^{(1)})_k \oplus (A_1^{(1)})_n}{(A_1^{(1)})_{k+n}}, \qquad k=\frac{nM}{M'-M}-2, \qquad \gcd\Big(\frac{M'-M}{n},M'\Big) \tag{2.1.1}$$

where $n = 1,2,3,\ldots$ is an integer fusion level and k is a fractional fusion level. The central charges of these coset CFTs are given by

$$c = c_k + c_n - c_{k+n} = \frac{3kn(k+n+4)}{(k+2)(n+2)(k+n+2)}, \qquad c_k = \frac{3k}{k+2} \tag{2.1.2}$$

where c_k is the central charge of the affine current algebra $(A_1^{(1)})_k$ and $\mathcal{M}(m,m',1) \equiv \mathcal{M}(m,m')$. Recently, it was argued [118] that the minimal cosets $\mathcal{M}(M,M',n)$ are given by the continuum scaling limit of the RSOS$(m,m')_{n\times n}$ lattice models with

$$(M,M') = (nm-(n-1)m',m'), \qquad nm > (n-1)\,m' \tag{2.1.3}$$

The extended family of RSOS lattice models and their related minimal CFTs, particularly the unitary theories $(M,M') = (m'-n,m')$, have been extensively studied and form a cornerstone of our understanding of statistical mechanics and its interrelation with conformal and quantum field theory.

Continuing the investigation initiated in [118] we address the question of what can happen if $nm < (n-1)\,m'$. In these cases, it was argued in [118] that the structure of the RSOS lattice models lacks the required "shaded n-bands" needed to support the ground states of the level-n coset CFTs. The expectation is that the continuum scaling limit of

these RSOS theories therefore defaults to a level-n' coset CFT with $n' < n$. Here we use the one-dimensional sums [31, 55, 56] associated with Baxter's off-critical Corner Transfer Matrices (CTMs) to argue that, at least for $n = 2$ and $m' > 2m$, the continuum scaling limit of the RSOS$(m, m')_{2\times 2}$ lattice models is given by the level $n' = 1$ coset CFTs $\mathcal{M}(m, m')$. Essentially, our arguments are based on *Physical Combinatorics* [59, 60, 105, 137–146].

The layout of this chapter is as follows. In Section 2.2.1, we introduce the RSOS(m, m') lattice models of Forrester and Baxter. From the known elliptic face weights for the $n \times n$ fused models for $n = 1, 2, 3$ we extract the local energies with a suitable choice of gauge. We also set up Baxter's one-dimensional sums and discuss the ground states for $n = 2$ and $m' > 2m$. In Section 2.3, we consider the sequence $m' = 2m + 1$ with $n = 2$. For these cases, we show that the one-dimensional sums agree with those of Jacob and Mathieu [139] based on half-integer RSOS paths. The simplest models in this sequence, namely RSOS$(2, 5)$ and RSOS$(3, 7)$, are analyzed. The conformal data of the nonunitary minimal models $\mathcal{M}(m, m')$ is presented in Section 2.4. In particular, for $m' > 2m$, we conjecture bosonic forms for the RSOS$(m, m')_{2\times 2}$ finitized characters. For modest system sizes N, these agree with the one-dimensional sums and give the standard Virasoro characters of nonunitary minimal model $\mathcal{M}(m, m')$ in the limit $N \to \infty$. Taking the logarithmic limit leads to conjectured bosonic forms for the the finitized characters for the logarithmic minimal models $\mathcal{LM}(p, p')_{2\times 2}$ with $p' \geq 2p$. We finish with some concluding remarks. We finish with some conjectures for the case of $n > 2$.

2.2 Forrester-Baxter RSOS(m, m') Models

2.2.1 RSOS(m, m') lattice models

The RSOS(m, m') lattice model is a Restricted Solid-On-Solid (RSOS) model [50, 54] defined on a square lattice with heights $a = 1, 2, \ldots, m' - 1$ restricted so that nearest neighbour heights differ by ± 1. The heights thus live on the $A_{m'-1}$ Dynkin diagram. The nonzero Boltzmann face weights are

$$W\left(\begin{matrix} a\pm 1 & a \\ a & a\mp 1 \end{matrix}\middle| u\right) = \quad = s(\lambda - u) \tag{2.2.1a}$$

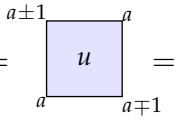

$$W\left(\begin{matrix} a & a\pm 1 \\ a\mp 1 & a \end{matrix}\middle| u\right) = \quad = -\frac{g_{a\pm 1}}{g_{a\mp 1}} \frac{s((a\pm 1)\lambda)}{s(a\lambda)} s(u) \tag{2.2.1b}$$

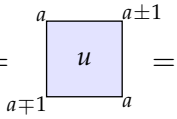

$$W\left(\begin{matrix} a & a\pm 1 \\ a\pm 1 & a \end{matrix}\middle| u\right) = \quad = \frac{s(a\lambda \pm u)}{s(a\lambda)} \tag{2.2.1c}$$

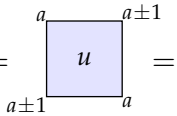

where $s(u) = \vartheta_1(u,t)/\vartheta_1(\lambda,t)$ is a quotient of the standard elliptic theta functions [147]

$$\vartheta_1(u,t) = 2t^{1/4}\sin u \prod_{n=1}^{\infty}(1-2t^{2n}\cos 2u + t^{4n})(1-t^{2n}), \qquad 0<u<\lambda, \quad 0<t<1 \tag{2.2.2}$$

u is the spectral parameter and g_a are arbitrary gauge factors. Unless stated otherwise, we work in the gauge $g_a = 1$. The elliptic nome $t = e^{-\varepsilon}$ is a temperature-like variable, with t^2 measuring the departure from criticality corresponding to the $\varphi_{1,3}$ integrable perturbation [133–135]. The crossing parameter is

$$\lambda = \frac{(m'-m)\pi}{m'}, \qquad 2 \le m < m', \qquad m, m' \text{ coprime} \tag{2.2.3}$$

The relevant properties of the elliptic functions are given in Appendix A.1. The restrictions on u and t mean that we are working in Regime III of [50, 54].

It was shown in [50, 54] that the off-critical face weights (2.2.1) satisfy the Yang-Baxter equations. The RSOS(m,m') lattice models are therefore exactly solvable. At the critical point $t = 0$, the Boltzmann face weights reduce to trigonometric functions. The algebraic structure of the solution to the Yang-Baxter equation for the critical RSOS$(m,m')_{2\times 2}$ models is discussed in Appendix A.2.

2.2.2 RSOS$(m, m')_{2\times 2}$ face weights

The normalized 2×2 fused RSOS are

$$W^{2,2}\left(\begin{matrix} d & c \\ a & b \end{matrix}\middle| u\right) = \frac{1}{\eta^{2,2}(u)}$$

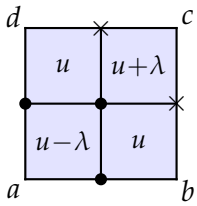

$$\eta^{2,2}(u) = s(2\lambda)s(u)s(u-\lambda) \tag{2.2.4}$$

The black dots indicate sums over all allowed heights at the site. The crosses indicate that the weight is independent of the allowed heights on these sites. The fused weights all have a common factor $\eta^{2,2}(u)$ which is removed so that the normalized weights are entire functions of u.

The explicit formulas for the 19 normalised weights are

$$W^{2,2}\left(\begin{matrix} a\pm 2 & a \\ a & a\mp 2 \end{matrix}\middle| u\right) = \frac{s(\lambda-u)s(2\lambda-u)}{s(2\lambda)} \tag{2.2.5a}$$

$$W^{2,2}\left(\begin{matrix} a & a \\ a & a\pm 2 \end{matrix}\middle| u\right) = W^{2,2}\left(\begin{matrix} a\pm 2 & a \\ a & a \end{matrix}\middle| u\right) = \frac{s(\lambda-u)s((a\pm 1)\lambda\mp u)}{s((a\pm 1)\lambda)} \tag{2.2.5b}$$

$$W^{2,2}\left(\begin{matrix} a & a \\ a\pm 2 & a \end{matrix}\middle| u\right) = -\frac{s((a\mp 1)\lambda)s(u)s(a\lambda\pm u)}{s(2\lambda)s(a\lambda)s((a\pm 1)\lambda)} \tag{2.2.5c}$$

$$W^{2,2}\left(\begin{matrix} a & a\pm 2 \\ a & a \end{matrix}\middle| u\right) = -\frac{s(2\lambda)s((a\pm 2)\lambda)s(u)s(a\lambda\pm u)}{s((a-1)\lambda)s((a+1)\lambda)} \tag{2.2.5d}$$

$$W^{2,2}\left(\begin{matrix} a & a\mp 2 \\ a\pm 2 & a \end{matrix}\middle| u\right) = \frac{s((a\mp 2)\lambda)s((a\mp 1)\lambda)s(u)s(\lambda+u)}{s(2\lambda)s(a\lambda)s((a\pm 1)\lambda)} \tag{2.2.5e}$$

$$W^{2,2}\left(\begin{matrix} a & a\pm 2 \\ a\pm 2 & a \end{matrix}\middle| u\right) = \frac{s(a\lambda\pm u)s((a\pm 1)\lambda\pm u)}{s(a\lambda)s((a\pm 1)\lambda)} \tag{2.2.5f}$$

$$W^{2,2}\left(\begin{matrix} a & a\pm 2 \\ a & a\pm 2 \end{matrix}\middle| u\right) = W^{2,2}\left(\begin{matrix} a\pm 2 & a\pm 2 \\ a & a \end{matrix}\middle| u\right) = \frac{s((a\pm 3)\lambda)s(u)s(u-\lambda)}{s(2\lambda)s((a\pm 1)\lambda)} \tag{2.2.5g}$$

$$W^{2,2}\left(\begin{matrix} a & a \\ a & a \end{matrix}\middle| u\right) = \frac{s(a\lambda\pm u)s((a\pm 1)\lambda\mp u)}{s(a\lambda)s((a\pm 1)\lambda)} + \frac{s((a\pm 1)\lambda)s((a\mp 2)\lambda)s(u)s(u-\lambda)}{s(2\lambda)s(a\lambda)s((a\mp 1)\lambda)} \tag{2.2.5h}$$

In contrast to the other equations, in the last equation, the choice of upper or lower signs gives two equivalent expressions for the same weight.

2.2.3 RSOS$(m, m')_{2\times 2}$ paths and shaded bands

A 2×2 fused RSOS lattice path $\sigma = \{\sigma_0, \sigma_1, \ldots, \sigma_N, \sigma_{N+1}\}$ is defined as a sequence of integer heights $\sigma_j \in A_{m'-1}$, $j = 0, 1, \ldots, N+1$ which satisfy the same adjacency rules as neighbouring heights on the corners of the 2×2 fused face weights. Explicitly, these adjacency conditions are

$$\sigma_{j+1} - \sigma_j = 0, \pm 2, \qquad \sigma_{j+1} + \sigma_j = 4, 6, \ldots, 2m' - 4, \qquad j = 0, 1, 2, \ldots, N \tag{2.2.6}$$

The boundary conditions are fixed by

$$(\sigma_0, \sigma_N, \sigma_{N+1}) = (s, \rho, \rho'), \qquad \rho' - \rho = 0, \pm 2 \tag{2.2.7}$$

The 2×2 fused RSOS lattice paths are used to define Baxter's one-dimensional configurational sum in Section 2.2.5.

The 2×2 fused RSOS lattice paths on a square lattice are interpreted as (N+1)-step walks that start at height s and then take N steps, respecting the 2×2 adjacency condition, until height ρ is reached. The last step is from height ρ to height ρ'. Each step consists of staying at the same height or moving up or down by 2 in height. Since the heights always change by an even number, paths have a definite parity — the heights are either all odd or all even. An example of such a path, represented as a walk on the $A_{m'-1}$ diagram, is given in Figure 2.1. In this figure some bands are shaded as we now explain.

Let us define the sequence

$$\rho = \rho(r) = \left\lfloor \tfrac{rm'}{m} \right\rfloor, \qquad r = 1, 2, 3, \ldots, m-1 \tag{2.2.8}$$

Following [105], we shade the bands in walk diagrams (such as Figure 2.1) between the heights $\rho(r)$ and $\rho(r)+1$ for $r = 1, 2, \ldots, m-1$. The shaded and unshaded bands interchange under the duality $m \leftrightarrow m'$. An *n-band* consists of n contiguous bands, which can be all shaded, all unshaded or mixed. An n-band is called a shaded n-band if all its 1-bands are shaded. An n-band is called an unshaded n-band if all its 1-bands are unshaded. In

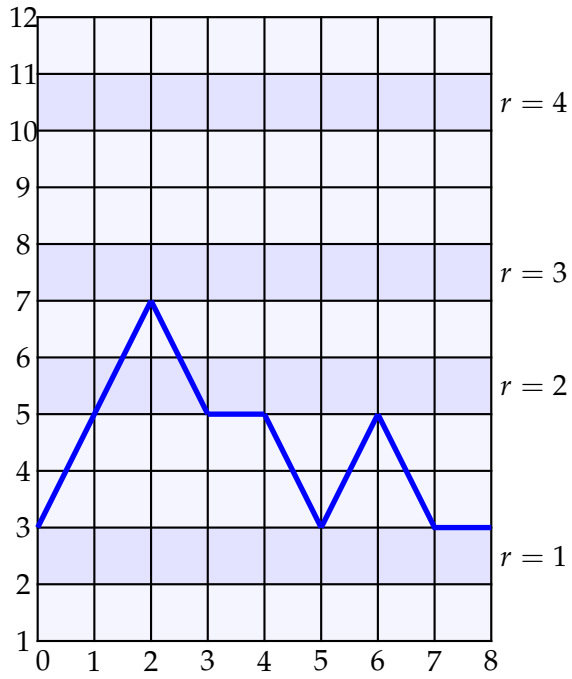

Figure 2.1: An example path $\sigma = \{3,5,7,5,5,3,5,3,3\}$ in model $(m, m') = (5,13)$ with boundary conditions $(s, \rho, \rho') = (3,3,3)$ and $N = 7$ steps from $s = 3$ to $\rho = 3$. The shaded 1-bands are labelled by $r = 1, 2, 3, \ldots$ from the bottom.

[118] it is shown that, for $0 < \lambda < \frac{\pi}{n}$, the number of shaded n-bands is

$$\#\text{shaded } n\text{-bands} := M - 1 = \begin{cases} nm - (n-1)m' - 1, & 0 < \lambda < \frac{\pi}{n} \\ 0, & \frac{\pi}{n} < \lambda < \pi \end{cases} \tag{2.2.9}$$

For $\frac{\pi}{n} < \lambda < \pi$ there are no shaded n-bands. In the unitary cases, with $\lambda = \frac{\pi}{m'}$ and $m = m' - 1$, all of the 1-bands are shaded. For nonunitary cases, with $2 \leq m < m' - 1$, there are both shaded and unshaded bands.

For the case of $\frac{\pi}{2} < \lambda < \pi$ of primary interest here, we note that there are only shaded 1-bands and no shaded n-bands for $n > 1$. The shaded 1-bands are separated by contiguous unshaded 1-bands as in Figure 2.1. We also note that s and ρ have the same parity. For later use, it is convenient to consider the union of the two sequences $\rho(r)$ and $\rho(r) + 1$ and to separate these into the union of two new sequences $\rho_0(r)$ and $\rho_1(r)$ consisting of the even and the odd members respectively. For the example in Figure 2.1, the two new sequences

are

$$\rho_0(r) = 2, 6, 8, 10, \qquad \rho_1(r) = 3, 5, 7, 11, \qquad r = 1, 2, 3, 4 \tag{2.2.10}$$

It follows that, if we wish to end a 2×2 fused RSOS lattice path on the edge of a shaded 1-band, we must have

$$\rho = \rho' = \rho_\mu(r), \qquad \mu = s \bmod 2 \tag{2.2.11}$$

for some $r = 1, 2, \ldots, m-1$.

2.2.4 Local energy functions

The local energy functions $H(d, a, b)$ are extracted from the low temperature limit $t = e^{-\varepsilon} \to 1$ of the Boltzmann weights (2.2.5) in a suitable normalization. Explicitly, with gauge factors g_a,

$$W^{n,n}\left(\begin{matrix} d & c \\ a & b \end{matrix}\middle| u\right) \sim \frac{g_a g_c}{g_b g_d} w^{H(d,a,b)} \delta_{a,c}, \qquad w = e^{-2\pi u/\varepsilon}, \quad \varepsilon \to 0, \quad u \to 0, \quad \tfrac{u}{\varepsilon} \text{ fixed} \tag{2.2.12}$$

In the following subsections, we consider the cases $n = 1, 2, 3$ separately. In each case, the local energies possess the reflection and height reversal symmetries

$$H(d, a, b) = H(b, a, d) = H(m'-d, m'-a, m'-b) \tag{2.2.13}$$

These are inherited from the properties of the Boltzmann face weights.

1×1 local energies

Working in the gauge $g_a = 1$ for $n = 1$, the local energy functions obtained by Forrester-Baxter [54] are

$$H^{\mathrm{FB}}(a, a \mp 1, a) = \pm \left\lfloor \tfrac{a\lambda}{\pi} \right\rfloor \tag{2.2.14a}$$

$$H^{\mathrm{FB}}(a \pm 1, a, a \mp 1) = \tfrac{1}{2} \tag{2.2.14b}$$

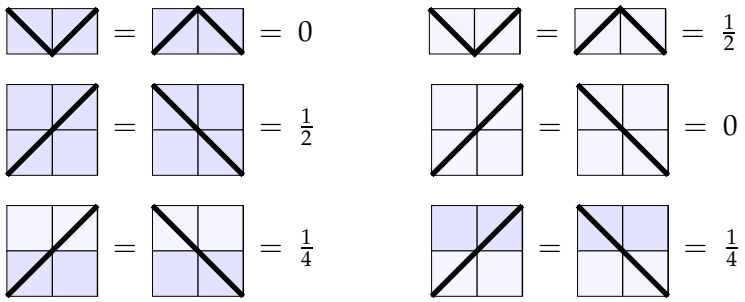

Figure 2.2: The gauged local energies of the 1×1 RSOS models in the interval $0 < \lambda < \pi$. In this gauge, the local energies take the values $0, \frac{1}{4}, \frac{1}{2}$.

Changing to a more suitable gauge [118], the local energies for the 1×1 models are given by

$$H(a+1, a, a+1) = \tfrac{1}{2}(h_{a+1} - h_a) \tag{2.2.15a}$$

$$H(a-1, a, a-1) = \tfrac{1}{2}(h_a - h_{a-1}) \tag{2.2.15b}$$

$$H(a \pm 1, a, a \mp 1) = \tfrac{1}{2} - \tfrac{1}{4}(h_{a+1} - h_{a-1}) \tag{2.2.15c}$$

These are all positive with values $0, \frac{1}{4}, \frac{1}{2}$ as shown in Figure 2.2. The sequences

$$h_a = \lfloor \frac{a(m'-m)}{m'} \rfloor = \lfloor \frac{a\lambda}{\pi} \rfloor \tag{2.2.16}$$

count the number of unshaded 1-bands below the height a. The value of h_a remains unchanged within any shaded n-band. Observing the duality

$$m \leftrightarrow m'-m, \qquad \lambda \leftrightarrow \pi-\lambda, \qquad \text{shaded 1-bands} \leftrightarrow \text{unshaded 1-bands}, \qquad h_a \leftrightarrow a-1-h_a \tag{2.2.17}$$

it follows that the $n = 1$ local energies satisfy

$$H^{m,m',1}(a, b, c) = \tfrac{1}{2} - H^{m'-m,m',1}(a, b, c) \tag{2.2.18}$$

2×2 **local energies**

To obtain the low temperature limit of the 2×2 fuesd RSOS face weights, it is convenient to first perform a *conjugate modulus transformation*

$$\vartheta_1(u, e^{-\varepsilon}) = ie^{-\varepsilon/4}e^{-iu}E(e^{2iu}, e^{-2\varepsilon}) = \sqrt{\frac{\pi}{\varepsilon}}\, e^{-(u-\pi/2)^2/\varepsilon}E(e^{-2\pi u/\varepsilon}, e^{-2\pi^2/\varepsilon}) \tag{2.2.19}$$

from nome $t = e^{-\varepsilon}$ to the conjugate nome $p = e^{-\pi^2/\varepsilon}$ where

$$E(w) = E(w,p) = \sum_{k=-\infty}^{\infty}(-1)^n p^{n(n-1)/2}w^n = \prod_{n=1}^{\infty}(1-p^{n-1}w)(1-p^n w^{-1})(1-p^n) \tag{2.2.20}$$

We introduce the variable $x = e^{-2\pi\lambda/\varepsilon} = p^{\lambda/\pi}$ so that $p = e^{-2\pi^2/\varepsilon} = x^{\pi/\lambda}$. The diagonal fused weights then become

$$W^{2,2}\left(\begin{smallmatrix} a\pm 2 & a \\ a & a\mp 2\end{smallmatrix}\right) = \frac{g_a^2}{g_{a-2}g_{a+2}}\,\frac{wE(x^2w^{-1})E(w^{-1}x)}{E(x^2)E(x)} \tag{2.2.21a}$$

$$W^{2,2}\left(\begin{smallmatrix} a & a \\ a & a\pm 2\end{smallmatrix}\right) = W^{2,2}\left(\begin{smallmatrix} a\pm 2 & a \\ a & a\end{smallmatrix}\right) = \frac{g_a}{g_{a\pm 2}}\,\frac{E(xw^{-1})E(x^{a\pm 1}w^{\mp 1})}{E(x)E(x^{a\pm 1})} \tag{2.2.21b}$$

$$W^{2,2}\left(\begin{smallmatrix} a & a\pm 2 \\ a\pm 2 & a\end{smallmatrix}\right) = \frac{g_{a\pm 2}^2}{g_a^2}\,\frac{E(x^a w^{\pm 1})E(x^{a\pm 1}w^{\pm 1})}{E(x^a)E(x^{a\pm 1})} \tag{2.2.21c}$$

$$W^{2,2}\left(\begin{smallmatrix} a & a \\ a & a\end{smallmatrix}\right) = \frac{xwE(w^{-1})E(xw^{-1})E(x^{a-1})E(x^{a+2})}{E(x)E(x^2)E(x^a)E(x^{a+1})} + \frac{E(x^{a-1})E(x^a w^{-1})}{E(x^{a-1})E(x^a)} \tag{2.2.21d}$$

where the gauge factors g_a are arbitrary.

The low-temperature limit is now given by $x \to 0$ or $p \to 0$ with w fixed. The E-functions satisfy the following properties

$$E(w,p) = E(pw^{-1}, p) = -wE(w^{-1}, p) \tag{2.2.22a}$$

$$E(p^n w, p) = p^{-n(n-1)/2}(-w)^{-n}E(w,p) \tag{2.2.22b}$$

$$\lim_{p\to 0} E(p^a w, p^b) = \begin{cases} 1, & 0 < a < b \\ 1-w, & a = 0 \end{cases} \tag{2.2.22c}$$

where n is an integer. Another useful property is

$$\lim_{x\to 0} \frac{E(x^a w^{-1})}{x^a} = w^{\lfloor a\lambda/\pi \rfloor} \tag{2.2.23}$$

These relations are used to derive the low temperature limit separately for the two intervals $0 < \lambda < \frac{\pi}{2}$ and $\frac{\pi}{2} < \lambda < \pi$.

Fixing the choice of gauge $g_a = w^{a(a\lambda-\pi)/4\pi}$ and removing the overall scale factor $\exp(-2u(\lambda-u)/\varepsilon)$, the local energy functions are

$$0 < \lambda < \tfrac{\pi}{2}: \qquad H(a\pm 2, a, a\mp 2) = 1 \tag{2.2.24a}$$

$$H(a\pm 2, a, a) = H(a, a, a\pm 2) = \tfrac{1}{2} \pm h_{a\pm 1} \tag{2.2.24b}$$

$$H(a, a\pm 2, a) = \mp\big(h_a + h_{a\pm 1}\big) \tag{2.2.24c}$$

$$H(a,a,a) = \begin{cases} 0, & h_{a-1} = h_a = h_{a+1} \\ 1, & \text{otherwise} \end{cases} \tag{2.2.24d}$$

$$\tfrac{\pi}{2} < \lambda < \pi: \qquad H(a\pm 2, a, a\mp 2) = 2 \tag{2.2.25a}$$

$$H(a\pm 2, a, a) = H(a, a, a\pm 2) = \tfrac{1}{2} \pm h_{a\pm 1} \tag{2.2.25b}$$

$$H(a, a\pm 2, a) = \mp(h_a + h_{a\pm 1}) \tag{2.2.25c}$$

$$H(a,a,a) = \begin{cases} 0, & h_{a-1} = h_a \text{ or } h_a = h_{a+1} \\ 1, & \text{otherwise} \end{cases} \tag{2.2.25d}$$

The above expressions for the local energy functions take both positive and negative values. This is not desirable because we would like nonnegative local energy functions. To achieve this we use another gauge $g'_a = w^{G_a}$ such that the new local energies $H'(a,b,c)$ are

$$H'(a,b,c) = H(a,b,c) + 2G_b - G_a - G_c \geq 0 \tag{2.2.26}$$

A gauge transformation that satisfies this is

$$G_a = \begin{cases} h_1 + h_3 + \dots h_{a-1}, & a \text{ even} \\ h_2 + h_4 + \dots h_{a-1}, & a \text{ odd} \end{cases} \qquad G_{a+1} - G_{a-1} = h_a \tag{2.2.27}$$

This transformation is performed more neatly by defining $G(a,b) = G_b - G_a$ so that

$$H'(a,b,c) = H(a,b,c) + G(a,b) - G(b,c) \geq 0, \qquad G(a,b) = \tfrac{1}{2}(b-a)h_{\frac{a+b}{2}} \tag{2.2.28}$$

The new expressions for local energies in this gauge, omitting the prime, are

$$0 < \lambda < \tfrac{\pi}{2}: \qquad H(a \pm 2, a, a \mp 2) = 1 - (h_{a+1} - h_{a-1}) \tag{2.2.29a}$$

$$H(a \pm 2, a, a) = H(a, a, a \pm 2) = \tfrac{1}{2} \tag{2.2.29b}$$

$$H(a, a \pm 2, a) = \pm\big(h_{a\pm1} - h_a\big) \tag{2.2.29c}$$

$$H(a,a,a) = \begin{cases} 0, & h_{a-1} = h_a = h_{a+1} \\ 1, & \text{otherwise} \end{cases} \tag{2.2.29d}$$

$$\tfrac{\pi}{2} < \lambda < \pi: \qquad H(a \pm 2, a, a \mp 2) = 2 - (h_{a+1} - h_{a-1}) \tag{2.2.30a}$$

$$H(a \pm 2, a, a) = H(a, a, a \pm 2) = \tfrac{1}{2} \tag{2.2.30b}$$

$$H(a, a \pm 2, a) = \pm(h_{a\pm1} - h_a) \tag{2.2.30c}$$

$$H(a,a,a) = \begin{cases} 0, & h_{a-1} = h_a \text{ or } h_a = h_{a+1} \\ 1, & \text{otherwise} \end{cases} \tag{2.2.30d}$$

These are shown in Figures 2.3 and 2.4.

The local energy functions are now nonnegative $H(a,b,c) \geq 0$ and take only the values $0, \frac{1}{2}, 1$, which is consistent with a spin-1 interpretation. The local energies only depend on

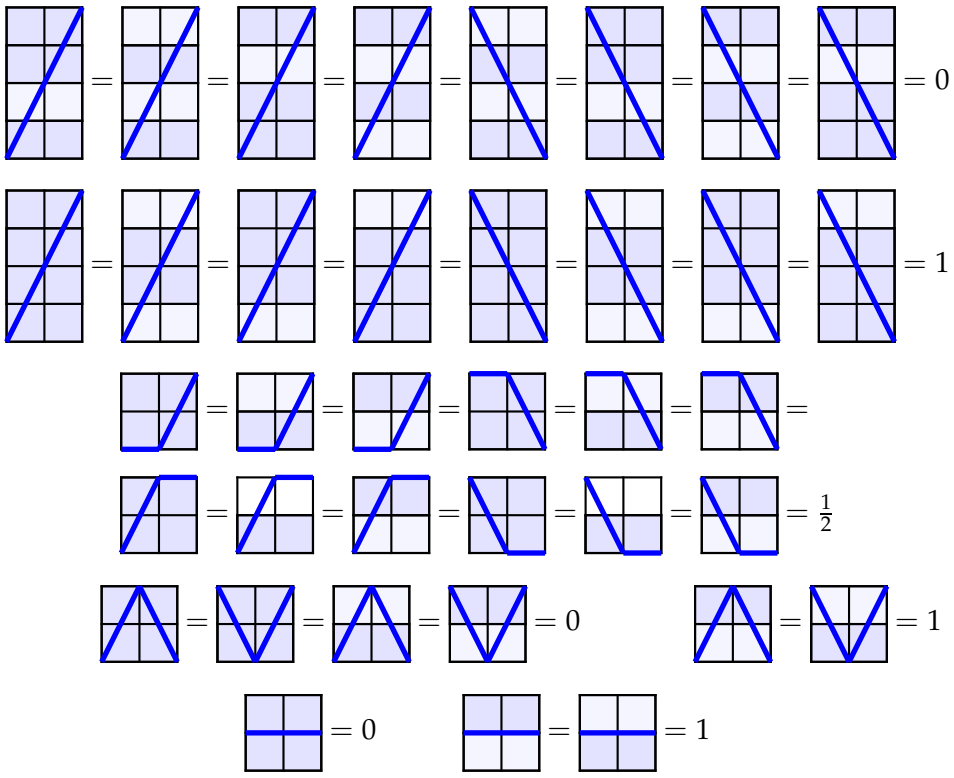

Figure 2.3: Local energies for 2×2 fused RSOS models in the interval $0 < \lambda < \frac{\pi}{2}$.

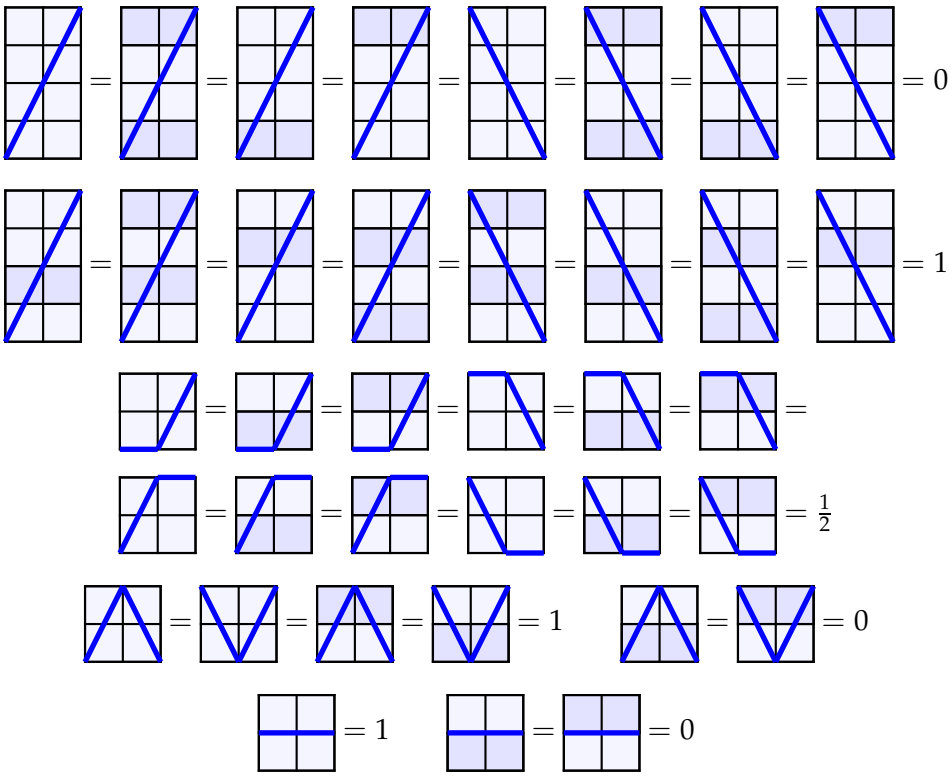

Figure 2.4: Local energies for 2×2 fused RSOS models in the interval $\frac{\pi}{2} < \lambda < \pi$.

the heights a through the shading of the 1-bands since they depend only on the differences

$$\delta_a = h_{a+1} - h_a = \begin{cases} 0, & \text{the 1-band } (a, a+1) \text{ is shaded} \\ 1, & \text{the 1-band } (a, a+1) \text{ is unshaded} \end{cases} \tag{2.2.31}$$

The shaded and unshaded 1-bands for the two intervals $0 < \lambda < \frac{\pi}{2}$ and $\frac{\pi}{2} < \lambda < \pi$ are interchanged under duality (2.2.17) with $\delta_a \leftrightarrow 1-\delta_a$. For $0 < \lambda < \frac{\pi}{2}$, there are no unshaded 2-bands and the local energies are shown in Figure 2.3. By contrast, in the dual interval $\frac{\pi}{2} < \lambda < \pi$, there are no shaded 2-bands and the local energies are shown in Figure 2.4. Under duality (2.2.17), the local energies are related by

$$H^{m,m',2}(a, b, c) = 1 - H^{m'-m,m',2}(a, b, c) \tag{2.2.32}$$

3×3 local energies

Starting with the 3×3 local energies for $0 < \lambda < \frac{\pi}{3}$ in [118], the local energies for $\frac{2\pi}{3} < \lambda < \pi$ can be obtained by applying, for $n = 3$, the conjectured duality relation

$$H^{m,m'}(a, b, c) = \tfrac{n}{2} - H^{m'-m,m'}(a, b, c), \qquad n = 1, 2, 3, \ldots \tag{2.2.33}$$

2.2.5 Energy statistic and one-dimensional sums

Following Baxter [31, 55, 56], the energy statistic of RSOS paths is

$$E(\sigma) = \sum_{j=1}^{N} jH(\sigma_{j-1}, \sigma_j, \sigma_{j+1}) \tag{2.2.34}$$

The associated one-dimensional sums are defined as

$$X_{abc}^{(N)}(q) = \sum_{\sigma} q^{E(\sigma)}, \qquad \sigma_0 = a,\ \sigma_N = b,\ \sigma_{N+1} = c \tag{2.2.35}$$

where the sum is over all RSOS paths $\sigma = \{\sigma_0, \sigma_1, \ldots, \sigma_N, \sigma_{N+1}\}$ at the given fusion level n. These sums satisfy the recursion

$$X^{(N)}_{abc}(q) = \sum_{d \sim b} q^{NH(d,b,c)} X^{(N-1)}_{adb}(q) \tag{2.2.36}$$

subject to the boundary conditions

$$X^{(N)}_{a0c}(q) = X^{(N)}_{am'c}(q) = 0, \qquad X^{(0)}_{abc}(q) = \delta_{a,b} \tag{2.2.37}$$

where $d \sim b$ denotes that the heights d and b are adjacent at fusion level n.

2.2.6 Ground states and sectors for $n = 2$ and $m' > 2m$

For the interval $0 < \lambda < \frac{\pi}{2}$, there are shaded 2-bands and the associated ground states relate to the superconformal minimal models in the Neveu-Schwarz and Ramond sectors as discussed in [118]. In contrast, for $\frac{\pi}{2} < \lambda < \pi$, there are no shaded 2-bands only shaded 1-bands. So, for these models, the superconformal groundstates are not supported and we find that the ground states are associated to shaded 1-bands. A comparison of ground states in the two different intervals is shown in Figure 2.5. Since the local energies are nonnegative $H(a,b,c) \geq 0$, any one-dimensional RSOS path σ with $E(\sigma) = 0$ is a ground state. The only RSOS paths with energy $E(\sigma) = 0$ are the $2(m-1)$ flat paths $\sigma = \{\rho, \rho, \ldots, \rho\}$ with $\rho = \rho_0(r)$ or $\rho = \rho_1(r)$ for some r.

Generically, for suitable choices of (a,b,c), the one-dimensional sums (2.2.35) are interpreted as finitized conformal characters

$$\chi^{(N)}_{\Delta}(q) = q^{-c/24+\Delta} X^{(N)}_{abc}(q) = q^{-c/24+\Delta} \sum_{\sigma} q^{E(\sigma)} \tag{2.2.38}$$

where $E(\sigma)$ are conformal energies of the infinite system. These are the spectrum generating functions for a finite truncated set of conformal energy levels in a given sector labelled by (a,b,c). The connection with characters is made by choosing the last step (b,c) of the one-dimensional walks to agree with a ground state RSOS path labelled by r. Restricting to models with $\frac{\pi}{2} < \lambda < \pi$, the precise connection between (a,b,c) and the conformal Kac

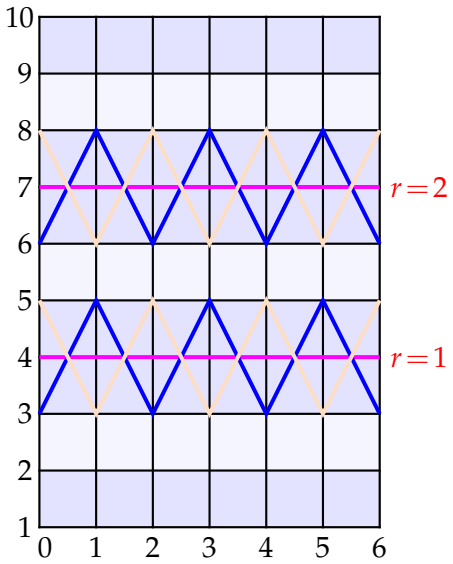

(a) Flat and alternating ground states for $0 < \lambda < \pi/2$.

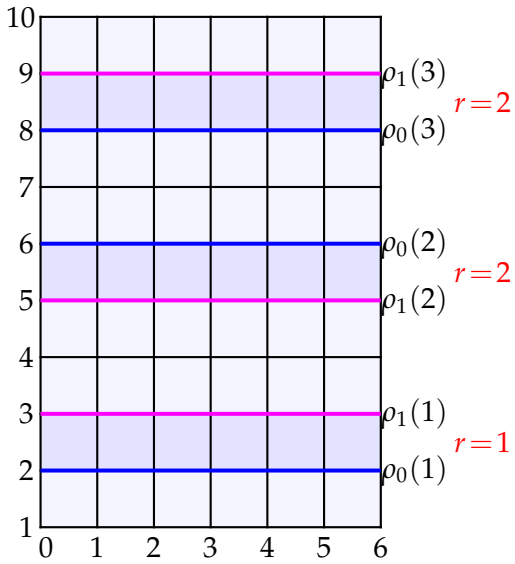

(b) Flat ground states for $\pi/2 < \lambda < \pi$.

Figure 2.5: A comparison of ground state RSOS paths for dual RSOS$(m, m')_{2\times 2}$ models with (a) $(m, m') = (7, 11)$ and (b) $(m, m') = (4, 11)$: (a) For $(m, m') = (7, 11)$, the shaded 1-bands occur at heights $\lfloor \frac{11r}{7} \rfloor = 1, 3, 4, 6, 7, 9$ for $r = 1, 2, \ldots, 6$. The 6 ground state (shaded) 2-bands occur centered at heights $a = 4, 7$. The ground states are either flat of the form $\{a, a, \ldots, a\}$ or alternating of the form $\{a \pm 1, a \mp 1, a \pm 1, a \mp 1, \ldots\}$. (b) For $(m, m') = (4, 11)$, there are no shaded 2-bands. The ground state (shaded) 1-bands occur at heights $\lfloor \frac{11r}{4} \rfloor = 2, 5, 8$ for $r = 1, 2, 3$. The 6 ground states are flat of the form $\{a, a, \ldots, a\}$ with a belonging to the even or odd sequences $\rho_0(r) = 2, 6, 8$ or $\rho_1(r) = 3, 5, 9$. (a) Flat and alternating ground states for $0 < \lambda < \pi/2$. (b) Flat ground states for $\pi/2 < \lambda < \pi$.

quantum numbers (r, s) is given by

$$a = s, \qquad b = c = \rho_\mu(r), \qquad \mu = s \bmod 2 \tag{2.2.39}$$

2.3 RSOS$(m, 2m+1)_{2\times 2}$ One-Dimensional Sums

In [139,144–146], a study has been carried out of the one-dimensional sums associated with a particular choice of local energy functions for RSOS lattice paths with half-integer steps. We call these half-integer RSOS paths JM paths. In these papers, the local energy functions of JM paths were not related to integrable lattice models. However, in the thermodynamic limit, these one-dimensional sums quite remarkably reproduce the Virasoro characters of

the sequences of nonunitary minimal models $\mathcal{M}(m, 2m+1)$ with $m = 2, 3, 4, \ldots$. In this section, we show that that there exists an energy-preserving bijection between the JM paths and RSOS$(m, 2m+1)_{2\times 2}$ paths. More precisely, we present a one-to-one mapping of RSOS spin-1 paths into equivalent spin-$\frac{1}{2}$ JM paths with equivalent local energies. We conclude that the JM paths are described by the RSOS$(m, 2m+1)_{2\times 2}$ Yang-Baxter integrable lattice models. This explains the remarkable observed properties of the JM one-dimensional sums.

We observe that when $m' = 2m+1$, the sequence of integers (2.2.8) defining the shaded bands simplifies to

$$\rho = \left\lfloor \tfrac{r(2m+1)}{m} \right\rfloor = \lfloor 2r + \tfrac{r}{m} \rfloor = 2r \qquad r = 1, 2, \ldots, m-1 \tag{2.3.1}$$

This means that every second band starting from the lowest height $a = 1$ is shaded and

$$\delta_a = \begin{cases} 0 & a \text{ even} \\ 1 & a \text{ odd} \end{cases} \qquad a = 1, \ldots, m'-2 \tag{2.3.2}$$

Since the adjacency graph decomposes for the 2×2 fused models, it suffices to restrict a, b, c to be odd in these cases.

In the next two subsections, we consider the two simplest nonunitary RSOS(m, m') models with crossing parameter in the interval $\frac{\pi}{2} < \lambda < \pi$, namely, the RSOS(2,5) (Yang-Lee model) and RSOS(3,7). The heights $a = 1, 2, \ldots ..., m'-1$ live on the $A_{m'-1}$ Dynkin diagrams which possess a $\mathbb{Z}_2$ symmetry. Specifically, the Boltzmann face weights are invariant under the height reversal $\sigma \leftrightarrow m' - \sigma$. As a consequence of this symmetry the Dynkin diagrams, which encode the adjacency rules among heights, can be folded into tadpole diagrams. Example foldings are shown in Figures 2.6a and 2.6c for the $n = 1$ adjacency. For RSOS$(2, 5)_{1\times 1}$, the nodes of the tadpole are interpreted as particles $\bullet$ or vacancies $\circ$ with nearest neighbour particle exclusion. Specifically, a particle $\bullet = 1 = 4$ is allowed next to a vacancy $\circ = 2 = 3$ but not allowed next to another particle. For RSOS$(3, 7)_{1\times 1}$, there are two types of particles $\bullet = 1 = 6$ and $\bullet = 2 = 5$ in addition to the vacancy $\circ = 3 = 4$. At fusion level $n = 2$, the RSOS$(2, 5)_{2\times 2}$ model is equivalent to two independent folded copies

of the original unfused model RSOS$(2,5)_{1\times 1}$ as indicated in Figure 2.6b. The situation is different for the RSOS$(3,7)_{2\times 2}$ fused model. The new tadpole diagram $T_3^{(n=2)}$, shown in Figure 2.6d, acquires an additional loop corresponding to the particle $\circ = 3$ and $\circ = 4$.

2.3.1 RSOS$(2,5)$

The Yang-Lee (YL) model [148] is associated with the exactly solvable RSOS(2,5) model. It is defined on a square lattice and its heights live on a A_4 Dynkin diagram. There is a single shaded 1-band between heights 2 and 3, and ground state configurations are alternating paths inside it as shown in Figure 2.7a. Identifying the heights related by this $\mathbb{Z}_2$ symmetry and using the notation $\bullet = 1, 4$, $\circ = 2, 3$, the face weights (2.2.1) with $g_a = 1$ become

$$W\left(\begin{smallmatrix}\circ & \circ\\ \circ & \bullet\end{smallmatrix}\middle| u\right) = W\left(\begin{smallmatrix}\bullet & \circ\\ \circ & \circ\end{smallmatrix}\middle| u\right) = s(\lambda - u) \tag{2.3.3a}$$

$$W\left(\begin{smallmatrix}\circ & \circ\\ \bullet & \circ\end{smallmatrix}\middle| u\right) = -s(u) \tag{2.3.3b}$$

$$W\left(\begin{smallmatrix}\circ & \bullet\\ \circ & \circ\end{smallmatrix}\middle| u\right) = -\frac{s(u)}{s(2\lambda)} \tag{2.3.3c}$$

$$W\left(\begin{smallmatrix}\circ & \bullet\\ \bullet & \circ\end{smallmatrix}\middle| u\right) = \frac{s(2\lambda - u)}{s(2\lambda)} \tag{2.3.3d}$$

$$W\left(\begin{smallmatrix}\bullet & \circ\\ \circ & \bullet\end{smallmatrix}\middle| u\right) = s(\lambda + u) \tag{2.3.3e}$$

$$W\left(\begin{smallmatrix}\circ & \circ\\ \circ & \circ\end{smallmatrix}\middle| u\right) = \frac{s(2\lambda + u)}{s(2\lambda)} \tag{2.3.3f}$$

In particle notation for RSOS$(2,5)$, $\bullet = 1$ is used for an occupied site and $\circ = 0$ for an unoccupied site. In this notation, the adjacency graph is the tadpole T_2. The local energy functions can be taken to be

$$H(a,b,c) = \begin{cases} 1, & (a,b,c) = (\circ, \bullet, \circ) \\ 0, & \text{other allowed triples} \end{cases} \tag{2.3.4}$$

Implementing the 2×2 fusion as in (2.2.4) with a gauge yields the following face

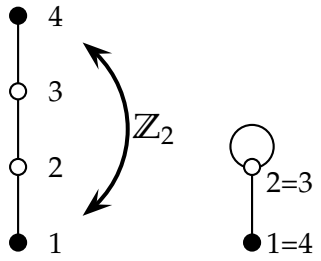

(a) RSOS$(2,5)_{1\times1}$: folding of the $A_4 = A_4^{(n=1)}$ and the corresponding T_2 tadpole.

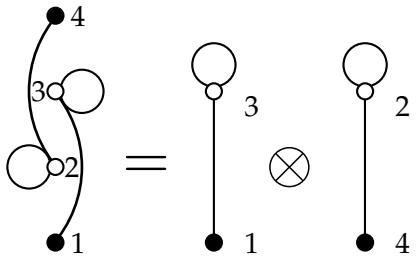

(b) RSOS$(2,5)_{2\times2}$: decomposition of $A_4^{(n=2)}$ into the tensor product of two T_2 tadpoles.

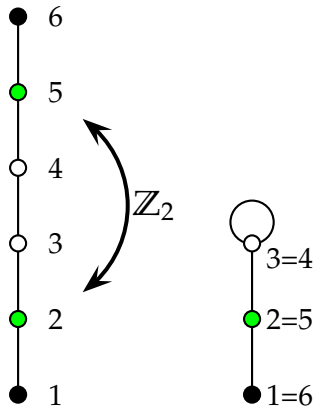

(c) RSOS$(3,7)_{1\times1}$: folding of the $A_6 = A_6^{(n=1)}$ and the corresponding $T_3^{(n=1)}$ tadpole.

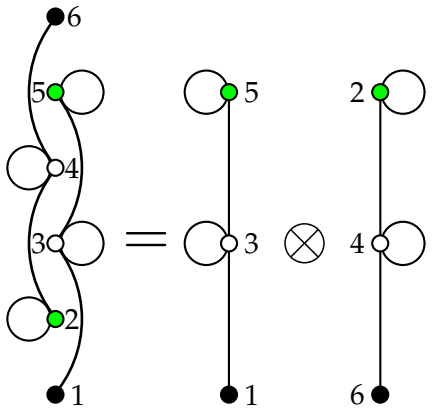

(d) RSOS$(3,7)_{2\times2}$: decomposition of $A_6^{(n=2)}$ into the tensor product of two $T_3^{(n=2)}$ tadpoles.

Figure 2.6: The RSOS$(2,5)$ and RSOS$(3,7)$ lattice models are identified with tadpole diagrams which encode the adjacency rules between heights. The RSOS$(2,5)_{1\times1}$ (a) and RSOS$(2,5)_{2\times2}$ (b) models share the same tadpole diagram. This results from the fact that the 2×2 lattice fusion gives back the original lattice model. In contrast, the RSOS$(3,7)_{1\times1}$(c) and RSOS$(3,7)_{2\times2}$ (d) models show different tadpole diagrams because the 2×2 lattice fusion produces a new lattice model. (a) RSOS$(2,5)_{1\times1}$: folding of the $A_4 = A_4^{(n=1)}$ and the corresponding $T_2^{(n=1)}$ tadpole. (b) RSOS$(2,5)_{2\times2}$: decomposition of $A_4^{(n=2)}$ into the tensor product of two $T_2^{(n=2)}$ tadpoles. (c) RSOS$(3,7)_{1\times1}$: folding of the $A_6 = A_6^{(n=1)}$ and the corresponding $T_3^{(n=1)}$ tadpole. (d) RSOS$(3,7)_{2\times2}$: decomposition of $A_6^{(n=2)}$ into the tensor product of two $T_3^{(n=2)}$ tadpoles.

weights for the RSOS(2,5)$_{2\times 2}$ model

$$W^{2,2}\left(\begin{smallmatrix}\circ & \circ\\ \circ & \bullet\end{smallmatrix}\middle| u\right) = W^{2,2}\left(\begin{smallmatrix}\bullet & \circ\\ \circ & \circ\end{smallmatrix}\middle| u\right) = \frac{s(\lambda-u)s(2\lambda+u)}{s(2\lambda)} \tag{2.3.5a}$$

$$W^{2,2}\left(\begin{smallmatrix}\circ & \circ\\ \bullet & \circ\end{smallmatrix}\middle| u\right) = -\frac{g_0}{g_1}\frac{s(u)s(2\lambda+u)}{s(2\lambda)^3} \tag{2.3.5b}$$

$$W^{2,2}\left(\begin{smallmatrix}\circ & \bullet\\ \circ & \circ\end{smallmatrix}\middle| u\right) = -\frac{g_1}{g_0}s(u)s(2\lambda+u) \tag{2.3.5c}$$

$$W^{2,2}\left(\begin{smallmatrix}\circ & \bullet\\ \bullet & \circ\end{smallmatrix}\middle| u\right) = \frac{s(2\lambda-u)s(2\lambda+u)}{s(2\lambda)^2} \tag{2.3.5d}$$

$$W^{2,2}\left(\begin{smallmatrix}\bullet & \circ\\ \circ & \bullet\end{smallmatrix}\middle| u\right) = \frac{s(\lambda+u)s(2\lambda+u)}{s(2\lambda)} \tag{2.3.5e}$$

$$W^{2,2}\left(\begin{smallmatrix}\circ & \circ\\ \circ & \circ\end{smallmatrix}\middle| u\right) = \frac{s(2\lambda+u)^2}{s(2\lambda)^2} \tag{2.3.5f}$$

Fixing the gauge to be $g_0/g_1 = s(2\lambda)^2$ and removing the overall scale factor $s(2\lambda+u)/s(2\lambda)$, these weights coincide with the 1×1 weights above (2.3.7). Consequently RSOS$(2,5)_{1\times 1}$ and RSOS$(2,5)_{2\times 2}$ coincide as lattice models.

The new local energies for the 2×2 fused model are

$$H(\circ,\bullet,\circ) = H(\circ,\circ,\circ) = 0, \qquad H(\circ,\circ,\bullet) = H(\bullet,\circ,\circ) = \tfrac{1}{2}, \qquad H(\bullet,\circ,\bullet) = 1 \tag{2.3.6}$$

The ground state configurations for the fused model are flat paths corresponding to the lower and upper height of the single shaded 1-band as seen in Figure 2.7b.

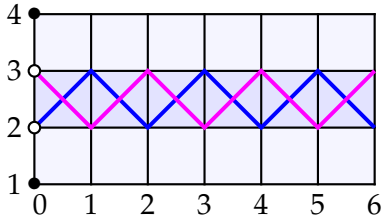

(a) RSOS$(2,5)_{1\times 1}$ has a single shaded 1-band and the 2 ground states corresponds to alternating paths inside it.

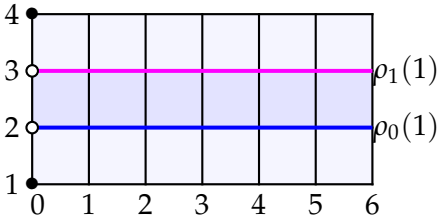

(b) RSOS$(2,5)_{2\times 2}$ has a single shaded 1-band and 2 flat ground states corresponding to the lower and upper height of this band.

Figure 2.7: Ground state configurations of RSOS$(2,5)_{1\times 1}$ and RSOS$(2,5)_{2\times 2}$ lattice models.(a) RSOS$(2,5)_{1\times 1}$ has a single shaded 1-band and the 2 ground states corresponds to alternating paths inside it. (b) RSOS$(2,5)_{2\times 2}$ has a single shaded 1-band and 2 flat ground states corresponding to the lower and upper height of this band.

2.3.2 RSOS$(3,7)$

The second simplest example of nonunitary RSOS model is RSOS(3,7), with heights living on the A_6 Dynkin diagram. Identifying the heights related by the $\mathbb{Z}_2$ symmetry and using the notation $\bullet = 1,6$, $\circ = 3,4$, $\color{green}\bullet = 5,2$, the face weights (2.2.1) with $g_a = 1$ become

$$W\left(\begin{smallmatrix}\circ & \color{green}\bullet\\ \color{green}\bullet & \bullet\end{smallmatrix}\middle|u\right) = W\left(\begin{smallmatrix}\bullet & \color{green}\bullet\\ \color{green}\bullet & \circ\end{smallmatrix}\middle|u\right) = W\left(\begin{smallmatrix}\color{green}\bullet & \circ\\ \circ & \circ\end{smallmatrix}\middle|u\right) = W\left(\begin{smallmatrix}\circ & \circ\\ \circ & \color{green}\bullet\end{smallmatrix}\middle|u\right) = s(\lambda-u) \tag{2.3.7a}$$

$$W\left(\begin{smallmatrix}\color{green}\bullet & \circ\\ \bullet & \color{green}\bullet\end{smallmatrix}\middle|u\right) = -\frac{s(3\lambda)s(u)}{s(2\lambda)} \tag{2.3.7b}$$

$$W\left(\begin{smallmatrix}\color{green}\bullet & \bullet\\ \circ & \color{green}\bullet\end{smallmatrix}\middle|u\right) = -\frac{s(u)}{s(2\lambda)} \tag{2.3.7c}$$

$$W\left(\begin{smallmatrix}\circ & \circ\\ \color{green}\bullet & \circ\end{smallmatrix}\middle|u\right) = -s(u) \tag{2.3.7d}$$

$$W\left(\begin{smallmatrix}\circ & \color{green}\bullet\\ \circ & \circ\end{smallmatrix}\middle|u\right) = -\frac{s(2\lambda)s(u)}{s(3\lambda)} \tag{2.3.7e}$$

$$W\left(\begin{smallmatrix}\color{green}\bullet & \bullet\\ \bullet & \color{green}\bullet\end{smallmatrix}\middle|u\right) = \frac{s(2\lambda-u)}{s(2\lambda)} \tag{2.3.7f}$$

$$W\left(\begin{smallmatrix}\bullet & \color{green}\bullet\\ \color{green}\bullet & \bullet\end{smallmatrix}\middle|u\right) = s(\lambda+u) \tag{2.3.7g}$$

$$W\left(\begin{smallmatrix}\circ & \color{green}\bullet\\ \color{green}\bullet & \circ\end{smallmatrix}\middle|u\right) = \frac{s(3\lambda-u)}{s(3\lambda)} \tag{2.3.7h}$$

$$W\left(\begin{smallmatrix}\color{green}\bullet & \circ\\ \circ & \color{green}\bullet\end{smallmatrix}\middle|u\right) = \frac{s(2\lambda+u)}{s(2\lambda)} \tag{2.3.7i}$$

$$W\left(\begin{smallmatrix}\circ & \circ\\ \circ & \circ\end{smallmatrix}\middle|u\right) = \frac{s(3\lambda+u)}{s(3\lambda)} \tag{2.3.7j}$$

In particle notation $\bullet = 1$, $\circ = 3$ and $\color{green}\bullet = 5$ are used for the three different occupation states. In this notation, the adjacency graph is the tadpole T_3. The RSOS$(3,7)_{1\times1}$ local energy functions are

$$H(\color{green}\bullet,\circ,\color{green}\bullet) = H(\circ,\color{green}\bullet,\circ) = 0 \tag{2.3.8a}$$

$$H(\circ,\circ,\color{green}\bullet) = H(\color{green}\bullet,\circ,\circ) = H(\circ,\color{green}\bullet,\bullet) = H(\bullet,\color{green}\bullet,\circ) = \tfrac{1}{4} \tag{2.3.8b}$$

$$H(\circ,\circ,\circ) = H(\color{green}\bullet,\bullet,\color{green}\bullet) = H(\bullet,\color{green}\bullet,\bullet) = \tfrac{1}{2} \tag{2.3.8c}$$

There are two shaded 1-bands, one between heights 2 and 3, the other between heights 4 and 5. The ground state configurations are alternating paths inside each shaded 1-band as

shown in Figure 2.8a.

Implementing the 2×2 fusion as in (2.2.4) and allowing gauge factors yields the fol-

lowing face weights for the RSOS(3,7)$_{2\times 2}$ model

$$W^{2,2}\left(\begin{smallmatrix}\bullet & \circ\\ \circ & \bullet\end{smallmatrix}\middle| u\right) = W^{2,2}\left(\begin{smallmatrix}\bullet & \circ\\ \circ & \bullet\end{smallmatrix}\middle| u\right) = \frac{s(\lambda-u)s(2\lambda-u)}{s(2\lambda)} \tag{2.3.9a}$$

$$W^{2,2}\left(\begin{smallmatrix}\circ & \circ\\ \circ & \bullet\end{smallmatrix}\middle| u\right) = W^{2,2}\left(\begin{smallmatrix}\bullet & \circ\\ \circ & \circ\end{smallmatrix}\middle| u\right) = \frac{s(\lambda-u)s(2\lambda+u)}{s(2\lambda)} \tag{2.3.9b}$$

$$W^{2,2}\left(\begin{smallmatrix}\circ & \circ\\ \circ & \bullet\end{smallmatrix}\middle| u\right) = W^{2,2}\left(\begin{smallmatrix}\bullet & \circ\\ \circ & \circ\end{smallmatrix}\middle| u\right) = \frac{s(\lambda-u)s(3\lambda+u)}{s(3\lambda)} \tag{2.3.9c}$$

$$W^{2,2}\left(\begin{smallmatrix}\bullet & \bullet\\ \bullet & \circ\end{smallmatrix}\middle| u\right) = W^{2,2}\left(\begin{smallmatrix}\circ & \bullet\\ \bullet & \bullet\end{smallmatrix}\middle| u\right) = \frac{s(\lambda-u)s(3\lambda-u)}{s(3\lambda)} \tag{2.3.9d}$$

$$W^{2,2}\left(\begin{smallmatrix}\circ & \circ\\ \bullet & \circ\end{smallmatrix}\middle| u\right) = -\frac{g_2}{g_1}\frac{s(u)s(3\lambda-u)}{s(2\lambda)^2} \tag{2.3.9e}$$

$$W^{2,2}\left(\begin{smallmatrix}\circ & \circ\\ \bullet & \circ\end{smallmatrix}\middle| u\right) = -\frac{g_2}{g_3}\frac{s(u)s(3\lambda+u)}{s(3\lambda)^2} \tag{2.3.9f}$$

$$W^{2,2}\left(\begin{smallmatrix}\bullet & \bullet\\ \circ & \bullet\end{smallmatrix}\middle| u\right) = -\frac{g_3}{g_2}\frac{s(u)s(2\lambda+u)}{s(2\lambda)s(3\lambda)} \tag{2.3.9g}$$

$$W^{2,2}\left(\begin{smallmatrix}\circ & \bullet\\ \circ & \circ\end{smallmatrix}\middle| u\right) = -\frac{g_1}{g_2}\frac{s(u)s(3\lambda-u)}{s(3\lambda)} \tag{2.3.9h}$$

$$W^{2,2}\left(\begin{smallmatrix}\circ & \bullet\\ \circ & \circ\end{smallmatrix}\middle| u\right) = -\frac{g_3}{g_2}\frac{s(u)s(3\lambda+u)s(2\lambda)}{s(3\lambda)} \tag{2.3.9i}$$

$$W^{2,2}\left(\begin{smallmatrix}\bullet & \circ\\ \bullet & \bullet\end{smallmatrix}\middle| u\right) = -\frac{g_2}{g_3}s(u)s(2\lambda+u)s(2\lambda) \tag{2.3.9j}$$

$$W^{2,2}\left(\begin{smallmatrix}\circ & \bullet\\ \bullet & \circ\end{smallmatrix}\middle| u\right) = \frac{g_1}{g_3}\frac{s(u)s(\lambda+u)}{s(3\lambda)^2} \tag{2.3.9k}$$

$$W^{2,2}\left(\begin{smallmatrix}\circ & \bullet\\ \bullet & \circ\end{smallmatrix}\middle| u\right) = \frac{g_3}{g_1}\frac{s(u)s(\lambda+u)}{s(2\lambda)} \tag{2.3.9l}$$

$$W^{2,2}\left(\begin{smallmatrix}\bullet & \circ\\ \circ & \bullet\end{smallmatrix}\middle| u\right) = \frac{s(\lambda+u)s(2\lambda+u)}{s(2\lambda)} \tag{2.3.9m}$$

$$W^{2,2}\left(\begin{smallmatrix}\circ & \bullet\\ \bullet & \circ\end{smallmatrix}\middle| u\right) = \frac{s(2\lambda-u)s(3\lambda-u)}{s(2\lambda)s(3\lambda)} \tag{2.3.9n}$$

$$W^{2,2}\left(\begin{smallmatrix}\bullet & \circ\\ \circ & \bullet\end{smallmatrix}\middle| u\right) = \frac{s(2\lambda+u)s(3\lambda+u)}{s(2\lambda)s(3\lambda)} \tag{2.3.9o}$$

$$W^{2,2}\left(\begin{smallmatrix}\circ & \bullet\\ \bullet & \circ\end{smallmatrix}\middle| u\right) = \frac{s(3\lambda+u)s(3\lambda-u)}{s(3\lambda)^2} \tag{2.3.9p}$$

$$W^{2,2}\left(\begin{smallmatrix}\circ & \bullet\\ \circ & \bullet\end{smallmatrix}\middle| u\right) = W^{2,2}\left(\begin{smallmatrix}\bullet & \bullet\\ \circ & \circ\end{smallmatrix}\middle| u\right) = \frac{g_3}{g_2}\frac{s(u)s(u-\lambda)}{s(2\lambda)s(3\lambda)} \tag{2.3.9q}$$

$$W^{2,2}\left(\begin{smallmatrix}\bullet & \circ\\ \bullet & \circ\end{smallmatrix}\middle| u\right) = W^{2,2}\left(\begin{smallmatrix}\circ & \circ\\ \bullet & \bullet\end{smallmatrix}\middle| u\right) = \frac{g_2}{g_3}\frac{s(u)s(u-\lambda)}{s(3\lambda)} \tag{2.3.9r}$$

$$W^{2,2}\left(\begin{smallmatrix}\circ & \circ\\ \circ & \circ\end{smallmatrix}\middle| u\right) = \frac{s(2\lambda+u)s(3\lambda-u)}{s(2\lambda)s(3\lambda)} + \frac{s(2\lambda)s(u)s(u-\lambda)}{s(3\lambda)^2} \tag{2.3.9s}$$

$$W^{2,2}\left(\begin{smallmatrix}\bullet & \bullet\\ \bullet & \bullet\end{smallmatrix}\middle| u\right) = \frac{s(2\lambda+u)s(3\lambda-u)}{s(2\lambda)s(3\lambda)} \tag{2.3.9t}$$

In contrast to the Yang-Lee case, no choice of gauge factors can map the fused weights onto the unfused ones. This implies that the RSOS$(3,7)_{1\times 1}$ and RSOS$(3,7)_{2\times 2}$ models are distinct Yang-Baxter integrable lattice models even though we will argue that they lie in the same universality class.

The local energies for the RSOS$(3,7)_{2\times 2}$ model are

$$H(\bullet,\circ,\bullet) = H(\bullet,\circ,\bullet) = H(\bullet,\circ,\bullet) = H(\circ,\bullet,\circ) = 1 \tag{2.3.10a}$$

$$H(\bullet,\circ,\circ) = H(\circ,\circ,\bullet) = H(\circ,\circ,\bullet) = H(\bullet,\circ,\circ) = H(\circ,\bullet,\bullet) = H(\bullet,\bullet,\circ) = \tfrac{1}{2} \tag{2.3.10b}$$

$$H(\circ,\bullet,\circ) = H(\bullet,\circ,\bullet) = H(\circ,\circ,\circ) = H(\bullet,\bullet,\bullet) = 0 \tag{2.3.10c}$$

The ground state configurations for this model are flat paths corresponding to the lower and upper height of each shaded 1-band as seen in Figure 2.8b.

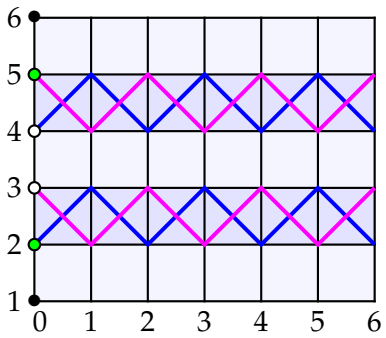

(a) RSOS$(3,7)_{1\times 1}$ has two shaded 1-bands and the 4 ground states corresponds to alternating paths inside them.

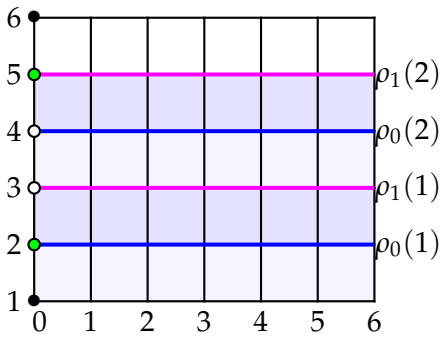

(b) RSOS$(3,7)_{2\times 2}$ has two shaded 1-bands and 4 flat ground states corresponding to the lower and upper height of these bands.

Figure 2.8: Ground state configurations for the 1×1 unfused and 2×2 fused A_6 RSOS models. (a) RSOS$(3,7)_{1\times 1}$ has two shaded 1-bands and the 4 ground states corresponds to alternating paths inside them. (b) RSOS$(3,7)_{2\times 2}$ has two shaded 1-bands and 4 flat ground states corresponding to the lower and upper height of these bands.

2.3.3 RSOS$(m, 2m+1)$ and JM$(m, 2m+1)$

Fix $k \in \mathbb{N}_{\geq 1}$ with $k = m-1$. A JM$(k+1, 2k+3)$ path [139]

$$\sigma = \{\sigma_0, \sigma_{\frac{1}{2}}, \sigma_1, \ldots, \sigma_N, \sigma_{N+\frac{1}{2}}\}, \qquad \sigma_j \in \{1, \tfrac{3}{2}, 2, \ldots, k+\tfrac{1}{2}, k+1\} \tag{2.3.11}$$

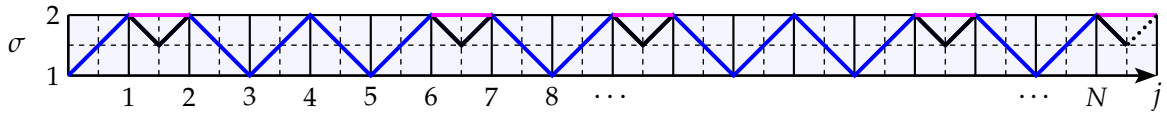

(a) JM(2,5) and RSOS$(2,5)_{2\times 2}$ paths with $k=1$ and $N=17$ integer steps: $\sigma=1,2$ corresponds to $1=\bullet$ and $2=\circ$ in the $T_2^{(n=2)}$ tadpole description of RSOS models.

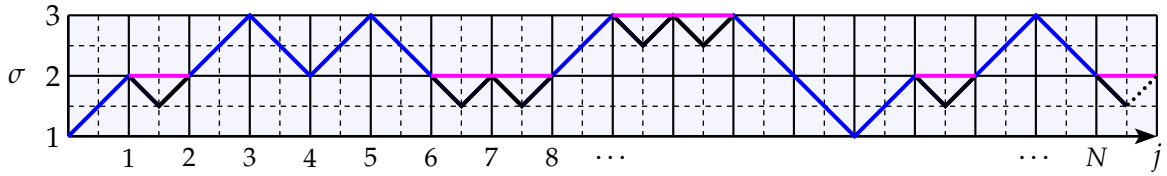

(b) JM(3,7) and RSOS$(3,7)_{2\times 2}$ paths with $k=2$ and $N=17$ integer steps: $\sigma_j=1,2,3$ corresponds to $1=\bullet$, $2=\bullet$ and $3=\circ$ in the $T_3^{(n=2)}$ tadpole description of RSOS models.

Figure 2.9: Two examples of the bijection between JM and RSOS paths. The edges of JM paths are black while their equivalent in the RSOS description are purple. The shared path is shown in blue. The bijection between JM and RSOS paths preserves the contour of the path except at local minima at half-integer heights where two consecutive half-integer steps in the JM path are replaced with a single horizontal step in the RSOS path. The last half-integer step of a JM path must be down and we add an additional half-integer up step shown dashed. The last RSOS step is therefore flat in the tadpole representation. (a) JM(2,5) and RSOS$(2,5)_{2\times 2}$ paths with $k=1$ and $N=7$ integer steps: $\sigma=1,2$ corresponds to $1=\bullet$ and $2=\circ$ in the $T_2^{(n=2)}$ tadpole description of RSOS models. (b) JM(3,7) and RSOS$(3,7)_{2\times 2}$ paths with $k=2$ and $N=17$ integer steps: $\sigma=1,2,3$ corresponds to $1=\bullet$, $2=\bullet$, and $3=\circ$ in the $T_3^{(n=2)}$ tadpole description of RSOS model.

is then a sequence of heights $\sigma_j \in \frac{1}{2}\mathbb{N}$ subject to the constraints

$$\sigma_0, \sigma_N \in \mathbb{N}, \quad \sigma_{N+\frac{1}{2}} = \sigma_N - \tfrac{1}{2}, \quad \sigma_N = \sigma_{N+1}, \quad \sigma_{j+\frac{1}{2}} - \sigma_j = \pm\tfrac{1}{2},\ j = 0, \tfrac{1}{2}, 1, \tfrac{3}{2}, \ldots, N$$

(2.3.12a)

$$(j, \sigma_j) \in \mathbb{N}^2 \text{ at all local peaks}$$

Examples are shown in Figure 2.9 for $k=1,2$. The JM paths are thus defined on lattices with half-integer spacing and half-integer heights, while in the RSOS description, only integer values of steps and heights are considered. Therefore, to map the energy of JM paths into the local energy functions of the RSOS paths with integer heights, we need to sum out (decimate) the half odd integer heights.

The energy of a JM path is given by

$$E(\sigma) = \sum_{j=\frac{1}{2}, j\in\frac{1}{2}\mathbb{N}}^{N} jw(j), \qquad w(j) = \tfrac{1}{2}\big|\sigma_{j+\frac{1}{2}} - \sigma_{j-\frac{1}{2}}\big| \tag{2.3.13}$$

Using $w(N+\frac{1}{2}) = 0$, this is gauge equivalent to the energy of the corresponding RSOS path with local energies (2.2.30)

$$\begin{aligned} E(\sigma) &= \sum_{j=\frac{1}{2}, j\in\frac{1}{2}\mathbb{N}}^{N+\frac{1}{2}} jw(j) = \tfrac{1}{4}w(\tfrac{1}{2}) + \tfrac{1}{2}\sum_{j=1}^{N}\big[(j-\tfrac{1}{2})w(j-\tfrac{1}{2}) + 2jw(j) + (j+\tfrac{1}{2})w(j+\tfrac{1}{2})\big] \\ &= \tfrac{1}{4}w(\tfrac{1}{2}) + \tfrac{1}{2}\sum_{j=1}^{N} j\big[w(j-\tfrac{1}{2}) + 2w(j) + w(j+\tfrac{1}{2})\big] + \tfrac{1}{4}\sum_{j=1}^{N}\big[w(j+\tfrac{1}{2}) - w(j-\tfrac{1}{2})\big] \\ &= \tfrac{1}{2}\sum_{j=1}^{N} j\big[w(j-\tfrac{1}{2}) + 2w(j) + w(j+\tfrac{1}{2})\big] \\ &= \sum_{j=1}^{N} j\big[\tilde{H}(\sigma_{j-1},\sigma_j,\sigma_{j+1}) + G_{j-1} - 2G_j + G_{j+1}\big] - G_0 + G_N \end{aligned} \tag{2.3.14}$$

Here $G_j = g(\sigma_j) = \frac{1}{4}\sigma_j$ and $G_{N+1} = G_N$ is a suitable gauge such that

$$\tilde{H}(\sigma_{j-1},\sigma_j,\sigma_{j+1}) = \tfrac{1}{2}\big[w(j-\tfrac{1}{2}) + 2w(j) + w(j+\tfrac{1}{2})\big] - G_{j-1} + 2G_j - G_{j+1} \tag{2.3.15}$$

and the constant shift of energy by $G_0 - G_N$ is irrelevant. Explicitly,

$$\tilde{H}(a\pm 1, a, a\mp 1) = 1 - g(a-1) + 2g(a) - g(a+1) = 1 \tag{2.3.16a}$$

$$\tilde{H}(a+1, a, a) = \tilde{H}(a, a, a+1) = \tfrac{3}{4} + g(a) - g(a+1) = \tfrac{1}{2} \tag{2.3.16b}$$

$$\tilde{H}(a-1, a, a) = \tilde{H}(a, a, a-1) = \tfrac{1}{4} + g(a) - g(a-1) = \tfrac{1}{2} \tag{2.3.16c}$$

$$\tilde{H}(a-1, a, a-1) = \tfrac{1}{2} + 2g(a) - 2g(a-1) = 1 \tag{2.3.16d}$$

$$\tilde{H}(a+1, a, a+1) = \tfrac{1}{2} + 2g(a) - 2g(a+1) = 0 \tag{2.3.16e}$$

$$\tilde{H}(a, a, a) = 0 \tag{2.3.16f}$$

The intermediate half-integer heights $a \pm \frac{1}{2}$ needed in (2.3.15) are uniquely determined by the adjacent integer heights. The local energies $\tilde{H}(\tilde{a}, \tilde{b}, \tilde{c})$ are related to the local energies

(2.2.30) by

$$\tilde{H}(\tilde{a},\tilde{b},\tilde{c}) = \tfrac{1}{2}H(a,b,c), \qquad a = 2\tilde{a}-1 = 1,3,5,\ldots,2k+1 \tag{2.3.17}$$

The factor of $\frac{1}{2}$ arises because the fused weights leading to (2.3.15) are calculated with integer fundamental steps rather than the half-integer fundamental steps of the JM paths, that is, $a-b = 0, \pm 2$ compared with $\tilde{a}-\tilde{b} = 0, \pm 1$.

2.4 Nonunitary Minimal Models $\mathcal{M}(m,m')$

2.4.1 Conformal data and characters

In the continuum scaling limit, the RSOS lattice models are described by the rational minimal models. The central charges of the $n = 1$ minimal models $\mathcal{M}(m,m')$, with $m < m'$ and m, m' coprime, are given by (1.2.20). The conformal weights and associated Virasoro characters are

$$\Delta_{r,s}^{m,m'} = \frac{(rm'-sm)^2-(m-m')^2}{4mm'}, \quad 1 \le r \le m-1, \;\; 1 \le s \le m'-1 \tag{2.4.1}$$

$$\mathrm{ch}_{r,s}^{m,m'}(q) = \frac{q^{-c/24+\Delta_{r,s}^{m,m'}}}{(q)_\infty} \sum_{k=-\infty}^{\infty} \left[q^{k(kmm'+m'r-ms)} - q^{(km+r)(km'+s)}\right] \tag{2.4.2}$$

where the q-factorials are defined by

$$(q)_n = \prod_{k=1}^{n}(1-q^k), \qquad (q)_\infty = \prod_{k=1}^{\infty}(1-q^k) \tag{2.4.3}$$

The minimal models are unitary if $m = m'-1$ and nonunitary if $m < m'-1$. In this section we consider the finitized characters of the 2×2 fused minimal models with $m < \frac{1}{2}m'$.

2.4.2 Finitized bosonic characters

From extensive numerics, we find empirically that the normalized finitized characters associated with the RSOS$(m,m')_{2\times 2}$ lattice models admit a bosonic form

$$\widehat{\mathrm{ch}}^{m,m';(N)}_{r,s}(q) = X^{m,m';(N)}_{abc}(q) \quad = \sum_{k=-\infty}^{\infty} \left[q^{k(kmm'+m'r-ms)} T^{(N)}_{km'+\frac{b-a}{2}}(q) - q^{(km+r)(km'+s)} T^{(N)}_{km'+\frac{b+a}{2}}(q) \right] \tag{2.4.4}$$

where

$$a = s, \qquad b = c = \rho_\mu(r), \qquad \mu = s \bmod 2 \tag{2.4.5}$$

The q-trinomial coefficients [149] are

$$T^{(N)}_k(q) = T^{(N)}_{-k}(q) = \begin{bmatrix} N \\ k \end{bmatrix}^{(0)}_2 = \sum_{j=0}^{N} q^{j(j+k)} \begin{bmatrix} N \\ j, j+k \end{bmatrix}_q \tag{2.4.6}$$

where the q-multinomial coefficients are defined in terms of q-factorials by

$$\begin{bmatrix} n \\ \ell, m \end{bmatrix}_q = \begin{cases} \frac{(q)_n}{(q)_\ell (q)_m (q)_{n-\ell-m}} & \ell, m, n-\ell-m \in \mathbb{Z}_{\geq 0} \\ 0, & \text{otherwise} \end{cases} \tag{2.4.7}$$

In the limit $q \to 1$, the q-multinomials reduce to multinomial coefficients

$$\lim_{q\to 1} \begin{bmatrix} n \\ \ell, m \end{bmatrix}_q = \begin{bmatrix} n \\ \ell, m \end{bmatrix} \tag{2.4.8}$$

which ensures the correct counting of states.

To arrive at the bosonic forms (2.4.4), we used the fact that the q-trinomial coefficient $T^{(N)}_k(q)$ is a q-deformed counting of weighted N step 2×2 fused paths on the A_∞ Dynkin diagram. This counting only respects the constraints $\sigma_{i+1} - \sigma_i = 0, \pm 2$, with $2k$ height difference between the initial and final state $\sigma_N - \sigma_0 = 2k$. This ensures correct counting, as $j+k$ is the number of up steps, j is the number of down steps, and $N-2j-k$ is the number of flat steps. Thus, given that the local energy functions are periodically ex-

tended, $T_k^{(N)}(q)$ gives the correct one-dimensional sums (without restricting to the fused $A_{m'}$). The required bosonic form of the one-dimensional sum on $A_{m'}$ is then obtained by summing and subtracting the respective generalized paths. These bosonic forms (2.4.4) were checked against the ground state one-dimensional sums with $b = c$ for all values of r, s using Mathematica [150] out to size $N = 12$ for $(m, m') = (2,5), (2,7), (3,7), (3,8)$, size $N = 11$ for $(m, m') = (2,9), (4,9)$, size $N = 10$ for $(m, m') = (3,10)$ and size $N = 9$ for $(m, m') = (2,11), (3,11), (4,11), (5,11)$. It would be of interest to obtain the bosonic expressions for $X_{abc}^{(N)}(q)$ more generally for $c = b, b \pm 2$ and to prove that these expressions satisfy the CTM recursions (2.2.36).

Using (2.4.6), it is straightforward to show that the finitized characters also satisfy the Kac symmetry

$$\hat{X}_{abc}^{m,m';(N)}(q) = \hat{X}_{m'-a,m'-b,m'-c}^{m,m';(N)}(q) \tag{2.4.9}$$

Since the shaded band structure is symmetric, the Kac labels on the right are $(r, s) = (m - r, m' - s)$.

2.4.3 $N \to \infty$ limit

The finitized characters also agree with the full characters in the thermodynamic limit $N \to \infty$. For fixed $k \in \mathbb{Z}$, the modified q-trinomials satisfy

$$\lim_{N\to\infty} T_k^{(N)}(q) = \lim_{N\to\infty} \sum_{j=0}^{\infty} q^{j(j+k)} \begin{bmatrix} N \\ j, j+k \end{bmatrix}_q = \frac{1}{(q)_\infty} \tag{2.4.10}$$

To establish this we take the limit inside the sum and use the elementary result

$$\lim_{N\to\infty} \begin{bmatrix} N \\ j, j+k \end{bmatrix}_q = \lim_{N\to\infty} \frac{(q)_N}{(q)_j\,(q)_{j+k}\,(q)_{N-2j-k}} = \frac{1}{(q)_j\,(q)_{j+k}} \tag{2.4.11}$$

to obtain

$$\lim_{N\to\infty} \sum_{j=0}^{\infty} q^{j(j+k)} \begin{bmatrix} N \\ j, j+k \end{bmatrix}_q = \sum_{j=0}^{\infty} \frac{q^{j(j+k)}}{(q)_j\,(q)_{j+k}} = \frac{1}{(q)_\infty} \tag{2.4.12}$$

The last equality follows by setting $z = q^{k+1}$ in the q-analogue of Kummer's theorem (see (2.2.8) of [151])

$$\sum_{j=0}^{\infty} \frac{q^{j(j-1)} z^j}{(1-q)\dots(1-q^j)(1-z)(1-zq)\dots(1-zq^{j-1})} = \prod_{j=0}^{\infty} \frac{1}{1-zq^j} \tag{2.4.13}$$

It follows that the limit of the finitized characters (2.4.4) precisely reproduces the $n = 1$ Virasoro characters

$$\lim_{N\to\infty} q^{-\frac{c}{24}+\Delta_{r,s}} \widehat{\mathrm{ch}}_{r,s}^{m,m';(N)}(q) = \mathrm{ch}_{r,s}^{m,m'}(q) \tag{2.4.14}$$

2.4.4 Logarithmic limit

Following [122,152] and [153], the Kac characters of the logarithmic minimal models $\mathcal{LM}(p,p')$ [123] and their $n \times n$ fusion hierarchies [154] are given by taking the *logarithmic limit*. Symbolically,

$$\lim_{m,m'\to\infty,\ \frac{m'}{m}\to\frac{p'}{p}+} \mathcal{M}(m,m')_{2\times 2} = \mathcal{LM}(p,p'), \qquad 1 \le p < \tfrac{1}{2}p', \quad p,p' \text{ coprime} \tag{2.4.15}$$

The (one-sided) limit is taken through coprime pairs (m,m') with $\frac{m'}{m} > \frac{p'}{p}$ and $\frac{p'}{p} \ge 2$. The one-sided limit is needed to ensure the sequences of minimal model ground states converge to the correct logarithmic minimal model ground states. Formally, the logarithmic limit is taken in the continuum scaling limit after the thermodynamic limit. The equality indicates the identification of the spectra of the chiral CFTs. In principle, the Jordan cells appearing in the reducible yet indecomposable representations of the logarithmic minimal models should emerge in this limit but there are subtleties [122,152].

Since finitized characters give the spectrum generating functions for finite truncated sets of conformal energies, the logarithmic limit can be applied directly to finitized characters. Assuming $m < \frac{1}{2}m'$, $0 < |q| < 1$ and taking the logarithmic limit of the finitized

characters (2.4.4) gives the finitized characters of $\mathcal{LM}(p,p')_{2\times 2}$ for $p < \frac{1}{2}p'$.

$$\widehat{\chi}^{p,p',(N)}_{r,s}(q) = \lim_{m,m'\to\infty,\ \frac{m'}{m}\to\frac{p'}{p}+} \widehat{\mathrm{ch}}^{m,m';(N)}_{r,s}(q) = T^{(N)}_{\frac{b-a}{2}}(q) - q^{rs}\, T^{(N)}_{\frac{b+a}{2}}(q) \tag{2.4.16}$$

where r, s, a, b, c are related by (2.4.5). Taking the thermodynamic limit, using (2.4.10), gives

$$\lim_{N\to\infty} q^{-\frac{c}{24}+\Delta_{r,s}} \widehat{\chi}^{p,p',(N)}_{r,s}(q) = q^{-\frac{c}{24}+\Delta_{r,s}} \frac{1-q^{rs}}{(q)_\infty} = \chi^{p,p'}_{r,s}(q) \tag{2.4.17}$$

which agrees with the Kac characters of the logarithmic minimal models $\mathcal{LM}(p,p')$.

2.5 Conclusion

Using the one-dimensional sums arising from Baxter's off-critical Corner Transfer Matrix (CTM) formalism, we have argued that, for $m' > 2m$, the $\mathrm{RSOS}(m,m')_{1\times 1}$ and $\mathrm{RSOS}(m,m')_{2\times 2}$ lattice models lie in the same universality class described by the nonunitary minimal CFT $\mathcal{M}(m,m')$. This result holds even though, in general, $\mathrm{RSOS}(m,m')_{1\times 1}$ and $\mathrm{RSOS}(m,m')_{2\times 2}$ are distinct lattice models. More specifically, we have conjectured the explicit bosonic form of the finitized characters and, for modest system sizes N, checked that these agree with the ground state one-dimensional sums. In the case $m' = 2m+1$, we have further shown that the ground state one-dimensional sums of $\mathrm{RSOS}(m,m')_{2\times 2}$ agree with those of Jacob and Mathieu [139] based on half-integer RSOS paths. This connection with a Yang-Baxter integrable lattice model nicely explains the remarkable observed properties of these half-integer one-dimensional sums. The more general methods used here allow these observations to be extended to all $\mathrm{RSOS}(m,m')_{2\times 2}$ lattice models.

Chapter 3

Yang-Baxter Solution of Dimers as a Free-Fermion Six-Vertex Model

The dimer model is formulated as a Yang-Baxter integrable free-fermion six-vertex model. At the free-fermion point the spectral parameter is $\lambda = \frac{\pi}{2}$. A one-to-many mapping of six-vertex configurations onto dimer configurations allows the free-fermion solutions to be applied to the anisotropic dimer model on a square lattice where the dimers are rotated by 45° compared to their usual orientation. This dimer model is exactly solvable in geometries of arbitrary finite size. In the present chapter, we establish and solve inversion identities for dimers with periodic boundary conditions on the cylinder. In the particle representation, the local face tile operators give a representation of the fermion algebra and the fermion particle trajectories play the role of nonlocal (logarithmic) degrees of freedom. In a suitable gauge, the dimer model is described by the Temperley-Lieb algebra with loop fugacity $\beta = 2\cos\lambda = 0$. At the isotropic point, $u = \frac{\lambda}{2} = \frac{\pi}{4}$, the exact solution allows for the explicit counting of 45° rotated dimer configurations on a periodic $M \times N$ square lattice. We show that the modular invariant partition function on the torus is the same as symplectic fermions and critical dense polymers.

3.1 Introduction

The dimer (domino tiling) model [70, 155] captures the molecular freedom in densely arranging (adsorbing) non-overlapping diatomic molecules (dimers) on a lattice substrate. In 1961, the dimer model on the square lattice was solved exactly [73, 74, 156, 157] by Pfaffians. While the original solutions were by Pfaffians, the idea of using a transfer matrix and free fermions was initiated in [75]. After more than 50 years, the dimer model continues to be the subject of extensive study [76, 82–87, 89] primarily to understand the finite-size effects of boundary conditions and steric effects under the influence of infinitely repulsive hard-core local interactions. These effects are manifest in the related problems of Aztec dia-

monds [158,159] and the six-vertex model with domain wall boundary conditions [69,160]. For these systems, even the thermodynamic limit can fail to exist. Although such boundary conditions clearly break conformal invariance in the continuum scaling limit there are other boundary conditions, such as periodic and free boundary conditions, which are conformally invariant. For dimers with the latter boundary conditions it has been argued [83,84] that the system is best described as a logarithmic Conformal Field Theory (CFT) with central charge $c = -2$ rather than the $c = 1$ Gaussian free field usually associated [62,79,80] with dimers and the six-vertex model at the free fermion point.

The six-vertex model [34–39, 161] is a ferroelectric model on the square lattice that is Yang-Baxter integrable [31]. Provided that the free-fermion condition (3.2.2) is satisfied, the six-vertex model reduces to a non-interacting free-fermion model [40, 41, 162]. It is well-known that the six-vertex free-fermion and dimer models are related, at least at the level of configurations. In fact, a one-to-many mapping exists [46, 61, 69] from six-vertex configurations to dimer configurations, where the dimers are rotated by 45° compared to their usual orientation parallel to the bonds of the square lattice. As shown in Figure 3.3, in this orientation, each dimer covers two sites of the medial lattice whose sites consist of midpoints of the bonds of the original square lattice. For an $M \times N$ square lattice with periodic boundary conditions, there are thus $2MN$ sites on the medial lattice covered by MN dimers.

In this chapter, we provide the exact solution of the anisotropic dimer model on the square lattice for dimers with the 45° rotated orientation. This is achieved by considering the dimer model as a free-fermion Yang-Baxter integrable six-vertex model and solving the associated inversion identity [31, 162, 163] satisfied by the transfer matrices. In this setting, we calculate the partition function at the isotropic point to obtain explicit formulas for the counting of dimer configurations on a *finite* $M \times N$ periodic square lattice. By using periodic boundary conditions on the cylinder which folds into a torus after taking a matrix trace, we calculate the modular invariant partition function (MIPF). Notably, the MIPF of dimers precisely agrees with symplectic fermions [121,164–166] and critical dense polymers [124,167–170]. The latter is nontrivial because, as a special six-vertex model, the usual matrix trace is used to close the cylinder to a torus for the dimer model whereas a modi-

fied trace [170] is needed for critical dense polymers. Remarkably, we find that the spectra of dimers agrees sector-by-sector with the spectra of critical dense polymers. However, an important difference with periodic boundary conditions is that the transfer matrix of critical dense polymers exhibits Jordan cells [169, 171] on the cylinder whereas the transfer matrix of dimers (six-vertex free-fermion model) is normal and diagonalizable so it does not exhibit Jordan cells. The similarity of the conformal spectra of these two models is a crucial observation because it hints to a possible logarithmic behaviour of dimers in the continuum scaling limit. This problem will be addressed more fully in the next chapter.

The layout of this chapter is as follows. In Section 3.2 we describe the dimer model, with dimers rotated by 45°, as a free-fermion six-vertex model and give the equivalence of the face tiles in the vertex, particle and dimer representations. We also describe the relations between the free-fermion algebra, the Temperley-Lieb algebra and the Yang-Baxter equation. We end this section by showing that the residual entropy is not changed by rotating the orientation of the dimers and agrees with the known result [157]. In Section 3.3, we introduce the periodic row transfer matrices and show that the associated dimer Hamiltonian reduces to the usual free-fermion hopping Hamiltonian. In this section, we also obtain the exact eigenvalues of the transfer matrices on finite cylinders. Following closely [169], we calculate the finite-size spectra in the $\mathbb{Z}_4$, Ramond and Neveu-Schwarz sectors. The N even sectors are combined to show that the MIPF is that of symplectic fermions [121, 164–166]. This completes the CFT description of dimers on the torus. Next, in Section 3.4, we consider the isotropic point and obtain explicit formulas for the counting of rotated dimer configurations on a periodic $M \times N$ square lattice. Although it displays the same asymptotic growth, the precise counting of these configurations differs from the counting in the usual orientation [73, 82, 156].

3.2 Dimers as a Free-Fermion Six-Vertex Model

3.2.1 Face tiles and equivalence of vertex, particle and dimer representations

The allowed six-vertex (arrow conserving) face configurations and the equivalent tiles in the particle (even and odd rows) and dimer [69] representations are shown in Figure 3.1.

For N columns, the vertex (arrow) degrees of freedom $\sigma_j = \pm 1$ and the particle occupation numbers $a_j = \frac{1}{2}(1-\sigma_j) = 0, 1$ live on the medial lattice with $j = 1, 2, \ldots, N$. The Boltzmann weights of the six-vertex tiles are

$$a(u) = \rho \frac{\sin(\lambda - u)}{\sin \lambda}, \quad b(u) = \rho \frac{\sin u}{\sin \lambda}, \quad c_1(u) = \rho g, \quad c_2(u) = \frac{\rho}{g}, \qquad \lambda \in (0, \pi), \quad \rho \in \mathbb{R} \tag{3.2.1}$$

The spectral parameter u plays the role of spatial anisotropy with $u = \frac{\lambda}{2}$ being the isotropic point. Geometrically [172], varying u effectively distorts a square tile into a rhombus with an opening anisotropy angle $\vartheta = \frac{\pi u}{\lambda}$. The arbitrary parameter ρ is an overall normalization. Assuming boundary conditions such that there are an equal number of sources and sinks of horizontal arrows (vertices c_1 and c_2) along any row, the transfer matrix entries (3.3.1) are all independent of the gauge factor g.

At the free-fermion point ($\lambda = \frac{\pi}{2}$), the six-vertex face weights reduce to

$$a(u) = \rho \cos u, \quad b(u) = \rho \sin u, \quad c_1(u) = \rho g, \quad c_2(u) = \frac{\rho}{g}, \qquad \rho \in \mathbb{R} \tag{3.2.2}$$

These weights satisfy the free-fermion condition

$$a(u)^2 + b(u)^2 = c_1(u) c_2(u) \tag{3.2.3}$$

As shown in Section 3.2.2, with the special choice of gauge $g = z = e^{iu}$, the tiles give a representation of the free-fermion algebra with generators $\{f_j, f_j^\dagger\}$ and, consequently, also a representation of the Temperley-Lieb algebra with generators $\{e_j\}$ and loop fugacity $\beta = 2\cos\lambda = 0$. Explicitly, the face transfer operators are

$$X_j(u) = \rho(\cos u \, I + \sin u \, e_j), \qquad j = 1, 2, \ldots, N \tag{3.2.4}$$

This Temperley-Lieb model is directly equivalent to an anisotropic dimer model as shown in Figures 3.1, 3.3 and 3.4. A dimer weight is assigned to the unique square face which is half-covered by the dimer as shown in Figure 3.4. The statistical weights assigned to

"horizontal" and "vertical" dimers are

$$\zeta_h(u) = a(u) = \rho \cos u, \qquad \zeta_v(u) = b(u) = \rho \sin u \tag{3.2.5}$$

Setting $g = \rho$, and allowing for the facts that (i) the c_1 face has two allowed configurations and (ii) no dimer covers the c_2 face, it follows that

$$c_1(u) = \zeta_h(u)^2 + \zeta_v(u)^2 = \rho^2(\cos^2 u + \sin^2 u) = \rho^2, \qquad c_2(u) = 1 \tag{3.2.6}$$

Alternatively, fixing $\rho = g = \sqrt{2}$ at the isotropic point ($u = \frac{\lambda}{2} = \frac{\pi}{4}$) gives

$$a(\tfrac{\pi}{4}) = 1, \qquad b(\tfrac{\pi}{4}) = 1, \qquad c_1(\tfrac{\pi}{4}) = 2, \qquad c_2(\tfrac{\pi}{4}) = 1 \tag{3.2.7}$$

It follows that, with this normalization and any gauge g, the partition function at the isotropic point gives the correct counting of distinct dimer configurations.

In addition to the vertex and dimer representations, the six-vertex free-fermion model admits a particle representation as shown in Figure 3.3. A reference state on the cylinder and strip is fixed as in Figure 3.2. An edge of a given vertex is a segment of a particle trajectory (and has particle occupation number $a_j = 1$) if its arrow points in the opposite direction to that of the reference state. Otherwise, if the edge arrow points in the same direction as the reference state, the edge is not a segment of a particle trajectory (and the particle occupation is $a_j = 0$). The segments of particle trajectories live on the medial lattice and are indicated with heavy lines in Figure 3.2. The number of particles is conserved and their trajectories are non-intersecting. On the cylinder (which is glued at the top and bottom to form the torus), the particle trajectories are constrained to move up and to the right through the lattice. The particle representation is the simplest of the three representations and is convenient for coding in Mathematica [150] and for manipulations in the diagrammatic planar algebra so we usually work in the particle representation.

With suitable face weights, the mapping between the six-vertex model, particle representation and dimers also holds for $\lambda \neq \frac{\pi}{2}$ and the model is still Yang-Baxter integrable. The difference is that, in the free-fermion case $\lambda = \frac{\pi}{2}$, the particles are non-

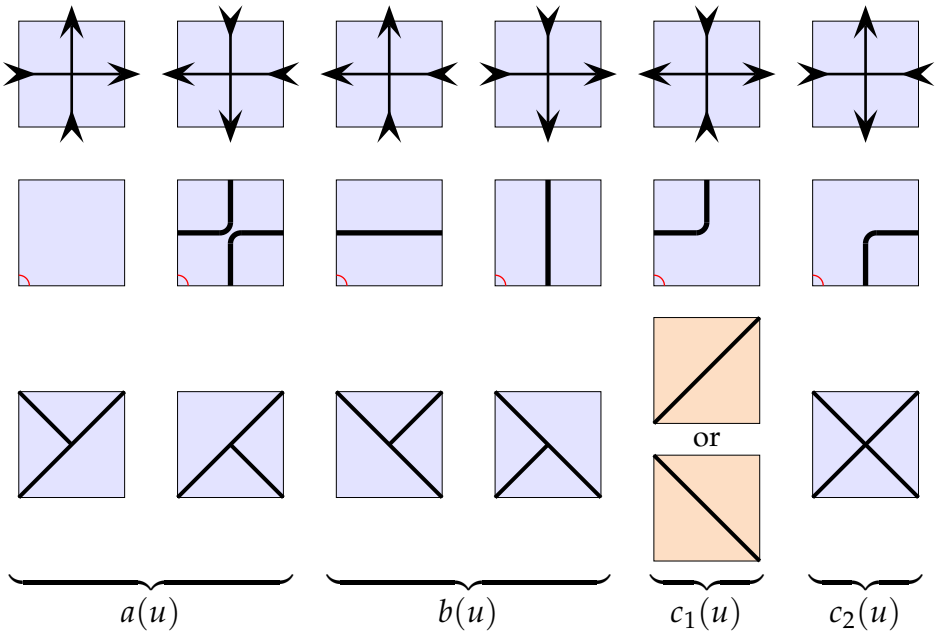

Figure 3.1: Equivalent face tiles of the six-vertex model in the vertex, particle and dimer representations.The heavy particle lines are drawn whenever the arrows disagree with the reference state as shown in Figure 3.2. The particles move up and to the right.

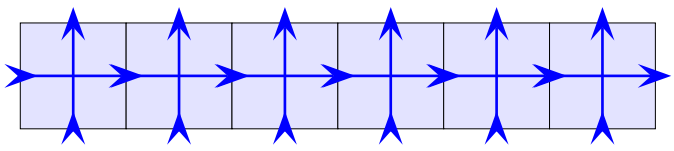

Figure 3.2: Reference states for the single row transfer matrix for mapping onto the particle representation. The reference arrows point up and to the right.

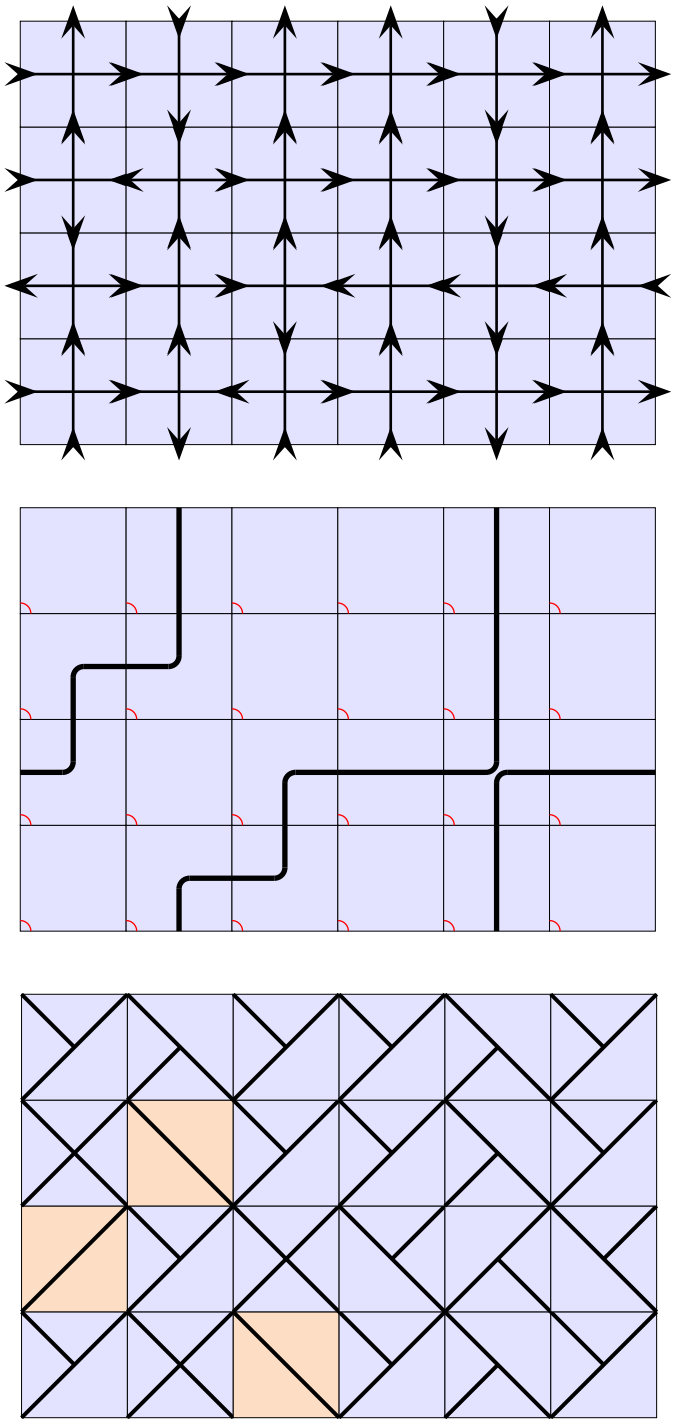

Figure 3.3: Typical periodic arrow configuration on a 6×4 rectangle corresponding to four applications of the single row transfer matrix. The associated particle and (one of the $2^3 = 8$) possible periodic dimer configurations are also shown. The boundary conditions are periodic such that the left/right edges and top/bottom edges are identified. The excess of up arrows over down arrows (2 in this case) is conserved. Particles travel up and to the right. They can wind around the torus but do not cross. An $M \times N$ square lattice is covered by MN dimers. Each dimer covers two adjacent sites of the medial lattice.

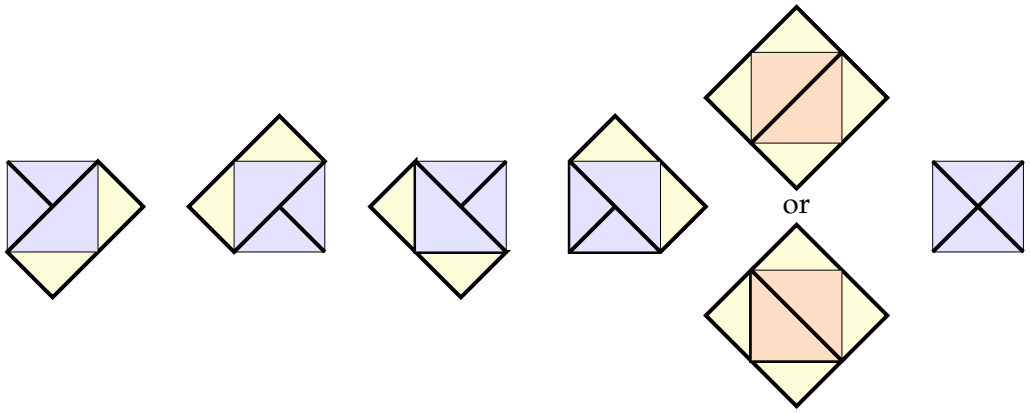

Figure 3.4: Face configurations showing (in light yellow) the one or two dimers associated with each face. No dimers are associated with the last face.

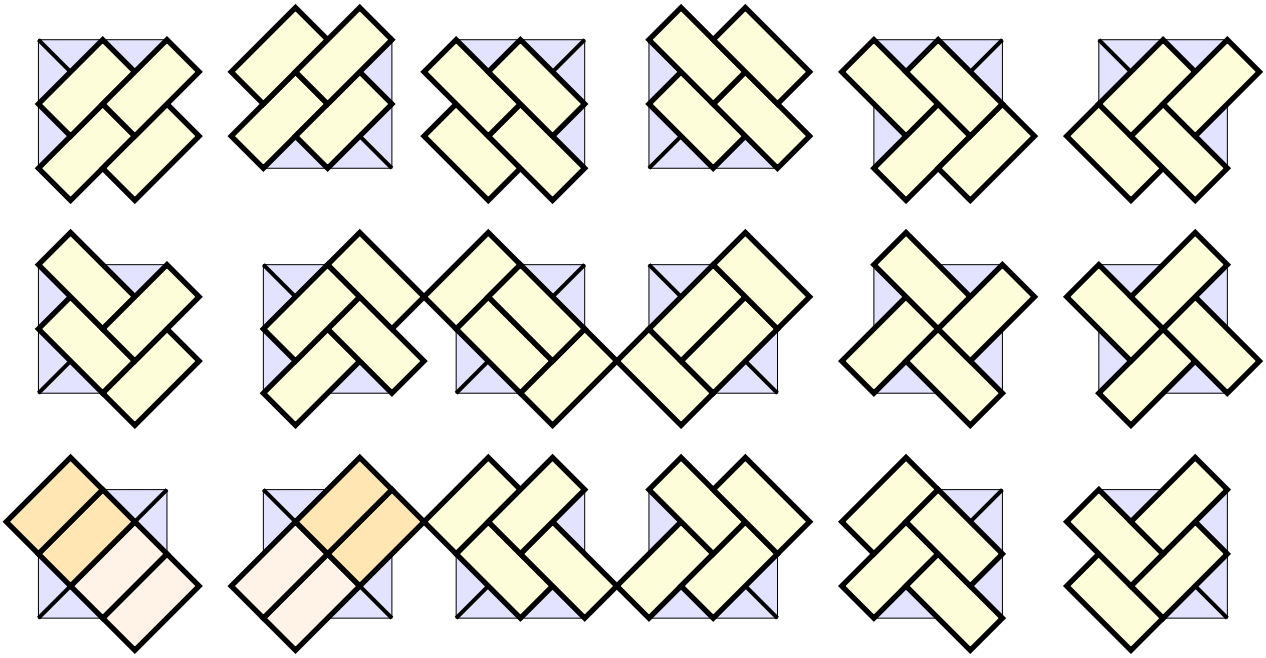

Figure 3.5: The 24 periodic configurations of rotated dimers on 2×2 square lattice. Each of the apricot shaded blocks of two dimers can occur in 2 local configurations related by a rotation through 90°.

interacting whereas, for $\lambda \neq \frac{\pi}{2}$, the particles interact. In terms of dimers, for $\lambda \neq \frac{\pi}{2}$, there are anisotropic 3-dimer interactions for the faces of vertices 1 through 4. In general, for $\lambda = \frac{(p'-p)\pi}{p'}$ with p, p' coprime, the (non-intersecting) fermion particle trajectories play the role of nonlocal degrees of freedom in these logarithmic Conformal Field Theories (CFTs). The $\mathbb{Z}_2$ arrow reversal symmetry of the vertex model implies a particle-hole duality in the particle representation.

3.2.2 Free-fermion, Temperley-Lieb algebras and Yang-Baxter equation

In this section, we consider the free-fermion model (3.2.2) with $\lambda = \frac{\pi}{2}$ and set $g = z = e^{iu}$ and $\rho = 1$. The overall normalization $\rho = \sqrt{2}$ is easily reinstated, as needed, to count dimer configurations at the isotropic point ($u = \frac{\pi}{4}$).

Free-fermion algebra

As elements of a planar algebra [173], the face operators of the free-fermion six-vertex model decompose [174] in the particle representation into a sum of contributions from six elementary tiles

$X_j(u) =$ 

$= a(u)\Big($  $+$  $\Big) + b(u)\Big($  $+$  $\Big) + c_1(u)$  $+ c_2(u)$  (3.2.8)

Multiplication of the tiles in the planar algebra is given by local tensor contraction of indices ($a, b, c, \ldots = 0, 1$) specifying the particle occupation numbers on the centers of the tile edges. Regarding the elementary tiles as operators acting on an upper (zigzag) row particle configuration to produce a lower (zigzag) row particle configuration, we write them respectively as

$$E_j = n_j^{00},\ n_j^{11},\ f_j^\dagger f_{j+1},\ f_{j+1}^\dagger f_j,\ n_j^{10},\ n_j^{01}, \qquad n_j^{00} + n_j^{11} + n_j^{10} + n_j^{01} = I \tag{3.2.9}$$

The four operators n_j^{ab} are (diagonal) orthogonal projection operators which factorize into single-site orthogonal projectors corresponding to left and right half (triangular) tiles

$$n_j^{ab} = n_j^a n_{j+1}^b, \qquad n_j^a n_j^b = \delta_{ab}\, n_j^a, \qquad n_j^0 + n_j^1 = I, \qquad a, b = 0, 1 \tag{3.2.10}$$

Here $n_j = n_j^1$ is the number operator counting single-site occupancy at position j and n_j^0 is the dual number operator counting the single-site vacancies at position j. The operators f_j and $f_j^\dagger$ are single-site particle annihilation and creation operators respectively which satisfy the Canonical Anticommutation Relations (CAR) for fermions

$$\{f_j, f_k\} = \{f_j^\dagger, f_k^\dagger\} = 0, \qquad \{f_j, f_k^\dagger\} = \delta_{jk}, \qquad n_j^1 = f_j^\dagger f_j, \qquad n_j^0 = f_j f_j^\dagger = 1 - f_j^\dagger f_j \tag{3.2.11}$$

It follows that all of the elementary tile operators can be written as combinations of bilinears in the fermion operators f_j and $f_j^\dagger$. Diagrammatically, the particle hopping terms $f_j^\dagger f_{j+1}$ and $f_{j+1}^\dagger f_j$ factorize into left and right half (triangular) tiles

$f_j^\dagger f_{j+1} =$  $f_{j+1}^\dagger f_j =$  (3.2.12)

so that the fermion generators are represented by half (triangular) tiles

$f_j^\dagger =$ 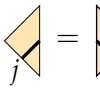 $=$  $, \qquad f_j =$ 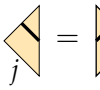 $=$  (3.2.13)

The action of the fermion operators (3.2.13) on states is given by

$$f_j^\dagger \big| \cdots, n_{j-1}, n_j, n_{j+1}, \cdots \big\rangle = (-1)^{\sum_{1\le k<j} n_k} (1 - n_j) \big| \cdots, n_{j-1}, (1 - n_j), n_{j+1}, \cdots \big\rangle \tag{3.2.14}$$

$$f_j \big| \cdots, n_{j-1}, n_j, n_{j+1}, \cdots \big\rangle = (-1)^{\sum_{1\le k<j} n_k}\, n_j \big| \cdots, n_{j-1}, (1 - n_j), n_{j+1}, \cdots \big\rangle \tag{3.2.15}$$

The presence of the "Jordan-Wigner string" $(-1)^{\sum_{1\le k<j} n_k}$ ensures the complete antisymmetry of the states and reflects the non-locality of the fermion operators. Notice that a particle

can only hop into a site that is vacant and that the action of the hopping terms on states is

$$f_j^\dagger f_{j+1} \big| \cdots, n_{j-1}, 0, 1, n_{j+2}, \cdots \big\rangle = \big| \cdots, n_{j-1}, 1, 0, n_{j+2}, \cdots \big\rangle \tag{3.2.16}$$

$$f_{j+1}^\dagger f_j \big| \cdots, n_{j-1}, 1, 0, n_{j+2}, \cdots \big\rangle = \big| \cdots, n_{j-1}, 0, 1, n_{j+2}, \cdots \big\rangle \tag{3.2.17}$$

since the contributions from the Jordan-Wigner strings cancel. This action applies for both open and periodic boundary conditions with the cyclic boundary condition $f_{j+N} = f_j$ on the fermions. Although the Jordan-Wigner strings seem to break translation invariance for periodic boundary conditions, this invariance is restored [162] for operators composed of an even number of fermion operators.

Temperley-Lieb algebra

To realise a Temperley-Lieb algebra, let us introduce $x = e^{i\lambda} = i$ and the generators

$e_j =$ 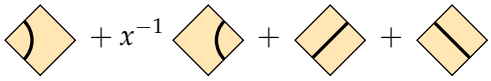 (3.2.18a)

$$= x f_j^\dagger f_j (1 - f_{j+1}^\dagger f_{j+1}) + x^{-1}(1 - f_j^\dagger f_j) f_{j+1}^\dagger f_{j+1} + f_j^\dagger f_{j+1} + f_{j+1}^\dagger f_j \tag{3.2.18b}$$

$$= x f_j^\dagger f_j + x^{-1} f_{j+1}^\dagger f_{j+1} + f_j^\dagger f_{j+1} + f_{j+1}^\dagger f_j \tag{3.2.18c}$$

The quartic (interacting) terms vanish, since $\beta = x + x^{-1} = 0$, leaving bilinears in fermion operators. Using the planar algebra of tiles, it is easily shown that these operators yield a representation of the Temperley-Lieb algebra [175]

$$e_j^2 = \beta e_j = 0, \qquad e_j e_{j\pm1} e_j = e_j, \qquad \beta = 2\cos\lambda = x + x^{-1} = 0 \tag{3.2.19}$$

Equivalently this follows, purely from fermionic algebra, by writing the generators in terms of the fermionic operators f_j and $f_j^\dagger$ as in (3.2.18c).

Yang-Baxter equation

Using the above algebra, it is straightforward to confirm that, in the gauge with $g = z = e^{iu}$, the face transfer operators (4.3.2) of the free-fermion six vertex model now take the form

$$X_j(u) = \quad = \cos u\, I + \sin u\, e_j \tag{3.2.20}$$

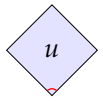

It immediately follows, from standard arguments [52], that they satisfy the Yang-Baxter Equation (YBE)

$$X_j(u)X_{j+1}(u+v)X_j(v) = X_{j+1}(v)X_j(u+v)X_{j+1}(u) \tag{3.2.21a}$$

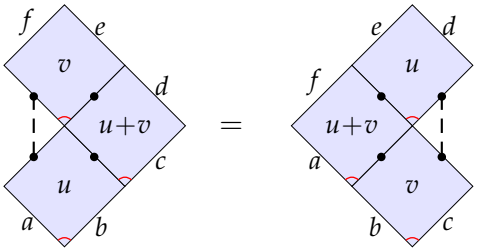

(3.2.21b)

The initial condition and inversion relation are

$$X_j(0) = I, \qquad X_j(u)X_j(-u) = \cos^2 u\, I \tag{3.2.22}$$

In the usual vertex model terminology, $X_j(u)$ is the $\check{R}$-matrix and not the R-matrix.

3.2.3 Free energy and residual entropy

Since the free-fermion six-vertex model is Yang-Baxter integrable, its partition function per site

$$\rho\,\kappa(u) = \rho \exp(-f_{\text{bulk}}(u)) \tag{3.2.23}$$

can be obtained by solving [52] the inversion relation $\kappa(u)\kappa(-u) = \cos^2 u$ or by using Euler-Maclaurin approach as in [124]. The two equivalent integrals for the bulk free energy

are

$$f_{\rm bulk}(u) = -\int_{-\infty}^{\infty} \frac{\sinh ut \sinh(\frac{\pi}{2}-u)t}{t \sinh \pi t \cosh \frac{\pi t}{2}}\, dt = \tfrac{1}{2}\log 2 - \frac{1}{\pi}\int_0^{\pi/2} \log(\operatorname{cosec} t + \sin 2u)dt \tag{3.2.24}$$

Setting $\rho = \sqrt{2}$ and $u = \frac{\pi}{4}$ gives the known [157] molecular freedom W and residual entropy S of dimers on the square lattice as

$$W = e^S = \sqrt{2}\exp(-f_{\rm bulk}(\tfrac{\pi}{4})) = \exp(\tfrac{2G}{\pi}) = 1.791\,622\,812\ldots, \qquad S = \tfrac{2G}{\pi} = .583\,121\,808\ldots \tag{3.2.25}$$

where the molecular freedom W and Catalan's constant G are given by

$$W = \sqrt{2}\,\kappa(\tfrac{\pi}{4}) = \lim_{M,N\to\infty} (Z_{M\times N})^{\frac{1}{MN}}, \qquad G = \tfrac{1}{2}\int_0^{\pi/2} \log(1+\operatorname{cosec} t)dt = .915\,965\,594\ldots \tag{3.2.26}$$

3.3 Solution on a Cylinder and Torus and Finite-Size Spectra

3.3.1 Commuting single row transfer matrices

The single row transfer matrix of the free-fermion model in the particle representation is defined by

$\boldsymbol{T}(u) =$ 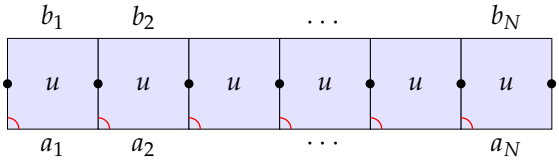

(3.3.1)

where there are N columns and the left and right edges are identified. The occupation numbers on the vertical edges (auxiliary space) are summed out. The quantum space consists of 2^N row configurations $\boldsymbol{a} = \{a_1, a_2, \ldots, a_N\}$ of particle occupation numbers. The Yang-Baxter equation (4.3.18) implies [31] that the single row transfer matrices commute

$$[\boldsymbol{T}(u), \boldsymbol{T}(v)] = 0 \tag{3.3.2}$$

From the crossing relation and commutation, it follows that the transfer matrices are normal

$$\boldsymbol{T}(u)^T = \boldsymbol{T}(\lambda - u) \quad \Rightarrow \quad [\boldsymbol{T}(u), \boldsymbol{T}(u)^T] = 0 \tag{3.3.3}$$

The transfer matrices are therefore simultaneously diagonalizable by a similarity transformation with a matrix $\boldsymbol{S}$ whose columns are the common u-independent right eigenvectors of $\boldsymbol{T}(u)$.

In the six-vertex arrow (or spin) representation, the total magnetization

$$S_z = \sum_{j=1}^{N} \sigma_j = -N, -N+2, \ldots, N-2, N \tag{3.3.4}$$

is conserved under the action of the transfer matrix. The magnetization S_z is thus a good quantum number separating the spectrum into sectors. For dimers, it therefore plays the role of the variation index in [76,85,87]. By the $\mathbb{Z}_2$ up-down symmetry, the spectrum for the sectors $S_z = m$ and $S_z = -m$ coincide for $m > 0$. So all these eigenvalues are exactly doubly degenerate. We will see that, for N even, the lowest energy (ground) state is unique and occurs in the sector $S_z = 0$ so that there are $\frac{1}{2}N$ up arrows (spins) and $\frac{1}{2}N$ down arrows (spins). More generally, the number of down spins is $d = \frac{1}{2}(N - S_z)$, the number of up spins is thus $N - d = \frac{1}{2}(N + S_z)$ and the counting of states in the S_z sector is given by the binomial $\binom{N}{d}$ with $S_z = N \bmod 2$. The number of particles $d = \sum_{j=1}^{N} a_j$ coincides with the number of down arrows and is also conserved. The transfer matrix and vector space of states thus decompose as

$$\boldsymbol{T}(u) = \bigoplus_{d=0}^{N} \boldsymbol{T}_d(u), \quad \dim \mathcal{V}^{(N)} = \sum_{d=0}^{N} \dim \mathcal{V}_d^{(N)} = \sum_{d=0}^{N} \binom{N}{d} = 2^N = \dim (\mathbb{C}^2)^{\otimes N} \tag{3.3.5}$$

Comparing the spectra sector-by-sector with critical dense polymers [169] gives a precise matching if the number of defects ℓ is identified as

$$\ell = |N - 2d| = |S_z| = \begin{cases} 0, 2, 4, \ldots, N, & N \text{ even} \\ 1, 3, 5, \ldots, N, & N \text{ odd} \end{cases} \tag{3.3.6}$$

Taking the logarithmic derivative of the single row transfer matrix (3.3.1) gives the Hermitian free-fermion Hamilitonian

$$\mathcal{H} = -\sum_{j=1}^{N} e_j = -\sum_{j=1}^{N} (x f_j^\dagger f_j + x^{-1} f_{j+1}^\dagger f_{j+1} + f_j^\dagger f_{j+1} + f_{j+1}^\dagger f_j) \tag{3.3.7a}$$

$$= -\sum_{j=1}^{N} (f_j^\dagger f_{j+1} + f_{j+1}^\dagger f_j) \tag{3.3.7b}$$

Using $\beta = x + x^{-1} = 0$ and cyclic symmetry, the first two fermionic terms cancel leaving the expected free-fermion hopping Hamiltonian. Since the Hamiltonian is a quadratic form in fermi operators it can be diagonalized by standard free-fermion techniques. Here we diagonalize the transfer matrices using inversion identities to make clear the relation to critical dense polymers. The methods we use, based on Yang-Baxter integrability, functional equations and physical combinatorics, are more general and can also be applied to percolation [176] and to the six-vertex model at other roots of unity.

3.3.2 Inversion identities on the cylinder

The inversion identities for the single row transfer matrix of the free-fermion six vertex model with periodic boundary conditions are

$$\boldsymbol{T}(u)\boldsymbol{T}(u+\lambda) = \big(\cos^{2N} u - \sin^{2N} u\big) I, \qquad N \text{ odd} \tag{3.3.8a}$$

$$\begin{aligned} \boldsymbol{T}_d(u)\boldsymbol{T}_d(u+\lambda) &= \big(\cos^{2N} u + \sin^{2N} u + 2(-1)^d \sin^N u \cos^N u\big) I \\ &= (\cos^N u + (-1)^{(N-\ell)/2} \sin^N u)^2 I, \qquad N \text{ even} \end{aligned} \tag{3.3.8b}$$

These are specializations of the elliptic inversion identities [162] of the eight-vertex free-fermion model. The derivation following [162] is given in Appendix B.1. For N even, the inversion identity is different in the sectors with even and odd parity for d. Alternatively, these inversion identities can be written as

$$\boldsymbol{T}(u)\boldsymbol{T}(u+\lambda) = \big(\cos^{2N} u + (-1)^N \sin^{2N} u\big) I + (\sin u \cos u)^N J \tag{3.3.9}$$

where $J = 0$ for N odd and, for N even, J is a diagonal matrix with entries ± 2 alternating in the different d sectors. The commuting transfer matrices $\boldsymbol{T}(u)$ admit a common set of right eigenvectors independent of u. They can therefore be simultaneously diagonalized by a similarity transformation. It therefore follows that the inversion identities are satisfied by the individual eigenvalues.

As in the case of critical dense polymers, J is related to the braid transfer matrices $\boldsymbol{B}^+$ and its inverse $\boldsymbol{B}^-$ by

$$\boldsymbol{B}^{\pm} = \lim_{u \to \pm i\infty} \frac{\boldsymbol{T}(u)}{\sin^N(u + \lambda/2)}, \qquad (\boldsymbol{B}^{\pm})^2 = \begin{cases} 2I + (-1)^{N/2} J, & N \text{ even} \\ 2I, & N \text{ odd} \end{cases} \tag{3.3.10}$$

3.3.3 Exact eigenvalues

The inversion identities (3.3.8a) and (3.3.8b), for N odd and N even, precisely coincide with the N odd and N even inversion identities of critical dense polymers [169]. In the rest of Section 3, we summarize the solution of these inversion identities and the relevant results of [169]. From the Temperley-Lieb equivalence, it is expected that the spectra of the free-fermion six-vertex model and critical dense polymers agree up to the possibility of different degeneracies. The new content of the following subsections is that we find empirically that the spectra of these two models precisely coincide sector-by-sector as matched by the identification (3.3.6) of the number of defects ℓ of critical dense polymers with $|S_z|$. In particular, the central charge $c = -2$ and conformal weights $\Delta = -\frac{1}{8}, 0, \frac{3}{8}$ of dimers are given by the same calculations using the Euler-Maclaurin formula carried out previously for critical dense polymers so we do not repeat these calculations.

For N and $\ell = |S_z|$ even, the transfer matrix eigenvalue spectra breaks up into Ramond and Neveu-Schwarz sectors according to the even or odd parity of $\ell/2 = |S_z|/2$. As in (5.24) and (5.25) of [169], the eigenvalues $T(u)$ factor into elementary contributions arising from zeros in the complex u-plane in the form of single or double 1-strings on the line

Re $u = \frac{\pi}{4}$ at ordinates

$$y_j = \begin{cases} -\frac{1}{2}\log\tan\frac{\frac{1}{2}(j-\frac{1}{2})\pi}{N}, & \mathbb{Z}_4\text{: } N,\ell \text{ odd}, \quad j = 1,2,\ldots,N \\ -\frac{1}{2}\log\tan\frac{(j-\frac{1}{2})\pi}{N}, & \text{R: } N,\ell/2 \text{ even}, \quad j = 1,2,\ldots,N/2 \\ -\frac{1}{2}\log\tan\frac{j\pi}{N}, & \text{NS: } N \text{ even}, \ell/2 \text{ odd}, \quad j = 1,2,\ldots,N/2-1 \end{cases} \tag{3.3.11}$$

A typical pattern of zeros is shown in Figure 3.6. From [169], the elementary excitation energy of a single 1-string at position j in the upper or lower half plane is

$$E_j = \begin{cases} \frac{1}{2}(j-\frac{1}{2}), & \mathbb{Z}_4\text{: } N,\ell \text{ odd} \\ j-\frac{1}{2}, & \text{R: } N,\ell/2 \text{ even} \\ j, & \text{NS: } N \text{ even}, \ell/2 \text{ odd} \end{cases} \tag{3.3.12}$$

For N odd, the contributions from 1-strings in each half-plane are encoded in one-column diagrams as shown in Figures 3.7 and 3.8. For N even, the contributions from the single or double 1-strings in each half-plane are encoded in double-column diagrams as shown in Figures 3.9–3.12. Each column of a two-column diagram has a 0- or 1-string at a given position or height, labelled by j. These combine to encode no 1-string, a single 1-string or a double 1-string at each height j or position (3.3.11) in the pattern of zeros. By convention, zeros on the real u-axis are regarded as being in the upper half plane.

Explicitly, as shown in [169, 170], the solution of the inversion identity (3.3.8b) by factorization of the eigenvalues yields

$$T(u) = \epsilon\,\frac{(-i)^{N/2}e^{-Niu}}{2^{N-1/2}}\prod_{j=1}^{N}\Big(e^{2iu} + i\epsilon_j\tan\frac{(2j-1)\pi}{4N}\Big), \quad \mathbb{Z}_4\text{: } N,\ell \text{ odd} \tag{3.3.13a}$$

$$T(u) = \frac{\epsilon(-i)^{\frac{N}{2}}e^{-Niu}}{2^{N-1}}\prod_{j=1}^{N}\Big(e^{2iu} + i\epsilon_j\tan\frac{(2j-1)\pi}{2N}\Big), \quad \text{R: } N,\ell/2 \text{ even} \tag{3.3.13b}$$

$$T(u) = \frac{\epsilon(-i)^{\frac{N}{2}}Ne^{-Niu}}{2^{N-1}}\prod_{\substack{j=1\\ j\neq N/2}}^{N}\Big(e^{2iu} + i\epsilon_j\tan\frac{j\pi}{N}\Big), \quad \text{NS: } N \text{ even}, \ell/2 \text{ odd} \tag{3.3.13c}$$

where $\epsilon_j = \pm 1$. The overall sign $\epsilon = \pm 1$ of each eigenvalue is not fixed by the inversion

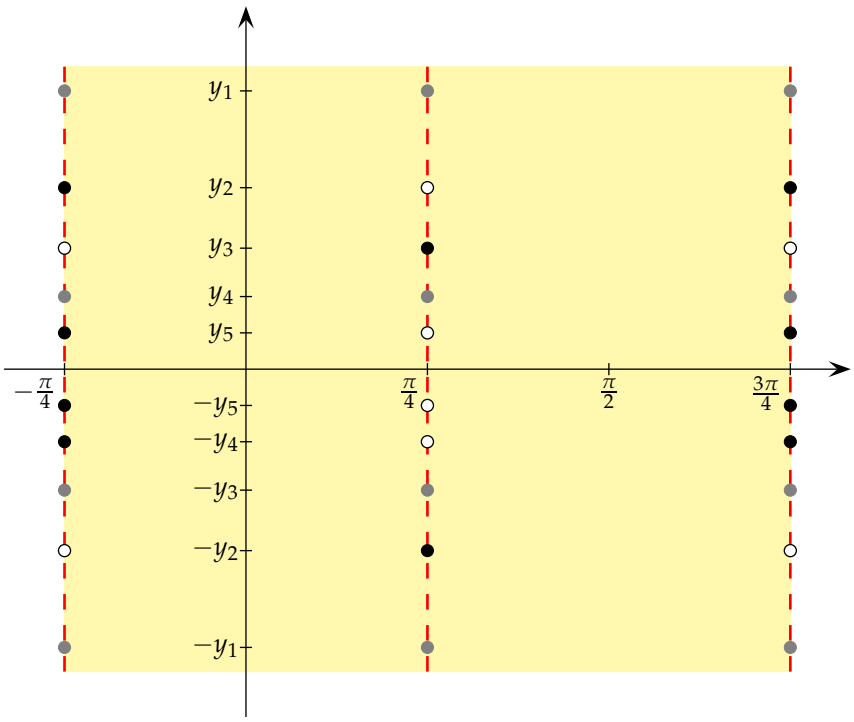

Figure 3.6: A typical pattern of zeros in the complex u-plane for the ℓ even sectors. Here, $N = 12$ and $\ell = |S_z| = 2$. The ordinates of the locations of the zeros u_j are $y_j = -\frac{1}{2}\log\tan\frac{j\pi}{N}, j = 1, 2, \ldots, N/2 - 1$. At each position j, there is either two 1-strings with $\mathrm{Re}\, u_j = \pi/4$, two 2-strings with real parts $\mathrm{Re}\, u_j = -\pi/4, 3\pi/4$ or one 1-string and one 2-string. A double zero is indicated by a black circle, a single zero by a grey circle and an unoccupied position by an open circle.

relation. These sign factors ϵ are fixed by [170]

$$\epsilon = (-1)^{\frac{N-s}{4}}, \qquad \epsilon^{\mathrm{R}} = \epsilon^{\mathrm{NS}} = (-1)^{\left\lfloor \frac{|s|+2}{4} \right\rfloor}, \qquad s = S_z \tag{3.3.14}$$

Separating the zeros in the upper and lower half planes leads to

$$T(u) = \frac{\mu\,(-i)^{N/2}}{2^{N-1/2}e^{Niu}} \prod_{j=1}^{\frac{N+1}{2}} \Big(e^{2iu} + i\epsilon_j \tan\frac{(2j-1)\pi}{4N}\Big) \prod_{j=1}^{\frac{N-1}{2}} \Big(\bar{\epsilon}_j e^{2iu} + i\cot\frac{(2j-1)\pi}{4N}\Big), \quad \mathbb{Z}_4\text{: } N, \ell \text{ odd} \tag{3.3.15a}$$

$$\begin{aligned} T(u) \;=\; & \frac{\mu(-i)^{\frac{N}{2}}e^{-Niu}}{2^{N-1}} \prod_{j=1}^{\lfloor (N+2)/4 \rfloor} \Big(e^{2iu} + i\epsilon_j \tan\frac{(2j-1)\pi}{2N}\Big)\Big(\bar{\epsilon}_j e^{2iu} + i\cot\frac{(2j-1)\pi}{2N}\Big) \\ & \times \prod_{j=1}^{\lfloor N/4 \rfloor} \Big(e^{2iu} + i\mu_j \tan\frac{(2j-1)\pi}{2N}\Big)\Big(\bar{\mu}_j e^{2iu} + i\cot\frac{(2j-1)\pi}{2N}\Big), \qquad \text{R: } N, \ell/2 \text{ even} \end{aligned} \tag{3.3.15b}$$

$$\begin{aligned} T(u) \;=\; & \frac{\mu(-i)^{\frac{N-2}{2}}Ne^{(2-N)iu}}{2^{N-1}} \prod_{j=1}^{\lfloor N/4 \rfloor} \Big(e^{2iu} + i\epsilon_j \tan\frac{j\pi}{N}\Big)\Big(\bar{\epsilon}_j e^{2iu} + i\cot\frac{j\pi}{N}\Big) \\ & \times \prod_{j=1}^{\lfloor (N-2)/4 \rfloor} \Big(e^{2iu} + i\mu_j \tan\frac{j\pi}{N}\Big)\Big(\bar{\mu}_j e^{2iu} + i\cot\frac{j\pi}{N}\Big), \qquad \text{NS: } N \text{ even}, \ell/2 \text{ odd} \end{aligned} \tag{3.3.15c}$$

where $\mu, \epsilon_j, \bar{\epsilon}_j, \mu_j, \bar{\mu}_j = \pm 1$. Up to the overall choice of sign μ, there are either 2^N or 2^{N-2} possible eigenvalues allowing for all excitations but they are not all physical and are subject to selection rules. The number of 1-strings m_j plus the number of 2-strings n_j at any given position is

$$m_j + n_j = \begin{cases} 1, & \mathbb{Z}_4 \\ 2, & \text{R, NS} \end{cases} \tag{3.3.16}$$

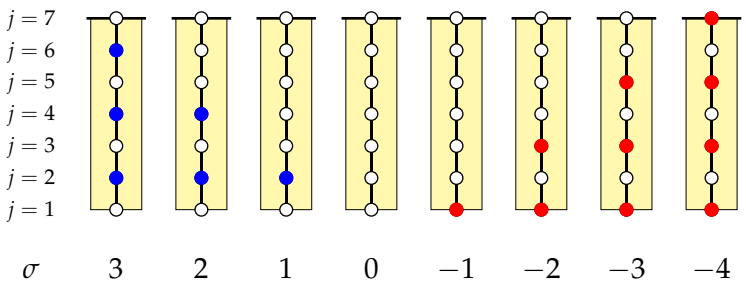

Figure 3.7: $\mathbb{Z}_4$ sectors (N, ℓ odd): Minimal configurations of single-columns with energy $E(\sigma) = \frac{1}{2}\sigma(\sigma+\frac{1}{2})$. The quantum number $\sigma = \lfloor n/2 \rfloor - m$ is given by the excess of blue (even j) over red (odd j) 1-strings. At each empty position j, there is a 2-string. This analyticity strip is in the upper-half complex u-plane rotated by 180°so that position $j = 1$ (furthest from the real axis) is at the bottom.

3.3.4 Patterns of zeros and selection rules

The combinatorial description of the spectra follows precisely as in [169]. The building blocks of the spectra in the upper half-plane consist of the "symplectic" q-binomials

$$\begin{bmatrix} n \\ m \end{bmatrix}_q = \begin{bmatrix} n \\ \lfloor n/2 \rfloor - \sigma \end{bmatrix}_q = \begin{cases} q^{-\frac{1}{2}\sigma(\sigma+\frac{1}{2})} \sum\limits_{\substack{\sigma\text{-single} \\ \text{columns}}} q^{\sum_j m_j E_j}, & \mathbb{Z}_4\text{: } N, \ell \text{ odd} \\ q^{-\frac{1}{2}\sigma^2} \sum\limits_{\substack{\sigma\text{-double} \\ \text{columns}}} q^{\sum_j m_j E_j}, & \text{R: } N, \ell/2 \text{ even} \\ q^{-\frac{1}{2}\sigma(\sigma+1)} \sum\limits_{\substack{\sigma\text{-double} \\ \text{columns}}} q^{\sum_j m_j E_j}, & \text{NS: } N \text{ even}, \ell/2 \text{ odd} \end{cases} \tag{3.3.17}$$

as shown in Figures 3.8, 3.10 and 3.12. For the one-column diagrams in the $\mathbb{Z}_4$ sectors, the excess σ of the number m_{even} of even 1-strings over the number m_{odd} of odd 1-strings is

$$\sigma = m_{\text{even}} - m_{\text{odd}} = \sum_{k=1}^{\lfloor n/2 \rfloor} m_{2k} - \sum_{k=1}^{\lfloor (n+1)/2 \rfloor} m_{2k-1}, \qquad \mathbb{Z}_4\text{: } N, \ell \text{ odd} \tag{3.3.18}$$

For R, NS sectors, the excess $\sigma = \lfloor n/2 \rfloor - m$ of the number of 1-strings in the right column minus the number of 1-strings in the left column of the double-column diagram is given

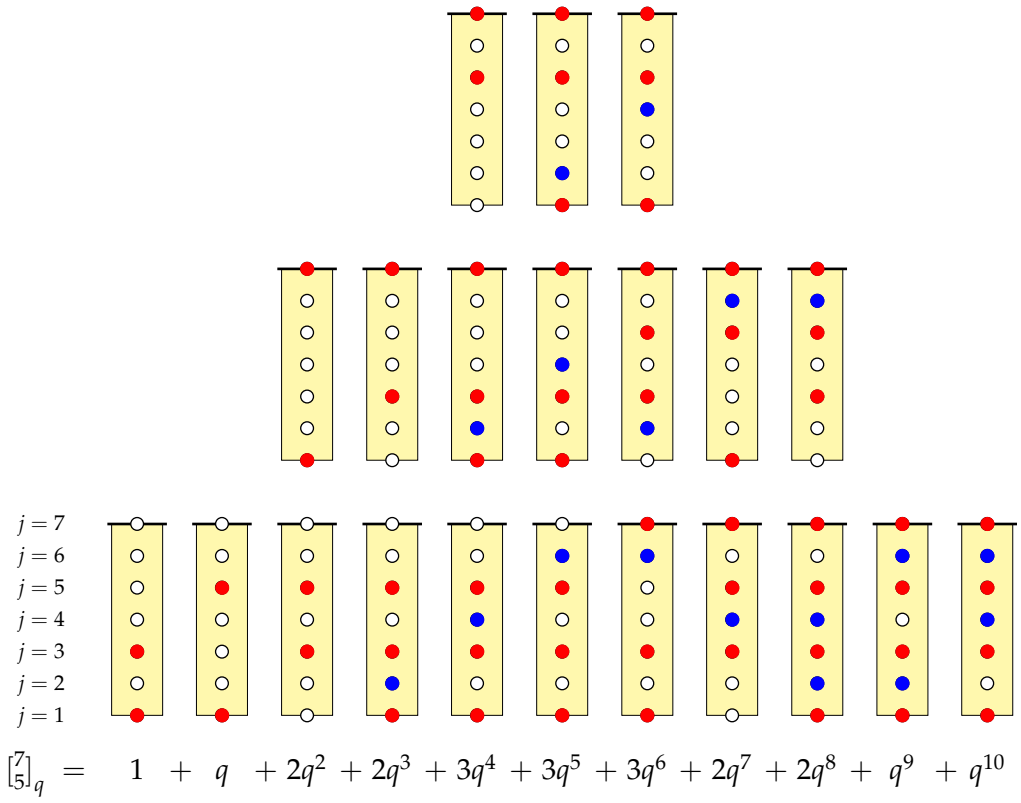

Figure 3.8: $\mathbb{Z}_4$ sectors (N, ℓ odd): Combinatorial enumeration by single-columns of the q-binomial $\begin{bmatrix}n\\m\end{bmatrix}_q = \begin{bmatrix}7\\5\end{bmatrix}_q = q^{-3/2}\sum q^{\sum_j m_j E_j}$. The excess of blue (even j) over red (odd j) 1-strings is given by the quantum number $\sigma = \lfloor n/2 \rfloor - m = -2$. The elementary excitation energy of a 1-string at position j is $E_j = \frac{1}{2}(j - \frac{1}{2})$. The lowest energy configuration has energy $E(\sigma) = 1/4 + 5/4 = 3/2 = \frac{1}{2}\sigma(\sigma + \frac{1}{2})$. At each empty position j, there is a 2-string. This analyticity strip is in the upper-half complex u-plane rotated by 180°so that position $j = 1$ (furthest from the real axis) is at the bottom. The elementary excitations (of energy 1) are generated by either inserting two 1-strings at positions $j = 1$ and $j = 2$ or promoting a 1-string at position j to position $j + 2$. Notice that $\begin{bmatrix}n\\m\end{bmatrix}_q = \begin{bmatrix}n\\n-m\end{bmatrix}_q$ as q-polynomials but they have different combinatorial interpretations because they have different quantum numbers σ. In the lower half-plane, q is replaced with $\bar{q}$ and no rotation is required. In this example, $\ell = 7$ and the value $\bar{\sigma} = -2$ of the quantum number in the lower half-plane is related to $\sigma = -2$ in the upper half-plane by the selection rules $\sigma + \bar{\sigma} = -(\ell + 1)/2$ and $\frac{1}{2}(\sigma - \bar{\sigma}) \in \mathbb{Z}$.

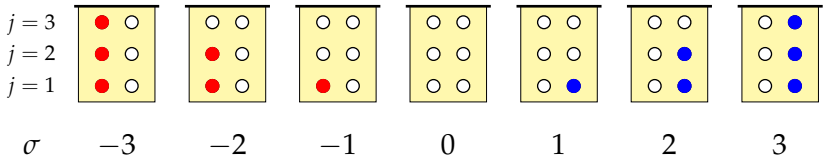

Figure 3.9: Ramond sectors (N even, $\ell/2$ even): Minimal configurations of double-columns with energy $E(\sigma) = \frac{1}{2}\sigma^2$. The quantum number $\sigma = \lfloor n/2 \rfloor - m$ is given by the excess of blue (right) over red (left) 1-strings. At each position j, the number of 1-strings m_j plus the number of 2-strings n_j is 2. This analyticity strip is in the upper-half complex u-plane rotated by 180°so that position $j = 1$ (furthest from the real axis) is at the bottom.

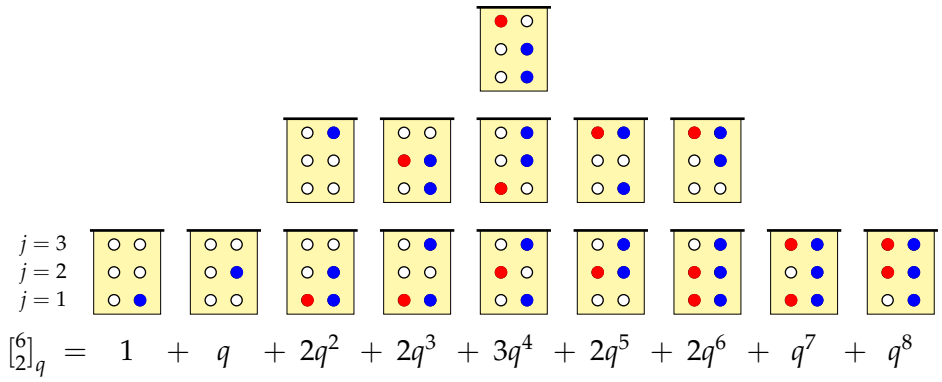

Figure 3.10: Ramond sectors (N even, $\ell/2$ even): Combinatorial enumeration by double-columns of the q-binomial $\begin{bmatrix} n \\ m \end{bmatrix}_q = \begin{bmatrix} 6 \\ 2 \end{bmatrix}_q = q^{-1/2} \sum q^{\sum_j m_j E_j}$. The excess of blue (right) over red (left) 1-strings is given by the quantum number $\sigma = \lfloor n/2 \rfloor - m = 1$. The elementary excitation energy of a 1-string at position j is $E_j = (j - \frac{1}{2})$. The lowest energy configuration has energy $E(\sigma) = \frac{1}{2}\sigma^2 = \frac{1}{2}$. At each position j, there are m_j 1-strings and $n_j = 2 - m_j$ 2-strings. This analyticity strip is in the upper-half complex u-plane rotated by 180°so that position $j = 1$ (furthest from the real axis) is at the bottom. The elementary excitations (of energy 1) are generated by either inserting a left-right pair of 1-strings at position $j = 1$ or promoting a 1-string at position j to position $j + 1$. Notice that $\begin{bmatrix} n \\ m \end{bmatrix}_q = \begin{bmatrix} n \\ n-m \end{bmatrix}_q$ as q-polynomials but they admit different combinatorial interpretations because they have different quantum numbers σ. In the lower half-plane, q is replaced with $\bar{q}$ and no rotation is required. The value $\bar{\sigma}$ of the quantum number in the lower half-plane is related to σ in the upper half-plane by the selection rules $\sigma + \bar{\sigma} = \ell/2$ and $\frac{1}{2}(\sigma - \bar{\sigma}) \in \mathbb{Z}$.

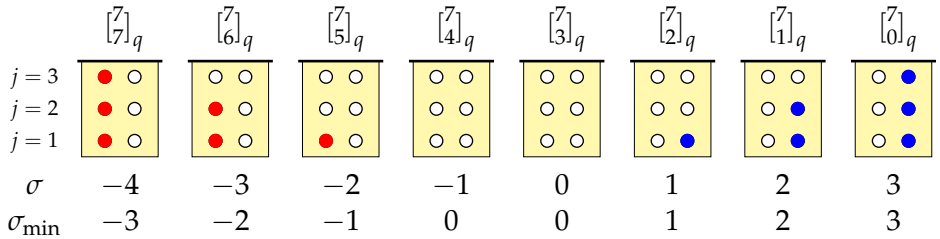

Figure 3.11: Neveu-Schwarz sectors (N even, $\ell/2$ odd): Minimal configurations of double-columns within the binomials $\begin{bmatrix}n\\m\end{bmatrix}_q = \begin{bmatrix}7\\m\end{bmatrix}_q$. The energy is $E(\sigma) = \frac{1}{2}\sigma(\sigma+1)$ where the quantum number is $\sigma = \lfloor n/2 \rfloor - m$. The excess of blue (right) over red (left) 1-strings in these minimal configurations is $\sigma_{\min}$ as given in (3.3.20). At each position j, the number of 1-strings m_j plus the number of 2-strings n_j is 2. This analyticity strip is in the upper-half complex u-plane rotated by 180°so that position $j = 1$ (furthest from the real axis) is at the bottom.

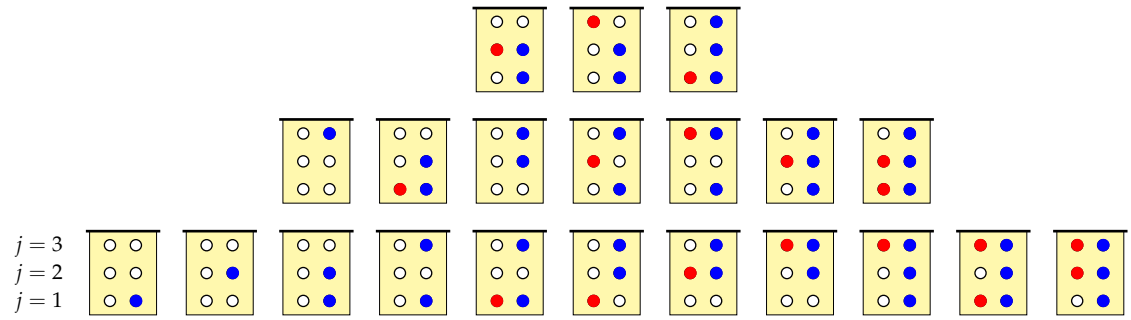

Figure 3.12: Neveu-Schwarz sectors (N even, $\ell/2$ odd): Combinatorial enumeration by double-columns of the q-binomial $\begin{bmatrix}n\\m\end{bmatrix}_q = \begin{bmatrix}7\\2\end{bmatrix}_q = q^{-1}\sum q^{\sum_j m_j E_j}$. The number of positions is $(n-1)/2 = 3$. The quantum number is $\sigma = \lfloor n/2 \rfloor - m = 1$. The excess of blue (right) over red (left) 1-strings is $\sigma = 1$ or $\sigma + 1 = 2$. The elementary excitation energy of a 1-string at position j is $E_j = j$. The lowest energy configuration has energy $E(\sigma) = \frac{1}{2}\sigma(\sigma+1) = 1$. At each position j, there are m_j 1-strings and $n_j = 2 - m_j$ 2-strings. This analyticity strip is in the upper-half complex u-plane rotated by 180°so that position $j = 1$ (furthest from the real axis) is at the bottom. The elementary excitations (of energy 1) are generated by either inserting a left or right 1-string at position $j = 1$ or promoting a 1-string at position j to position $j+1$. Notice that $\begin{bmatrix}n\\m\end{bmatrix}_q = \begin{bmatrix}n\\n-m\end{bmatrix}_q$ as q-polynomials but they admit different combinatorial interpretations because they have different quantum numbers σ and $\sigma' = -\sigma - 1$. In calculating σ', we have used the fact that n in (3.3.27) is odd. In the lower half-plane, q is replaced with $\bar{q}$ and no rotation is required. The value $\bar{\sigma}$ of the quantum number in the lower half-plane is related to σ in the upper half-plane by the selection rules $\sigma + \bar{\sigma} = (\ell - 2)/2$ and $\frac{1}{2}(\sigma - \bar{\sigma}) \in \mathbb{Z}$.

by

$$m_{\text{right}} - m_{\text{left}} = \begin{cases} \sigma, & \text{R: } \ell/2 \text{ even} \\ \sigma \text{ or } \sigma+1, & \text{NS: } \ell/2 \text{ odd} \end{cases} \tag{3.3.19}$$

The minimal configurations in the upper half-plane with energy $E(\sigma)$ are as shown in Figures 3.7, 3.9 and 3.11.

There are similar building blocks in the lower half-plane with σ replaced by $\bar{\sigma}$. In each half-plane, the *minimum* energy configurations satisfy

$$m_{\text{right}} - m_{\text{left}} = \sigma_{\text{min}} = \begin{cases} \sigma, & \sigma \geq 0 \\ \sigma+1, & \sigma < 0 \end{cases} \tag{3.3.20}$$

By convention, any zeros on the real u axis are pushed into the upper half plane. Empirically determined selection rules dictate that, in a sector with ℓ defects, the quantum numbers of the groundstate satisfy

$$\sigma = \bar{\sigma} = \begin{cases} (\ell-1)/4, & \ell = 1 \bmod 4, \quad \mathbb{Z}_4\text{: } N \text{ odd} \\ -(\ell+1)/4, & \ell = 3 \bmod 4, \quad \mathbb{Z}_4\text{: } N \text{ odd} \\ \ell/4, & \text{R: } \ell/2 \text{ even} \\ (\ell-2)/4, & \text{NS: } \ell/2 \text{ odd} \end{cases} \tag{3.3.21}$$

with $\ell = |4\sigma+1| = 1, 3, 5, 7, \ldots$ in the $\mathbb{Z}_4$ sectors. Similarly, it is found that all excitations satisfy the selection rules

$$\sigma + \bar{\sigma} = \begin{cases} \frac{1}{2}(\ell-1), & \ell = 1 \bmod 4 \\ -\frac{1}{2}(\ell+1), & \ell = 3 \bmod 4 \end{cases} \qquad \mathbb{Z}_4\text{: } N \text{ odd} \qquad \tfrac{1}{2}(\sigma - \bar{\sigma}) \in \mathbb{Z} \tag{3.3.22}$$

$$\sigma + \bar{\sigma} = \begin{cases} \ell/2, & \text{R: } \ell/2 \text{ even} \\ (\ell-2)/2, & \text{NS: } \ell/2 \text{ odd} \end{cases} \qquad \tfrac{1}{2}(\sigma - \bar{\sigma}) \in \mathbb{Z} \tag{3.3.23}$$

These selection rules hold [170] equally for critical dense polymers and the free-fermion six-vertex model.

3.3.5 Modular invariant partition function

Using the q-binomial building blocks and empirical selection rules for N odd or even, gives the finitized partition functions as in [169]. In the $\mathbb{Z}_4$ sectors with N, ℓ odd

$$Z_\ell^{(N)}(q) = \begin{cases} (q\bar{q})^{-c/24} \sum_{k\in\mathbb{Z}} q^{\Delta_{2k+\ell/2}} \begin{bmatrix} \frac{N+1}{2} \\ \frac{N-\ell}{4} - k \end{bmatrix}_q \bar{q}^{\Delta_{2k-\ell/2}} \begin{bmatrix} \frac{N-1}{2} \\ \frac{N-\ell}{4} + k \end{bmatrix}_{\bar{q}} \\ (q\bar{q})^{-c/24} \sum_{k\in\mathbb{Z}} q^{\Delta_{2k+\ell/2}} \begin{bmatrix} \frac{N+1}{2} \\ \frac{N+\ell+2}{4} + k \end{bmatrix}_q \bar{q}^{\Delta_{2k-\ell/2}} \begin{bmatrix} \frac{N-1}{2} \\ \frac{N+\ell-2}{4} - k \end{bmatrix}_{\bar{q}} \end{cases} \quad N-\ell = 0 \bmod 4 \tag{3.3.24}$$

$$Z_\ell^{(N)}(q) = \begin{cases} (q\bar{q})^{-c/24} \sum_{k\in\mathbb{Z}} q^{\Delta_{2k+\ell/2}} \begin{bmatrix} \frac{N+1}{2} \\ \frac{N-\ell+2}{4} - k \end{bmatrix}_q \bar{q}^{\Delta_{2k-\ell/2}} \begin{bmatrix} \frac{N-1}{2} \\ \frac{N-\ell-2}{4} + k \end{bmatrix}_{\bar{q}} \\ (q\bar{q})^{-c/24} \sum_{k\in\mathbb{Z}} q^{\Delta_{2k+\ell/2}} \begin{bmatrix} \frac{N+1}{2} \\ \frac{N+\ell}{4} + k \end{bmatrix}_q \bar{q}^{\Delta_{2k-\ell/2}} \begin{bmatrix} \frac{N-1}{2} \\ \frac{N+\ell}{4} - k \end{bmatrix}_{\bar{q}} \end{cases} \quad N-\ell = 2 \bmod 4 \tag{3.3.25}$$

For given mod 4 parities of $N-\ell$, these expressions are equivalent as partition functions but, in each case, the first form is used for the combinatorial interpretation when $\ell = 1 \bmod 4$ and the second form when $\ell = 3 \bmod 4$. As in [169], this leads to

$$\sum_{\ell\in 2\mathbb{N}-1}^{\ell\le N} Z_\ell^{(N)}(q) = \tfrac{1}{2}(q\bar{q})^{-\frac{c}{24}-\frac{3}{32}} \left[\prod_{n=1}^{\frac{N+1}{2}} (1+q^{\frac{2n-1}{4}}) \prod_{n=1}^{\frac{N-1}{2}} (1+\bar{q}^{\frac{2n-1}{4}}) + \prod_{n=1}^{\frac{N+1}{2}} (1-q^{\frac{2n-1}{4}}) \prod_{n=1}^{\frac{N-1}{2}} (1-\bar{q}^{\frac{2n-1}{4}}) \right] \tag{3.3.26}$$

In the R and NS sectors with N even

$$Z_\ell^{(N)}(q) = \begin{cases} (q\bar{q})^{-c/24} \sum_{k\in\mathbb{Z}} q^{\Delta_{2k+\ell/2}} \begin{bmatrix} 2\lfloor \frac{N+2}{4} \rfloor \\ \lfloor \frac{N+2-\ell}{4} \rfloor - k \end{bmatrix}_q \bar{q}^{\Delta_{2k-\ell/2}} \begin{bmatrix} 2\lfloor \frac{N}{4} \rfloor \\ \lfloor \frac{N-\ell}{4} \rfloor + k \end{bmatrix}_{\bar{q}}, & \text{R: } \ell/2 \text{ even} \\ (q\bar{q})^{-c/24} \sum_{k\in\mathbb{Z}} q^{\Delta_{2k+\ell/2}} \begin{bmatrix} 2\lfloor \frac{N}{4} \rfloor + 1 \\ \lfloor \frac{N+2-\ell}{4} \rfloor - k \end{bmatrix}_q \bar{q}^{\Delta_{2k-\ell/2}} \begin{bmatrix} 2\lfloor \frac{N+2}{4} \rfloor - 1 \\ \lfloor \frac{N-\ell}{4} \rfloor + k \end{bmatrix}_{\bar{q}}, & \text{NS: } \ell/2 \text{ odd} \end{cases} \tag{3.3.27}$$

In these formulas the central charge and conformal weights, given by the Euler-Maclaurin formula, are

$$c=-2,\qquad \Delta=\bar{\Delta}=\Delta_j=-\frac{1}{8},0,\frac{3}{8},\qquad j=0,1,2,\qquad \Delta_j=\frac{j^2-1}{8} \tag{3.3.28}$$

The modular invariant partition function $Z(q)$ of the free-fermion six-vertex model is given by taking the trace over all S_z sectors with N even. Using the explicit expressions in terms of products, as in [169], and summing over the ℓ sectors with multiplicities 2 arising from $S_z=\pm\ell$ yields the finitized partition function of the free-fermion six-vertex model

$$Z^N(q)=Z_0^{(N)}+2\sum_{\ell\in 4\mathbb{N}}^{\ell\leq N}Z_\ell^{(N)}(q)+2\sum_{\ell\in 4\mathbb{N}-2}^{\ell\leq N}Z_\ell^{(N)}(q) \tag{3.3.29a}$$

$$\begin{aligned}&=\tfrac{1}{2}(q\bar{q})^{-\frac{c}{24}-\frac{1}{8}}\Big[\prod_{n=1}^{\lfloor\frac{N+2}{4}\rfloor}(1+q^{n-\frac{1}{2}})^2\prod_{n=1}^{\lfloor\frac{N}{4}\rfloor}(1+\bar{q}^{n-\frac{1}{2}})^2+\prod_{n=1}^{\lfloor\frac{N+2}{4}\rfloor}(1-q^{n-\frac{1}{2}})^2\prod_{n=1}^{\lfloor\frac{N}{4}\rfloor}(1-\bar{q}^{n-\frac{1}{2}})^2\Big]\\&\quad+2(q\bar{q})^{-\frac{c}{24}}\prod_{n=1}^{\lfloor\frac{N}{4}\rfloor}(1+q^n)^2\prod_{n=1}^{\lfloor\frac{N-2}{4}\rfloor}(1+\bar{q}^n)^2\end{aligned} \tag{3.3.29b}$$

It is easily checked that the counting of states $Z^N(1)=2^N$ is correct at $q=\bar{q}=1$.

Taking the thermodynamic limit $N\to\infty$ gives the conformal modular invariant partition function

$$\begin{aligned}Z_0(q)+2\sum_{\ell\in 4\mathbb{N}}Z_\ell(q)&=\frac{|\vartheta_{0,2}(q)|^2+|\vartheta_{2,2}(q)|^2}{|\eta(q)|^2}=|\hat{\chi}_{-1/8}(q)|^2+|\hat{\chi}_{3/8}(q)|^2\\2\sum_{\ell\in 4\mathbb{N}-2}Z_\ell(q)&=\frac{|\vartheta_{1,2}(q)|^2+|\vartheta_{3,2}(q)|^2}{|\eta(q)|^2}=\frac{2|\vartheta_{1,2}(q)|^2}{|\eta(q)|^2}=2|\hat{\chi}_0(q)+\hat{\chi}_1(q)|^2\\Z(q)=Z_0(q)+2\sum_{\ell\in 2\mathbb{N}}Z_\ell(q)&=\frac{1}{|\eta(q)|^2}\sum_{j=0}^{3}|\vartheta_{j,2}(q)|^2=|\hat{\chi}_{-1/8}(q)|^2+2|\hat{\chi}_0(q)+\hat{\chi}_1(q)|^2+|\hat{\chi}_{3/8}(q)|^2\\&=|\varkappa_0^2(q)|^2+2|\varkappa_1^2(q)|^2+|\varkappa_2^2(q)|^2\end{aligned} \tag{3.3.30}$$

where the $u(1)$ and $\mathcal{W}$-irreducible characters are

$$\varkappa_j^n(q)=\frac{1}{\eta(q)}\,\vartheta_{j,n}(q),\qquad \begin{aligned}\hat{\chi}_{-1/8}(q)&=\frac{1}{\eta(q)}\,\vartheta_{0,2}(q),\ \hat{\chi}_0(q)=\frac{1}{2\eta(q)}[\vartheta_{1,2}(q)+\eta(q)^3]\\\hat{\chi}_{3/8}(q)&=\frac{1}{\eta(q)}\,\vartheta_{2,2}(q),\ \hat{\chi}_1(q)=\frac{1}{2\eta(q)}[\vartheta_{1,2}(q)-\eta(q)^3]\end{aligned} \tag{3.3.31}$$

and the Dedekind eta and theta functions are

$$\eta(q) = q^{1/24}\prod_{n=1}^{\infty}(1-q^n), \qquad \vartheta_{j,n}(q) = \sum_{k\in\mathbb{Z}} q^{\frac{(j+2kn)^2}{4n}} \tag{3.3.32}$$

The MIPF $Z(q)$ of the free-fermion six-vertex model thus precisely agrees with the MIPF of dimers in the usual orientation [83] and critical dense polymers [170]. The latter coincidence is nontrivial as a modified trace is needed to close the cylinder to a torus for this lattice loop model. Although the MIPF agrees with symplectic fermions [121, 164–166], which is a logarithmic theory, there are no Jordan cells and no indication of logarithmic behaviour for dimers on the cylinder. Indeed, viewing the free-fermion model as the critical eight-vertex model at the decoupling point [177], the MIPF reduces to the square of the Ising model MIPF with central charge $c = \frac{1}{2}$

$$Z(q) = Z_{\text{Ising}}(q)^2 \tag{3.3.33}$$

Comparing (3.3.29b) with [163] shows that this relation also holds at the level of the finitized MIPFs. To see Jordan cells for dimers, we consider the vacuum boundary condition on the strip in the next chapter 4.

3.4 Periodic Dimers on a Finite $M \times N$ square Lattice

The problem of counting of periodic dimers on a finite $M \times N$ square lattice, in the usual orientation, has been solved exactly [73, 82, 156]. The number of periodic dimer configurations is given by

$$\tilde{Z}_{M\times N} = \tfrac{1}{2}(\tilde{Z}^{1/2,1/2}_{M\times N} + \tilde{Z}^{0,1/2}_{M\times N} + \tilde{Z}^{1/2,0}_{M\times N}) \tag{3.4.1}$$

where

$$\tilde{Z}^{\alpha,\beta}_{M\times N} = \prod_{n=0}^{N/2-1}\prod_{m=0}^{M/2-1} 4\Big(\sin^2\frac{2\pi(n+\alpha)}{N} + \sin^2\frac{2\pi(m+\beta)}{M}\Big), \qquad M,N = 2,4,6,\ldots \tag{3.4.2}$$

Explicitly, arranging the entries in a symmetric matrix gives

$$(\tilde{Z}_{M\times N}) = \begin{pmatrix} 8 & 36 & 200 & 1156 & \cdots \\ 36 & 272 & 3{,}108 & 39{,}952 & \cdots \\ 200 & 3{,}108 & 90{,}176 & 3{,}113{,}860 & \cdots \\ 1{,}156 & 39{,}952 & 3{,}113{,}860 & 311{,}853{,}312 & \cdots \\ \vdots & \vdots & \vdots & \vdots & \ddots \end{pmatrix}, \qquad M, N = 2, 4, 6, \ldots \tag{3.4.3}$$

The exact counting of periodic dimer configurations on a finite $M \times N$ square lattice, in the 45 degree rotated orientation, is given by taking the trace of the Mth power of the transfer matrix (3.3.1) with eigenvalues (3.3.13). The expressions, however, are more involved than for the usual orientation. Explicitly, setting $\rho = \sqrt{2}$ at the isotropic point $u = \pi/4$ with $\epsilon_j = \pm 1$, the number of periodic dimer configurations with the rotated orientation is

$$Z_{M\times N} = \begin{cases} 2^{MN+1} \displaystyle\sum_{s=-N+2;4}^{N} \sum_{\sum_{j=1}^{N}\epsilon_j = s} (-1)^{\frac{M(N-s)}{4}} \prod_{j=1}^{N} \cos^M\!\big(\epsilon_j t_j - \tfrac{\pi}{4}\big), & N \text{ odd} \\ 2^{MN} \displaystyle\sum_{\substack{s=-N \\ s\,=\,0 \bmod 4}}^{N} \sum_{\sum_{j=1}^{N}\epsilon_j = -|s|} (-1)^{\frac{M(2N+s)}{4}} \prod_{j=1}^{N} \cos^M\!\big(\epsilon_j t_j^{\mathrm{R}} - \tfrac{\pi}{4}\big) & \\ \quad + 2^{MN} \displaystyle\sum_{\substack{s=-N \\ s\,=\,2 \bmod 4}}^{N} \sum_{\sum_{j=1}^{N}\epsilon_j = -|s|} (-1)^{\frac{M(2N+|s|+2)}{4}} \prod_{j=1}^{N} \cos^M\!\big(\epsilon_j t_j^{\mathrm{NS}} - \tfrac{\pi}{4}\big), & N \text{ even} \end{cases} \tag{3.4.4}$$

where $s = S_z$ in the sums increments in steps of 4 as indicated and

$$t_j = \frac{(2j-1)\pi}{4N}, \qquad t_j^{\mathrm{R}} = \frac{(2j-1)\pi}{2N}, \qquad t_j^{\mathrm{NS}} = \begin{cases} \frac{j\pi}{N}, & j \neq N/2 \\ 0, & j = N/2 \end{cases} \tag{3.4.5}$$

The restrictions on s are compatible with the selection rules and the signs ϵ in (3.3.14) ensure that the eigenvalues contribute with the correct overall sign. The trigonometric iden-

tities [178]

$$\prod_{j=1}^{N} \cos t_j = 2^{1/2-N}, \qquad \prod_{j=1}^{N} \cos t_j^{\mathrm{R}} = (-1)^{N/2}\, 2^{1-N}, \qquad \prod_{j=1, j\neq N/2}^{N} \cos t_j^{\mathrm{NS}} = (-1)^{N/2} N\, 2^{1-N} \tag{3.4.6}$$

are used to evaluate the products in the denominators arising from the simplification

$$1 + \epsilon_j \tan t_j = \frac{\cos t_j + \epsilon_j \sin t_j}{\cos t_j} = \sqrt{2}\, \frac{\cos(\epsilon_j t_j - \frac{\pi}{4})}{\cos t_j}, \qquad \epsilon_j = \pm 1 \tag{3.4.7}$$

For N even, precisely half the eigenvalues in (3.4.4) come from the Ramond sectors and half from the Neveu-Schwarz sectors in accord with the binomial identity

$$\sum_{s=-N;4}^{N} \binom{N}{\frac{N-s}{2}} = \sum_{s=-N+2;4}^{N-2} \binom{N}{\frac{N-s}{2}} = 2^{N-1}, \qquad s = S_z \tag{3.4.8}$$

Arranging the entries in a symmetric matrix, the number of periodic dimer configurations for the rotated orientation is

$$(Z_{M\times N}) = \begin{pmatrix} 4 & 8 & 16 & 32 & 64 & \dots \\ 8 & 24 & 80 & 288 & 1{,}088 & \dots \\ 16 & 80 & 448 & 2{,}624 & 15{,}616 & \dots \\ 32 & 288 & 2{,}624 & 26{,}752 & 280{,}832 & \dots \\ 64 & 1{,}088 & 15{,}616 & 280{,}832 & 5{,}080{,}064 & \dots \\ \vdots & \vdots & \vdots & \vdots & \vdots & \ddots \end{pmatrix}, \qquad M, N = 1, 2, 3, \dots \tag{3.4.9}$$

It is easy to recognize the integer sequences [179] in the first 3 rows. The formulas (3.4.4) look unwieldy but are straightforward to code in Mathematica [150]. In particular, for comparison, the number of periodic dimer configurations $\tilde{Z}_{8\times 8}$ on an 8×8 square lattice in the usual orientation and the number $Z_{8\times 8}$ in the rotated orientation are

$$\tilde{Z}_{8\times 8} = 311{,}853{,}312, \qquad Z_{8\times 8} = 38{,}735{,}278{,}017{,}380{,}352 \tag{3.4.10}$$

The difference in magnitude observed here is due to the difference in the unit cells by a

linear factor $\sqrt{2}$ on each edge of the rectangle. This is in accord with the fact that an $M \times N$ rectangle in the original orientation has $MN/2$ dimers compared to MN dimers in the rotated orientation. While the precise counting of dimer configurations differs in the two orientations, the asymptotic growth (3.2.26) per dimer coincide

$$(\tilde{Z}_{2M,N})^{\frac{1}{MN}} \sim (\tilde{Z}_{M,2N})^{\frac{1}{MN}} \sim (Z_{M,N})^{\frac{1}{MN}} \sim \exp(\tfrac{2G}{\pi}) \tag{3.4.11}$$

3.5 Conclusion

It is often stated that two-dimensional lattice models are exactly solvable if their Boltzmann weights satisfy the local Yang-Baxter equation so that they admit a family of commuting transfer matrices with an infinite number of conserved quantities. In a sense, Yang-Baxter integrability is the *gold standard* for solvability on the lattice. Until now, dimers has been solved exactly by Pfaffian and other techniques but not by Yang-Baxter methods. Now, dimers is brought firmly into the framework of Yang-Baxter integrability. For periodic transfer matrices, through the special inversion identity, this has enabled the detailed calculation of the dimer model spectra on the cylinder in the $\mathbb{Z}_4$, Ramond and Neveu-Schwarz sectors for arbitrary finite sizes. Taking a trace to form a torus and combining these sectors at the isotropic point $u = \frac{\lambda}{2} = \frac{\pi}{4}$ yields explicit formulas for the counting of dimer configurations on arbitrary periodic $M \times N$ square lattices. Because the orientation of the dimers is rotated by 45°, the precise counting of these states differs from the counting of configurations for the usual orientation on the square lattice even though the residual entropies coincide.

The inclusion of a spatial anisotropy in the form of a spectral parameter u enables the analytic calculation of the complete finite-size spectra of dimers yielding the central charge $c = -2$ and conformal weights $\Delta = -\frac{1}{8}, 0, \frac{3}{8}$. Remarkably, the modular invariant partition function precisely coincides with that of critical dense polymers sector-by-sector even though in critical dense polymers it is required the implementation of a modified trace.

Since the bulk CFTs appear to be the same, at least in terms of spectra, it is tempting to argue that dimers and critical dense polymers lie in the same *universality class*. However, to

reach a definitive answer it is necessary to research further if the Virasoro dilatation operator L_0 for the dimer model manifests a non-trivial Jordan cell structure in other geometries iwith different boundary conditions. This question motivated a successive investigation, presented and explained in the third chapter of my thesis, where the the anisotropic dimer model is studied on a strip with certain types of Kac boundary conditions.

Chapter 4

Yang-Baxter Integrable Dimers on a Strip

Using the theory of the Yang-Baxter integrable free-fermion dimer model, as it has been outlined in the previous chapter, we can now study dimers on the strip geometry. We establish and solve inversion identities for the dimer model on a strip of arbitrary finite size N with vacuum boundary conditions and r-type seam of width $w = 1$. In the continuum scaling limit, in sectors with magnetization S_z, we obtain the conformal weights $\Delta_s = \big((2-s)^2 - 1\big)/8$ where $s = |S_z| + 1 = 1, 2, 3, \ldots$. We further show that the corresponding finitized characters $\chi_s^{(N)}(q)$ decompose into sums of q-Narayana numbers or, equivalently, skew q-binomials. In the particle representation, the local face tile operators give a representation of the fermion algebra and the fermion particle trajectories play the role of nonlocal (logarithmic) degrees of freedom. We argue that, in the continuum scaling limit, there exists nontrivial Jordan cells in the Virasoro dilatation operator L_0. This confirms that the dimer model gives rise to a logarithmic *conformal field theory with central charge $c = -2$, minimal conformal weight $\Delta_{min} = -\frac{1}{8}$ and effective central charge $c_{eff} = 1$.*

4.1 Introduction

The dimer model [70, 155] was solved exactly [73–75, 157] in the early sixties. After more than 50 years, the dimer model continues to be the subject of extensive study [76, 82–87, 89]. The current interest is twofold: (i) to understand the finite-size effects of boundary conditions and steric effects [69, 158–160] under the influence of infinitely repulsive hard-core local interactions and (ii) to understand the conformal description of dimers in the continuum scaling limit. Traditionally, it is asserted that dimers is described [62, 79, 80] by a $c = 1$ Gaussian free field and a number of authors [83, 84] have suggested that dimers is

described by a logarithmic Conformal Field Theory (CFT). However, without full access to various sectors and boundary conditions on the strip, it is difficult to distinguish between a $c = 1$. Recently, the dimer model was shown [132] to be Yang-Baxter integrable [31] by mapping [46, 61, 69] it onto the free-fermion six-vertex model [34, 36–40, 161]. Notably, this maps six-vertex configurations onto dimer configurations where the dimers are rotated by 45°, as shown in Figures 4.2, 3.4 and 4.4, compared to their usual orientation parallel to the bonds of the square lattice. This technique combined with inversion identities [31, 162, 163] enables dimers to be solved exactly for finite lattices with various boundary conditions and topologies. The conformal properties can therefore be readily extracted from the finite-size scaling behaviour. On this basis, it was argued in [132] that dimers is best described as a logarithmic CFT with effective central charge $c_{\text{eff}} = 1$ but central charge $c = -2$ in agreement with the findings of [83, 84]. The primary characterization of logarithmic CFTs is the appearance of nontrivial Jordan cells in the Virasoro dilation operator L_0. Indeed for simple boundary conditions on the strip, corresponding to the $U_q(sl(2))$-invariant XX Hamiltonian $\mathcal{H}$ of the free-fermion six-vertex model, it was shown [132] that $\mathcal{H}$ admits nontrivial Jordan cells for finite systems. Since the appearance of these cells is stable as the system size increases these cells are expected to persist for large sizes and appear in the Virasoro dilation operator L_0.

In this chapter, we solve exactly the anisotropic square lattice dimer model with the 45° rotated orientation on the strip in sectors labelled by the magnetization S_z of the related free-fermion six-vertex model. This is achieved, using Yang-Baxter integrability, by mapping the dimer model with given boundary conditions onto a free-fermion six-vertex model and solving the associated inversion [31, 162, 163] identities satisfied by the double row transfer matrices. The solution of the inversion identities allows to obtain the exact finite spectra in the various sectors. Finite-size scaling then yields the central charge and the conformal weights. In addition, combinatorial analysis of the patterns of zeros, in the complex spectral parameter plane, of the double row transfer matrix eigenvalues allows us to obtain finitized characters. We confirm the central charge $c = -2$ and the conformal weights $\Delta_s = \left((2-s)^2 - 1\right)/8$ with $s = 1, 2, 3, \ldots$. Remarkably, although the characters are different, the conformal weights coincide with those in the first column of the infinitely

s							
	$\vdots$	$\vdots$	$\vdots$	$\vdots$	$\vdots$	$\vdots$	$\iddots$
10	$\frac{63}{8}$	$\frac{35}{8}$	$\frac{15}{8}$	$\frac{3}{8}$	$-\frac{1}{8}$	$\frac{3}{8}$	$\cdots$
9	6	3	1	0	0	1	$\cdots$
8	$\frac{35}{8}$	$\frac{15}{8}$	$\frac{3}{8}$	$-\frac{1}{8}$	$\frac{3}{8}$	$\frac{15}{8}$	$\cdots$
7	3	1	0	0	1	3	$\cdots$
6	$\frac{15}{8}$	$\frac{3}{8}$	$-\frac{1}{8}$	$\frac{3}{8}$	$\frac{15}{8}$	$\frac{35}{8}$	$\cdots$
5	1	0	0	1	3	6	$\cdots$
4	$\frac{3}{8}$	$-\frac{1}{8}$	$\frac{3}{8}$	$\frac{15}{8}$	$\frac{35}{8}$	$\frac{63}{8}$	$\cdots$
3	0	0	1	3	6	10	$\cdots$
2	$-\frac{1}{8}$	$\frac{3}{8}$	$\frac{15}{8}$	$\frac{35}{8}$	$\frac{63}{8}$	$\frac{99}{8}$	$\cdots$
1	0	1	3	6	10	15	$\cdots$
	1	2	3	4	5	6	r

Figure 4.1: Kac table of conformal weights $\Delta_{r,s}$ of critical dense polymers taken from [168]. The conformal weights of dimers coincide with the conformal weights in the first ($r = 1$) column of this Kac table. Both theories are described by CFTs with $c = -2$ although their conformal characters are different.

extended Kac table of critical dense polymers [124, 167–170, 180] as shown in Figure 4.1.

The layout of the chapter is as follows. In Section 4.2, we recall the rotated dimer model on the square lattice and review its relation to the free-fermion six-vertex model. We also describe the underlying free-fermion and Temperley-Lieb algebras. In Section 4.3, we present the local Yang-Baxter relations of the six-vertex model using the particle representation of the planar algebra and establish the commutation of the double row transfer matrices. In Section 4.4, we specialize to the dimer model and solve the associated inversion identities on the strip for the finite size-spectra. This involves the combinatorial analysis of the patterns of zeros of the eigenvalues and the empirical determination of selection rules to fix the eigenvalue degeneracies which are not fixed by the functional equa-

tions alone. Jordan decompositions of the isotropic double row transfer matrices and their quantum Hamiltonians, for some small system sizes, are presented in Section 4.5 to reveal the existence of nontrivial Jordan cells of rank 2 . Assuming the stability of these Jordan cells for large system sizes N, the persistence of these Jordan cells in the continuum scaling limit implies that the CFT describing the dimer model is logarithmic. We finish with some concluding remarks in Section 4.6 comparing dimers with critical dense polymers. Details of the proof of the inversion identities and the properties of the skew q-binomials appearing in the selection rules are relegated to Appendices.

4.2 Dimers as a Free-Fermion Six-Vertex Model

4.2.1 Face tiles and equivalence of vertex, particle and dimer representations

The mapping between the free-fermion six-vertex model and dimer configurations was given in [132]. The allowed six-vertex (arrow conserving) face configurations and the equivalent tiles in the particle (even and odd rows) and dimer [69] representations are shown in Figure 4.2. The vertex (arrow) degrees of freedom $\sigma_j = \pm 1$ and the particle occupation numbers $a_j = \frac{1}{2}(1-\sigma_j) = 0, 1$ live on the medial lattice. The Boltzmann weights of the six-vertex tiles are

$$a(u) = \rho\,\frac{\sin(\lambda-u)}{\sin\lambda}, \quad b(u) = \rho\,\frac{\sin u}{\sin\lambda}, \quad c_1(u) = \rho g, \quad c_2(u) = \frac{\rho}{g}, \qquad \lambda \in (0,\pi), \quad \rho \in \mathbb{R} \tag{4.2.1}$$

The spectral parameter u plays the role of spatial anisotropy with $u = \frac{\lambda}{2}$ being the isotropic point. Geometrically [172], varying u effectively distorts a square tile into a rhombus with an opening anisotropy angle $\vartheta = \frac{\pi u}{\lambda}$. The arbitrary parameter ρ is an overall normalization. Assuming boundary conditions such that there are an equal number of sources and sinks of horizontal arrows (vertices c_1 and c_2) along any row, the transfer matrix entries are all independent of the gauge factor g.

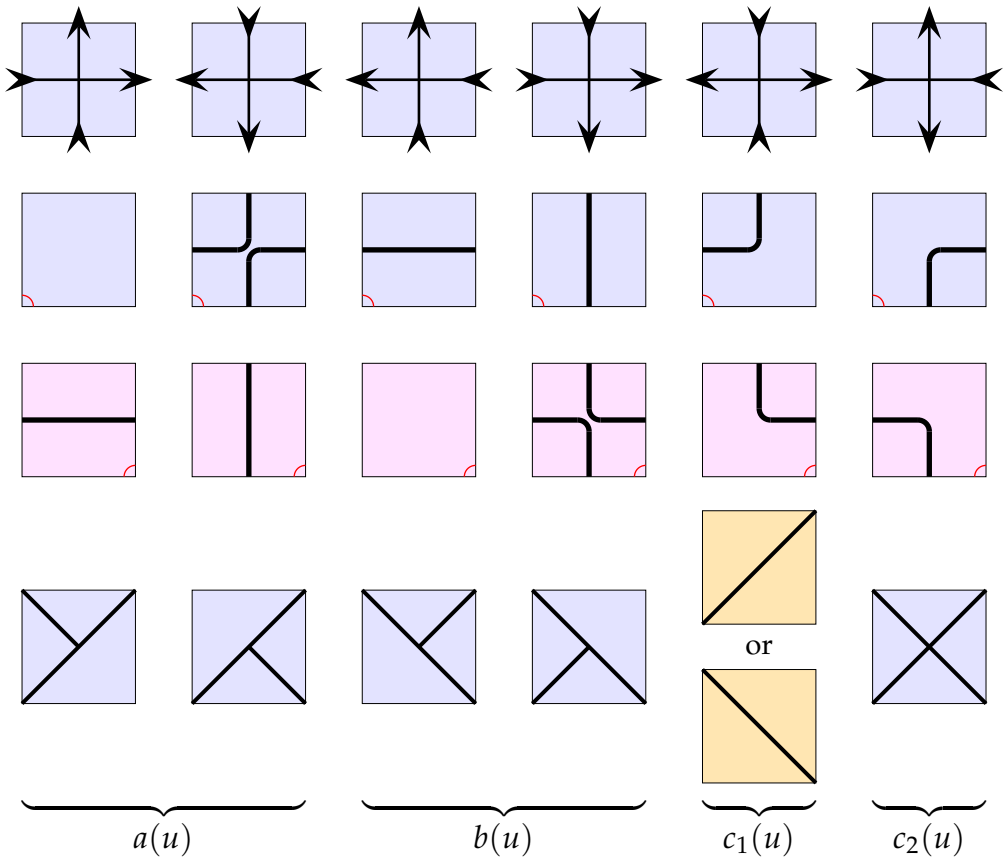

Figure 4.2: Equivalent face tiles of the six-vertex model in the vertex, particle (even and odd rows) and dimer representations. On the strip, the odd and even rows alternate. For periodic boundary conditions, all rows are odd. The heavy particle lines are drawn whenever the arrows disagree with the reference state as shown in Figure 4.3. The particles move up and to the right on odd rows and up and to the left on even rows.

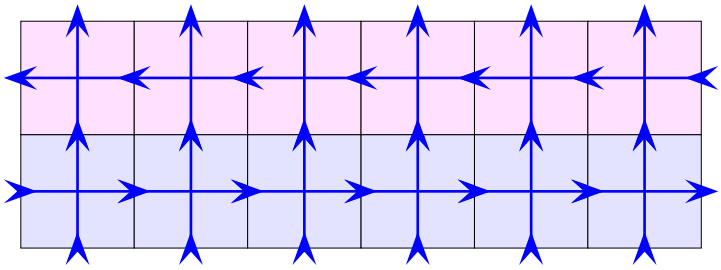

Figure 4.3: Reference states for the single and double row transfer matrices for mapping onto the particle representation. The reference arrows point up and to the right for the single row transfer matrices. For the double row transfer matrices, the reference arrows point up and right on odd rows and up and left on even rows.

At the free-fermion point ($\lambda = \frac{\pi}{2}$), the six-vertex face weights reduce to

$$a(u) = \rho \cos u, \quad b(u) = \rho \sin u, \quad c_1(u) = \rho g, \quad c_2(u) = \frac{\rho}{g}, \qquad \rho \in \mathbb{R} \tag{4.2.2}$$

These weights satisfy the free-fermion condition

$$a(u)^2 + b(u)^2 = c_1(u)c_2(u) \tag{4.2.3}$$

As shown in Section 3.2.2, with the special choice of gauge $g = z = e^{iu}$, the tiles give a representation of the free-fermion algebra with generators $\{f_j, f_j^\dagger\}$ and, consequently, also a representation of the Temperley-Lieb algebra [175] with generators $\{e_j\}$ and loop fugacity $\beta = 2\cos\lambda = 0$. Explicitly, the face transfer operators are

$$X_j(u) = \rho(\cos u\, I + \sin u\, e_j) \tag{4.2.4}$$

This Temperley-Lieb model is directly equivalent to an anisotropic dimer model as shown in Figures 4.2, 3.4 and 4.4. A dimer weight is assigned to the unique square face which is half-covered by the dimer as shown in Figure 3.4. The statistical weights assigned to "horizontal" and "vertical" dimers are

$$\zeta_h(u) = a(u) = \rho \cos u, \qquad \zeta_v(u) = b(u) = \rho \sin u \tag{4.2.5}$$

Setting $g = \rho$, and allowing for the facts that (i) the c_1 face has two allowed configurations and (ii) no dimer covers the c_2 face, it follows that

$$c_1(u) = \zeta_h(u)^2 + \zeta_v(u)^2 = \rho^2(\cos^2 u + \sin^2 u) = \rho^2, \qquad c_2(u) = 1 \tag{4.2.6}$$

Additionally, fixing $\rho = \sqrt{2}$ at the isotropic point ($u = \frac{\lambda}{2} = \frac{\pi}{4}$) gives

$$a(\tfrac{\pi}{4}) = 1, \qquad b(\tfrac{\pi}{4}) = 1, \qquad c_1(\tfrac{\pi}{4}) = 2, \qquad c_2(\tfrac{\pi}{4}) = 1 \tag{4.2.7}$$

It follows that, with this gauge and normalization, the partition function at the isotropic point gives the correct counting of distinct dimer configurations.

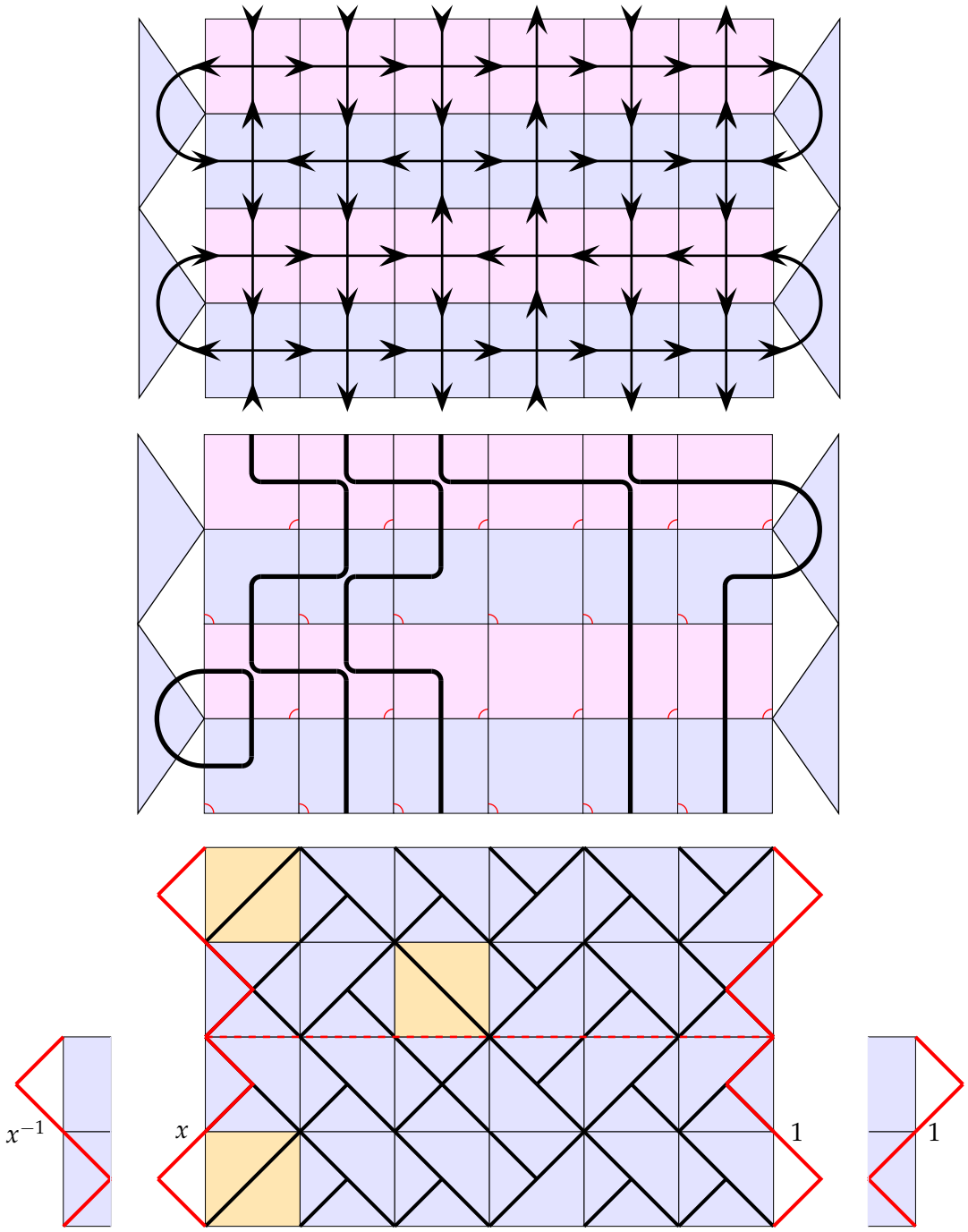

Figure 4.4: Typical dimer configuration on a 6×4 strip with vacuum boundary conditions in the vertex, particle and dimer representations. For the vertex representation, the boundary arrows can be in either one of the two possible directions (corresponding to a particle or vacancy in the particle representation). Particles move up and right on odd rows and up and left on even rows. The number of particles/down arrows inside the strip is conserved from double row to double row but not necessarily in intermediate rows. For dimers, there are two different zigzag edges allowed independently on the left and right edges of each double row. The left boundary zigzags have weights x, x^{-1} as shown. The right boundary zigzags have weight 1.

In addition to the vertex and dimer representations, the six-vertex free-fermion model admits a particle representation as shown in Figures 4.2 and 4.4. A reference state on the strip is fixed as in Figure 4.3. An edge of a given vertex is a segment of a particle trajectory (and has particle occupation number $a_j = 1$) if its arrow points in the opposite direction to that of the reference state. Otherwise, if the edge arrow points in the same direction as the reference state, the edge is not a segment of a particle trajectory (and the particle occupation is $a_j = 0$). The segments of particle trajectories live on the medial lattice and are indicated with heavy lines in Figure 4.3. The number of particles is conserved and their trajectories are non-intersecting. The particle representation is the simplest of the three representations and is convenient for coding in Mathematica [150] and for manipulations in the diagrammatic planar algebra [51] so we usually work in the particle representation. The $\mathbb{Z}_2$ arrow reversal symmetry of the vertex model implies a particle-hole duality in the particle representation.

4.2.2 Free-fermion and Temperley-Lieb algebras

In this section we refer to the previous chapter (section 3.2.2), where the fermionic and Temperley-Lieb algebras of the free-fermion model (4.3) with $\lambda = \frac{\pi}{2}$ and $\rho = 1$ in the specific gauge $g = z = e^{iu}$ have been exhaustively treated.

4.3 Six Vertex Model on the Strip

The commuting double row transfer matrices of the six-vertex model were constructed algebraically by Sklyanin [181]. In this section, we develop a diagrammatic construction of the commuting double row transfer matrices of the six-vertex model by generalizing the methods of [182] and using planar algebras [183].

4.3.1 Local relations

We describe the local relations satisfied by the six-vertex face operators in the planar and linear algebra settings. Because it has local degrees of freedom, in the form of particle oc-

cupation numbers, the planar algebra of the six vertex model just involves local tensor contractions of the indices giving the particle numbers. By fixing the planar algebra operators to act in an arbitrary fixed direction, the local relations presented in this section are easily established concretely using matrix representations (for example in Mathematica [150]). Alternatively, a local relation can be established diagrammatically directly in the planar algebra setting. It then follows that the local relation holds for all matrix representations and for all choices of the direction of action.

Face operators, symmetries and face weights

As elements of a planar algebra [183], the face operators of the six-vertex model in the particle representation decompose [174] into a sum of contributions from six elementary tiles

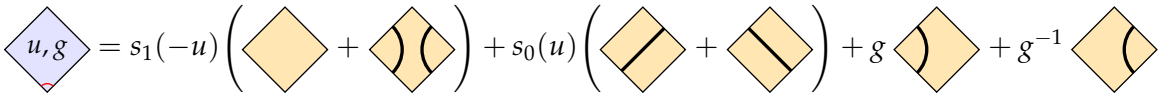

(4.3.1)

where $s_k(u) = \frac{\sin(u+k\lambda)}{\sin\lambda}$ and g is a gauge factor. Multiplication of the tiles in the planar algebra is given [132,174] by local tensor contraction of indices $a, b, c, d, \ldots = 0, 1$ specifying the particle occupation numbers on the centers of the tile edges. The face operators are invariant under reflection about the principal (vertical) diagonal indicated by the marked corner. Rotating the face operator by 90° gives

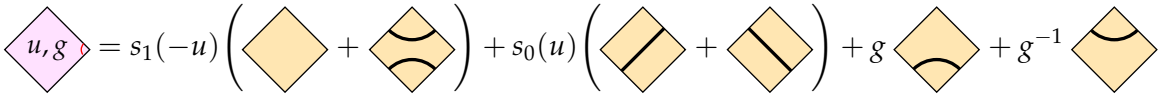

(4.3.2)

Further rotations by 90° give

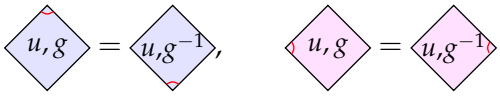

(4.3.3)

Only the occupation numbers $a, b, c, d = 0, 1$ of the edges are important. The colors of the face operators (indicating their relative orientation) and the internal particle trajectories are just for easy visual identification so that

(4.3.4)

Later, we work in the fixed gauge $g = z = e^{iu}$ with $x = e^{i\lambda}$

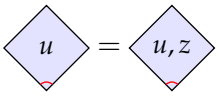

(4.3.5)

Specializing with this gauge gives the generators of the planar Temperley-Lieb algebra

(4.3.6a)

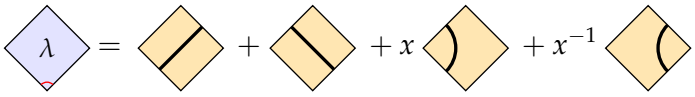

(4.3.6b)

where, acting vertically, the first operator acts as the identity and the second acting at position j acts as the Temperley-Lieb generator e_j. Moreover,

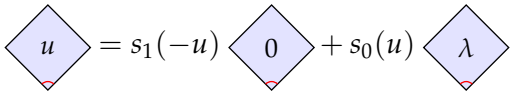

(4.3.7)

More conventionally, the bulk 1×1 face weights of the six-vertex model are

$$
\begin{aligned}
W\left(\begin{smallmatrix} 0 & 0 \\ 0 & 0 \end{smallmatrix}\middle| z,g\right) &= 0 \quad \begin{smallmatrix} & 0 & \\ 0 & & 0 \\ & 0 & \end{smallmatrix} \quad = s_1(-u) \\
W\left(\begin{smallmatrix} 1 & 0 \\ 1 & 0 \end{smallmatrix}\middle| z,g\right) &= 0 \quad \begin{smallmatrix} & 1 & \\ 0 & & 0 \\ & 1 & \end{smallmatrix} \quad = s_0(u) \\
W\left(\begin{smallmatrix} 0 & 1 \\ 1 & 0 \end{smallmatrix}\middle| z,g\right) &= 0 \quad \begin{smallmatrix} & 0 & \\ 0 & & 1 \\ & 1 & \end{smallmatrix} \quad = g^{-1} \\
W\left(\begin{smallmatrix} 1 & 0 \\ 0 & 1 \end{smallmatrix}\middle| z,g\right) &= 1 \quad \begin{smallmatrix} & 1 & \\ 0 & & 0 \\ & 0 & \end{smallmatrix} \quad = g \\
W\left(\begin{smallmatrix} 0 & 1 \\ 0 & 1 \end{smallmatrix}\middle| z,g\right) &= 1 \quad \begin{smallmatrix} & 0 & \\ 0 & & 0 \\ & 0 & \end{smallmatrix} \quad = s_0(u) \\
W\left(\begin{smallmatrix} 1 & 1 \\ 1 & 1 \end{smallmatrix}\middle| z,g\right) &= 1 \quad \begin{smallmatrix} & 1 & \\ 1 & & 1 \\ & 1 & \end{smallmatrix} \quad = s_1(-u)
\end{aligned}
\tag{4.3.8}
$$

The set of six allowed (blue) faces is not invariant under rotations through 90°. There is therefore no crossing symmetry. Instead, we distinguish the set of six rotated faces (pink) by the position of the corner marked by the (red) arc. In the blue faces the particles move up and to the right and in the pink faces they move up and to the left. The face weights are unchanged under rotations if both the face configurations and the marked corner are rotated together. Again, the colour of the faces is just for easy visual identification.

The six-vertex face weights can be organized into an $\check{R}$-matrices. Explicitly, choosing

the particular basis $\{(0,0),(0,1),(1,0),(1,1)\}$ gives

$$W\left(\begin{smallmatrix} & d & \\ a & & c \\ & b & \end{smallmatrix}\middle| z,g\right) = X(u,g)_{ab}{}^{dc}, \qquad X(u,g) = \begin{pmatrix} s_1(-u) & 0 & 0 & 0 \\ 0 & g^{-1} & s_0(u) & 0 \\ 0 & s_0(u) & g & 0 \\ 0 & 0 & 0 & s_1(-u) \end{pmatrix} \tag{4.3.9a}$$

$$W\left(\begin{smallmatrix} & d & \\ a & & c \\ & b & \end{smallmatrix}\middle| z,g\right) = \tilde{X}(u,g)_{da}{}^{cb}, \qquad \tilde{X}(u,g) = \begin{pmatrix} s_1(-u) & 0 & 0 & g^{-1} \\ 0 & 0 & s_0(u) & 0 \\ 0 & s_0(u) & 0 & 0 \\ g & 0 & 0 & s_1(-u) \end{pmatrix} \tag{4.3.9b}$$

Let us define

$$X_j(u,g) = I \otimes I \otimes \cdots I \otimes X(u,g) \otimes I \cdots \otimes I \otimes I \tag{4.3.10}$$

acting on $(\mathbb{C}^2)^{\otimes N}$ where $X(u,g)$ acts in the slots j and $j+1$ and similarly for $\tilde{X}(u,g)$. Setting $X(u) = X(u,z)$ the generators of the linear Temperley-Lieb algebra are then

$$X_j(0) = I, \qquad X_j(\lambda) = e_j, \quad j = 1,2,\ldots,N \tag{4.3.11}$$

satisfying

$$e_j^2 = \beta e_j, \qquad e_j e_{j\pm1} e_j = e_j, \qquad j = 1,2,\ldots,N, \qquad \beta = x + x^{-1} \tag{4.3.12}$$

This corresponds to the linear vertical action of the planar algebra. In particular, defining the local face operator

$$X_j(u) = X_j(u,z) = s_1(-u)\, I + s_0(u)\, e_j \tag{4.3.13}$$

leads to the Yang-Baxter equation

$$X_j(u) X_{j+1}(u+v) X_j(v) = X_{j+1}(v) X_j(u+v) X_{j+1}(u) \tag{4.3.14}$$

Inversion relations

The elementary 1×1 face weights satisfy two distinct inversion relations. In the planar algebra they are

Inv1 :

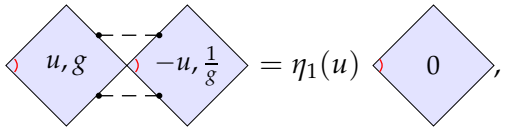

$$\eta_1(u) = s_1(u)s_1(-u) \tag{4.3.15a}$$

Inv2 :

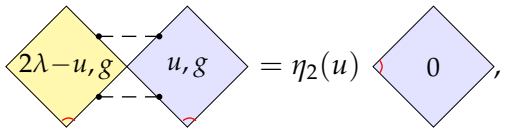

$$\eta_2(u) = s_0(u)s_2(-u) \tag{4.3.15b}$$

In the linear algebra acting from left to right, these become

$$X_j(u,g)X_j(-u,1/g) = s_1(u)s_1(-u)\, I \tag{4.3.16a}$$

$$\tilde{X}_j(2\lambda - u, g)\tilde{X}_j(u,g) = s_0(u)s_2(-u)\, I \tag{4.3.16b}$$

Up to the scalar on the right side, the face $\tilde{X}_j(2\lambda - u, g)$ (shown in yellow) is the inverse of the face $\tilde{X}_j(u,g)$. We observe the commutation relations

$$[X_j(u), X_j(v)] = 0, \qquad \tilde{X}_j(u,g), \tilde{X}_j(v,g)] = 0 \tag{4.3.17}$$

Yang-Baxter equations

The fundamental Yang-Baxter Equation [31] (YBE) in the planar and linear algebra is

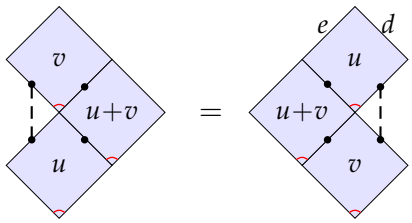

(4.3.18a)

$$X_j(u)X_{j+1}(u+v)X_j(v) = X_{j+1}(v)X_j(u+v)X_{j+1}(u) \tag{4.3.18b}$$

Distorting the faces into rhombi leads to the alternative representation of the YBE as the equality, for all values of the indices $a, b, c, d, e, f = 0, 1$, of the two partition functions

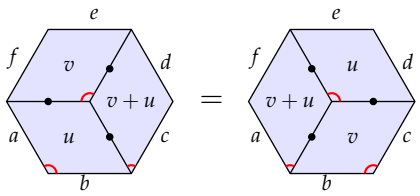

(4.3.19)

To establish commuting transfer matrices with Kac boundary conditions, we need three independent YBEs. In the planar algebra, these are

YBE1 :

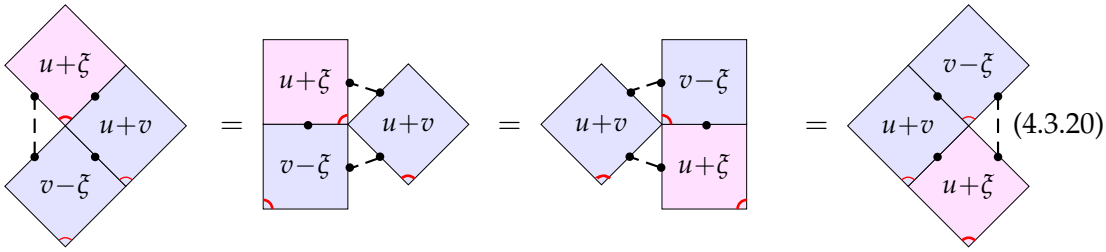

(4.3.20)

YBE2 :

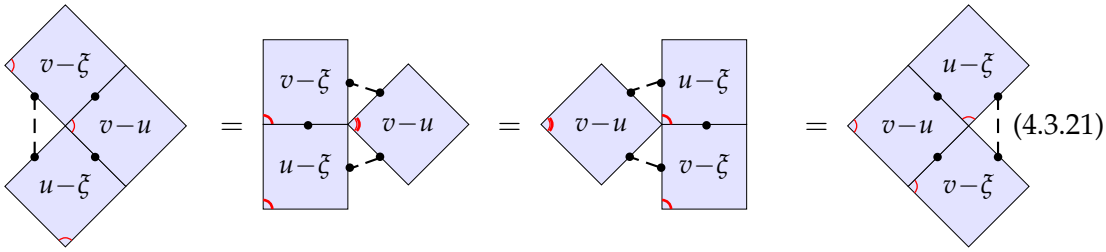

(4.3.21)

YBE3 :

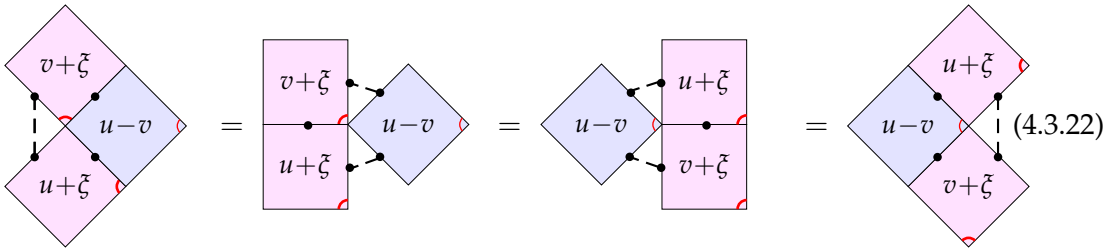

(4.3.22)

Here ξ is an arbitrary boundary field and the faces with two bold edges are the $n \times 1$

boundary seams.

Boundary Yang-Baxter equations

In the presence of a boundary, there are addtional local relations in the form of boundary Yang-Baxter or reflection equations [181, 182, 184]. The nonzero left and right boundary triangle weights and the corresponding planar operators are independent of u and given by

$$K^L\left(\begin{smallmatrix} b \\ a \end{smallmatrix}\right) = x^{1-2a}\delta(a,b), \qquad K^R\left(\begin{smallmatrix} b \\ a \end{smallmatrix}\right) = \delta(a,b) \tag{4.3.23a}$$

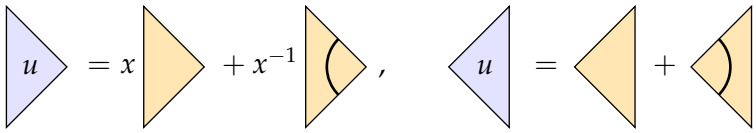

(4.3.23b)

The general right boundary Yang-Baxter equation is

$$X_j(u-v)K^R_{j+1}(u)X_j(u+v)K^R_{j+1}(v) = K^R_{j+1}(v)X_j(u+v)K^R_{j+1}(u)X_j(u-v) \tag{4.3.24a}$$

RBYBE:

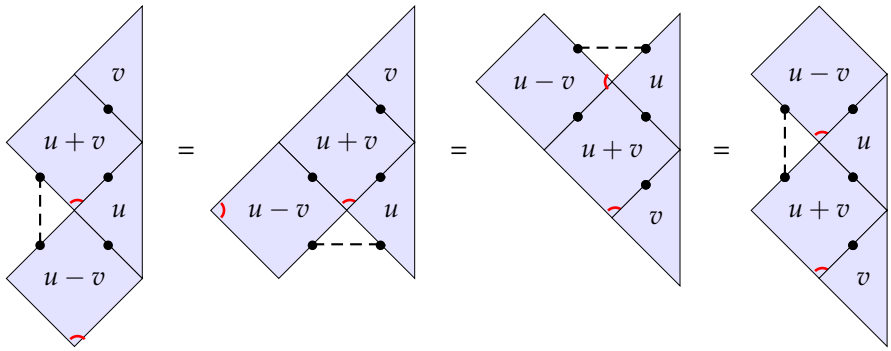

(4.3.24b)

After removing the right boundary triangles $K^R_j(u) = I$, this reduces to the commutation relation $[X_j(u-v), X_j(u+v)] = 0$.

With $z = e^{iu}$, $w = e^{iv}$, the general left boundary Yang-Baxter equation is

$$X_{j+1}(v-u,\frac{z}{w})K^L_j(u)\tilde{X}_{j+1}(2\lambda-u-v,zw)K^L_j(v) = K^L_j(v)\tilde{X}_{j+1}(2\lambda-u-v,zw)K^L_j(u)X_{j+1}(v-u,\frac{z}{w}) \tag{4.3.25a}$$

LBYBE: 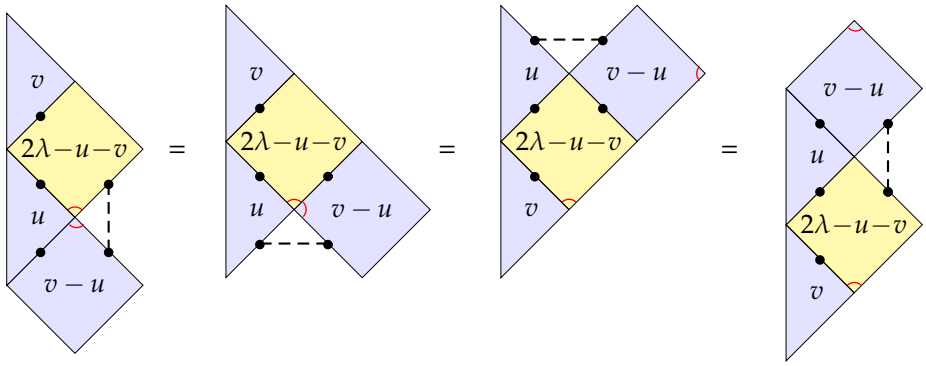

(4.3.25b)

where the gauge factors have been omitted in the diagrams. For the dimer models under consideration, the boundary triangles are independent of the spectral parameters.

4.3.2 Commuting double row transfer matrices

The general double row transfer matrices are defined by

$\boldsymbol{D}(u) =$ 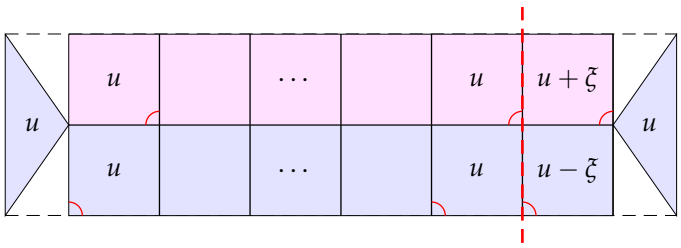

(4.3.26)

where ξ is an arbitrary boundary field. There are a total of N columns in the bulk and $w = 0, 1$ columns in the boundary. We are primarily interested in two cases (i) $w = 0$ in which case there is no boundary column and the system is homogeneous and (ii) $w = 1$ for which the boundary consists of the right-most column with $\xi = \frac{\lambda}{2}$. The specialization $\xi = \frac{\lambda}{2}$ has nice properties compared to other nonzero values of ξ. In particular the inversion identity can be solved exactly for $\xi = \frac{\lambda}{2}$.

In the six-vertex arrow (or spin) representation, the total magnetization

$$S_z = \sum_{j=1}^{\mathcal{N}} \sigma_j = -\mathcal{N}, -\mathcal{N}+2, \ldots, \mathcal{N}-2, \mathcal{N}, \qquad \mathcal{N} = N + w \tag{4.3.27}$$

is conserved under the action of the transfer matrix. By the $\mathbb{Z}_2$ up-down symmetry, the spectrum for the sectors $S_z = \pm m$ coincide for $m > 0$. More generally, the number of down

spins is $d = \frac{1}{2}(\mathcal{N} - S_z)$. The number of up spins is thus $\mathcal{N} - d = \frac{1}{2}(\mathcal{N} + S_z)$ and the counting of states in the S_z sector is given by the binomial $\binom{\mathcal{N}}{d}$ with $S_z = \mathcal{N} \bmod 2$. In the particle representation, a particle configuration along a row of the double row transfer matrix takes the form

$$a = \{a, a_2, \ldots, a_{\mathcal{N}-1}, a_{\mathcal{N}}\}, \qquad a_j = 0, 1 \text{ for } j = 1, 2, \ldots, \mathcal{N} \tag{4.3.28}$$

The total number of particles $d = \sum_{j=1}^{\mathcal{N}} a_j$ coincides with the number of down arrows and is also conserved. The transfer matrix and vector space of states thus decompose as

$$\boldsymbol{D}(u) = \bigoplus_{d=0}^{\mathcal{N}} \boldsymbol{D}_d(u), \qquad \dim \mathcal{V}^{(\mathcal{N})} = \sum_{d=0}^{\mathcal{N}} \dim \mathcal{V}_d^{(\mathcal{N})} = \sum_{d=0}^{\mathcal{N}} \binom{\mathcal{N}}{d} = 2^{\mathcal{N}} = \dim (\mathbb{C}^2)^{\otimes \mathcal{N}} \tag{4.3.29}$$

For comparing the spectra sector-by-sector with critical dense polymers [169] it is useful to define

$$\ell = |\mathcal{N} - 2d| = |S_z| = \begin{cases} 0, 2, 4, \ldots, \mathcal{N}, & \mathcal{N} \text{ even} \\ 1, 3, 5, \ldots, \mathcal{N}, & \mathcal{N} \text{ odd} \end{cases} \tag{4.3.30}$$

In the context of critical dense polymers, ℓ is the number of defects.

Setting $\eta_1 = \eta_1(u - v), \eta_2 = \eta_2(u + v)$ as in (4.3.15), the commutation of the double row transfer matrices is established diagrammatically

$\boldsymbol{D}(u)\boldsymbol{D}(v) \;=$

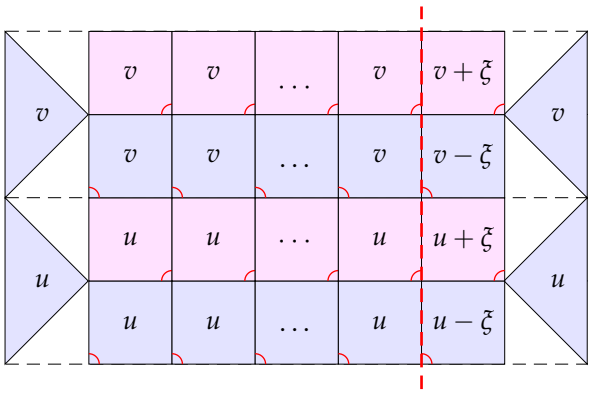

(4.3.31a)

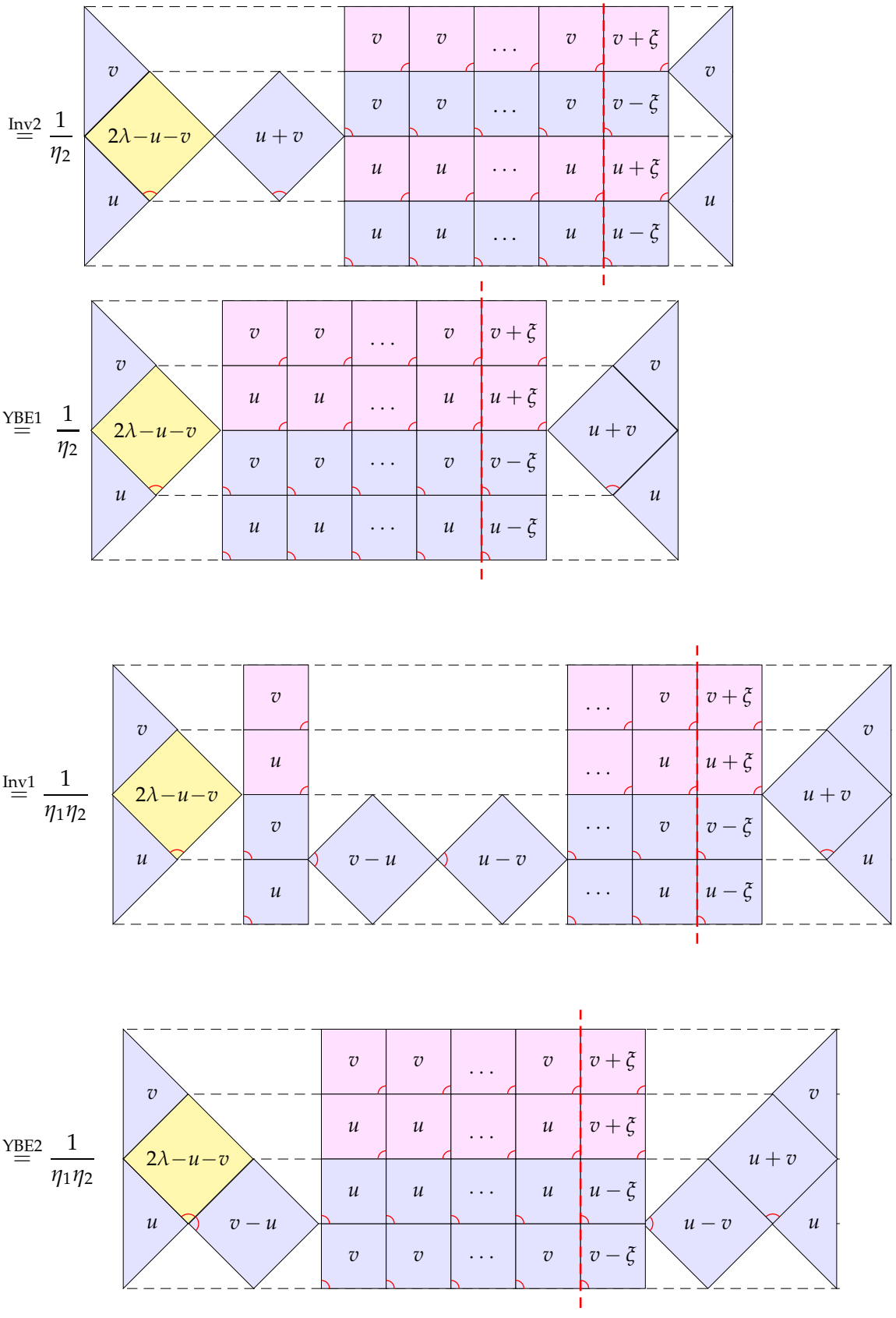
Inv2 $\frac{1}{\eta_2}$
YBE1 $\frac{1}{\eta_2}$
Inv1 $\frac{1}{\eta_1\eta_2}$
YBE2 $\frac{1}{\eta_1\eta_2}$
$2\lambda-u-v$
$u+v$
$v-u$
$u-v$
$v+\xi$
$v-\xi$
$u+\xi$
$u-\xi$

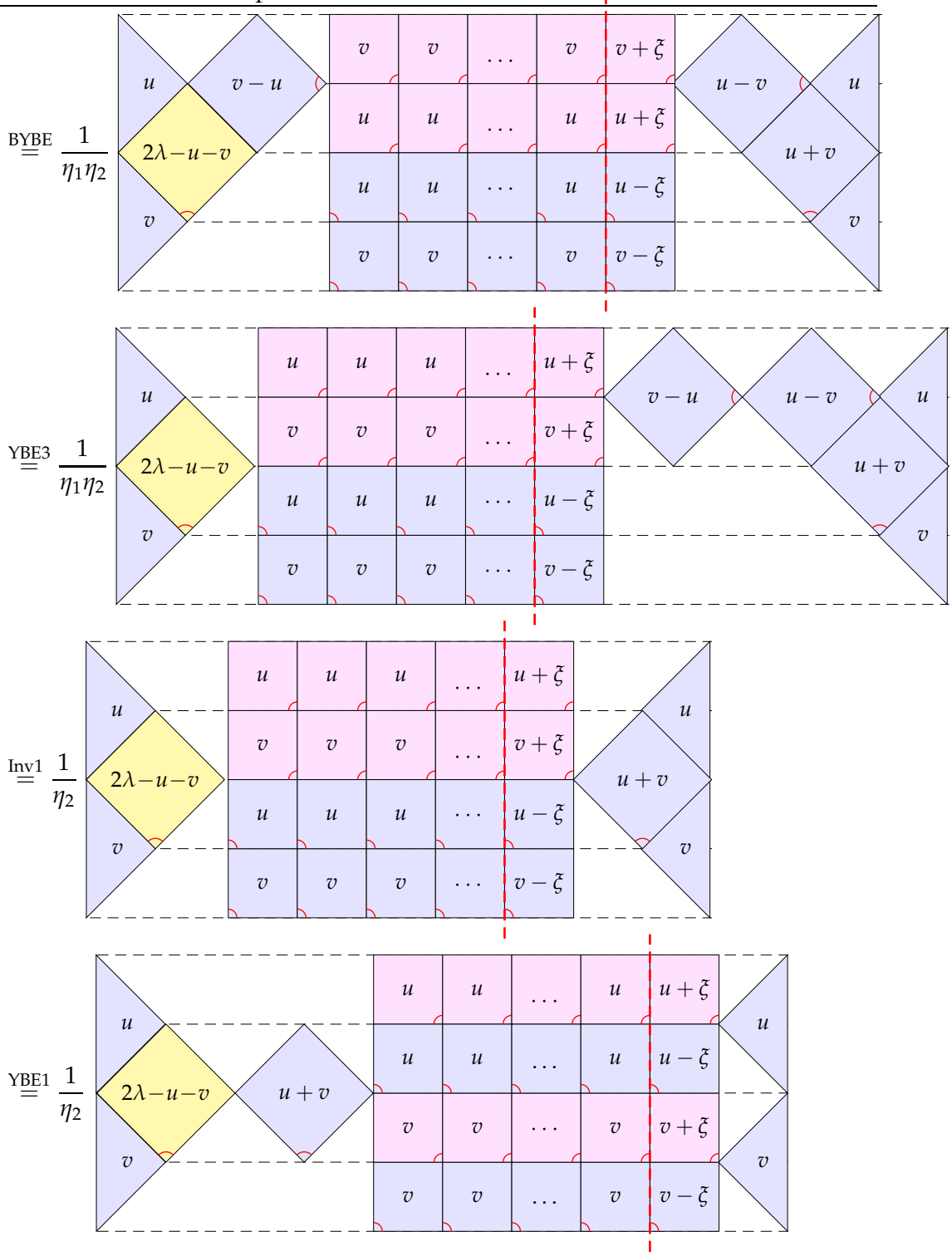
BYBE
1
η1η2
2λ−u−v
u
v
v − u
v
v
...
v
v + ξ
u
u
...
u
u + ξ
u
u
...
u
u − ξ
v
v
...
v
v − ξ
u − v
u
u + v
v
YBE3
1
η1η2
2λ−u−v
u
v
v − u
u − v
u
u + v
v
Inv1
1
η2
2λ−u−v
u
v
u + v
u
v
YBE1
1
η2
2λ−u−v
u
v
u + v
u
v

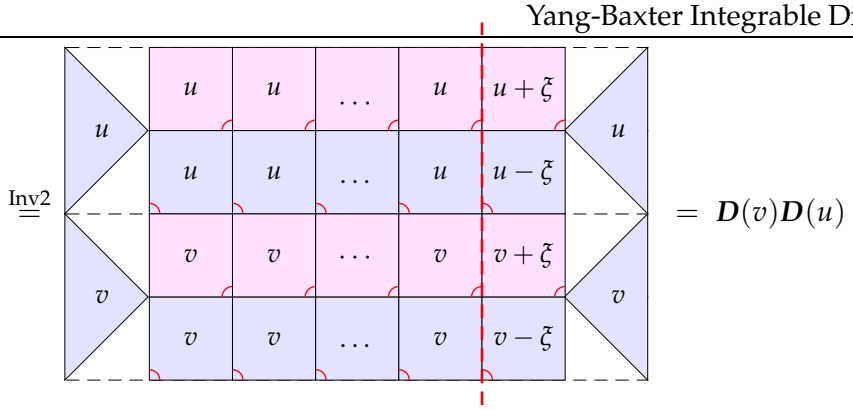

4.4 Solution of Dimers on a Strip and Finite-Size Spectra

In this section, we specialize to the six-vertex model at the free-fermion point with $\lambda = \frac{\pi}{2}$ and $x = i$ corresponding to dimers.

4.4.1 Inversion identities on the strip

In Appendix A, we show that the double row transfer matrices (4.3.26) satisfy the inversion identities

$$w = 0 : \ \boldsymbol{D}(u)\boldsymbol{D}(u+\lambda) = -\tan^2 2u \Big[\cos^{2N} u - \sin^{2N} u \Big]^2 \boldsymbol{I} \tag{4.4.1}$$

$$w = 1 : \ \boldsymbol{D}(u)\boldsymbol{D}(u+\lambda) = -\tan^2 2u \Big[\sin(u+\xi)\sin(u-\xi)\cos^{2N} u - \cos(u+\xi)\cos(u-\xi)\sin^{2N} u \Big]^2 \boldsymbol{I} \tag{4.4.2}$$

The first inversion identity is obtained from the second by dividing both sides by $\cos^4 \xi$ and taking the braid limit $\xi \to i\infty$. Remarkably, after suitable normalization and specialization, the commuting double row transfer matrices (4.3.26) satisfy precisely the same inversion identities as critical dense polymers [124, 168]. Specifically, we find

$$w = 0 : \qquad \boldsymbol{d}(u) = \frac{\boldsymbol{D}(u)}{\sin 2u}, \qquad \boldsymbol{d}(u)\boldsymbol{d}(u+\lambda) = \Big(\frac{\cos^{2N} u - \sin^{2N} u}{\cos^2 u - \sin^2 u} \Big)^2 \boldsymbol{I} \tag{4.4.3a}$$

$$w = 1,\ \xi = \frac{\lambda}{2} : \qquad \boldsymbol{d}(u) = \frac{2\boldsymbol{D}(u)}{\sin 2u}, \qquad \boldsymbol{d}(u)\boldsymbol{d}(u+\lambda) = \big(\cos^{2N} u + \sin^{2N} u \big)^2 \boldsymbol{I} \tag{4.4.3b}$$

Using standard inversion identity techniques [31, 162, 163], the last two functional equations can be solved, for arbitrary finite sizes N, for the eigenvalues $d(u)$ of $\boldsymbol{d}(u)$ subject to the initial condition and crossing symmetry

$$d(0) = 1, \qquad d(\lambda - u) = d(u) \tag{4.4.4}$$

The calculation of the eigenvalues by solving the functional equations (4.4.3a) and (4.4.3b) follows exactly the same path as in [168]. So let us just summarize the salient facts. The eigenvalues $d(u)$ are Laurent polynomials in $z = e^{iu}$. Consequently, they are determined by their complex zeros in the analyticity strip $-\frac{\pi}{4} \leq \mathrm{Re}\, u \leq \frac{3\pi}{4}$. Following [168], these zeros occur as 1-strings in the center of the analyticity strip or as "2-strings" with one zero on the boundary $\mathrm{Re}\, u = -\frac{\pi}{4}$ of the analyticity strip and its periodic image on the other boundary $\mathrm{Re}\, u = \frac{3\pi}{4}$. The ordinates of the 1- and 2-strings are quantized and given by

$$y_j = -\frac{i}{2} \ln \tan \frac{E_j \pi}{2N}, \qquad E_j = \begin{cases} j, & N + w \text{ even} \\ j - \frac{1}{2}, & N + w \text{ odd} \end{cases} \qquad j \in \mathbb{Z} \tag{4.4.5}$$

At each allowed ordinate, there is either two 1-strings, two 2-strings or one 1-string and one 2-string. The fact that double zeros occur has its origins in the relation between critical dense polymers and symplectic fermions [121, 164, 165]. Due to complex conjugation symmetry, the pattern of zeros in the upper and lower half-planes is the same. We can therefore focus solely on the lower half-plane. A typical pattern of zeros is shown in Figure 4.5.

A pattern of zeros is completely determined by specifying the location of the 1-strings. A 1-string at position j is a local elementary excitation with associated conformal energy E_j. In the ground state, with energy E_0, there are no 1-strings. The conformal excitation energy above the ground state is given by

$$E = E_0 + \sum_j E_j, \qquad j = \text{position of 1-strings} \tag{4.4.6}$$

The lowest state energy is $E_0 = -\frac{c}{24} + \Delta_s$ where c is the central charge and Δ_s is the conformal weight associated with the particular sector labelled by $s = |S_z| + 1$. The lowest

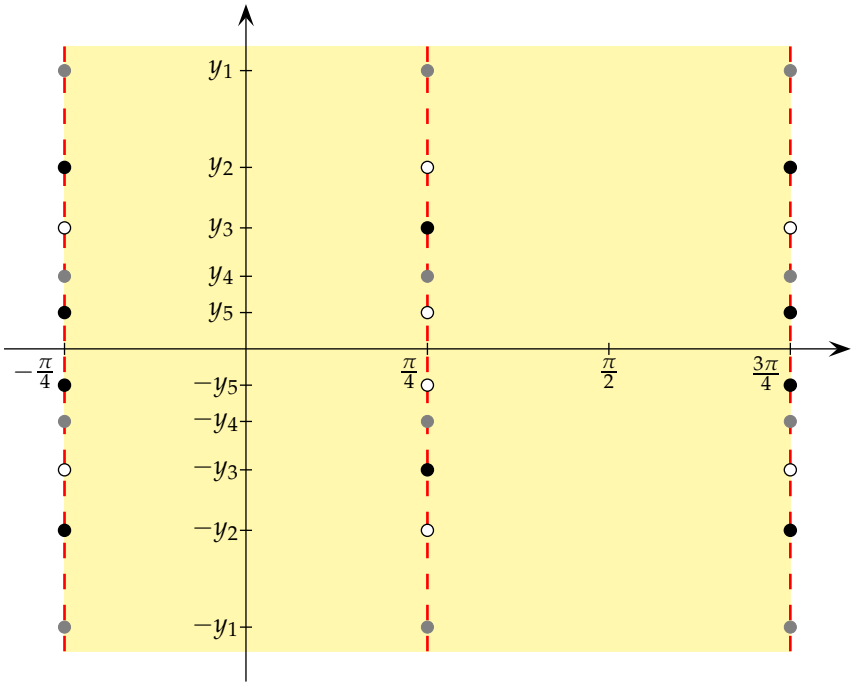

Figure 4.5: A typical pattern of zeros in the complex u-plane associated to a transfer matrix eigenvalue. Single zeros are shown by grey disks, double zeros are shown by black disks and the absence of zeros is shown by white disks. The upper and lower half-planes are related under the $\mathbb{Z}_2$ complex conjugation symmetry.

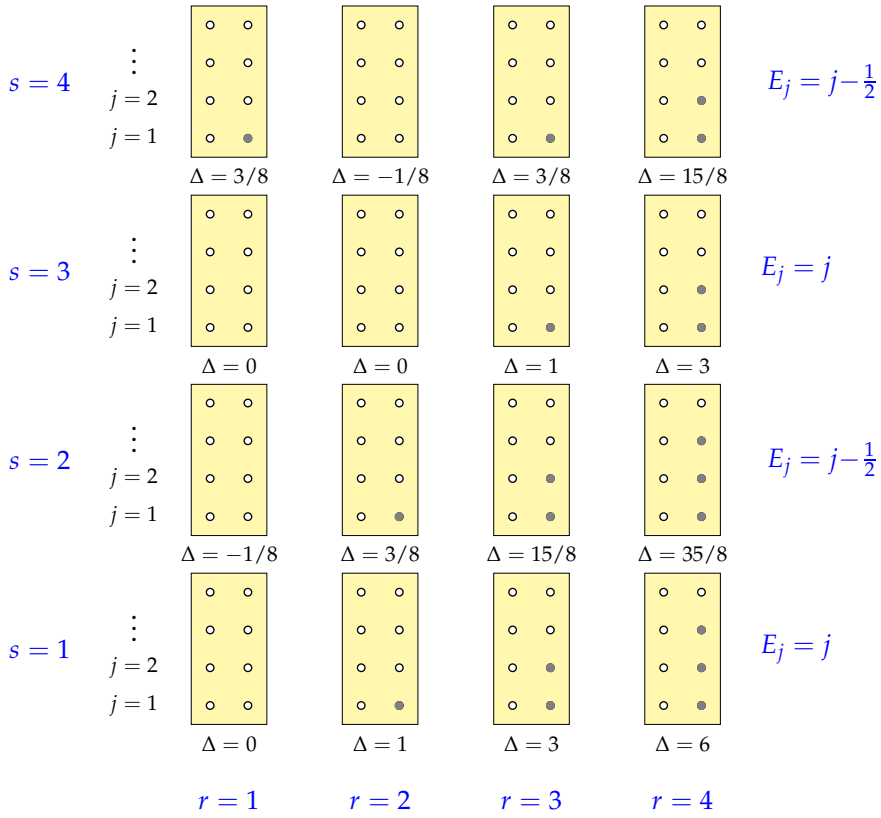

Figure 4.6: Lowest or groundstate double-column configurations arranged by sectors in a Kac table for $r,s=1,2,3,4$ for critical dense polymers. The continuation of the pattern for larger values of r and s is clear. Only the first column with $r=1$ relates to dimers. The solid grey dots represent single 1-strings in the center of the analyticity strip. There are no double zeros in the center of the analyticity strip for these groundstates. The vacuum sector with $\Delta=0$ lies at $(r,s)=(1,1)$.

states in each sector exactly coincide with those of critical dense polymers for arbitrary finite sizes. The zero patterns for these lowest states are encoded as double column diagrams in Figure 4.6. On the strip, the only difference between dimers and critical dense polymers with $(r,s)=(1,1)$ boundary conditions resides in the degeneracy of energy levels and the counting of states. The finite-size corrections therefore also coincide and the central charge $c=-2$ and conformal weights $\Delta_s=\left((2-s)^2-1\right)/8$ with $s=|S_z|+1=1,2,3,\ldots$ follow from the same calculation based on Euler-Maclaurin methods.

It follows that the finitized characters take the form

$$\chi_s^{(N)}(q)=q^{-c/24+\Delta_s}\sum_E q^E, \qquad E=\text{eigenvalue excitation energy} \tag{4.4.7}$$

This is a truncated set of conformal eigenenergies of the infinite system. The finitized characters are the spectrum generating functions for the finite set of conformal energies. The parameter q is the modular nome and arises through the finite-size calculation as

$$q = \exp(-2\pi \frac{N'}{N} \sin 2u) \tag{4.4.8}$$

where N'/N is the lattice aspect ratio. The remaining problem is thus to classify the allowed patterns of zeros and their degeneracies. This is a combinatorial problem and, since not all patterns of zeros occur, it entails certain selection rules. We determine the classification of zero patterns empirically based on examining the patterns of zeros for modest sizes N. For critical dense polymers on the strip the empirical selection rules obtained were shown rigorously to be correct [185].

4.4.2 Combinatorial analysis of patterns of zeros

Combinatorially, the key building blocks are q-Narayana numbers (or equivalently skew q-binomials) enumerated by double-column diagrams with dominance.

The information in a zero pattern is simply encoded in a double-column diagram. A double-column configuration $S = (L, R)$ is called *admissible* if $L \preceq R$ with respect to the partial ordering

$$L \preceq R \quad \text{if} \quad L_j \leq R_j, \ \ j = 1, \ldots, m \tag{4.4.9}$$

which presupposes that

$$0 \leq m \leq n \leq M \tag{4.4.10}$$

Admissibility is characterized diagrammatically as in the following example

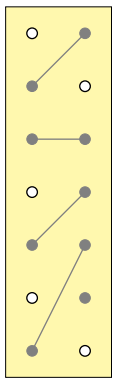

(4.4.11)

One draws line segments between the occupied sites of greatest height in the two columns, then between the occupied sites of second-to-greatest height and so on. The double-column configuration is now admissible if it does *not* involve line segments with a *strictly negative slope*. Thus, in an admissible double-column configuration, there are either no line segments ($m = 0$) or each line segment appears with a non-negative slope. Such admissible diagrams are said to satisfy dominance. At each position or height j, there is zero, one or two occupied sites corresponding to zero, one or two 1-strings in the lower half-plane.

Combinatorially, the (generalized) q-Narayana numbers $\left\langle \begin{matrix} M \\ m, n \end{matrix} \right\rangle_q$ are defined as the sum of the monomials associated to all admissible double-column configurations of height M with exactly m and n occupied sites in the left and right columns respectively

$$\left\langle \begin{matrix} M \\ m, n \end{matrix} \right\rangle_q = \sum_{S:\,|L|=m,|R|=n} q^{E(S)} \tag{4.4.12}$$

These are the basic building blocks to describe the allowed patterns of zeros in each sector. Physically, these are the generating functions for the spectrum encoded in a double column diagram with conformal energies $E_j = j$. The monomials $q^{E(S)}$ need to be scaled by the factor $q^{-\frac{1}{2}(m+n)}$ in sectors with $E_j = j - \frac{1}{2}$. The q-Narayana numbers admit the closed-form

expressions

$$\left\langle \begin{matrix} M \\ m,n \end{matrix} \right\rangle_q = q^{\frac{1}{2}m(m+1)+\frac{1}{2}n(n+1)} \left\{ \begin{matrix} M \\ m,n \end{matrix} \right\}_q \tag{4.4.13}$$

$$= q^{\frac{1}{2}m(m+1)+\frac{1}{2}n(n+1)} \left(\begin{bmatrix} M \\ m \end{bmatrix}_q \begin{bmatrix} M \\ n \end{bmatrix}_q - q^{n-m+1} \begin{bmatrix} M \\ m-1 \end{bmatrix}_q \begin{bmatrix} M \\ n+1 \end{bmatrix}_q \right) \tag{4.4.14}$$

where $\begin{bmatrix} M \\ m \end{bmatrix}_q$ is a q-binomial (Gaussian polynomial) and $\left\{ \begin{matrix} M \\ m,n \end{matrix} \right\}_q$ are skew q-binomials, as in Appendix D.1. The (generalized) q-Narayana numbers coincide with q-Narayana numbers [186, 187] when $m = n$.

4.4.3 Empirical selection rules

In this Section we consider the empirical classification of patterns of zeros for the cases $w = 0, 1$. Empirically, using Mathematica [150] to examine the spectra out to $\mathcal{N} = N + w = 8$, we find that the finitized characters are classified in terms of patterns of zeros, double column diagrams and q-Narayana numbers by

$$\chi_s^{(N)}(q) = \begin{cases} q^{-c/24+\Delta_1} \sum_{m,n=0}^{\lfloor \frac{\mathcal{N}-1}{2} \rfloor} A_{m,n}^{(s)} \left\langle \begin{matrix} \lfloor \frac{\mathcal{N}-1}{2} \rfloor \\ m,n \end{matrix} \right\rangle_q, & s \text{ odd}, \Delta_1 = 0 \\ q^{-c/24+\Delta_2} \sum_{m,n=0}^{\lfloor \frac{\mathcal{N}-1}{2} \rfloor} B_{m,n}^{(s)} q^{-\frac{1}{2}(m+n)} \left\langle \begin{matrix} \lfloor \frac{\mathcal{N}-1}{2} \rfloor \\ m,n \end{matrix} \right\rangle_q, & s \text{ even}, \Delta_2 = -\frac{1}{8} \end{cases} \tag{4.4.15}$$

The $\lfloor\frac{\mathcal{N}+1}{2}\rfloor \times \lfloor\frac{\mathcal{N}+1}{2}\rfloor$ matrices $A^{(s)}$ and $B^{(s)}$ have a simple structure as indicated in the following examples

$$\mathcal{N}=8:\ A^{(1)}=\begin{pmatrix}2&2&2&2\\0&2&2&2\\0&0&2&2\\0&0&0&2\end{pmatrix},\ A^{(3)}=\begin{pmatrix}1&2&2&2\\0&1&2&2\\0&0&1&2\\0&0&0&1\end{pmatrix},\ A^{(5)}=\begin{pmatrix}0&1&2&2\\0&0&1&2\\0&0&0&1\\0&0&0&0\end{pmatrix},\ \ldots,\ A^{(9)}=\begin{pmatrix}0&0&0&1\\0&0&0&0\\0&0&0&0\\0&0&0&0\end{pmatrix} \tag{4.4.16}$$

$$\mathcal{N}=7:\ B^{(2)}=\begin{pmatrix}1&1&1&1\\0&1&1&1\\0&0&1&1\\0&0&0&1\end{pmatrix},\ B^{(4)}=\begin{pmatrix}0&1&1&1\\0&0&1&1\\0&0&0&1\\0&0&0&0\end{pmatrix},\ B^{(6)}=\begin{pmatrix}0&0&1&1\\0&0&0&1\\0&0&0&0\\0&0&0&0\end{pmatrix},\ B^{(8)}=\begin{pmatrix}0&0&0&1\\0&0&0&0\\0&0&0&0\\0&0&0&0\end{pmatrix} \tag{4.4.17}$$

For $w=0,1$ and s odd or even, the finitized characters can be written in terms of q-binomials

$$\chi_s^{(N)}(q)=q^{-c/24+\Delta_s}\,\frac{1+q^{(s-1)/2}}{1+q^{\mathcal{N}/2}}\begin{bmatrix}\mathcal{N}\\ \frac{1}{2}(\mathcal{N}+s-1)\end{bmatrix}_q,\qquad \mathcal{N}=N+w \tag{4.4.18}$$

where

$$\Delta_s=\frac{(2-s)^2-1}{8} \tag{4.4.19}$$

Setting $q=1$ gives the correct counting of states $\chi_s^{(N)}(1)=\binom{\mathcal{N}}{\frac{1}{2}(\mathcal{N}+s-1)}$. Observing that $|q|<1$ and using the result

$$\lim_{M\to\infty}\begin{bmatrix}M\\ m\end{bmatrix}_q=\frac{1}{(q)_m},\qquad (q)_m=\prod_{k=1}^{m}(1-q^k) \tag{4.4.20}$$

it follows that in the thermodynamic limit

$$\chi_s(q)=\lim_{N\to\infty}\chi_s^{(N)}(q)=\frac{q^{-c/24+\Delta_s}}{(q)_\infty}\,(1+q^{(s-1)/2}) \tag{4.4.21}$$

Notice that, for $s=1$, all states are doubly degenerate and that, for s even, the characters involve half-integer powers of q.

4.5 Jordan Decompositions

4.5.1 Isotropic double row transfer matrices

It is easy to verify that, at the isotropic point $u = \frac{\lambda}{2}$, the double row transfer matrix $\boldsymbol{D}(u)$ is not Hermitian. Remarkably, it has real eigenvalues but the Jordan decomposition admits nontrivial Jordan cells of rank 2:

$$N = 2,\ s = 1: \qquad \begin{pmatrix} 1 & 1 \\ 0 & 1 \end{pmatrix} \tag{4.5.1}$$

$$N = 4,\ s = 1: \qquad \tfrac{1}{2} \oplus \begin{pmatrix} \frac{3}{2} - \sqrt{2} & 1 \\ 0 & \frac{3}{2} - \sqrt{2} \end{pmatrix} \oplus \begin{pmatrix} \frac{3}{2} + \sqrt{2} & 1 \\ 0 & \frac{3}{2} + \sqrt{2} \end{pmatrix} \oplus \tfrac{1}{2} \tag{4.5.2}$$

4.5.2 Quantum Hamiltonians

As pointed out in [132], the quantum Hamiltonian

$$\mathcal{H} = -\tfrac{1}{2} \frac{d}{du} \log \boldsymbol{D}(u)\Big|_{u=0} \tag{4.5.3}$$

for dimers on the strip with $w = 0$ precisely coincides with the $U_q(sl(2))$-invariant XX Hamiltonian of the free-fermion six-vertex model

$$\mathcal{H} = -\sum_{j=1}^{N-1} e_j = -\tfrac{1}{2} \sum_{j=1}^{N-1} (\sigma_j^x \sigma_{j+1}^x + \sigma_j^y \sigma_{j+1}^y) - \tfrac{1}{2} i (\sigma_1^z - \sigma_N^z) \tag{4.5.4}$$

$$= -\sum_{j=1}^{N-1} (f_j^\dagger f_{j+1} + f_{j+1}^\dagger f_j) - i(f_1^\dagger f_1 - f_N^\dagger f_N) \tag{4.5.5}$$

where $\sigma_j^{x,y,z}$ are Pauli matrices and $f_j = \sigma_j^x - i\sigma_j^y$, $f_j^\dagger = \sigma_j^x + i\sigma_j^y$. This Hamiltonian is manifestly not Hermitian. Nevertheless, the spectra of this Hamiltonian is real [188]. Including all S_z sectors, the Jordan canonical forms for $N = 2$ and $N = 4$ respectively are

$$N = 2: \quad 0 \oplus \begin{pmatrix} 0 & 1 \\ 0 & 0 \end{pmatrix} \oplus 0 \tag{4.5.6}$$

$$N = 4: \quad 0 \oplus \begin{pmatrix} 0 & 1 \\ 0 & 0 \end{pmatrix} \oplus 0 \oplus 0 \oplus \begin{pmatrix} 0 & 1 \\ 0 & 0 \end{pmatrix} \oplus 0 \oplus (-\sqrt{2}) \oplus \begin{pmatrix} -\sqrt{2} & 1 \\ 0 & -\sqrt{2} \end{pmatrix} \oplus (-\sqrt{2}) \oplus \sqrt{2} \oplus \begin{pmatrix} \sqrt{2} & 1 \\ 0 & \sqrt{2} \end{pmatrix} \oplus \sqrt{2} \tag{4.5.7}$$

Such Jordan cells for the quantum group invariant XX Hamiltonian were observed in [189]. By comparison, the transfer matrices and Hamiltonians of the (r,s) sectors of critical dense polymers are diagonalizable [124] and do not exhibit Jordan cells.

In the continuum scaling limit, the Hamiltonian gives the Virasoro dilatation operator L_0. Assuming that the Jordan cells persist in this scaling limit, we see that dimers admits reducible yet indecomposable representations and so we conclude that, as a CFT, dimers is logarithmic.

4.6 Conclusion

Although dimers was first solved many years ago, there remain a number of unanswered questions concerning the Conformal Field Theory (CFT) description of the dimer model on the square lattice. In a previous paper [132], the dimer model on a cylinder, with 45° rotated dimers, was solved exactly. Moreover, the modular invariant conformal partition function was obtained from finite-size corrections and shown to precisely agree with the modular invariant partition function of critical dense polymers.

In this thesis, we solved exactly the dimer model on a strip by viewing it as a free-fermion six-vertex model and using Yang-Baxter techniques. The key is to show that the commuting double row transfer matrices satisfy special functional equations in the form of inversion identities. Due to a common underlying Temperley-Lieb algebra, these inversion identities precisely coincide with those of critical dense polymers. This implies, essentially through the Temperley-Lieb equivalence, that the two models have eigenvalues exactly in common but the degeneracy and counting of states differ. Indeed, the lowest eigenvalues in each sector (labelled by $(r,s) = (1,s)$) coincide and so the two models share the same central charge and a common infinite set of conformal weights

$$c = -2, \qquad \Delta_s = \Delta_{1,s} = \frac{(2-s)^2 - 1}{8}, \quad s = 1,2,3,\ldots \tag{4.6.1}$$

The common negative conformal weight

$$\Delta_2 = -\frac{1}{8} \tag{4.6.2}$$

implies that both CFTs are nonunitary. However, despite these similarities, combinatorial analysis of the patterns of zeros of the transfer matrix eigenvalues of dimers leads to finitized and conformal characters (4.4.18) and (4.4.21) that are distinct from those of critical dense polymers. So clearly, the dimer model must be regarded as lying in a different "universality class" to critical dense polymers.

Finally, it is shown that the Jordan canonical form of the isotropic double row transfer matrices and quantum Hamiltonians of dimers on the strip both exhibit Jordan cells. Assuming that these Jordan cells persist in the scaling limit, this implies that the Virasoro dilatation operator L_0 admits reducible yet indecomposable representations. All this confirms that the dimer model is not a rational CFT, rather, we argue that it is described by a logarithmic CFT with central charge $c = -2$, minimal conformal weight $\Delta_{\text{min}} = -\frac{1}{8}$ and effective central charge $c_{\text{eff}} = 1$.

Chapter 5
Conclusion

Yang-Baxter integrability in two-dimensions is the reference test for solvability on the lattice: if the Yang-Baxter equation is locally satisfied, there exists a family of commuting transfer matrices with an infinite number of conserved quantities, and so the two-dimensional lattice model under consideration is exactly solvable.

RSOS models form a class of well-known Yang-Baxter integrable lattice models of statistical mechanics. Although their first formulation dates back to 1984, they continue to be subject of intensive studies due to the fact that the critical models give rise to a particular type of conformal field theories, minimal models, which finds many important applications in condensed matter physics, string theory and statistical mechanics.

In the nonunitary cases, RSOS lattice models are still integrable in the Yang-Baxter sense. Using the one-dimensional sums arising from Baxter's off-critical corner transfer matrix formalism, we have argued that, for $m' > 2m$, the nonunitary RSOS$(m, m')_{1\times1}$ and RSOS$(m, m')_{2\times2}$ lattice models lie in the same universality class described by the nonunitary minimal CFT $\mathcal{M}(m, m')$. This result holds even though, in general, RSOS$(m, m')_{1\times1}$ and RSOS$(m, m')_{2\times2}$ are distinct lattice models. More specifically, we have conjectured the explicit bosonic form of the finitized characters and, for modest system sizes N, checked that these agree with the ground state one-dimensional sums.

In the case $m' = 2m + 1$, we have further shown that the ground state one-dimensional sums of RSOS$(m, m')_{2\times2}$ agree with those of Jacob and Mathieu [139] based on half-integer RSOS paths. This connection with a Yang-Baxter integrable lattice model nicely explains the remarkable observed properties of these half-integer one-dimensional sums. The more general methods used here allow these observations to be extended to a larger family of

RSOS$(m, m')_{2\times 2}$ lattice models(or possibly all of them). Understanding the connection between these two different formulations of RSOS paths, which lead to either bosonic or fermionic forms of the finitized characters, could be an interesting subject of further investigations.

Until now dimers has been solved exactly by Pfaffian and other techniques but not by Yang-Baxter methods. The study shown in this thesis brings dimers firmly into the framework of Yang-Baxter integrability. For periodic transfer matrices, through the special inversion identity, this has enabled the detailed calculation of the dimer model spectra on the cylinder in the $\mathbb{Z}_4$, Ramond and Neveu-Schwarz sectors for arbitrary finite sizes. Taking a trace to form a torus and combining these sectors at the isotropic point $u = \frac{\lambda}{2} = \frac{\pi}{4}$ yields explicit formulas for the counting of dimer configurations on arbitrary periodic $M \times N$ square lattices. Because the orientation of the dimers is rotated by 45°, the precise counting of these states differs from the counting of configurations for the usual orientation on the square lattice even though the residual entropies coincide.

The inclusion of a spatial anisotropy in the form of a spectral parameter u enables the analytic calculation of the complete finite-size spectra of dimers yielding the central charge $c = -2$ and conformal weights $\Delta = -\frac{1}{8}, 0, \frac{3}{8}$. Remarkably, the modular invariant partition function precisely coincides with that of critical dense polymers sector-by-sector even though critical dense polymers requires the implementation of a modified trace.

Thanks to the mapping to the six-vertex model at the free fermion point and Yang-Baxter integrability, the dimer model can be also solved on a strip geometry of arbitrary finite size. The key point is that the commuting double row transfer matrices satisfy special functional equations in the form of inversion identities. Due to a common underlying Temperley-Lieb algebra, these inversion identities precisely coincide with those of critical dense polymers. This implies, essentially through the Temperley-Lieb equivalence, that the two models have eigenvalues exactly in common but the degeneracy and counting of states differs. Indeed, the combinatorial analysis of the pattern of zeros of the transfer matrix eigenvalues results in finitized characters that are distinct from those of critical dense polymers. In the continuum scaling limit, as expected, the expressions for the conformal characters of dimers and critical dense polymers are also different. However, despite the

dissimilarities, the two models share the same central charge and a common infinite set of conformal weights corresponding to sectors with $r = 1$ and $s = 1, 2, 3, \ldots$. The presence of a common negative conformal weight $\Delta_{\text{min}} = -\frac{1}{8}$ implies that both CFTs are nonunitary.

Finally, it is shown that the Jordan canonical form of the isotropic double row transfer matrices and quantum Hamiltonians of dimers on the strip both exhibit Jordan cells. Assuming that these Jordan cells persist in the scaling limit, this implies that the Virasoro dilatation operator L_0 admits reducible yet indecomposable representations. All this confirms that the dimer model is not a rational CFT, rather, we argue that it is described by a logarithmic CFT with central charge $c = -2$, minimal conformal weight $\Delta_{\text{min}} = -\frac{1}{8}$ and effective central charge $c_{\text{eff}} = 1$.

Looking at future perspectives of research on dimers, we could take advantage of the Yang-Baxter integrability and use commuting double row transfer matrices and inversion identities to extend our study to other boundary conditions on the strip or other geometries. These are expected to include boundary conditions analogous to the "current" (horizontal boundary arrows point to the right) and domain wall (horizontal boundary arrows point outwards and vertical boundary arrows point inwards) boundaries on the square lattice. Besides, an extensive study of Kac and Robin (r, s) type boundary conditions on the strip of the square lattice may help to gain a deeper insight into the conformal properties of dimers. Regarding different lattice geometries, it would be interesting to investigate the integrability of the dimer model on the checkerboard lattice with periodic boundary conditions using a more general form of the Yang-Baxter equation [190], and compare this result with a known solution by the Pfaffian method [191]. As a final remark, it is known that the inversion identity methods extend off criticality to the elliptic eight-vertex free-fermion model [162]. It would be of interest to study the off-critical dimer model given by the free-fermion eight-vertex model at $\lambda = \frac{\pi}{2}$. An extension of the mapping of [69] (Figure 4.2) suggests that this should involve horizontal and vertical dimers in addition to their 45° rotated counterparts.

Appendix A

One-Dimensional Sums and Finitized Characters of 2×2 Fused RSOS Models

A.1 Elliptic Functions

We summarize the definitions and properties of the elliptic functions used throughout this paper. The standard elliptic theta function $\vartheta_1(u,t)$ [192] is

$$\vartheta_1(u,t) = 2t^{1/4}\sin u \prod_{n=1}^{\infty}(1-2t^{2n}\cos 2u + t^{4n})(1-t^{2n}) \tag{A.1.1}$$

Its conjugate modulus transformation is

$$\vartheta_1(u,e^{-\varepsilon}) = \sqrt{\frac{\pi}{\varepsilon}}\, e^{-(u-\pi/2)^2/\varepsilon} E(e^{-2\pi u/\varepsilon}, e^{-2\pi^2/\varepsilon}) \tag{A.1.2}$$

where

$$E(w,p) = \sum_{k=-\infty}^{\infty}(-1)^k p^{k(k-1)/2} w^k = \prod_{n=1}^{\infty}(1-p^{n-1}w)(1-p^n w^{-1})(1-p^n) \tag{A.1.3}$$

The elliptic $\vartheta_1(u) = \vartheta_1(u,t)$ function satisfies the fundamental identity

$$\begin{aligned}\vartheta_1(u+x)\vartheta_1(u-x)\vartheta_1(v+y)\vartheta_1(v-y) - \vartheta_1(u+y)\vartheta_1(u-y)\vartheta_1(v+x)\vartheta_1(v-x)\\ = \vartheta_1(x-y)\vartheta_1(x+y)\vartheta_1(u+v)\vartheta_1(u-v)\end{aligned} \tag{A.1.4}$$

A.2 Yang-Baxter Equation of Critical Fused RSOS$(m, m')_{2\times 2}$ Models

In this Appendix we discuss the algebraic structure of the solution to the Yang-Baxter equations for the critical 2 × 2 RSOS models. Following [154], the face transfer operators can be written as

$$\mathbb{X}_j(u) = \frac{s(\lambda-u)s(2\lambda-u)}{s(2\lambda)} I + s(u)s(\lambda-u)X_j + \frac{s(u)s(u+\lambda)}{s(2\lambda)} E_j, \qquad s(u) = \frac{\sin u}{\sin\lambda} \tag{A.2.1}$$

where the identity I and the generalized monoids E_j and X_j

$I =$ 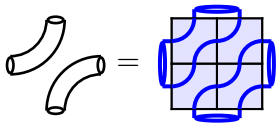 $E_j =$ 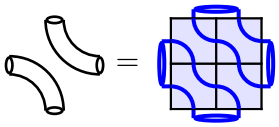 $X_j =$ 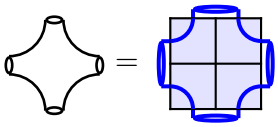

(A.2.2)

generate the 2 × 2 fused Temperley-Lieb (TL) algebra. This algebra is a one-parameter specialization of the two-parameter BMW algebra. The properties of the generator X_j were studied by a number of authors [193–196]. Here it is useful to replace the generator X_j with the generator

$\Xi_j =$ 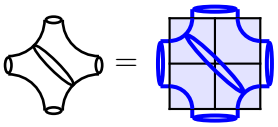 $= X_j - \beta^{-1}E_j, \qquad \Xi_j E_j = X_j E_j - \beta^{-1}E_j^2 = 0$ (A.2.3)

where

$$\beta = \beta_1 = \bigcirc = x + x^{-1} = 2\cos\lambda, \qquad x = e^{i\lambda}, \qquad \beta_{n-1} = [x]_n = \frac{x^n - x^{-n}}{x - x^{-1}} = \frac{\sin n\lambda}{\sin\lambda} \tag{A.2.4}$$

The generator Ξ_j is obtained by cabling the two central strings of X_j by decomposing the identity into orthogonal projectors

$$I \;=\; \Big|\;\Big| \;=\; \Big|\!\Big|\!\Big| \;+\beta^{-1}\;\cup\cap \;=\; p_j+\beta^{-1}e_j \tag{A.2.5}$$

The face transfer operator can now be written as

$$\mathbb{X}_j(u)=\frac{s(\lambda-u)s(2\lambda-u)}{s(2\lambda)}I+s(u)s(\lambda-u)\,\Xi_j+\frac{s(2u)}{s(2\lambda)}E_j \tag{A.2.6}$$

In the RSOS representation, the matrices representing E_j and $\beta\,\Xi_j$ admit the following non-zero rank-1 factorized blocks

E_j :

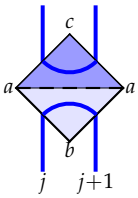

$$= \boldsymbol{e}^T_{b,a,a}\tilde{\boldsymbol{e}}_{a,a,c} \tag{A.2.7}$$

$\beta\,\Xi_j$:

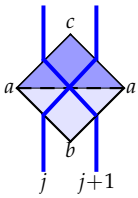

$$= \boldsymbol{x}^T_{b,a,a}\tilde{\boldsymbol{x}}_{a,a,c},$$

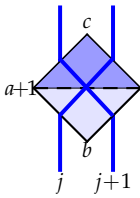

$$=$$

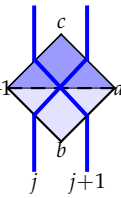

$$= \boldsymbol{y}^T_{b,a,a}\tilde{\boldsymbol{y}}_{a,a,c} \tag{A.2.8}$$

Here T denotes the transpose and the triangle weights are given by the row vectors

$$\boldsymbol{e}_{b,a,a}=\frac{1}{S_{a-1}S_{a+1}}(S_{a-1},S_a,S_{a+1}),\qquad \tilde{\boldsymbol{e}}_{a,a,c}=\frac{1}{S_a}(S_{a+1}S_{a+2},S_{a-1}S_{a+1},S_{a-2}S_{a-1}) \tag{A.2.9a}$$

$$\boldsymbol{x}_{b,a,a}=\frac{1}{S_{a-1}S_{a+1}}(-S^2_{a-1},S_{2a},S^2_{a+1}),\qquad \tilde{\boldsymbol{x}}_{a,a,c}=\frac{1}{S^2_a}(-S_aS_{a+2},S_{2a},S_{a-2}S_a) \tag{A.2.9b}$$

$$\boldsymbol{y}_{b,a,a}=(1,1),\qquad \tilde{\boldsymbol{y}}_{a,a,c}=\frac{1}{S_a}(S_{a+2},S_{a-2}) \tag{A.2.9c}$$

where, for fixed a, the vector entries are labelled by $b,c=a+2,a,a-2$ and $b,c=a+1,a-$

1 respectively. Using the relations

$$\tilde{\boldsymbol{e}}_{a,a,b}\cdot\boldsymbol{e}_{b,a,a} = \quad = \frac{S_{a+2}+S_a+S_{a-2}}{S_a} = x^2+1+x^{-2} = \beta_2 \tag{A.2.10a}$$

$$\tilde{\boldsymbol{x}}_{a,a,b}\cdot\boldsymbol{x}_{b,a,a} = \quad = \frac{S_{a-1}^2S_aS_{a+2}+S_{2a}^2+S_{a-2}S_aS_{a+1}^2}{S_{a-1}S_a^2S_{a+1}} = x^2+x^{-2} = \frac{\beta_3}{\beta} \tag{A.2.10b}$$

$$\tilde{\boldsymbol{y}}_{a,a,b}\cdot\boldsymbol{y}_{b,a,a} = \quad = \quad = \frac{S_{a+2}+S_{a-2}}{S_a} = x^2+x^{-2} = \frac{\beta_3}{\beta} \tag{A.2.10c}$$

$$\tilde{\boldsymbol{e}}_{a,a,b}\cdot\boldsymbol{x}_{b,a,a} = \quad = \frac{-S_{a-1}S_{a+2}+S_{2a}+S_{a-2}S_{a+1}}{S_a} = 0 \tag{A.2.10d}$$

$$\tilde{\boldsymbol{x}}_{a,a,b}\cdot\boldsymbol{e}_{b,a,a} = \quad = \frac{-S_{a-1}S_{a+2}+S_{2a}+S_{a-2}S_{a+1}}{S_{a-1}S_aS_{a+1}} = 0 \tag{A.2.10e}$$

it follows that, after suitable normalization, E_j and Ξ_j are commuting orthogonal idempotents. This is seen graphically as

$$E_j^2 = \quad = \beta_2 \quad = \beta_2 E_j, \qquad \beta^2\Xi_j^2 = \quad = \frac{\beta_3}{\beta} \quad = \frac{\beta_3}{\beta}\,\Xi_j \tag{A.2.11}$$

Similarly, the relations $E_jE_{j\pm1}E_j = E_j$ and $E_j\,\Xi_{j\pm1}E_j = E_j$ follows graphically as

$E_jE_{j+1}E_j =$ 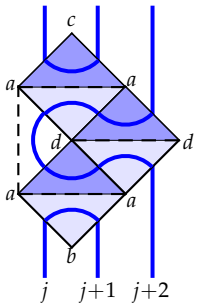

$=$ 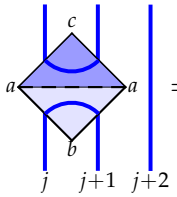

$= E_j,$ 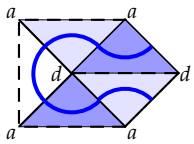

$= 1$ (A.2.12)

$\beta E_j\,\Xi_{j\pm1}E_j =$ 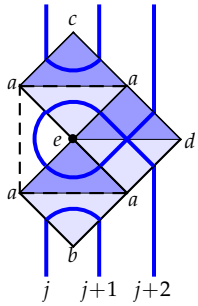

$= \dfrac{\beta_3}{\beta}$ 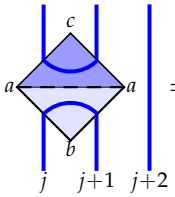

$= \dfrac{\beta_3}{\beta}\,E_j,$ 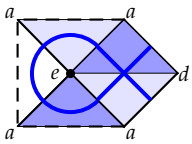

$= \dfrac{\beta_3}{\beta}$

(A.2.13)

In addition, setting $Y_j = \beta\Xi_j$, the generators satisfy the following cubic relations in accord with (3.34) of [118]

$$E_jY_{j\pm1}E_j = \tfrac{\beta_3}{\beta}\,E_j \tag{A.2.14a}$$

$$Y_jE_{j\pm1}E_j = (Y_{j\pm1} + E_{j\pm1} - 1)E_j \tag{A.2.14b}$$

$$Y_jY_{j\pm1}E_j = \big(\tfrac{\beta_3}{\beta} - 1\big)(Y_{j\pm1} + E_{j\pm1} - 1)E_j \tag{A.2.14c}$$

$$(Y_j + E_j)E_{j\pm1}(Y_j + E_j) = (Y_{j\pm1} + E_{j\pm1})E_j(Y_{j\pm1} + E_{j\pm1}) \tag{A.2.14d}$$

$$Y_jY_{j\pm1}Y_j - Y_{j\pm1}Y_jY_{j\pm1} = \beta^2(E_{j\pm1}Y_j - E_jY_{j\pm1} + Y_jE_{j\pm1} - Y_{j\pm1}E_j + E_j - E_{j\pm1}) + Y_j - Y_{j\pm1} \tag{A.2.14e}$$

Let $Z_j = Y_j + E_j$, then

$$E_j Z_{j\pm1} E_j = \beta_2 \, E_j \tag{A.2.15a}$$

$$Z_j E_{j\pm1} E_j = Z_{j\pm1} \, E_j \tag{A.2.15b}$$

$$Z_j Z_{j\pm1} E_j = ((\beta_2 - 1) Z_{j\pm1} + 1) E_j \tag{A.2.15c}$$

$$Z_j \, E_{j\pm1} Z_j = Z_{j\pm1} \, E_j \, Z_{j\pm1} \tag{A.2.15d}$$

$$Y_j Y_{j\pm1} Y_j - Y_{j\pm1} Y_j Y_{j\pm1} = \beta^2 (E_{j\pm1} Y_j - E_j Y_{j\pm1} + Y_j E_{j\pm1} - Y_{j\pm1} E_j + E_j - E_{j\pm1}) + Y_j - Y_{j\pm1} \tag{A.2.15e}$$

Expanding the Yang-Baxter equation

$$\mathbb{X}_j(u)\mathbb{X}_{j\pm1}(u+v)\mathbb{X}_j(v) = \mathbb{X}_{j\pm1}(v)\mathbb{X}_j(u+v)\mathbb{X}_{j\pm1}(u) \tag{A.2.16}$$

in terms of the face operators (A.2.6) as a multivariable Laurent polynomial in $z = e^{iu}$ and $w = e^{iv}$, equating coefficients and using these cubic relations, it follows that the Yang-Baxter equations is satisfied.

Appendix B

Yang-Baxter Solution of Dimers as a Free-Fermion Six-Vertex Model

B.1 Proof of Inversion Identities on the Cylinder

For completeness, in this appendix, we present the derivation following Felderhof [162] of the inversion identities (3.3.8) for periodic boundary conditions on the cylinder

$$\boldsymbol{T}_d(u)\boldsymbol{T}_d(u+\lambda) = \left(\cos^{2N} u - \sin^{2N} u\right) I, \qquad N \text{ odd} \tag{B.1.1a}$$

$$\boldsymbol{T}_d(u)\boldsymbol{T}_d(u+\lambda) = \left(\cos^{2N} u + \sin^{2N} u + 2(-1)^d \sin^N u \cos^N u\right) I, \qquad N \text{ even} \tag{B.1.1b}$$

For simplicity, since the transfer matrix is independent of the gauge, we work in the gauge $g = \rho = 1$.

For a 2-column at position j with fixed a_j, b_j, let us define the following four 4×4 matrices

$$R\begin{pmatrix} b_j \\ a_j \end{pmatrix} = \begin{array}{ccc} & b_j & \\ c' & u+\lambda & d' \\ c & u & d \\ & a_j & \end{array} \tag{B.1.2}$$

Ordering the four intermediate basis states as

$$\begin{pmatrix} c' \\ c \end{pmatrix} = \begin{pmatrix} 0 \\ 0 \end{pmatrix}, \begin{pmatrix} 1 \\ 0 \end{pmatrix}, \begin{pmatrix} 0 \\ 1 \end{pmatrix}, \begin{pmatrix} 1 \\ 1 \end{pmatrix} \tag{B.1.3}$$

the explicit form of these R matrices is

$$R\begin{pmatrix}0\\0\end{pmatrix}=\begin{pmatrix}-\sin u\cos u & 0 & 0 & 0\\ 0 & \cos^2 u & 0 & 0\\ 0 & 1 & -\sin^2 u & 0\\ 0 & 0 & 0 & \sin u\cos u\end{pmatrix},\quad R\begin{pmatrix}1\\1\end{pmatrix}=\begin{pmatrix}\sin u\cos u & 0 & 0 & 0\\ 0 & -\sin^2 u & 1 & 0\\ 0 & 0 & \cos^2 u & 0\\ 0 & 0 & 0 & -\sin u\cos u\end{pmatrix}$$

$$R\begin{pmatrix}1\\0\end{pmatrix}=\begin{pmatrix}0 & 0 & 0 & 0\\ \cos u & 0 & 0 & 0\\ \cos u & 0 & 0 & 0\\ 0 & -\sin u & \sin u & 0\end{pmatrix},\qquad R\begin{pmatrix}0\\1\end{pmatrix}=\begin{pmatrix}0 & \sin u & -\sin u & 0\\ 0 & 0 & 0 & \cos u\\ 0 & 0 & 0 & \cos u\\ 0 & 0 & 0 & 0\end{pmatrix}\tag{B.1.4}$$

It follows that the matrix entries of the left-side of the inversion identity are given by the trace of an ordered matrix product

$$[\boldsymbol{T}_d(u)\boldsymbol{T}_d(u+\lambda)]_{\boldsymbol{a},\boldsymbol{b}}=\mathrm{Tr}\prod_{j=1}^{N}R\begin{pmatrix}b_j\\a_j\end{pmatrix},\qquad a_j,b_j=0,1\tag{B.1.5}$$

where the lower and upper row configurations are $\boldsymbol{a}=\{a_1,a_2,\ldots,a_N\},\boldsymbol{b}=\{b_1,b_2,\ldots,b_N\}$.

Carrying out a similarity transformation with the matrices

$$S=\begin{pmatrix}0 & x_1 & x_2 & 0\\ x_3 & 0 & 0 & x_4\\ x_5 & 0 & 0 & x_6\\ 0 & x_7 & x_8 & 0\end{pmatrix}=\begin{pmatrix}0 & 0 & 1 & 0\\ 0 & 0 & 0 & -1\\ 1 & 0 & 0 & 0\\ 0 & 1 & -1 & 0\end{pmatrix},\qquad x_1=x_3=x_6=0,\quad x_2=x_5=x_7=1,\quad x_4=x_8=-1\tag{B.1.6}$$

$$S^{-1}=\begin{pmatrix}0 & y_1 & y_2 & 0\\ y_3 & 0 & 0 & y_4\\ y_5 & 0 & 0 & y_6\\ 0 & y_7 & y_8 & 0\end{pmatrix}=\begin{pmatrix}0 & 0 & 1 & 0\\ 1 & 0 & 0 & 1\\ 1 & 0 & 0 & 0\\ 0 & -1 & 0 & 0\end{pmatrix},\qquad y_1=y_6=y_8=0,\quad y_2=y_3=y_4=y_5=1,\quad y_7=-1\tag{B.1.7}$$

brings the four "diagonal" R matrices simultaneously to upper triangular form

$$SR\begin{pmatrix}0\\0\end{pmatrix}S^{-1} = \begin{pmatrix}\cos^2 u & 0 & 0 & 1\\ 0 & \sin u\cos u & 0 & 0\\ 0 & 0 & -\sin u\cos u & 0\\ 0 & 0 & 0 & -\sin^2 u\end{pmatrix} \tag{B.1.8a}$$

$$SR\begin{pmatrix}1\\1\end{pmatrix}S^{-1} = \begin{pmatrix}\cos^2 u & 0 & 0 & 0\\ 0 & -\sin u\cos u & 0 & 0\\ 0 & 0 & \sin u\cos u & 0\\ 0 & 0 & 0 & -\sin^2 u\end{pmatrix} \tag{B.1.8b}$$

$$SR\begin{pmatrix}1\\0\end{pmatrix}S^{-1} = \begin{pmatrix}0 & 0 & \cos u & 0\\ 0 & 0 & 0 & \sin u\\ 0 & 0 & 0 & 0\\ 0 & 0 & 0 & 0\end{pmatrix} \tag{B.1.8c}$$

$$SR\begin{pmatrix}0\\1\end{pmatrix}S^{-1} = \begin{pmatrix}0 & -\cos u & 0 & 0\\ 0 & 0 & 0 & 0\\ 0 & 0 & 0 & \sin u\\ 0 & 0 & 0 & 0\end{pmatrix} \tag{B.1.8d}$$

The required inversion identities (B.1.1) then follow immediately

$$\boldsymbol{T}_d(u)\boldsymbol{T}_d(u+\lambda) = \big[(\cos^2 u)^N + (-\sin^2 u)^N + (-1)^{N-d}(\sin u\cos u)^N + (-1)^d(\sin u\cos u)^N\big] \tag{B.1.9}$$

Appendix C

Yang-Baxter Integrable Dimers on a Strip

C.1 Proof of Inversion Identities on the Strip

In this appendix, we prove the inversion identity (4.4.1) for dimers on the strip

$$\boldsymbol{D}(u)\boldsymbol{D}(u+\lambda) = \left(\cos^{2N} u - \sin^{2N} u\right)^2 \boldsymbol{I}, \quad w = 0 \tag{C.1.1}$$

where $\boldsymbol{D}(u)$ is the double row transfer matrix (4.3.26). The inversion identity (4.4.2) is proved similarly. Throughout this section, we work in the Temperley-Lieb representation with the gauge $g = z = e^{iu}$.

For a column at position j with fixed $a_j, b_j = 0, 1$, let us define the four 16×16 matrices

$R\begin{pmatrix} a_j \\ b_j \end{pmatrix} =$

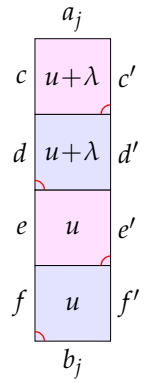

(C.1.2)

The matrix elements of the product of double row transfer matrices, with upper and lower

particle state configurations $\boldsymbol{a} = \{a_1, a_2, \ldots, a_N\}$ and $\boldsymbol{b} = \{b_1, b_2, \ldots, b_N\}$, are then given by

$$\left[\boldsymbol{D}(u)\boldsymbol{D}(u+\lambda)\right]_{\boldsymbol{b},\boldsymbol{a}} = \langle \text{left}| \prod_{j=1}^{N} R \begin{pmatrix} a_j \\ b_j \end{pmatrix} |\text{right}\rangle, \qquad a_j, b_j = 0, 1 \tag{C.1.3}$$

where the left and right boundary vectors are

$$\langle \text{left}| = (-1, 1, 1, -1, 0, 0, 0, 0, 0, 0, 0, 0, 0, 0, 0, 0) \in \mathcal{V}_6 \tag{C.1.4}$$

$$|\text{right}\rangle = (1, 1, 1, 1, 0, 0, 0, 0, 0, 0, 0, 0, 0, 0, 0, 0)^T \in \mathcal{V}_6 \tag{C.1.5}$$

Setting

$$s = \sin u,\ c = \cos u,\ z = e^{iu},\ x = i \tag{C.1.6}$$

and ordering the sixteen intermediate basis states as

$$\begin{pmatrix}0\\0\\0\\0\end{pmatrix}, \begin{pmatrix}0\\0\\1\\1\end{pmatrix}, \begin{pmatrix}1\\1\\0\\0\end{pmatrix}, \begin{pmatrix}1\\1\\1\\1\end{pmatrix}, \begin{pmatrix}0\\1\\1\\0\end{pmatrix}, \begin{pmatrix}1\\0\\0\\1\end{pmatrix}; \quad \begin{pmatrix}0\\0\\0\\1\end{pmatrix}, \begin{pmatrix}0\\0\\1\\0\end{pmatrix}, \begin{pmatrix}0\\1\\0\\0\end{pmatrix}, \begin{pmatrix}0\\1\\0\\1\end{pmatrix}, \begin{pmatrix}0\\1\\1\\1\end{pmatrix}, \begin{pmatrix}1\\0\\0\\0\end{pmatrix}, \begin{pmatrix}1\\0\\1\\0\end{pmatrix}, \begin{pmatrix}1\\0\\1\\1\end{pmatrix}, \begin{pmatrix}1\\1\\0\\1\end{pmatrix}, \begin{pmatrix}1\\1\\1\\0\end{pmatrix} \tag{C.1.7}$$

the four $R\begin{pmatrix} a_j \\ b_j \end{pmatrix}$ matrices are given explicitly by

$$R\begin{pmatrix} 0 \\ 0 \end{pmatrix} = \begin{pmatrix}
c^2s^2 & 0 & 0 & 0 & \frac{ics}{z^2} & 0 & 0 & 0 & 0 & 0 & 0 & 0 & 0 & 0 & 0 & 0 \\
s^2z^2 & s^4 & 0 & 0 & ics & 0 & 0 & 0 & 0 & 0 & 0 & 0 & 0 & 0 & 0 & 0 \\
-c^2z^2 & 0 & c^4 & 0 & -ics & 0 & 0 & 0 & 0 & 0 & 0 & 0 & 0 & 0 & 0 & 0 \\
-z^4 & -s^2z^2 & c^2z^2 & c^2s^2 & -icsz^2 & 0 & 0 & 0 & 0 & 0 & 0 & 0 & 0 & 0 & 0 & 0 \\
0 & 0 & 0 & 0 & -c^2s^2 & 0 & 0 & 0 & 0 & 0 & 0 & 0 & 0 & 0 & 0 & 0 \\
icsz^2 & ics & -ics & -\frac{ics}{z^2} & 0 & -c^2s^2 & 0 & 0 & 0 & 0 & 0 & 0 & 0 & 0 & 0 & 0 \\
0 & 0 & 0 & 0 & 0 & 0 & cs^3 & 0 & is^2 & 0 & \frac{is^2}{z^2} & 0 & 0 & 0 & 0 & 0 \\
0 & 0 & 0 & 0 & 0 & 0 & 0 & cs^3 & 0 & 0 & 0 & 0 & 0 & 0 & 0 & 0 \\
0 & 0 & 0 & 0 & 0 & 0 & 0 & 0 & -c^3s & 0 & 0 & 0 & 0 & 0 & 0 & 0 \\
0 & 0 & 0 & 0 & 0 & 0 & 0 & 0 & 0 & -c^2s^2 & 0 & 0 & 0 & 0 & 0 & 0 \\
0 & 0 & 0 & 0 & 0 & 0 & 0 & 0 & -csz^2 & 0 & -cs^3 & 0 & 0 & 0 & 0 & 0 \\
0 & 0 & 0 & 0 & 0 & 0 & 0 & ic^2 & 0 & 0 & 0 & -c^3s & 0 & 0 & 0 & -\frac{ic^2}{z^2} \\
0 & 0 & 0 & 0 & 0 & 0 & 0 & 0 & 0 & 0 & 0 & 0 & -c^2s^2 & 0 & 0 & 0 \\
0 & 0 & 0 & 0 & 0 & 0 & 0 & ic^2z^2 & 0 & 0 & 0 & -csz^2 & 0 & -cs^3 & 0 & -ic^2 \\
0 & 0 & 0 & 0 & 0 & 0 & -csz^2 & 0 & -is^2z^2 & 0 & -is^2 & 0 & 0 & 0 & c^3s & 0 \\
0 & 0 & 0 & 0 & 0 & 0 & 0 & -csz^2 & 0 & 0 & 0 & 0 & 0 & 0 & 0 & c^3s
\end{pmatrix} \tag{C.1.8}$$

$$R\begin{pmatrix} 1 \\ 1 \end{pmatrix} = \begin{pmatrix}
c^2s^2 & \frac{c^2}{z^2} & -\frac{s^2}{z^2} & -\frac{1}{z^4} & 0 & \frac{ics}{z^2} & 0 & 0 & 0 & 0 & 0 & 0 & 0 & 0 & 0 & 0 \\
0 & c^4 & 0 & -\frac{c^2}{z^2} & 0 & ics & 0 & 0 & 0 & 0 & 0 & 0 & 0 & 0 & 0 & 0 \\
0 & 0 & s^4 & \frac{s^2}{z^2} & 0 & -ics & 0 & 0 & 0 & 0 & 0 & 0 & 0 & 0 & 0 & 0 \\
0 & 0 & 0 & c^2s^2 & 0 & -icsz^2 & 0 & 0 & 0 & 0 & 0 & 0 & 0 & 0 & 0 & 0 \\
icsz^2 & ics & -ics & -\frac{ics}{z^2} & -c^2s^2 & 0 & 0 & 0 & 0 & 0 & 0 & 0 & 0 & 0 & 0 & 0 \\
0 & 0 & 0 & 0 & 0 & -c^2s^2 & 0 & 0 & 0 & 0 & 0 & 0 & 0 & 0 & 0 & 0 \\
0 & 0 & 0 & 0 & 0 & 0 & c^3s & 0 & 0 & 0 & 0 & 0 & 0 & 0 & -\frac{cs}{z^2} & 0 \\
0 & 0 & 0 & 0 & 0 & 0 & 0 & c^3s & 0 & 0 & 0 & is^2 & 0 & \frac{is^2}{z^2} & 0 & -\frac{cs}{z^2} \\
0 & 0 & 0 & 0 & 0 & 0 & ic^2 & 0 & -cs^3 & 0 & -\frac{cs}{z^2} & 0 & 0 & 0 & -\frac{ic^2}{z^2} & 0 \\
0 & 0 & 0 & 0 & 0 & 0 & 0 & 0 & 0 & -c^2s^2 & 0 & 0 & 0 & 0 & 0 & 0 \\
0 & 0 & 0 & 0 & 0 & 0 & ic^2z^2 & 0 & 0 & 0 & -c^3s & 0 & 0 & 0 & -ic^2 & 0 \\
0 & 0 & 0 & 0 & 0 & 0 & 0 & 0 & 0 & 0 & 0 & -cs^3 & 0 & -\frac{cs}{z^2} & 0 & 0 \\
0 & 0 & 0 & 0 & 0 & 0 & 0 & 0 & 0 & 0 & 0 & 0 & -c^2s^2 & 0 & 0 & 0 \\
0 & 0 & 0 & 0 & 0 & 0 & 0 & 0 & 0 & 0 & 0 & 0 & 0 & -c^3s & 0 & 0 \\
0 & 0 & 0 & 0 & 0 & 0 & 0 & 0 & 0 & 0 & 0 & 0 & 0 & 0 & cs^3 & 0 \\
0 & 0 & 0 & 0 & 0 & 0 & 0 & 0 & 0 & 0 & 0 & -is^2z^2 & 0 & -is^2 & 0 & cs^3
\end{pmatrix} \tag{C.1.9}$$

$$R\begin{pmatrix}0\\1\end{pmatrix} = \begin{pmatrix}
0 & 0 & 0 & 0 & 0 & 0 & \frac{cs^2}{z} & 0 & \frac{is^3}{z} & 0 & \frac{is}{z^3} & 0 & 0 & 0 & 0 & 0\\
0 & 0 & 0 & 0 & 0 & 0 & cs^2z & 0 & 0 & 0 & \frac{ic^2s}{z} & 0 & 0 & 0 & 0 & 0\\
0 & 0 & 0 & 0 & 0 & 0 & -cz & 0 & -is^3z & 0 & -\frac{is}{z} & 0 & 0 & 0 & \frac{c^3}{z} & 0\\
0 & 0 & 0 & 0 & 0 & 0 & -cz^3 & 0 & 0 & 0 & -ic^2sz & 0 & 0 & 0 & c^3z & 0\\
0 & 0 & 0 & 0 & 0 & 0 & 0 & 0 & -cs^2z & 0 & -\frac{cs^2}{z} & 0 & 0 & 0 & 0 & 0\\
0 & 0 & 0 & 0 & 0 & 0 & ic^2sz & 0 & 0 & 0 & 0 & 0 & 0 & 0 & -\frac{ic^2s}{z} & 0\\
0 & 0 & 0 & 0 & 0 & 0 & 0 & 0 & 0 & \frac{ics^2}{z} & 0 & 0 & 0 & 0 & 0 & 0\\
s^3z & \frac{s^3}{z} & 0 & 0 & \frac{ics^2}{z} & 0 & 0 & 0 & 0 & 0 & 0 & 0 & 0 & 0 & 0 & 0\\
0 & 0 & 0 & 0 & 0 & 0 & 0 & 0 & 0 & -\frac{c^2s}{z} & 0 & 0 & 0 & 0 & 0 & 0\\
0 & 0 & 0 & 0 & 0 & 0 & 0 & 0 & 0 & 0 & 0 & 0 & 0 & 0 & 0 & 0\\
0 & 0 & 0 & 0 & 0 & 0 & 0 & 0 & 0 & -c^2sz & 0 & 0 & 0 & 0 & 0 & 0\\
ics^2z & \frac{ic}{z} & -\frac{ics^2}{z} & -\frac{ic}{z^3} & 0 & -\frac{c^2s}{z} & 0 & 0 & 0 & 0 & 0 & 0 & 0 & 0 & 0 & 0\\
0 & 0 & 0 & 0 & 0 & 0 & 0 & ic^2sz & 0 & 0 & 0 & -cs^2z & 0 & -\frac{cs^2}{z} & 0 & -\frac{ic^2s}{z}\\
0 & ic^3z & 0 & -\frac{ic^3}{z} & 0 & -c^2sz & 0 & 0 & 0 & 0 & 0 & 0 & 0 & 0 & 0 & 0\\
0 & 0 & 0 & 0 & 0 & 0 & 0 & 0 & 0 & -ics^2z & 0 & 0 & 0 & 0 & 0 & 0\\
-sz^3 & -sz & c^2sz & \frac{c^2s}{z} & -ics^2z & 0 & 0 & 0 & 0 & 0 & 0 & 0 & 0 & 0 & 0 & 0
\end{pmatrix} \tag{C.1.10}$$

$$R\begin{pmatrix}1\\0\end{pmatrix} = \begin{pmatrix}
0 & 0 & 0 & 0 & 0 & 0 & 0 & \frac{c^3}{z} & 0 & 0 & 0 & \frac{ic^2s}{z} & 0 & 0 & 0 & -\frac{c}{z^3}\\
0 & 0 & 0 & 0 & 0 & 0 & 0 & c^3z & 0 & 0 & 0 & isz & 0 & \frac{is^3}{z} & 0 & -\frac{c}{z}\\
0 & 0 & 0 & 0 & 0 & 0 & 0 & 0 & 0 & 0 & 0 & -ic^2sz & 0 & 0 & 0 & \frac{cs^2}{z}\\
0 & 0 & 0 & 0 & 0 & 0 & 0 & 0 & 0 & 0 & 0 & -isz^3 & 0 & -is^3z & 0 & cs^2z\\
0 & 0 & 0 & 0 & 0 & 0 & 0 & ic^2sz & 0 & 0 & 0 & 0 & 0 & 0 & 0 & -\frac{ic^2s}{z}\\
0 & 0 & 0 & 0 & 0 & 0 & 0 & 0 & 0 & 0 & 0 & -cs^2z & 0 & -\frac{cs^2}{z} & 0 & 0\\
c^2sz & \frac{c^2s}{z} & -\frac{s}{z} & -\frac{s}{z^3} & 0 & \frac{ics^2}{z} & 0 & 0 & 0 & 0 & 0 & 0 & 0 & 0 & 0 & 0\\
0 & 0 & 0 & 0 & 0 & 0 & 0 & 0 & 0 & 0 & 0 & 0 & \frac{ics^2}{z} & 0 & 0 & 0\\
ic^3z & 0 & -\frac{ic^3}{z} & 0 & -\frac{c^2s}{z} & 0 & 0 & 0 & 0 & 0 & 0 & 0 & 0 & 0 & 0 & 0\\
0 & 0 & 0 & 0 & 0 & 0 & ic^2sz & 0 & -cs^2z & 0 & -\frac{cs^2}{z} & 0 & 0 & 0 & -\frac{ic^2s}{z} & 0\\
icz^3 & ics^2z & -icz & -\frac{ics^2}{z} & -c^2sz & 0 & 0 & 0 & 0 & 0 & 0 & 0 & 0 & 0 & 0 & 0\\
0 & 0 & 0 & 0 & 0 & 0 & 0 & 0 & 0 & 0 & 0 & 0 & -\frac{c^2s}{z} & 0 & 0 & 0\\
0 & 0 & 0 & 0 & 0 & 0 & 0 & 0 & 0 & 0 & 0 & 0 & 0 & 0 & 0 & 0\\
0 & 0 & 0 & 0 & 0 & 0 & 0 & 0 & 0 & 0 & 0 & 0 & -c^2sz & 0 & 0 & 0\\
0 & 0 & s^3z & \frac{s^3}{z} & 0 & -ics^2z & 0 & 0 & 0 & 0 & 0 & 0 & 0 & 0 & 0 & 0\\
0 & 0 & 0 & 0 & 0 & 0 & 0 & 0 & 0 & 0 & 0 & 0 & -ics^2z & 0 & 0 & 0
\end{pmatrix} \tag{C.1.11}$$

The matrices $R\begin{pmatrix}0\\0\end{pmatrix}$ and $R\begin{pmatrix}1\\1\end{pmatrix}$ are block diagonal under a direct sum decomposition of

the intermediate basis of states

$$\mathcal{V} = \mathcal{V}_6 \oplus \mathcal{V}_{10} \tag{C.1.12}$$

so that

$$R\begin{pmatrix} a \\ a \end{pmatrix} : \quad \mathcal{V}_6 \mapsto \mathcal{V}_6, \quad \mathcal{V}_{10} \mapsto \mathcal{V}_{10} \tag{C.1.13}$$

We show that non-diagonal matrix elements with $\boldsymbol{a \neq b}$ vanish. In this case, the states on the left and right in (C.1.3) are built up by the action of $R\begin{pmatrix} a \\ b \end{pmatrix}$ on the left and right boundaries $\langle \text{left}|$ and $|\text{right}\rangle$ with the occurrence of at least one $R\begin{pmatrix} a \\ 1-a \end{pmatrix}$ matrix. We begin building up the states by acting with $R\begin{pmatrix} a \\ a \end{pmatrix}$ on the left and right states. We find that

$$v_{\text{left}} = \langle \text{left}| \prod_{j=0}^{n} R\begin{pmatrix} a_j \\ a_j \end{pmatrix} \in \mathcal{V}_{\text{left}}, \qquad v_{\text{right}} = \prod_{j=0}^{n} R\begin{pmatrix} a_j \\ a_j \end{pmatrix} |\text{right}\rangle \in \mathcal{V}_{\text{right}}, \qquad n \geq 0 \tag{C.1.14}$$

where the vector spaces $\mathcal{V}_{\text{left}}, \mathcal{V}_{\text{right}}$ are given by the linear spans

$$\mathcal{V}_{\text{left}} = \left\langle \left\{ \langle \text{left}|, \ \langle \text{left}|R\begin{pmatrix} 0 \\ 0 \end{pmatrix}, \ \langle \text{left}|R\begin{pmatrix} 1 \\ 1 \end{pmatrix}, \ \langle \text{left}|R\begin{pmatrix} 0 \\ 0 \end{pmatrix}^2 \right\} \right\rangle \tag{C.1.15}$$

$$\mathcal{V}_{\text{right}} = \left\langle \left\{ |\text{right}\rangle, \ R\begin{pmatrix} 0 \\ 0 \end{pmatrix}|\text{right}\rangle, \ R\begin{pmatrix} 1 \\ 1 \end{pmatrix}|\text{right}\rangle, \ R\begin{pmatrix} 0 \\ 0 \end{pmatrix}^2 |\text{right}\rangle \right\} \right\rangle \tag{C.1.16}$$

These spaces are stable under the action of further $R\begin{pmatrix} a \\ a \end{pmatrix}$ matrices. The linear independence of vectors is easily checked by calculating the rank of suitable matrices in Mathematica [150]. Since

$$v_{\text{left}} R\begin{pmatrix} a \\ 1-a \end{pmatrix} v_{\text{right}} = 0 \tag{C.1.17}$$

let assume next that there are at least two $R\begin{pmatrix} a \\ 1-a \end{pmatrix}$ matrices. In this case, we similarly find that

$$v'_{\text{left}} = v_{\text{left}} R\begin{pmatrix} a \\ 1-a \end{pmatrix} \prod_{j=0}^{n} R\begin{pmatrix} a_j \\ a_j \end{pmatrix} \in \left\langle \left\{ \langle \text{left}| R\begin{pmatrix} a \\ 1-a \end{pmatrix}, \langle \text{left}| R\begin{pmatrix} 0 \\ 0 \end{pmatrix} R\begin{pmatrix} a \\ 1-a \end{pmatrix} \right\} \right\rangle = \mathcal{V}'_{\text{left}}, \quad n \geq 0 \tag{C.1.18}$$

$$v'_{\text{right}} = \prod_{j=0}^{n} R\begin{pmatrix} a_j \\ a_j \end{pmatrix} R\begin{pmatrix} a \\ 1-a \end{pmatrix} v_{\text{right}} \in \left\langle \left\{ R\begin{pmatrix} a \\ 1-a \end{pmatrix} |\text{right}\rangle, R\begin{pmatrix} a \\ 1-a \end{pmatrix} R\begin{pmatrix} 0 \\ 0 \end{pmatrix} |\text{right}\rangle \right\} \right\rangle = \mathcal{V}'_{\text{right}}, \ n \geq 0 \tag{C.1.19}$$

where the vector spaces are orthogonal. So next suppose that there are three or more $R\begin{pmatrix} a \\ 1-a \end{pmatrix}$ matrices. In this case, we observe that

$$v_{\text{left}} R\begin{pmatrix} a \\ 1-a \end{pmatrix} \prod_{j=0}^{n} R\begin{pmatrix} a_j \\ a_j \end{pmatrix} R\begin{pmatrix} a \\ 1-a \end{pmatrix} = R\begin{pmatrix} a \\ 1-a \end{pmatrix} \prod_{j=0}^{n} R\begin{pmatrix} a_j \\ a_j \end{pmatrix} R\begin{pmatrix} a \\ 1-a \end{pmatrix} v_{\text{right}} = \mathbf{0} \tag{C.1.20}$$

so that the occurrence of the matrices $R\begin{pmatrix} 0 \\ 1 \end{pmatrix}$ and $R\begin{pmatrix} 1 \\ 0 \end{pmatrix}$ must alternate along the segment. Moreover, we observe that

$$v^{\text{eig}}_{\text{left}} = v'_{\text{left}} R\begin{pmatrix} a \\ 1-a \end{pmatrix} R\begin{pmatrix} 1-a \\ a \end{pmatrix}, \ v'_{\text{left}} \in \mathcal{V}'_{\text{left}}, \qquad v^{\text{eig}}_{\text{right}} = R\begin{pmatrix} a \\ 1-a \end{pmatrix} R\begin{pmatrix} 1-a \\ a \end{pmatrix} v'_{\text{right}}, \ v'_{\text{right}} \in \mathcal{V}'_{\text{right}} \tag{C.1.21}$$

are simultaneous (respectively left and right) eigenvectors of $R\begin{pmatrix} 0 \\ 0 \end{pmatrix}$ and $R\begin{pmatrix} 1 \\ 1 \end{pmatrix}$ satisfying the orthogonality

$$v^{\text{eig}}_{\text{left}} \cdot v^{\text{eig}}_{\text{right}} = 0, \qquad v^{\text{eig}}_{\text{left}} R\begin{pmatrix} a \\ 1-a \end{pmatrix} = \mathbf{0}, \qquad R\begin{pmatrix} a \\ 1-a \end{pmatrix} v^{\text{eig}}_{\text{right}} = \mathbf{0} \tag{C.1.22}$$

It follows that the only nonzero matrix elements in (C.1.3) are diagonal with $\boldsymbol{a} = \boldsymbol{b}$ and

$$\big[\boldsymbol{D}(u)\boldsymbol{D}(u+\lambda)\big]_{\boldsymbol{a},\boldsymbol{a}} = {}_6\langle \text{left}| \prod_{j=1}^{N} R \begin{pmatrix} a_j \\ a_j \end{pmatrix}_6 |\text{right}\rangle_6, \qquad a_j = 0, 1. \tag{C.1.23}$$

where $R \begin{pmatrix} a \\ a \end{pmatrix}_6$ denotes the 6×6 diagonal block of $R \begin{pmatrix} a \\ a \end{pmatrix}$ and

$${}_6\langle \text{left}| = (-1, 1, 1, -1, 0, 0), \qquad |\text{right}\rangle_6 = (1, 1, 1, 1, 0, 0)^T \tag{C.1.24}$$

Let us now suppose that $\boldsymbol{a} = \boldsymbol{b} = (0, 0, 0, \ldots, 0, 0)$ and observe that $R \begin{pmatrix} 0 \\ 0 \end{pmatrix}$ can be diagonalized by a similarity transformation

$$S^{-1} R \begin{pmatrix} 0 \\ 0 \end{pmatrix} S = \begin{pmatrix} s^4 & 0 & 0 & 0 & 0 & 0 \\ 0 & c^4 & 0 & 0 & 0 & 0 \\ 0 & 0 & s^2c^2 & 0 & 0 & 0 \\ 0 & 0 & 0 & s^2c^2 & 0 & 0 \\ 0 & 0 & 0 & 0 & -s^2c^2 & 0 \\ 0 & 0 & 0 & 0 & 0 & -s^2c^2 \end{pmatrix}, \quad S = \begin{pmatrix} 0 & 0 & -\frac{(z^4-1)^2(z^4+1)}{4z^8} & \frac{z^8-1}{2z^8} & 0 & \frac{z^4+1}{z^4} \\ -\frac{(z^4+1)^2}{2z^4} & 0 & -\frac{(z^4-1)^2}{2z^4} & \frac{z^4-1}{z^4} & 0 & \frac{(z^4+1)^2}{2z^4} \\ 0 & -\frac{(z^4+1)^2}{2z^4} & -\frac{(z^4-1)^2}{2z^4} & \frac{z^4-1}{z^4} & 0 & \frac{(z^4+1)^2}{2z^4} \\ -z^4-1 & -z^4-1 & 0 & \frac{z^8-1}{2z^4} & 0 & z^4+1 \\ 0 & 0 & 0 & 0 & 0 & \frac{z^8-1}{2z^4} \\ \frac{z^8-1}{2z^4} & \frac{z^8-1}{2z^4} & \frac{z^8-1}{2z^4} & 0 & \frac{z^8-1}{2z^4} & 0 \end{pmatrix} \tag{C.1.25}$$

with

$${}_6\langle \text{left}|S = \left\{ \tfrac{z^8-1}{2z^4}, \tfrac{z^8-1}{2z^4}, -\tfrac{(z^4-1)^2(3z^4-1)}{4z^8}, -\tfrac{(z^4-1)^3}{2z^8}, 0, 0 \right\} \tag{C.1.26}$$

$$S^{-1}|\text{right}\rangle_6 = \left\{ \tfrac{2z^4(z^4-1)}{(z^4+1)^3}, \tfrac{2z^4(z^4-1)}{(z^4+1)^3}, -\tfrac{4z^4(z^4-1)}{(z^4+1)^3}, \tfrac{2z^4(5z^8-2z^4+1)}{(z^4-1)(z^4+1)^3}, 0, 0 \right\} \tag{C.1.27}$$

Putting everything together, it follows that

$${}_6\langle \text{left}|\, R \begin{pmatrix} 0 \\ 0 \end{pmatrix}_6^N |\text{right}\rangle_6 = -\tan^2 2u \left[c^{4N} - 2(sc)^{2N} + s^{4N}\right] = -\tan^2 2u \left[c^{2N} - s^{2N}\right]^2 \tag{C.1.28}$$

The last step is to extend this result to all the other diagonal segments. To do this let us

define

$$\Delta R = \frac{2z^2}{1-z^4}\Big[R\begin{pmatrix}0\\0\end{pmatrix} - R\begin{pmatrix}1\\1\end{pmatrix}\Big] \tag{C.1.29}$$

We then find, by induction on N, that

$$\prod_{j=1}^{N-1} R\begin{pmatrix}a_j\\a_j\end{pmatrix}\ \Delta R\,|\text{right}\rangle_6 = (-s^2c^2)^{N-1}(z^{-2},\cos 2u,\cos 2u,z^2,i\sin 2u,i\sin 2u)^T,\quad a_j=0,1 \tag{C.1.30}$$

It follows that

$${}_6\langle\text{left}|\prod_{j=1}^{N-1} R\begin{pmatrix}a_j\\a_j\end{pmatrix}\ \Delta R\,|\text{right}\rangle_6 = 0 \tag{C.1.31}$$

So the weight of the diagonal matrix elements with $\boldsymbol{b}=\boldsymbol{a}$ are independent of $\boldsymbol{a}$

$$\big[\boldsymbol{D}(u)\boldsymbol{D}(u+\lambda)\big]_{\boldsymbol{a},\boldsymbol{a}} = {}_6\langle\text{left}|\prod_{j=1}^{N} R\begin{pmatrix}a_j\\a_j\end{pmatrix}_6|\text{right}\rangle_6 = -\tan^2 2u\,[c^{2N}-s^{2N}]^2 \tag{C.1.32}$$

Appendix D

Yang-Baxter Integrable Dimers on a Strip

D.1 Skew q-Binomials

The skew q-binomials, related to generalized q-Narayana numbers (4.4.13), are [124, 180]

$$\begin{aligned}\begin{Bmatrix} M \\ m,n \end{Bmatrix}_q &= \begin{bmatrix} M \\ m \end{bmatrix}_q \begin{bmatrix} M \\ n \end{bmatrix}_q - q^{n-m+1} \begin{bmatrix} M \\ m-1 \end{bmatrix}_q \begin{bmatrix} M \\ n+1 \end{bmatrix}_q \\ &= q^{-M+n}\Big(\begin{bmatrix} M \\ m \end{bmatrix}_q \begin{bmatrix} M+1 \\ n+1 \end{bmatrix}_q - \begin{bmatrix} M+1 \\ m \end{bmatrix}_q \begin{bmatrix} M \\ n+1 \end{bmatrix}_q \Big), \qquad 0 \le m \le n \le M \end{aligned} \tag{D.1.1}$$

At $q=1$, the skew binomials $\begin{Bmatrix} M \\ m,m \end{Bmatrix}_{q=1}$ are determinants of ordinary binomials

Binomials	Skew Binomials ($n=m$)	Catalan
1	1	1
1 1	1 1	2
1 2 1	1 3 1	5
1 3 3 1	1 6 6 1	14
1 4 6 4 1	1 10 20 10 1	42
1 5 10 10 5 1	1 15 50 50 15 1	132

(D.1.2)

The skew q-binomials are enumerated by double column diagrams with dominance

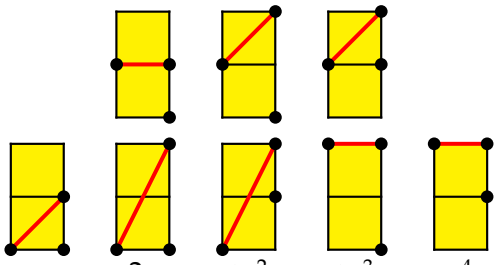

$$1 \quad + \quad 2q \quad + \quad 2q^2 \quad + \quad 2q^3 \quad + \quad q^4 \quad = \quad \left\{ \begin{matrix} 3 \\ 1,2 \end{matrix} \right\}_q \tag{D.1.3}$$

A partition λ is equivalent to a Young diagram Y. A skew Young diagram Y_2/Y_1 is equivalent to the pair (Y_1, Y_2) with $Y_1 \subseteq Y_2$. Let us define

$$\begin{aligned} E(Y) &= \text{Energy} = \{\#\text{ of boxes in the Young digram } Y\} \\ Y_{m,n} &= \{m \times n \text{ rectangular Young diagram}\} \end{aligned} \tag{D.1.4}$$

A skew q-binomial can be written as an energy weighted sum over skew Young diagrams

$$\left\{ \begin{matrix} M \\ m,n \end{matrix} \right\}_q = q^{(m-n)n} \sum_{\substack{Y_1 \subseteq Y_2 \\ \emptyset \subseteq Y_1 \subseteq Y_{M-m,m} \\ Y_{n-m,n} \subseteq Y_2 \subseteq Y_{M-m,n}}} q^{E(Y_1)+E(Y_2)}, \qquad 0 \le m \le n \le M \tag{D.1.5}$$

The bijection is implemented by interpreting the left and right column (particle) configurations in the double column diagrams as Maya diagrams and using the standard bijection between Maya diagrams and Young diagrams. For example, shading Y_1, gives

$$\left\{ \begin{matrix} 3 \\ 1,2 \end{matrix} \right\}_q = q^{-2} \left[\right. \quad \left. \right], \qquad \begin{matrix} \emptyset \subseteq Y_1 \subseteq Y_{2,1} \\ Y_{1,2} \subseteq Y_2 \subseteq Y_{2,2} \end{matrix} \tag{D.1.6}$$

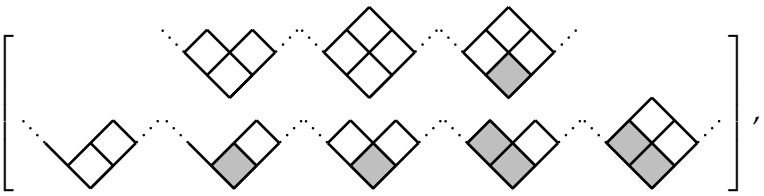

$$1 \quad + \quad 2q \quad + \quad 2q^2 \quad + \quad 2q^3 \quad + \quad q^4$$

Bibliography

[1] J. W. Gibbs, *Elementary principles in statistical mechanics*. Courier Corporation, 2014.

[2] P. Ehrenfest and T. Ehrenfest, *The conceptual foundations of the statistical approach in mechanics*. Courier Corporation, 2002.

[3] L. Landau and E. Lifshitz, "Statistical physics, vol. 5," *Course of theoretical physics*, vol. 30, 1980.

[4] H. E. Stanley, *Introduction to phase transitions and critical phenomena*. Clarendon Press, Oxford, 1971.

[5] C. Domb, J. Lebowitz, and M. Green, *Phase transitions and critical phenomena*, vol. 1-19. Elsevier. Vol. 9,11,13-20 edited by C. Domb and J.L. Lebowitz.

[6] L. P. Kadanoff, "Scaling laws for Ising models near T_c," *Physics Physique Fizika*, vol. 2, no. 6, p. 263, 1966.

[7] K. G. Wilson, "Renormalization group and critical phenomena. —. Renormalization group and the Kadanoff scaling picture," *Physical review B*, vol. 4, no. 9, p. 3174, 1971.

[8] K. G. Wilson, "Renormalization group and critical phenomena. ——. Phase-space cell analysis of critical behavior," *Physical Review B*, vol. 4, no. 9, p. 3184, 1971.

[9] K. G. Wilson and J. Kogut, "The renormalization group and the ϵ expansion," *Physics Reports*, vol. 12, no. 2, pp. 75–199, 1974.

[10] K. G. Wilson, "The renormalization group: Critical phenomena and the Kondo problem," *Reviews of modern physics*, vol. 47, no. 4, p. 773, 1975.

[11] K. G. Wilson and M. E. Fisher, "Critical exponents in 3.99 dimensions," *Physical Review Letters*, vol. 28, no. 4, p. 240, 1972.

[12] M. E. Fisher, S.-k. Ma, and B. Nickel, "Critical exponents for long-range interactions," *Physical Review Letters*, vol. 29, no. 14, p. 917, 1972.

[13] M. E. Fisher, "The renormalization group in the theory of critical behavior," *Reviews of Modern Physics*, vol. 46, no. 4, p. 597, 1974.

[14] J. Cardy, *Scaling and Renormalization in Statistical Physics*. Cambridge University Press, Apr. 1996.

[15] A. Pelissetto and E. Vicari, "Critical phenomena and renormalization-group theory," *Physics Reports*, vol. 368, no. 6, pp. 549–727, 2002.

[16] J. Zinn-Justin, "Critical phenomena: field theoretical approach," *Scholarpedia*, vol. 5, no. 5, p. 8346, 2010.

[17] M. E. Fisher, "The theory of equilibrium critical phenomena," *Reports on progress in physics*, vol. 30, no. 2, p. 615, 1967.

[18] C.-K. Hu, "Historical review on analytic, monte carlo, and renormalization group approaches to critical phenomena of some lattice models," *Chinese Journal of Physics*, vol. 52, no. 1, pp. 1–76, 2014.

[19] H. Kleinert and V. Schulte-Frohlinde, *Critical properties of φ4-theories*. World Scientific, 2001.

[20] E. Ising, "Beitrag zur Theorie des Ferromagnetismus," *Zeitschrift für Physik*, vol. 31, no. 1, pp. 253–258, 1925.

[21] L. Onsager, "Crystal statistics. I. A two-dimensional model with an order-disorder transition," *Physical Review*, vol. 65, pp. 117–149, Feb. 1944.

[22] M. E. Fisher, "The susceptibility of the plane ising model," *Physica*, vol. 25, no. 1, pp. 521 – 524, 1959.

[23] C. N. Yang, "The spontaneous magnetization of a two-dimensional ising model," *Phys. Rev.*, vol. 85, pp. 808–816, 1952.

[24] T. T. Wu, "Theory of toeplitz determinants and the spin correlations of the two-dimensional ising model. i," *Phys. Rev.*, vol. 149, pp. 380–401, 1966.

[25] M. Lakshmanana and R. Sahadevan, "Painlev analysis, Lie symmetries, and integrability of coupled nonlinear oscillators of polynomial type," *Physics Reports*, vol. 224, no. 1-2, pp. 1–93, 1993.

[26] M. J. Ablowitz, D. J. Kaup, A. C. Newell, and H. Segur, "Nonlinear-evolution equations of physical significance," *Phys. Rev. Lett.*, vol. 31, p. 125, 1973.

[27] S. Novikov, V. Manakov, L. Pitaevskii, and V. Zakharov, *Theory of Solitons*. Plenum, NY, 2nd ed., 1984.

[28] V. E. Korepin, N. M. Bogoliubov, and A. G. Izergin, *Quantum inverse scattering method and correlation functions*, vol. 3. Cambridge university press, 1997.

[29] L. Faddeev, *How Algebraic Bethe Ansatz works for integrable models*, ch. 2, pp. 370–439. World Scientific, 2016.

[30] H. Bethe, "Zur theorie der metalle. i. eigenwerte und eigenfunktionen der linearen atomkette," *Zeitschrift fr Physik*, vol. 71, pp. 205–226, 1931.

[31] R. J. Baxter, *Exactly solved models in statistical mechanics*. Academic Press, Inc. [Harcourt Brace Jovanovich Publishers], 1982.

[32] R. B. Potts and C. Domb, "Some generalized order-disorder transformations," *Proc. Camb.Phil. Soc.*, vol. 48, p. 106, 1952.

[33] H. E. Stanley, "Dependence of critical properties on dimensionality of spins," *Phys. Rev. Lett.*, vol. 20, no. 12, pp. 589–592, 1968.

[34] L. Pauling, "The structure and entropy of ice and of other crystals with some randomness of atomic arrangement," *Journal of the American Chemical Society*, vol. 57, no. 12, pp. 2680–2684, 1935.

[35] E. H. Lieb, "Exact solution of the problem of the entropy of two-dimensional ice," *Phys. Rev. Lett.*, vol. 18, no. 17, pp. 692–694, 1967.

[36] E. H. Lieb, "Residual entropy of square ice," *Phys. Rev.*, vol. 162, no. 1, pp. 162–172, 1967.

[37] E. H. Lieb, "Exact solution of the two-dimensional slater KDP model of a ferroelectric," *Phys. Rev. Lett.*, vol. 19, no. 3, pp. 108–110, 1967.

[38] E. H. Lieb, "Exact solution of the *F* model of an antiferroelectric," *Phys. Rev. Lett.*, vol. 18, no. 24, pp. 1046–1048, 1967.

[39] B. Sutherland, "Exact solution of a two-dimensional model for hydrogen-bonded crystals," *Phys. Rev. Lett.*, vol. 19, no. 3, pp. 103–104, 1967.

[40] C. Fan and F. Y. Wu, "Ising model with second neighbor interaction. i. Some exact results and an approximate solution," *Phys. Rev. B*, vol. 179, no. 2, pp. 560–570, 1969.

[41] C. Fan and F. Y. Wu, "General Lattice Models of Phase Transition," *Phys. Rev. B*, vol. 2, pp. 723–733, 1970.

[42] B. Sutherland, "Two dimensional hydrogen bonded crystals without the ice rule," *Journal of Mathematical Physics*, vol. 11, no. 11, pp. 3183–3186, 1970.

[43] W. Heisenberg, "Zur theorie des ferromagnetismus," in *Original Scientific Papers Wissenschaftliche Originalarbeiten*, pp. 580–597, Springer, 1985.

[44] F. Bloch, "Zur theorie des ferromagnetismus," *Zeitschrift für Physik*, vol. 61, no. 3-4, pp. 206–219, 1930.

[45] F. Bloch, "Zur theorie des austauschproblems und der remanenzerscheinung der ferromagnetika," in *Zur Theorie des Austauschproblems und der Remanenzerscheinung der Ferromagnetika*, pp. 295–335, Springer, 1932.

[46] R. J. Baxter, "Partition function of the eight-vertex lattice model," *Annals of Physics*, vol. 70, no. 1, pp. 193 – 228, 1972.

[47] R. Baxter, "One-dimensional anisotropic Heisenberg chain," *Physical Review Letters*, vol. 26, no. 14, p. 834, 1971.

[48] R. J. Baxter, "Hard hexagons: exact solution," *J. Phys. A: Math. Gen.*, vol. 13, pp. L61–L70, 1980.

[49] R. J. Baxter, "Rogers-Ramanujan identities in the hard hexagonal model," *Journal of Statistical Physics*, vol. 26, pp. 427–452, 1981.

[50] G. E. Andrews, R. J. Baxter, and P. J. Forrester, "Eight-vertex SOS model and generalized Rogers-Ramanujan-type identities," *Journal of Statistical Physics*, vol. 35, no. 3-4, pp. 193–266, 1984.

[51] V. F. R. Jones, "Planar algebras, I," *arXiv preprint math/9909027*, 1999.

[52] R. J. Baxter, "The inversion relation method for some two-dimensional exactly solved models in lattice statistics," *Journal of Statistical Physics*, vol. 28, pp. 1–41, May 1982.

[53] A. L. Owczarek and R. J. Baxter, "A class of Interaction-Round-a-Face models and its equivalence with an Ice-type model," *J. Stat. Phys.*, vol. 49, no. 5-6, pp. 1093–1115, 1987.

[54] P. Forrester and R. Baxter, "Further exact solutions of the eight-vertex SOS model and generalizations of the Rogers-Ramanujan identities," *Journal of Statistical Physics*, vol. 38, no. 3-4, pp. 435–472, 1985.

[55] R. J. Baxter, "Corner transfer matrices of the eight-vertex model. I. Low-temperature expansions and conjectured properties," *Journal of Statistical Physics*, vol. 15, pp. 485–503, Dec. 1976.

[56] R. J. Baxter, "Corner transfer matrices of the eight-vertex model. II. The Ising model case," *Journal of Statistical Physics*, vol. 17, pp. 1–14, July 1977.

[57] M. Jimbo and T. Miwa, *Algebraic Analysis of Solvable Lattice Models*. American Mathematical Soc., 1994.

[58] E. Melzer, "Fermionic character sums and the corner transfer matrix," *International Journal of Modern Physics A*, vol. 9, no. 07, pp. 1115–1136, 1994.

[59] S. O. Warnaar, "Fermionic solution of the Andrews-Baxter-Forrester model. i. Unification of TBA and CTM methods," *Journal of statistical physics*, vol. 82, no. 3-4, pp. 657–685, 1996.

[60] S. O. Warnaar, "Fermionic solution of the Andrews-Baxter-Forrester model. ii. Proof of Melzer's polynomial identities," *Journal of statistical physics*, vol. 84, no. 1-2, pp. 49–83, 1996.

[61] P. L. Ferrari and H. Spohn, "Domino tilings and the six-vertex model at its free-fermion point," *Journal of Physics A: Mathematical and General*, vol. 39, no. 33, p. 10297, 2006.

[62] R. Kenyon, "Lectures on dimers," *arXiv preprint arXiv:0910.3129*, 2009.

[63] R. J. Baxter, "Dimers on a rectangular lattice," *Journal of Mathematical Physics*, vol. 9, no. 4, pp. 650–654, 1968.

[64] O. J. Heilmann and E. H. Lieb, "Theory of monomer-dimer systems," in *Statistical Mechanics*, pp. 45–87, 1972.

[65] W.-J. Tzeng and F. Wu, "Dimers on a simple-quartic net with a vacancy," *Journal of statistical physics*, vol. 110, no. 3-6, pp. 671–689, 2003.

[66] F. Wu, "Pfaffian solution of a dimer-monomer problem: single monomer on the boundary," *Physical Review E*, vol. 74, no. 2, p. 020104, 2006.

[67] J. Bouttier, M. Bowick, E. Guitter, and M. Jeng, "Vacancy localization in the square dimer model," *Physical Review E*, vol. 76, no. 4, p. 041140, 2007.

[68] F. Wu, W.-J. Tzeng, and N. S. Izmailian, "Exact solution of a monomer-dimer problem: A single boundary monomer on a nonbipartite lattice," *Physical Review E*, vol. 83, no. 1, p. 011106, 2011.

[69] V. Korepin and P. Zinn-Justin, "Thermodynamic limit of the six-vertex model with domain wall boundary conditions," *Journal of Physics A*, vol. 33, pp. 7053–7066, 2000.

[70] R. H. Fowler and G. S. Rushbrooke, "An attempt to extend the statistical theory of perfect solutions," *Transactions of the Faraday Society*, vol. 33, p. 1272, 1937.

[71] H. S. Green and R. Leipnik, "Exact solution of the association problem by a matrix-spinor method with applications to statistical mechanics," *Rev. Mod. Phys.*, vol. 32, p. 129, 1960.

[72] H. N. V. Temperley and F. M. E., "Association problem in statistical mechanics-critique of the treatment of H. S. Green and R. Leipnik," *Rev. Mod. Phys.*, vol. 32, p. 1029, 1960.

[73] P. W. Kasteleyn, "The statistics of dimers on a lattice," *Physica*, vol. 27, pp. 1209–1225, 1961.

[74] H. N. V. Temperley and F. M. E., "Dimer problem in statistical mechanics-an exact result," *The Philosophical Magazine: A Journal of Theoretical Experimental and Applied Physics*, vol. 6, no. 68, pp. 1601–1603, 1961.

[75] E. H. Lieb, "Solution of the dimer problem by the transfer matrix method," *Journal of Mathematical Physics*, vol. 8, p. 2339, 1967.

[76] A. Morin-Duchesne, J. Rasmussen, and P. Ruelle, "Dimer representations of the Temperley-Lieb algebra," *Nucl. Phys. B*, vol. 890, pp. 363–387, 2015.

[77] D. S. Rokhsar and S. A. Kivelson, "Superconductivity and the quantum hard-core dimer gas," *Physical review letters*, vol. 61, no. 20, p. 2376, 1988.

[78] H. Cohn, N. Elkies, and J. Propp, "Local statistics for random domino tilings of the aztec diamond," *arXiv preprint math/0008243*, 2000.

[79] R. Kenyon, "Conformal invariance of domino tiling," *Annals of probability*, pp. 759–795, 2000.

[80] R. Kenyon, "Dominos and the Gaussian Free Field," *The Annals of Probability*, vol. 29, no. 3, pp. 1128–1137, 2001.

[81] S. Chakravarty, "Theory of the d-density wave from a vertex model and its implications," *Physical Review B*, vol. 66, no. 22, p. 224505, 2002.

[82] N. S. Izmailian, K. Oganesyan, and C.-K. Hu, "Exact finite-size corrections of the free energy for the square lattice dimer model under different boundary conditions," *Physical Review E*, vol. 67, p. 066114, 2003.

[83] N. S. Izmailian, V. B. Priezzhev, P. Ruelle, and H. Chin-Kun, "Logarithmic conformal field theory and boundary effects in the dimer model," *Phys. Rev. Lett.*, vol. 95, p. 260602, 2005.

[84] N. S. Izmailian, V. B. Priezzhev, and P. Ruelle, "Non-local finite-size effects in the dimer model," *Sigma. Symmetry, Integrability and Geometry: Methods and Applications*, vol. 3, p. 001, 2007.

[85] J. Rasmussen and P. Ruelle, "Refined conformal spectra in the dimer model," *J. Stat. Mech.:Theor. Exp.*, vol. 2012, no. 3, p. P10002, 2012.

[86] A. Nigro, "Finite size corrections for dimers," *arXiv preprint arXiv:1208.2110*, 2012.

[87] A. Morin-Duchesne, J. Rasmussen, and P. Ruelle, "Integrability and conformal data of the dimer model," *Journal of Physics A: Mathematical and Theoretical*, vol. 49, no. 17, p. 174002, 2016.

[88] N. S. Izmailian, R. Kenna, W. Guo, and X. Wu, "Exact finite-size corrections and corner free energies for the $c = -2$ universality class," *Nucl. Phys. B*, vol. 884, pp. 157–171, 2014.

[89] N. Allegra, "Exact solution of the 2d dimer model: corner free energy, correlation functions and combinatorics," *Nucl. Phys. B*, vol. 894, pp. 685–732, 2015.

[90] N. S. Izmailian, "Finite size and boundary effects in critical two-dimensional free-fermion models," *Eur. Phys. J. B*, vol. 90, p. 160, 2017.

[91] P. Di Francesco, P. Mathieu, and D. Sénéchal, *Conformal field theory*. Springer Science & Business Media, 2012.

[92] P. Ginsparg, "Applied conformal field theory," *arXiv preprint hep-th/9108028*, 1988.

[93] A. A. Belavin, A. M. Polyakov, and A. B. Zamolodchikov, "Infinite conformal symmetry in two-dimensional quantum field theory," *Nuclear Physics B*, vol. 241, no. 2, pp. 333 – 380, 1984.

[94] A. A. Belavin, A. M. Polyakov, and A. B. Zamolodchikov, "Infinite conformal symmetry of critical fluctuations in two dimensions," *Journal of Statistical Physics*, vol. 34, no. 5,6, pp. 763–774, 1984.

[95] B. L. Feigin and D. B. Fuks, "Invariant skew-symmetric differential operators on the line and Verma modules over the Virasoro algebra," *Functional Analysis and its Applications*, vol. 16, no. 2, pp. 114–126, 1982.

[96] A. Rocha-Caridi, "Vacuum Vector Representations of the Virasoro Algebra," in *Vertex Operators in Mathematics and Physics* (J. Lepowsky, S. Mandelstam, and I. M. Singer, eds.), no. 3 in Mathematical Sciences Research Institute Publications, pp. 451–473, Springer US, 1985. DOI: 10.1007/978-1-4613-9550-8_22.

[97] J. L. Cardy, "Conformal Invariance," in *Phase transisitons and critical phenomena* (C. Domb and J. Lebowitz, eds.), vol. 11, Academic Press, 1987.

[98] D. A. Huse, "Exact exponents for infinitely many new multicritical points," *Physical Review B*, vol. 30, no. 7, pp. 3908–3915, 1984.

[99] V. Pasquier, "Two-dimensional critical systems labelled by Dynkin diagrams," *Nuclear Physics B*, vol. 285, pp. 162–172, Jan. 1987.

[100] P. Di Francesco, H. Saleur, and J.-B. Zuber, "Generalized coulomb-gas formalism for two dimensional critical models based on su (2) coset construction," *Nuclear Physics B*, vol. 300, pp. 393–432, 1988.

[101] T. Nakanishi, "Non-unitary minimal models and RSOS models," *Nuclear Physics B*, vol. 334, pp. 745–766, Apr. 1990.

[102] J. L. Cardy, "Conformal invariance and the Yang-Lee edge singularity in two dimensions," *Physical Review Letters*, vol. 54, no. 13, pp. 1354–1356, 1985.

[103] C. Itzykson, H. Saleur, and J.-B. Zuber, "Conformal invariance of nonunitary 2d-models," *EPL (Europhysics Letters)*, vol. 2, no. 2, p. 91, 1986.

[104] H. Riggs, "Solvable lattice models with minimal and nonunitary critical behaviour in two dimensions," *Nuclear Physics B*, vol. 326, no. 3, pp. 673–688, 1989.

[105] O. Foda and T. A. Welsh, "On the Combinatorics of Forrester-Baxter Models," in *Physical Combinatorics* (M. Kashiwara and T. Miwa, eds.), no. 191 in Progress in Mathematics, pp. 49–103, Birkhäuser Boston, 2000. DOI: 10.1007/978-1-4612-1378-9_2.

[106] H. Fitzgerald, *Physical Combinatorics of Non-Unitary Minimal Models*. Honours thesis, University of Melbourne, 2006.

[107] R. J. Baxter and G. E. Andrews, "Lattice gas generalization of the hard hexagon model. I. Star-triangle relation and local densities," *Journal of Statistical Physics*, vol. 44, pp. 249–271, July 1986.

[108] E. Date, M. Jimbo, T. Miwa, and M. Okado, "Fusion of the eight vertex SOS model," *Letters in Mathematical Physics*, vol. 12, pp. 209–215, Oct. 1986.

[109] P. Kulish, N. Reshetikhin, and E. Sklyanin, "Yang-Baxter equation and representation theory: I," *Letters in Mathematical Physics*, vol. 5, no. 5, pp. 393–403, 1981.

[110] G. E. Andrews and R. J. Baxter, "Lattice gas generalization of the hard hexagon model. II. The local densities as elliptic functions," *Journal of Statistical Physics*, vol. 44, pp. 713–728, Sept. 1986.

[111] G. E. Andrews and R. J. Baxter, "Lattice gas generalization of the hard hexagon model. III.q-Trinomial coefficients," *Journal of Statistical Physics*, vol. 47, pp. 297–330, May 1987.

[112] E. Date, M. Jimbo, T. Miwa, and M. Okado, "Automorphic properties of local height probabilities for integrable solid-on-solid models," *Physical Review B*, vol. 35, pp. 2105–2107, Feb. 1987.

[113] E. Date, M. Jimbo, A. Kuniba, T. Miwa, and M. Okado, "Exactly solvable SOS models: Local height probabilities and theta function identities," *Nuclear Physics B*, vol. 290, pp. 231–273, 1987.

[114] E. Date, M. Jimbo, A. Kuniba, T. Miwa, and M. Okado, "Exactly Solvable SOS Models II: Proof of the star-triangle relation and combinatorial identities," *Yang-Baxter Equation In Integrable Systems. Series: Advanced Series in Mathematical Physics, ISBN: 978-981-02-0120-3. WORLD SCIENTIFIC, Edited by Michio Jimbo, vol. 10, pp. 509-614*, vol. 10, pp. 509–614, Mar. 1990.

[115] V. V. Bazhanov and N. Y. Reshetikhin, "Critical RSOS models and conformal field theory," *International Journal of Modern Physics A*, vol. 04, pp. 115–142, Jan. 1989.

[116] A. Klümper and P. A. Pearce, "Conformal weights of RSOS lattice models and their fusion hierarchies," *Physica A: Statistical Mechanics and its Applications*, vol. 183, no. 3, pp. 304 – 350, 1992.

[117] A. Schilling, "Multinomials and polynomial bosonic forms for the branching functions of the su(2)M x su(2)N/su(2)M+N conformal coset models," *Nuclear Physics B*, vol. 467, pp. 247–271, May 1996.

[118] E. Tartaglia and P. A. Pearce, "Fused RSOS lattice models as higher-level nonunitary minimal cosets," *Journal of Physics A: Mathematical and Theoretical*, vol. 49, no. 18, p. 184002, 2016.

[119] M. A. I. Flohr, "On modular invariant partition functions of conformal field theories with logarithmic operators," *International Journal of Modern Physics A*, vol. 11, no. 22, pp. 4147–4172, 1996.

[120] M. A. Flohr, "On fusion rules in logarithmic conformal field theories," *International Journal of Modern Physics A*, vol. 12, no. 10, pp. 1943–1958, 1997.

[121] M. R. Gaberdiel and H. G. Kausch, "A rational logarithmic conformal field theory," *Physics Letters B*, vol. 386, pp. 131–137, Oct. 1996.

[122] J. Rasmussen, "Logarithmic limits of minimal models," *Nuclear Physics B*, vol. 701, no. 3, pp. 516 – 528, 2004.

[123] P. A. Pearce, J. Rasmussen, and J.-B. Zuber, "Logarithmic minimal models," *Journal of Statistical Mechanics: Theory and Experiment*, vol. 2006, p. P11017, Nov. 2006.

[124] P. A. Pearce and J. Rasmussen, "Solvable critical dense polymers," *Journal of Statistical Mechanics: Theory and Experiment*, vol. 2007, no. 02, p. P02015, 2007.

[125] P. Mathieu and D. Ridout, "From percolation to logarithmic conformal field theory," *Physics Letters B*, vol. 657, no. 1, pp. 120–129, 2007.

[126] E. V. Ivashkevich, N. S. Izmailian, and C.-K. Hu, "Kronecker's double series and exact asymptotic expansions for free models of statistical mechanics on torus," *J. Phys. A: Math. Gen.*, vol. 35, pp. 5543–5561, 2002.

[127] A. E. Ferdinand, "Statistical mechanics of dimers on a quadratic lattice," *J. Math. Phys.*, vol. 8, pp. 2332–2339, 1967.

[128] P. Ruelle, "Wind on the boundary for the Abelian sandpile model," *J. Stat. Mech.:Theor. Exp.*, vol. 2007, p. P09013, 2007.

[129] J. Dubédat, "Dimers and families of Cauchy-Riemann operators i," *arXiv:1110.2808v2 [math:PR]*, June 2014.

[130] B. Duplantier, "Exact critical exponents for two-dimensional dense polymers," *J. Phys. A: Math. Gen.*, vol. 19, p. L1009, 1986.

[131] V. Priezzhev and F. Ruelle, "Boundary monomers in the dimer model," *Physical Review E*, vol. 77, p. 061126, 2008.

[132] P. A. Pearce and A. Vittorini-Orgeas, "Yang-baxter solution of dimers as a free-fermion six-vertex model," *Journal of Physics A: Mathematical and Theoretical*, vol. 50, no. 434001, pp. 1–28, 2017.

[133] A. Zamolodchikov, "Integrals of motion in scaling 3-state potts model field theory," *International Journal of Modern Physics A*, vol. 03, pp. 743–750, Mar. 1988.

[134] A. B. Zamolodchikov, "Integrable field theory from conformal field theory," *Adv. Stud. Pure Math*, vol. 19, p. 641, 1989.

[135] A. B. Zamolodchikov, "Higher order integrals of motion in two-dimensional models of the field theory with a broken conformal symmetry," *JETP Lett*, vol. 46, no. 4, 1987.

[136] P. Goddard, A. Kent, and D. Olive, "Virasoro algebras and coset space models," *Physics Letters B*, vol. 152, no. 12, pp. 88 – 92, 1985.

[137] C. H. O. Chui, C. Mercat, and P. A. Pearce, "Integrable boundaries and universal TBA functional equations," in *MathPhys Odyssey 2001* (M. Kashiwara and T. Miwa, eds.), no. 23 in Progress in Mathematical Physics, pp. 391–413, Birkhäuser Boston, 2002. DOI: 10.1007/978-1-4612-0087-1_14.

[138] G. Hatayama, A. Kuniba, M. Okado, T. Takagi, and Z. Tsuboi, "Paths, Crystals and Fermionic Formulae," in *MathPhys Odyssey 2001* (M. Kashiwara and T. Miwa, eds.), no. 23 in Progress in Mathematical Physics, pp. 205–272, Birkhäuser Boston, 2002. DOI: 10.1007/978-1-4612-0087-1_9.

[139] P. Jacob and P. Mathieu, "A new path description for the $\Updownarrow(k+1, 2k+3)$ models and the dual ${}_k$ graded parafermions," *J. Stat. Mech.*, vol. 2007, no. 11, p. P11005, 2007.

[140] P. Jacob and P. Mathieu, "Particles in RSOS paths," *Journal of Physics A: Mathematical and Theoretical*, vol. 42, no. 12, p. 122001, 2009.

[141] P. Mathieu, "Paths and partitions: combinatorial descriptions of the parafermionic states," *Journal of Mathematical Physics*, vol. 50, no. 9, p. 095210, 2009.

[142] J. Fortin, P. Jacob, and P. Mathieu, "fermionic characters and restricted jagged partitions," *Journal of Physics A: Mathematical and General*, vol. 38, no. 8, p. 1699, 2005.

[143] G. Feverati, P. A. Pearce, and N. S. Witte, "Physical combinatorics and quasiparticles," *Journal of Statistical Mechanics: Theory and Experiment*, vol. 2009, no. 10, p. P10013, 2009.

[144] O. Blondeau-Fournier, P. Mathieu, and T. A. Welsh, "A bijection between paths for the $\Updownarrow(p, 2p+1)$ minimal model Virasoro characters," in *Annales Henri Poincaré*, vol. 11, pp. 101–125, 2010.

[145] O. Blondeau-Fournier, P. Mathieu, and T. A. Welsh, "Half-lattice paths and Virasoro characters," *Fundamenta Informaticae*, vol. 117, no. 1-4, pp. 57–83, 2012.

[146] O. Blondeau-Fournier, P. Mathieu, and T. A. Welsh, "A quartet of fermionic expressions for $m(k, 2k \pm 1)$ virasoro characters via half-lattice paths," *Nuclear Physics B*, vol. 924, pp. 643–683, 2017.

[147] I. S. Gradshteyn and I. M. Ryzhik, *Tables of Integrals, Series and Products*. Academic Press, 1980.

[148] C. N. Yang and T. D. Lee, "Statistical theory of equations of state and phase transitions. I. Theory of condensation," *Physical Review*, vol. 87, pp. 404–409, Aug. 1952.

[149] K. A. Seaton and L. C. Scott, "q-Trinomial coefficients and the dilute A model," *Journal of Physics A: Mathematical and General*, vol. 30, no. 21, p. 7667, 1997.

[150] S. Wolfram, "Mathematica Edition: Version 8.0," 2010.

[151] G. E. Andrews, *The theory of partitions*. No. 2, 1998.

[152] J. Rasmussen, "Jordan cells in logarithmic limits of conformal field theory," *International Journal of Modern Physics A*, vol. 22, no. 1, pp. 67–82, 2007.

[153] P. A. Pearce and J. Rasmussen, "Coset construction of logarithmic minimal models: branching rules and branching functions," *Journal of Physics A: Mathematical and Theoretical*, vol. 46, no. 35, p. 355402, 2013.

[154] P. A. Pearce, J. Rasmussen, and E. Tartaglia, "Logarithmic superconformal minimal models," *Journal of Statistical Mechanics: Theory and Experiment*, vol. 2014, no. 5, p. P05001, 2014.

[155] J. K. Roberts, "Some properties of adsorbed films of oxygen on tungsten," *Proc. Roy. Soc. (London) A*, vol. 152, pp. 464–477, 1935.

[156] P. W. Kasteleyn, "Dimer statistics and phase transition," *J. Math. Phys.*, vol. 4, pp. 287–293, 1963.

[157] F. M. E., "Statistical mechanics of dimers on a plane lattice," *Phys. Rev.*, vol. 124, pp. 1664–1672, 1961.

[158] N. Elkies, G. Kuperberg, M. Larsen, and J. Propp, "Alternating-sign matrices and domino tilings (part i)," *Journal of Algebraic Combinatorics*, vol. 1, no. 2, pp. 111–132, 1992.

[159] N. Elkies, G. Kuperberg, M. Larsen, and J. Propp, "Alternating-sign matrices and domino tilings (part ii)," *Journal of Algebraic Combinatorics*, vol. 1, no. 3, pp. 219–234, 1992.

[160] V. E. Korepin, "Calculation of norms of bethe wave functions," *Communications in Mathematical Physics*, vol. 86, no. 3, pp. 391–418, 1982.

[161] E. H. Lieb and F. Y. Wu, "Two dimensional ferroelectric models," in *Phase transisitons and critical phenomena* (C. Domb and M. Green, eds.), vol. 1, Academic Press, 1972.

[162] B. U. Felderhof, "Direct diagonalization of the transfer matrix of the zero-field free-fermion model," *Physica*, vol. 65, pp. 421–451, 1973.

[163] D. L. O'Brien, P. A. Pearce, and S. O. Warnaar, "Finitized conformal spectrum of the Ising model on the cylinder and torus," *Physica A: Statistical Mechanics and its Applications*, vol. 228, no. 1–4, pp. 63 – 77, 1996.

[164] M. R. Gaberdiel and H. G. Kausch, "A local logarithmic conformal field theory," *Nuclear Physics B*, vol. 538, no. 3, pp. 631–658, 1999.

[165] H. G. Kausch, "Symplectic fermions," *Nuclear Physics B*, vol. 583, no. 3, pp. 513–541, 2000.

[166] M. R. Gaberdiel and I. Runkel, "From boundary to bulk in logarithmic cft," *Journal of Physics A: Mathematical and Theoretical*, vol. 41, no. 7, p. 075402, 2008.

[167] H. Saleur, "Polymers and percolation in two dimensions and twisted N= 2 supersymmetry," *Nuclear Physics B*, vol. 382, no. 3, pp. 486–531, 1992.

[168] P. A. Pearce, J. Rasmussen, and S. P. Villani, "Infinitely extended Kac table of solvable critical dense polymers," *Journal of Physics A: Mathematical and Theoretical*, vol. 46, no. 17, p. 175202, 2013.

[169] P. A. Pearce, J. Rasmussen, and S. P. Villani, "Solvable critical dense polymers on the cylinder," *Journal of Statistical Mechanics: Theory and Experiment*, vol. 2010, no. 02, p. P02010, 2010.

[170] A. Morin-Duchesne, P. A. Pearce, and J. Rasmussen, "Modular invariant partition function of critical dense polymers," *Nuclear Physics B*, vol. 874, pp. 312–357, Sept. 2013.

[171] A. Morin-Duchesne and Y. Saint-Aubin, "Jordan cells of periodic loop models," *Journal of Physics A: Mathematical and Theoretical*, vol. 46, no. 49, p. 494013, 2013.

[172] D. Kim and P. A. Pearce, "Scaling dimensions and conformal anomaly in anisotropic lattice spin models," *Journal of Physics A: Mathematical and General*, vol. 20, no. 7, p. L451, 1987.

[173] V. F. Jones, "A quotient of the affine hecke algebra in the brauer algebra," *ENSEIGNEMENT MATHEMATIQUE*, vol. 40, pp. 313–313, 1994.

[174] D. Bianchini, E. Ercolessi, P. A. Pearce, and F. Ravanini, "RSOS quantum chains associated with off-critical minimal models and Z_n parafermions," *Journal of Statistical Mechanics: Theory and Experiment*, vol. 2015, no. 3, p. P03010, 2015.

[175] H. N. V. Temperley and E. H. Lieb, "Relations between the 'percolation' and 'colouring' problem and other graph-theoretical problems associated with regular planar lattices: some exact results for the 'percolation' problem," *Proceedings of the Royal Society of London. Series A, Mathematical and Physical Sciences*, vol. 322, no. 1549, pp. 251–280, 1971.

[176] A. Morin-Duchesne, A. Klümper, and P. A. Pearce, "Conformal partition functions of critical percolation from D_3 thermodynamic Bethe Ansatz equations," *Journal of Statistical Mechanics: Theory and Experiment*, vol. 2017, no. 8, p. 083101, 2017.

[177] J.-Y. Choi, D. Kim, and P. A. Pearce, "Boundary conditions and inversion indentities for solvable lattice models with a sublattice symmetry," *Journal of Physics A: Mathematical and General*, vol. 22, no. 10, p. 1661, 1989.

[178] L. B. W. Jolley, *Summation of series*. Courier Corporation, 2012.

[179] N. Sloane, "The On-Line Encyclopedia of Integer Sequences."

[180] P. Pearce and J. Rasmussen, "Physical combinatorics of critical dense polymers," 2006.

[181] E. K. Sklyanin, "Boundary conditions for integrable quantum systems," *Journal of Physics A: Mathematical and General*, vol. 21, no. 10, p. 2375, 1988.

[182] R. E. Behrend, P. A. Pearce, and D. L. O'Brien, "Interaction-Round-a-Face models with fixed boundary conditions: the ABF fusion hierarchy," *Journal of Statistical Physics*, vol. 84, no. 1-2, pp. 1–48, 1996.

[183] V. F. R. Jones, "A polynomial invariant for knots via von Neumann algebras," *Bulletin of the American Mathematical Society*, vol. 12, Jan. 1985.

[184] I. V. Cherednik, "Factorizing particles on a half-line and root systems," *Theoretical and Mathematical Physics*, vol. 61, pp. 977–983, Oct. 1984.

[185] A. Morin-Duchesne, "A proof of selection rules for critical dense polymers," *Journal of Physics A: Mathematical and Theoretical*, vol. 44, no. 49, p. 495003, 2011.

[186] J. Fürlinger and J. Hofbauer, "q-catalan numbers," *Journal of Combinatorial Theory, Series A*, vol. 40, no. 2, pp. 248–264, 1985.

[187] P. Brändén, "q-narayana numbers and the flag h-vector of j (2× n)," *Discrete mathematics*, vol. 281, no. 1-3, pp. 67–81, 2004.

[188] A. Morin-Duchesne, J. Rasmussen, P. Ruelle, and Y. Saint-Aubin, "On the reality of spectra of $U_q(sl2)$-invariant XXZ Hamiltonians," *Journal of Statistical Mechanics: Theory and Experiment*, vol. 2016, no. 5, p. 053105, 2016.

[189] A. M. Gainutdinov, W. Hao, R. I. Nepomechie, and A. J. Sommese, "Counting solutions of the bethe equations of the quantum group invariant open xxz chain at roots of unity," *Journal of Physics A: Mathematical and Theoretical*, vol. 48, no. 49, p. 494003, 2015.

[190] J. H. Perk and H. Au-Yang, "Yang-baxter equations," *arXiv preprint math-ph/0606053*, 2006.

[191] N. S. Izmailian, C.-K. Hu, and R. Kenna, "Exact solution of the dimer model on the generalized finite checkerboard lattice," *Physical Review E*, vol. 91, no. 6, p. 062139, 2015.

[192] I. Gradshteyn and I. Ryzhik, *Tables of Integrals, Series and Products*. Academic Press, Inc., 1980.

[193] P. Fendley and N. Read, "Exact S-matrices for supersymmetric sigma models and the Potts model," *Journal of Physics A: Mathematical and General*, vol. 35, no. 50, p. 10675, 2002.

[194] P. Fendley, "Loop models and their critical points," *Journal of Physics A: Mathematical and General*, vol. 39, no. 50, p. 15445, 2006.

[195] P. Fendley and J. L. Jacobsen, "Critical points in coupled Potts models and critical phases in coupled loop models," *Journal of Physics A: Mathematical and Theoretical*, vol. 41, no. 21, p. 215001, 2008.

[196] P. Fendley and V. Krushkal, "Link invariants, the chromatic polynomial and the Potts model," *Advances in theoretical and mathematical physics*, vol. 14, no. 2, pp. 507–540, 2010.